Conceptual Design and Analysis of Orbital Cryogenic Liquid Storage and Supply Systems

**Final Report
May 1981**

by R. N. Eberhardt, G. R. Cunnington
and W. A. Johns

**Martin Marietta Corporation
Denver Aerospace**

CONCEPTUAL DESIGN AND ANALYSIS

OF ORBITAL CRYOGENIC LIQUID

STORAGE AND SUPPLY SYSTEMS

Final Report

May 1981

by R.N. Eberhardt, G.R. Cunnington
and W.A. Johns

Martin Marietta Corporation
Denver Aerospace

Prepared for

NATIONAL AERONAUTICS AND SPACE ADMINISTRATION

NASA Lewis Research Center

Contract NAS3-22264

FOREWORD

This report was prepared by the Martin Marietta Corporation, Denver Aerospace, under Contract NAS3-22264. The contract was administered by the Lewis Research Center of the National Aeronautics and Space Administration, Cleveland, Ohio. The study was performed from December 1979 to March 1981 and the NASA LeRC Project Manager was Mr. John C. Aydelott.

The Authors wish to acknowledge the contributions of the following individuals to this program:

Dale A. Fester - Program Manager
Ralph N. Eberhardt - Technical Director

Howard L. Paynter	Fluid Dynamic Analysis
William A. Johns	
William A. Johns	Thermal Analysis
G.R. Cunnington	
John P. Gille	
Robert L. Berry	Dynamics and
Terry M. Small	Structural Analysis
Terence Coxall	
John S. Marino	Design
Paul E. Bingham	Technology Evaluation

The data in this report are presented with the International System of Units as the primary units and English Units as secondary units. All Calculations and graphs were made in English Units and converted to the International Units.

ii

TABLE OF CONTENTS

LIST OF FIGURES

LIST OF TABLES

SUMMARY

Mission plans for future NASA and DOD payloads include a wide variety of applications which require orbital cryogenic liquid storage and supply systems. These applications range from the use of small quantities of liquid helium for experiment cooling to the use of thousands of liters of cryogens in the next generation of orbit-to-orbit transfer vehicles. Liquid storage requires the use of a fluid management system in low-g to accomplish gas-free liquid expulsion and efficient thermal control. One means of thermal control is to feed single-phase liquid to a thermodynamic vent system (TVS) to intercept heat leak and control tank pressure. A cryogenic storage and supply concept, which utilizes a fine mesh screen fluid management device and a vapor cooled shield TVS, known as the Cryogenic Fluid Management Experiment (CFME), is being developed by Martin Marietta under contract NAS3-21591 to the NASA-Lewis Research Center. The CFME is to be flown with liquid hydrogen as a Shuttle/Spacelab experiment.

A conceptual design and trade study was completed to extend the usefulness of the CFME storage tank concept to other fluids and tank sizes. Specifically, the fluids and tank sizes studied, included:

1) Spherical 0.62 m^3 (22 ft^3) argon, helium, oxygen and methane tanks;

2) Spherical 12.5 m^3 (440 ft^3) argon, oxygen and methane tanks; and a

3) Spherical and Cylindrical 37.4 m^3 (1320 ft^3) hydrogen tank.

Missions for each of the tank/fluid combinations were specified; they included constant liquid or gaseous supply, low-earth-orbit (LEO) to geosynchronous orbit (GEO) transfer, GEO stationkeeping, or on-orbit liquid resupply. For all cases except orbital resupply, each mission represented a relatively long-term (years) storage. Each tank configuration was assumed to be transported to low Earth orbit by the Shuttle.

Conceptual designs for each tank/fluid combination were generated. Fluid dynamic, steady-state thermal and preliminary structural analyses were made for each storage and supply tank concept. Numerous conceptual design trades were made to address the design paradox of a conservative support structure and minimum thermal input.

Relatively low weight and thermally efficient designs were configured for shuttle application for each tank/fluid combination. Parametric data, generated for each conceptual design to describe the orbital performance, include: 1) maximum liquid outflow rates and residuals, 2) rate of heat addition, 3) vent rate, 4) helium pressurant requirements, and 5) weight. A technology evaluation was completed, outlining deficiencies and recommendations for future analytical and experimental work.

Mission plans for future NASA and DOD payloads include a wide variety of applications which require orbital cryogenic liquid storage and supply systems. These applications range from the use of small quantities of liquid helium for experiment cooling to the use of thousands of pounds of cryogens in the next generation of orbit-to-orbit transfer vehicles. Liquid storage requires the use of a fluid management system in low-g to accomplish gas-free liquid expulsion and efficient thermal control.

Recent analytical and experimental efforts have resulted in designs that include cryogenic tankage containing fine-mesh screen liquid acquisition devices and thermal control systems consisting of thermodynamic vent systems (TVS) to intercept heat leak and control tank pressure (Ref. 1-4). However, a thorough characterization of low-g liquid expulsion and thermal performance has not been made for cryogenic tankage. This information is needed to provide an adequate data base from which efficient thermal designs can be generated. An orbital flight test is required because ground-based low-g test facilities are limited to a maximum of 25 seconds and thermal stabilization may require two to four days.

The Martin Marietta Corporation is currently developing a Shuttle/Spacelab experiment under contract NAS3-21591 to the NASA-Lewis Research Center (LeRC). The experiment, designated as the Cryogenic Fluid Management Experiment (CFME), consists of the systems necessary to store and expel liquid hydrogen in a low-g environment and to measure the performance of these systems. The CFME liquid hydrogen storage and supply tank is mounted on a Spacelab pallet and carried into orbit within the cargo bay of the Space Shuttle Orbiter.

The CFME storage and supply tank, shown schematically in Figure I-1, consists of the following major elements:

o   a pressure vessel containing a liquid acquisition device (LAD);
o   a thermodynamic vent system (TVS) consisting of heat exchangers attached to a vapor-cooled shield (VCS);
o   multilayer insulation (MLI); and
o   a vacuum jacket and girth ring assembly with trunnion supports for holding the pressure vessel.

The LAD is the key element of the storage and supply tank because it provides the means of expelling gas-free liquid in a low-g environment. The single-phase liquid feed is available for satisfying user requirements or supplying the thermodynamic vent system. The TVS uses the liquid hydrogen to control tank pressure. The hydrogen flows through two heat exchangers, each having an orifice that reduces the hydrogen temperature. These heat exchangers are mounted to the tank penetrations and the vapor-cooled shield, which is located concentrically between the tank and the vacuum jacket.
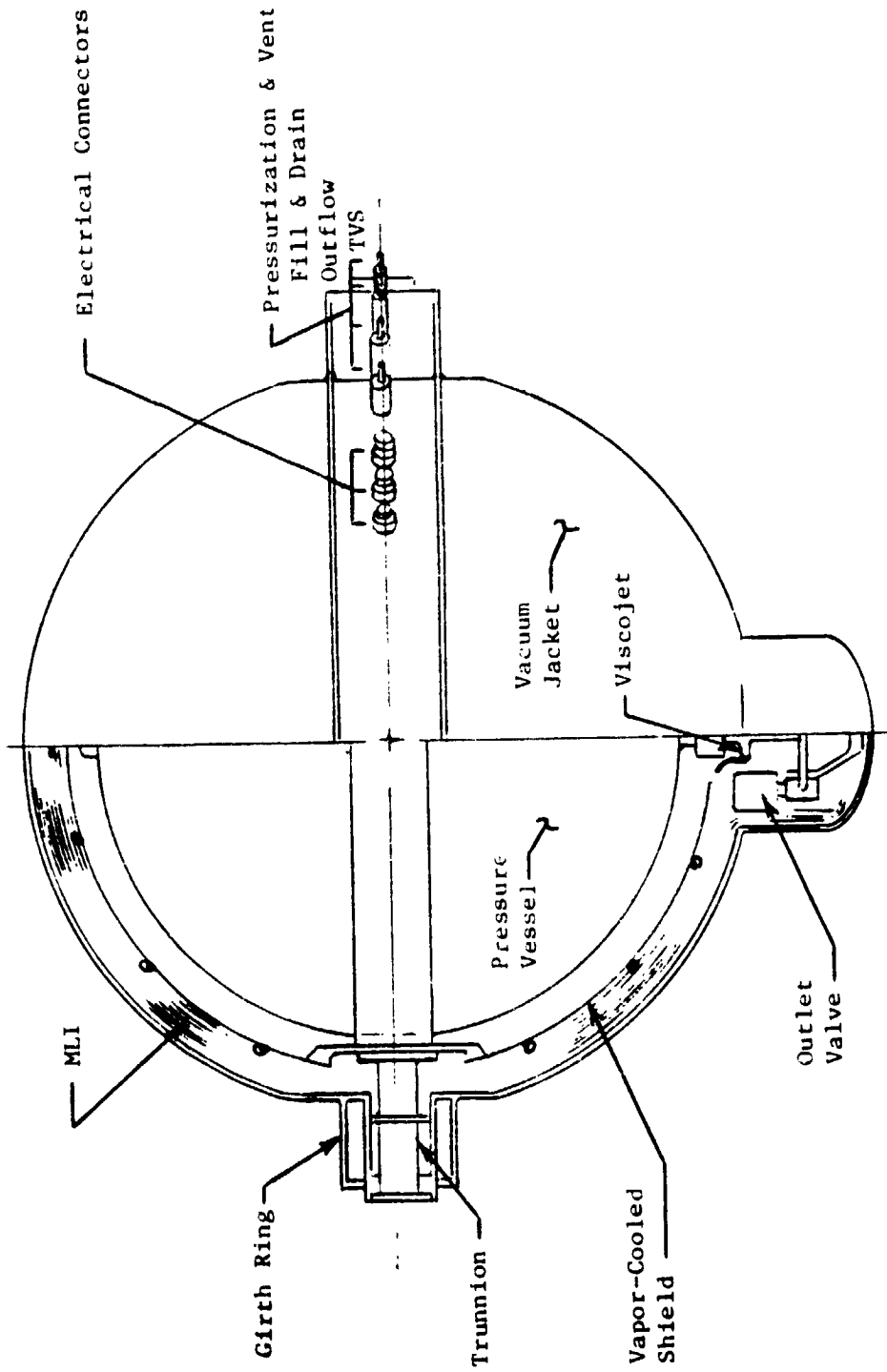
Figure I-1 CFME Liquid Hydrogen Storage and Supply Tank Assembly

Electrical Connectors

Pressurization & Vent
Fill & Drain
Outflow
TVS

Vacuum
Jacket

Viscojet

Pressure
Vessel

MLI

Girth Ring

Trunnion

Vapor-Cooled
Shield

Outlet
Valve

The MLI configuration consists of a 0.15-mil double aluminized mylar radiation shield separated by two Dacron B4A net spacers, assembled to a layer density of 60 reflectors per inch. This insulation blanket surrounds the vapor-cooled shield, and the entire tank assembly is contained within a vacuum jacket which provides efficient thermal control during launch operations and ascent.

A pressurization system, data acquisition and control system (DACS) and instrumentation make up the other major elements of CFME flight hardware. A sketch of the experiment hardware mounted on a Spacelab pallet is shown in Figure I-2.

The objective of this Orbital Cryogenic Storage and Supply System study was to establish the range of application of the CFME storage and supply tank assembly design, and determine modifications, as required, for other cryogenic liquids and large tank sizes. More specifically, the study involved expanding the CFME liquid hydrogen fluid dynamic, thermal and structural analyses to the matrix of tank sizes and cryogenic liquids presented in Table I-1. The CFME 0.62 m^3 (22 ft^3) hydrogen tank assembly was the "baseline" for the study, and this designation is used in the remainder of the report. As part of the study, changes to the CFME were identified, as required, to accommodate storage requirements. Total liquid acquisition devices and thermodynamic vent techniques for thermal control were ground-ruled for the study. Emphasis was placed on concepts and designs (e.g., support structure, components, control systems, etc) suitable for more than one cryogenic fluid.

Table I-1   Study Matrix of Tank Size/Cryogenic Liquid Combinations

Tank Volume	Cryogenic Liquid				
m^3 (ft^3)	Hydrogen	Methane	Argon	Oxygen	Helium
0.62 (22)	CFME (Baseline)	X	X	X	X
12.5 (440)		X	X	X	
37.4 (1320)	X				

A simplified schematic of the CFME baseline is presented in Figure I-3. A dark boundary line is drawn around the elements of the CFME that represent the tankage system evaluated in this study. The outflow, fill and drain, ground servicing vent and thermodynamic vent lines and valves were considered part of the tank assembly. Additional description of the CFME baseline is included as Section B of this chapter.

CFME Interface Panel

Liquid Acquisition Device
Pressure Vessel
Vapor-cooled Shield
MLI
Vacuum Jacket

Pressurization Spheres (4)

Power Distribution Units

DACS

Tape Recorder
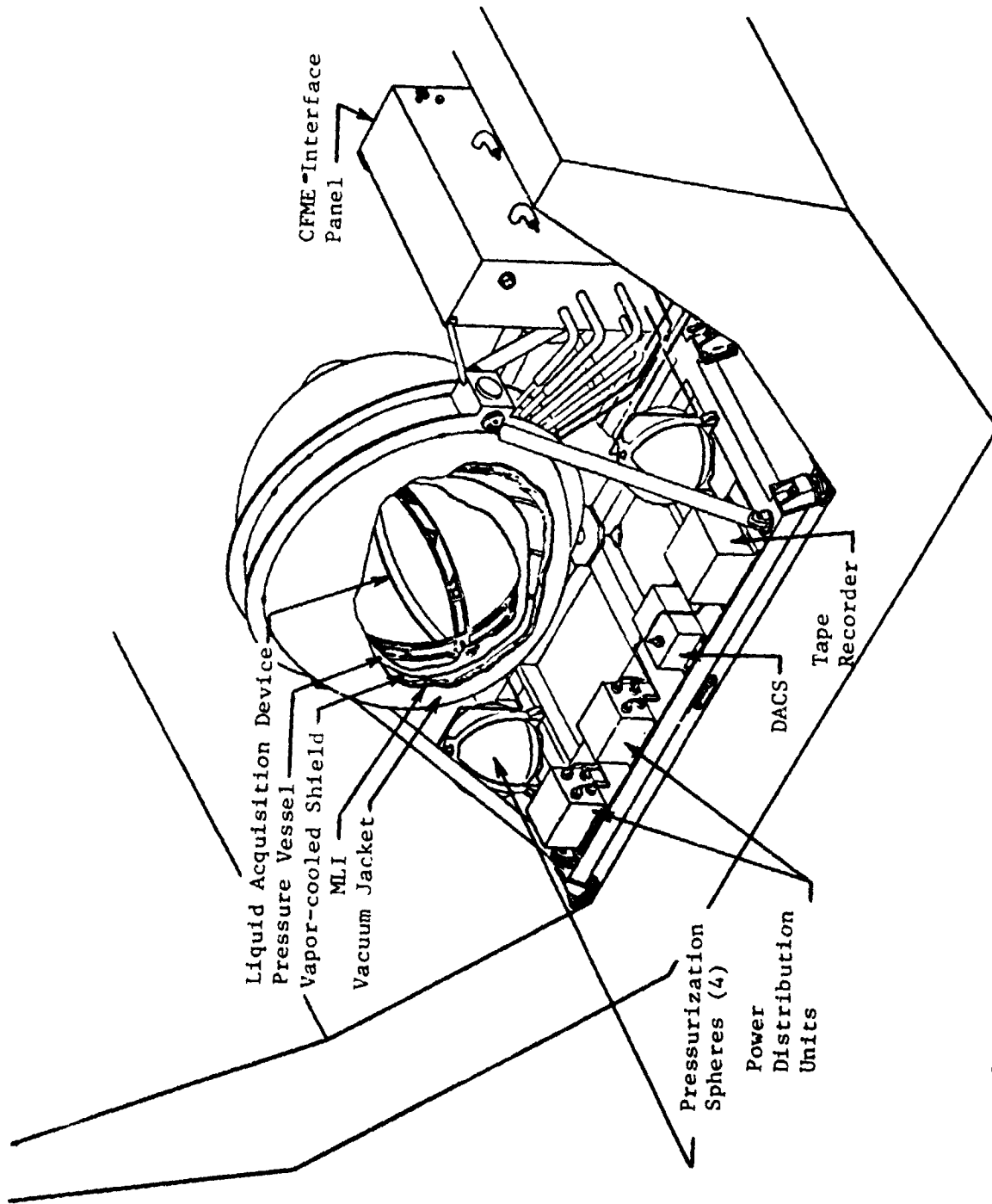
Figure I-2 CFME (Baseline) Mounted on a Spacelab Pallet
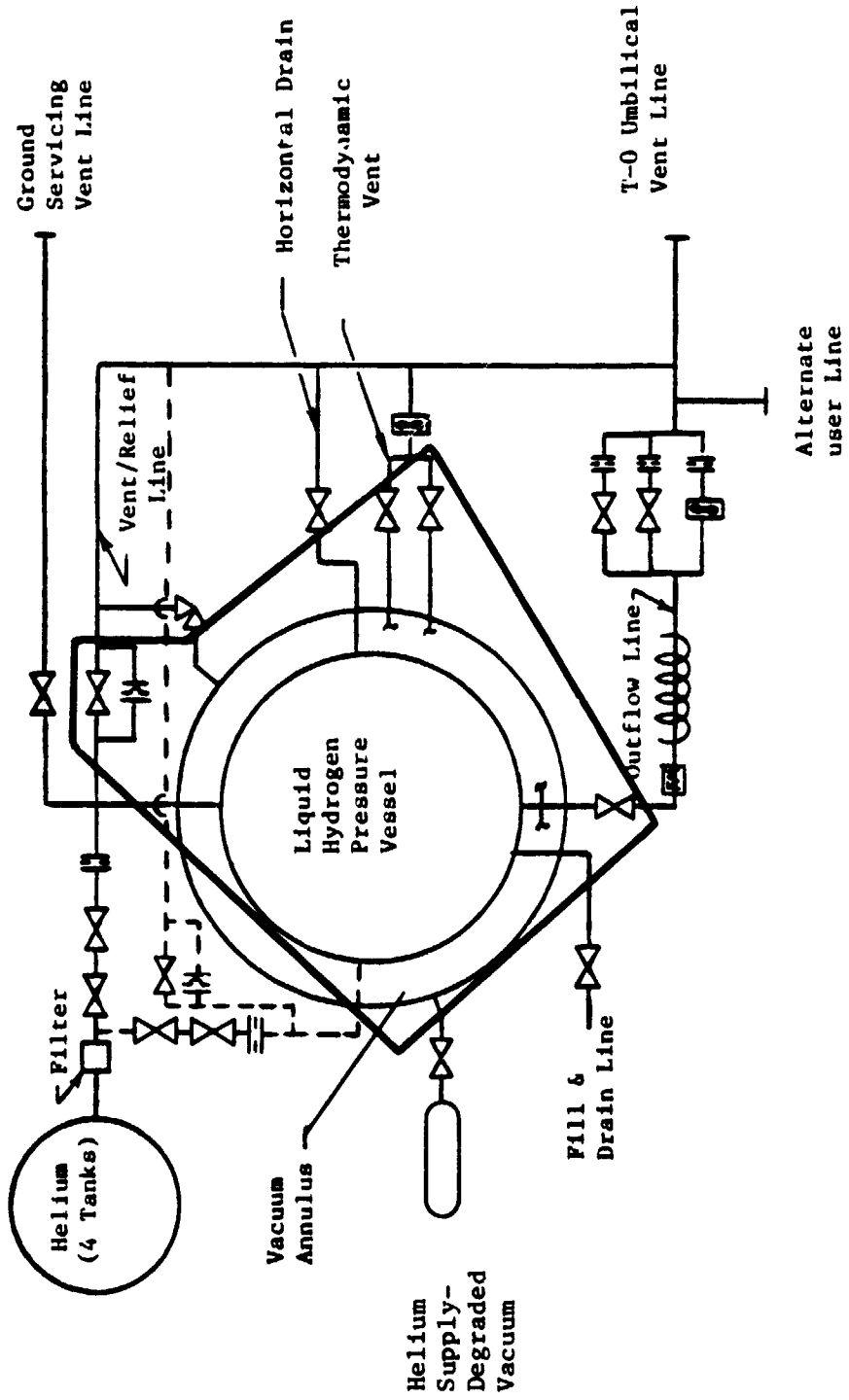
Figure I-3 CFME Schematic

A. Study Approach

The plan for conducting the study is presented in Figure I-4. It consisted of three tasks: Task I - Conceptual Design, Task II - Fluid, Thermal and Structural Analysis, and Task III - Technology Evaluation. The baseline CFME design was used as the initial conceptual design for each tank size/fluid combination. Mission requirements and study ground rules specified by NASA-LeRC at the beginning of the study effort guided the trade studies, resulting in preliminary conceptual designs of each system in the study matrix.

The Task II analysis effort was then performed, using techniques, computer models, and data previously used for the CFME detailed design and analysis. The fluid dynamic analysis consisted of hand calculations to establish the behavior of the liquid in the tanks, acquisition devices, inflow and outflow lines and thermodyanmic vent systems. Orbital performance predictions were prepared similar to those compiled for the CFME (Ref. 5). The steady state thermal analysis was conducted using the Cryogenic Storage Analysis Model (CSAM) thermal model and computer program. This program is a general thermal analyzer program, and includes a transient heat transfer network analysis, internal tank thermodynamics and a heat exchanger simulating the thermodynamic vent system. A brief description of the program is included as Appendix A, and a compilation of the preliminary analysis performed for CFME is contained in Reference 6. Fluid property subroutines were added to the program for the oxygen, argon, methane and helium cases. Thermodynamic vent system operations and helium pressurant requirements were determined.

A preliminary structural analysis was performed for each conceptual design to establish that the structural integrity was adequate for transport to low earth orbit by the Shuttle. Hand calculations were used to define the dynamic loads, hand calculations and selected Buckling of Shells of Revolution (BOSOR) runs were used to size the storage vessels, and hand calculations were used for the vacuum jacket buckling analysis. Similar analyses for CFME are documented in Reference 7.

A conceptual design iteration and update was performed following the fluid, thermal and structural analyses. The resulting conceptual designs were used as the basis for conducting the technology evaluation and determining recommendations for future analytical and experimental efforts.

B. CFME (Baseline) Description

The specific configuration of the CFME storage and supply tank assembly was influenced by the experimental objective of evaluating a thermodynamic vent system in combination with a fine mesh screen acquisition device for thermal control. A total communication device was selected for the LAD. The configuration of the LAD is shown schematically in Figure I-5. A four-channel arrangement encircles the interior of the tank, providing a flow path between the liquid in its low-g orientation and the tank outlet. One side of each channel is covered with 325x2300 Dutch Twill fine-mesh screen.
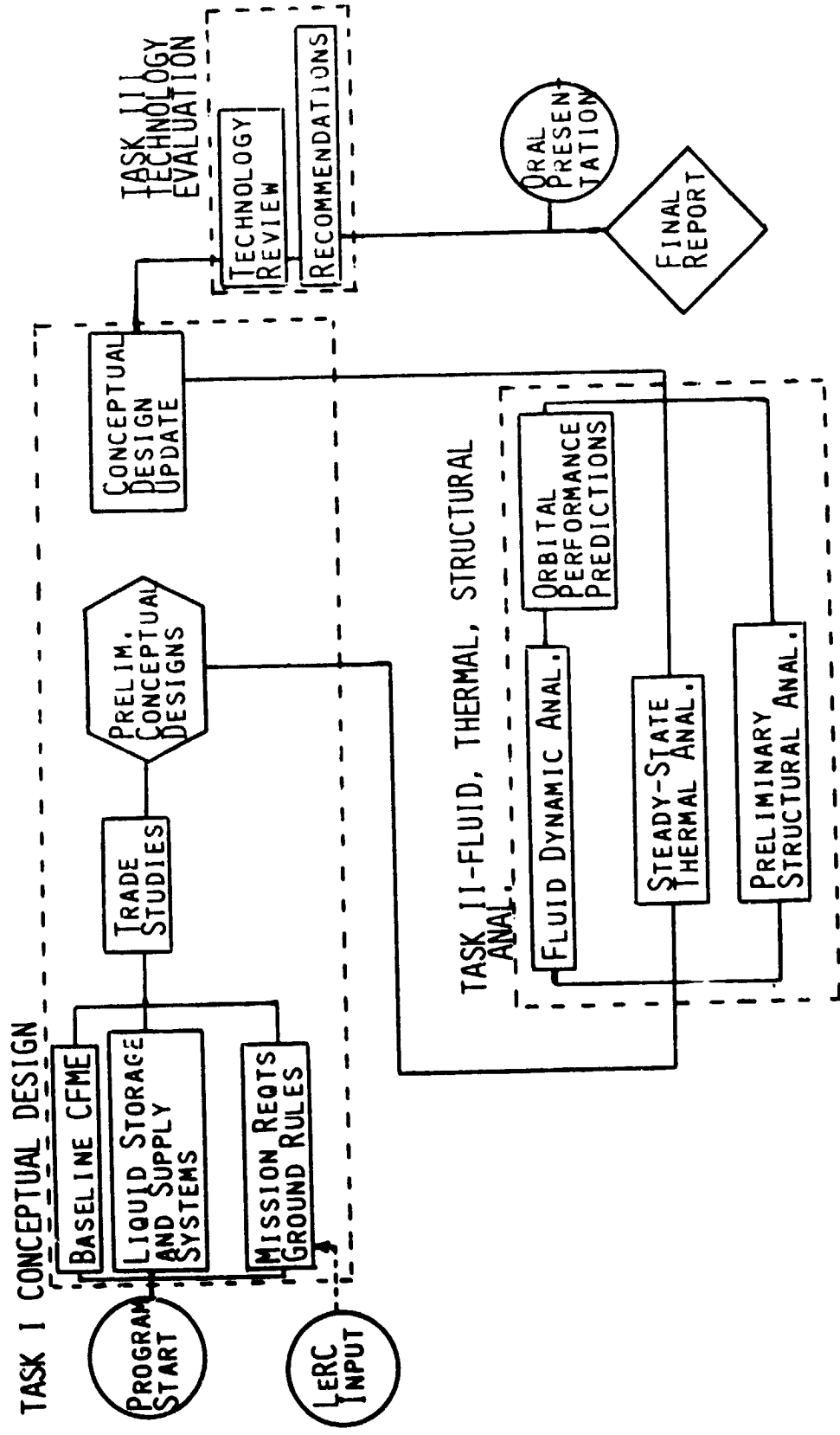
Figure I-4 Study Approach

Detail of
Upper Channel
Junction

Outlet Manifold
Detail

Typical
4 Channels

Outlet

Detail of
Truncated
Channel

Structural
Support
Truss

Screen Covered
Surface Facing
Tank Wall
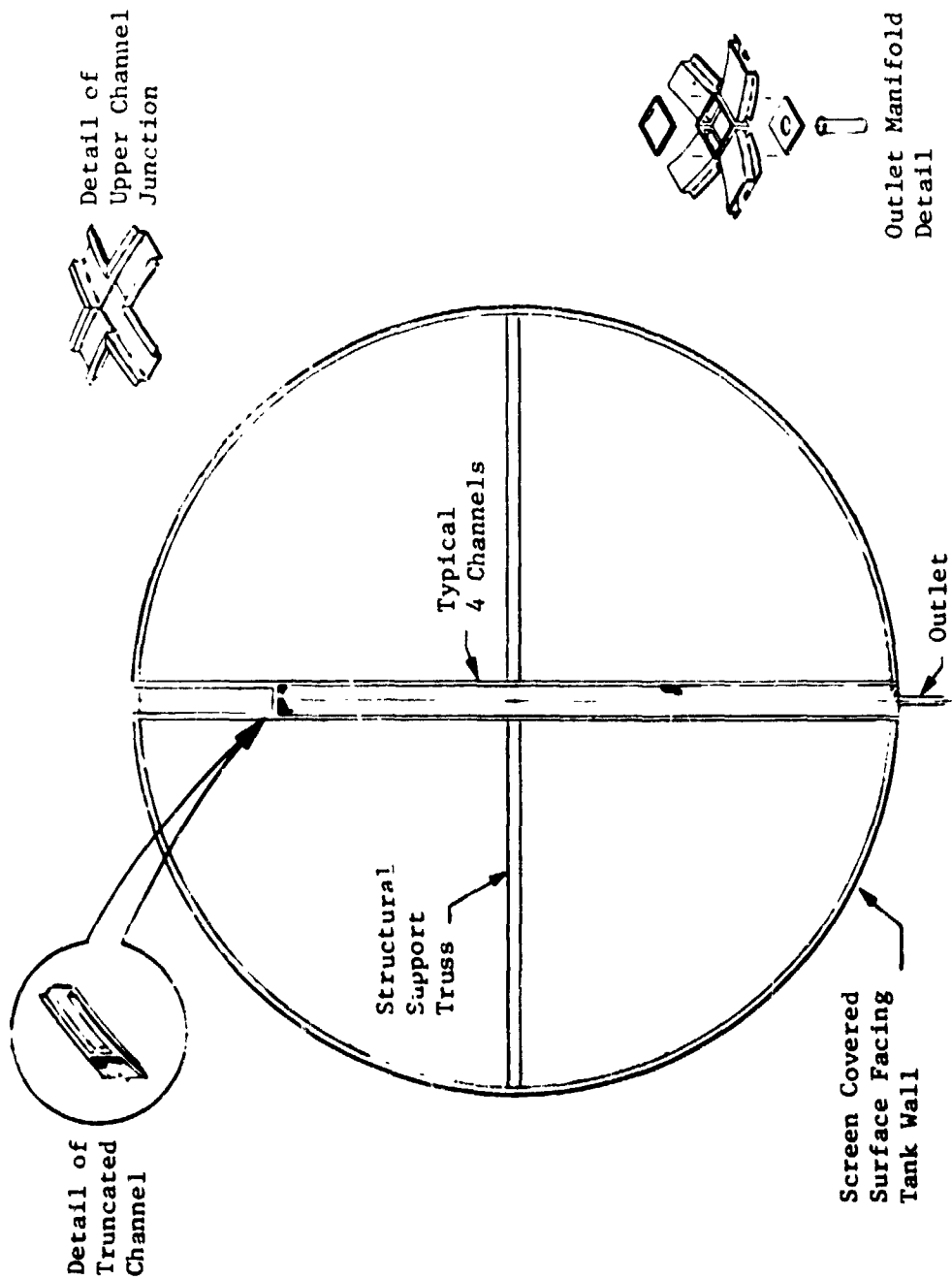
Figure I-5 CFME Liquid Acquisition Device

The screen on the flow channels is truncated to keep the
screen-covered portions completely submerged within the liquid during
the ground hold and boost phases of the mission. The truncation is at
the 10 percent level, and the initial ullage volume is approximately 5
percent, allowing some margin for liquid sloshing and venting. A 4.0-cm
(1.6-in) by 2.0-cm (0.39-in) channel cross-section was selected to
provide a residual of less than one percent at a minimum nominal flow
rate of 1.5 Kg/hr (3.3 lb/hr). Performance was considered in both the
omnidirectional acceleration environment produced by the Shuttle
Reaction Control System of 0.04-g and the settling acceleration
environment due to the Shuttle Orbital Maneuvering System of 0.077-g.
Safety considerations required propellant outflow (and dump) in a low-g
environment (non-RCS operational at point of depletion) at a flow rate
of 81.8 Kg/hr (180 lb/hr). In this case a residual of less than two
percent can be achieved with the selected channel configuration.

The location of the ullage in low-g is not controlled to permit
efficient (gas only) venting, so the increase in pressure due to heat
leak is relieved by withdrawing liquid through the acquisition device to
feed the thermodynamic vent system, which is illustrated schematically
in Figure I-6. The vented liquid is used as a refrigerant to reduce the
heat input to the tank. This is accomplished by routing the vent fluid
through heat exchangers which intercept heat entering through the
insulation and along tank penetrations. Liquid withdrawn from the tank
outlet flows through a Viscojet (Trademark, the Lee Co.) at the entrance
to each heat exchanger. The Viscojet is a multiorifice flow restrictor
(Joule-Thompson device) which meters the vent flow while reducing the
pressure and temperature.
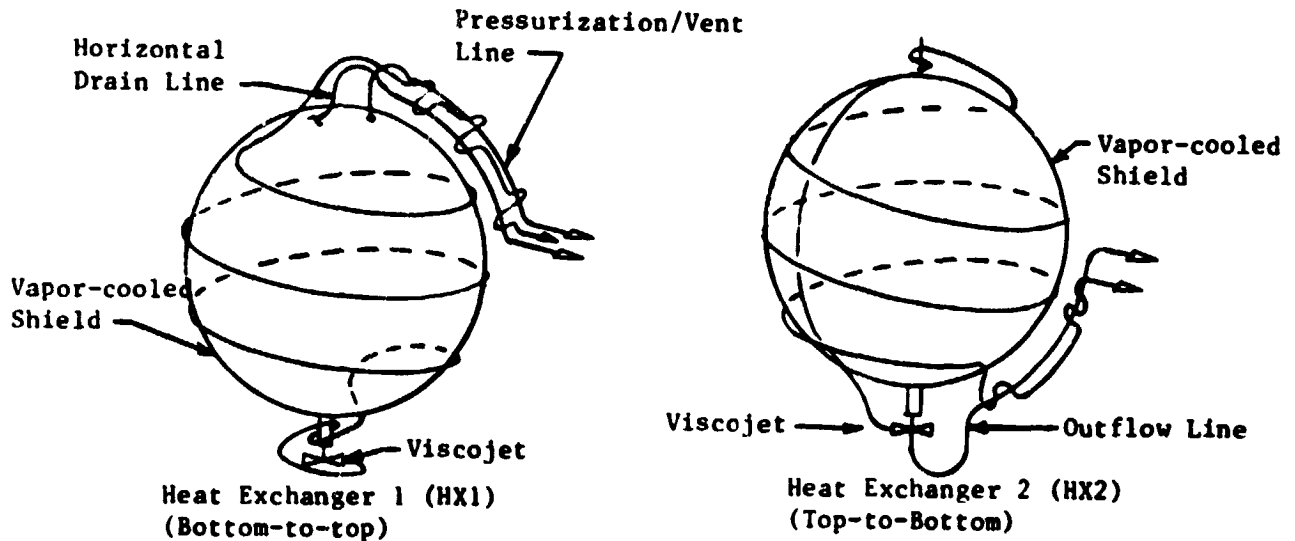
Figure I-6   CFME Thermodynamic Vent System

Heat exchanger one (HX1) is configured in a bottom-to-top direction and provides greater cooling to the bottom of the tank. The flow of heat exchanger two (HX2) is in the top-to-bottom direction, providing a means for limiting the temperature difference between the poles of the tank. The heat exchangers provide some degree of cooling to the entire tank since they are attached to the vapor-cooled shield. A thermal short is provided between the heat exchangers and composite trunnions to decrease heat input to the storage tank through these support members. Additional cooling capacity of the vent gas leaving the VCS is used to reduce heat leak along fill, vent, drain and outflow lines. Flow in the two heat exchangers is controlled by on-off latching solenoid valves actuated by a microprocessor. HX1 is designed to remove approximately 60-80 percent of the input heat leak and HX2 is sized to remove 150-200 percent.

A summary of the steady state heat leaks for the CFME is presented in Table I-2. Heat leaks are listed for cases with and without HX1 of the TVS operating. The major heat input is through the MLI, accounting for 42 percent of the total heat leak when the TVS is inoperative. With HX1 operating at a flow rate of 0.023 Kg/hr (0.05 lb/hr), a heat leak of 1.8 W (6.1 Btu/hr) is obtained (accompanied by a slow tank pressure rise). This table will be useful for comparison purposes as the thermal performance results are reviewed in Chapter IV.

Experiment flexibility and safety considerations resulted in the numerous servicing line penetrations of the storage and supply tank, and the relatively large safety factors used in the design. The relatively severe environments encountered in the Shuttle cargo bay, and the purposely conservative design approach associated with the safety aspects of hydrogen, resulted in a quite heavy tank assembly weight, which is presented in Table I-3.

The liquid hydrogen tank consists of two 6061-T6 aluminum alloy hemispherical domes which are welded to a ring. The wall thickness is a minimum of 0.142-cm (0.056-in) with increased thickness at the poles and the support ring. The wall thickness in these areas tapers from 0.64-cm (0.25-in) to 0.142-cm (0.056-in). The wall thicknesses resulted from a 2.5 safety factor imposed on the design yield point. A factor of 1.5 was applied to limit load to obtain ultimate load.

The vacuum jacket and girth ring are 6061-T6 aluminum. The vacuum jacket consists of two hemispherical domes of thickness 0.28-cm (0.110-in) which are welded to the girth ring. This thickness provides a safety factor of 1.5 against a collapse pressure of 101 KN/m^2 (14.7 psi). The girth ring has a diameter of 1.16-m (45.7-in) and is a forged and machined channel section.

Table I-2 Steady State Heat Leaks for CFME (Baseline) Configuration

Conductor	TVS Inoperative Heat Input		% of Total	TVS Operative (HX1) Heat Input	
	Watts (Btu/hr)	Watts/m^2 (Btu/hr ft^2)		Watts (Btu/hr)	Watts/m^2 (Btu/hr ft^2)
Multi-layer Insulation (Thickness = 31.8 mm)	3.0 (10.2)	0.85 (0.27)	42	2.7 (9.2)	0.77 (0.25)
Supports	2.1 (7.2)	0.59 (0.19)	30	1.8 (6.1)	0.51 (.16)
Penetrations	1.6 (5.5)	0.45 (0.14)	23	0.9 (3.1)	0.26 (0.08)
Thermodynamic Vent System (Flowrate = 0.023 kg/hr)	0.4 (1.4)	0.11 (0.03)	5	3.6* (12.3)*	1.03* (0.33)*
TOTAL	7.1 (24.3)	2.0 (0.63)	100	1.8 (6.1)	0.51 (0.16)

* Indicates heat flow from tank to conductor

Table I-3 Storage and Supply Tank Assembly Weight Summary

Tank Assembly Element	Weight	
	Kg	(1b)
LH$_2$ Storage Tank	32.3	(71.1)
Thermal Control System (TVS and VCS)	29.5	(64.8)
LH$_2$ Tank Supports	3.4	(7.4)
Outflow Valves	3.2	(7.0)
Vacuum Jacket	36.9	(81.1)
Girth Ring	23.4	(51.6)
Total	128.7	283.0

II. MISSION AND OPERATIONAL REQUIREMENTS

Mission criteria were specified by NASA-LeRC for each of the tank/fluid combinations in the study matrix. Operational requirements such as tank pressure, user system and abort flowrates, and duty cycle, were then established as the criteria for preparing the conceptual designs and evaluating performance. Shuttle environments were also defined for each of the tank/fluid combinations. Because the weight and thermal performance of each tank assembly are so closely tied to the methods of support, particular emphasis was directed toward the dynamic environments associated with launch. The mission and environmental requirements are presented in Sections A and B, and fluid properties and material properties summarized in Sections C and D, respectively.

A. Mission Requirements

The following mission functions were defined for each fluid/tank combination in the study:

1) Methane 0.62 m^3 (22 ft^3) - Experiment cooling

2) Argon 0.62 m^3 (22 ft^3) - Electric propulsion for stationkeeping

3) Oxygen 0.62 m^3 (22 ft^3) - Life support

4) Helium 0.62 m^3 (22 ft^3) - Experiment cooling

5) Argon 12.5 m^3 (440-ft^3) - Electric propulsion for orbit raising and stationkeeping

6) Methane 12.5 m^3 (440 ft^3) - Low thrust chemical stage

7) Oxygen 12.5 m^3 (440 ft^3) - Orbital Supply module (Tanker) for OTV

8) Hydrogen 37.4 m^3 (1320 ft^3) - Orbital Supply Module (Tanker) for OTV

From these basic mission designations, a typical set of specifications for duty cycle, loaded mass, mission flowrate and abort flowrate were defined, as shown in Table II-1. The loaded liquid mass for each storage and supply system represents a 95-percent liquid load, except for the 12.5 m^3 (440 ft^3) methane tank which has a 91.1 percent load. All of the 0.62 m^3 (22 ft^3) tanks have a constant outflow throughout the mission duration except the argon tank. The methane and helium tanks are for a 180-day mission with

II-1

TABLE II-1 - Typical Missions for Orbital Storage and Supply Systems

Tank Volume	Cryogen	Typical Mission	Duration	Liquid Mass Loaded	Mission Flowrate	Abort Flowrate/ Abort Time
0.62 m³ (22 ft³)	Hydrogen (Baseline-CFME)	Spacelab Experiment Supply Tank	7 days	39 kg (85 lbs)	27 kg/hr (60 lb/hr)	0.02 kg/sec (0.05 lb/sec) [0.5 hr]
0.62 m³ (22 ft³)	Argon	GEO stationkeeping; 25% - on cycle	7 years	814 kg (1795 lbs)	0.14 kg/hr (0.3 lb/hr)	0.15 kg/sec (0.33 lb/sec) [1.5 hr]
	Methane	Experiment/Spacecraft cooling; liquid supply, constant flowrate	180 days	250 kg (550 lbs)	0.06 kg/hr (0.13 lb/hr)	0.07 kg/sec (0.15 lb/sec) [1.0 hr]
	Oxygen	Life Support; gaseous supply, constant flowrate	180 days	668 kg (1473 lbs)	0.15 kg/hr (0.34 lb/hr)	0.37 kg/sec (0.82 lb/sec) [0.5 hr]
	Helium	Experiment/Spacecraft cooling; liquid supply, constant flowrate	180 days	74 kg (163 lbs)	0.02 kg/hr (0.04 lb/hr)	0.014 kg/sec (0.03 lb/sec) [1.5 hr]

TABLE II-1 - Typical Missions for Orbital Storage and Supply Systems (Continued)

Tank Volume	Cryogen	Typical Mission	Duration	Liquid Mass Loaded	Mission Flowrate	Abort Flowrate
12.5 m³ (440 ft³)	Argon	LEO-to-GEO transfer, plus 7-year station-keeping; 75%-transfer, 25%-stationkeeping	200 days (transfer) 7 years (station-keeping)	16,301 kg (35,906 lbs)	2.55 kg/hr (5.61 lb/hr) (transfer) 0.14 kg/hr (0.3 lb/hr) (station-keeping)	3.02 kg/sec (6.65 lb/sec) (1.5 hr)
	Methane	LEO-to-GEO transfer; (100 lb) thrust, 8 burns 45.4 kg	56.7 hours (transfer time),40 hours on-orbit prior to transfer	4787 kg (10,545 lbs) (8.9% ullage)	103 kg/hr (227 lb/hr)	1.33 kg/sec (2.93 lb/sec) (1.0 hr)
	Oxygen	OTV Resupply	3 hours (outflow time) several day mission	13,380 kg (29,470 lbs)	1.24 kg/sec (2.73 lb/sec)	7.4 kg/sec (16.4 lb/sec) (0.5 hr)
37. m³ (1320 ft³)	Hydrogen	OTV Resupply	3 hours (outflow time) several day mission	2447 Kg (5390 lbs)	0.23 Kg/sec (0.5 lb/sec)	0.7 Kg/sec (1.5 lb/sec) (1.0 hr)

constan. liquid outflow; the oxygen tank is for a 180-day life support mission with constant gaseous outflow. The argon flowrate represents a state-of-the-art electric propulsion system with an Isp of 3000 sec and a maximum thrust of 1.1 N (0.25 lb), as designated by NASA-LeRC. The seven-year mission requirement was an upper limit design goal outside the capability of a $0.64 \, m^3$ (22 ft^3) tank. Determination of the mission duration potential for this application was the key focus of the thermal and structural trade studies.

The 12.5 m^3 (440 ft^3) argon tank was specified to use 75 percent of the propellant for LEO-to-GEO transfer and the remainder for stationkeeping, with a seven-year design goal as previously discussed for the smaller argon tank. The flowrate during transfer represents constant flow of 75 percent of the loaded liquid over 200 days. The flowrate during stationkeeping again represents feeding thrusters with a total thrust of 1.1 N (0.25 lb). With the quantity of liquid remaining in the tank following transfer, it would be possible to operate the thrusters on a 50-percent-on duty cycle during the remainder of the seven-year mission. This neglects any loss of fluid due to boil-off. If the boil-off rate exceeds the equivalent flowrate of 0.14 kg/hr (0.3 lb/hr) then the percentage of on-time would be reduced. Since the thrusters can accept a low pressure gaseous supply, the approach was to configure the thermal control system such that the flowrate requirement for the thrusters matched as closely as possible the vent rate required to maintain tank pressure.

The 12.5 m^3 (440 ft^3) methane tank was applied to a CH_4/LO_2 low thrust chemical orbit-to-orbit propulsion system, as defined in Reference 8. The methane tank outflow rate is based on a 445 N (100 lb) thrust nine-burn mission scenario, as defined in Table II-2. A mixture ratio of 3.7 was used for the CH_4/LO_2 propulsion system. The total payload mass was 27,000 kg (60,000 lbs). A 40-hour on-orbit storage period precedes the LEO-to-GEO transfer.

The 12.5 m^3 (440 ft^3) LO_2 and 37.4 m^3 (1320 ft^3) LH_2 tanks are for OTV resupply. General Dynamics has specified three-hour OTV resupply sequences (Ref. 9) with actual durations for outflow from the supply tanks of 1.0 hour for LH_2 and 0.5 hours for LO_2. The remainder of these three-hour transfer times include line hook-up, cooldown, purging, etc. For the purposes of this study, a three-hour outflow time was agreed upon, resulting in the flowrates specified in Table II-1, with abort rates corresponding to the outflow times of the General Dynamics study.

The other abort flowrates specified in Table II-1 were based on the following rationale. For the argon and helium tanks, which contain inert fluids, the desire is to abort while on-orbit so that designing for crash landing does not over-penalize the system. An abort time of 1.5 hours was assumed to be representative of a single orbit commitment to return from orbit. It was assumed that for fuels and oxidizers the dumping on-orbit must be accomplished sequentially. Thus, one hour was assumed for fuels and one-half hour for the oxygen oxidizer.

II-4

Table II-2   Methane 12.5 m^3 (440 ft^3) Storage Tank Duty Cycle

Burn	Duration (sec)	(Hr)	Mass Used		Mass Remaining	
			kg	(lb)	kg	(lb)
					4503	(9907)
1	22528	6.26	645	(1419)	3858	(8488)
Coast		1.7				
2	19976	5.55	572	(1258)	3286	(7230)
Coast		1.9				
3	17709	4.92	507	(1116)	2779	(6114)
Coast		2.3				
4	15697	4.36	450	(989)	2330	(5125)
Coast		2.8				
5	13910	3.86	398	(876)	1931	(4249)
Coast		3.5				
6	12324	3.42	353	(776)	1579	(3473)
Coast		4.5				
7	10915	3.03	313	(588)	1266	(2785)
Coast		6.2				
8	9664	2.68	277	(609)	989	(2176)
Coast		1.0				
Circularize	32397	9.0	928	(2041)	62	(135)
		66.98	4443	(9772)		

An initial study ground rule of 414 KN/m^2 (60 psia) maximum tank supply pressure was established for all cases except helium. Performance limitations or advantages associated with this pressure level were identified later in the study as structural and thermal performance results were generated. In most cases, decreases in the maximum operating pressure were possible, resulting in potential tank weight reductions. Because the critical pressure for helium is 227.5 KN/m^2 (33 psia), the maximum operating pressure must be below this level to maintain a liquid supply in the tank. Critical pressures for argon, methane and oxygen are all above 4140 KN/m^2 (600 psi), and the critical pressure of hydrogen is 1300 KN/m^2 (188 psi), giving adequate design and performance margins. (Fluid property data are presented in Section C.)

B. Shuttle Interfaces and Environments

Two separate acceleration/vibration environments were identified for conducting the conceptual design and structural analysis tasks. For the initial conceptual design activity, the 0.62 m^3 (22 ft^3) tank assemblies were assumed to be Spacelab pallet-mounted like the CFME design. This environment is summarized in Table II-3, and the random vibration environment for the pallet-mounted tank assembly is included as Figure II-1. These environments are specified in the Spacelab Payload Accommodations Handbook (SPAH), Reference 10.

Table II-3 Acceleration/Vibration Environment for Spacelab
Pallet-Mounted Tank Assemblies (SLP/2104)

Boost/Ascent and Landing

1) Quasi-Static Accelerations (g)

Event	$\ddot{X}$	$\ddot{Y}$	$\ddot{Z}$
Lift-Off	+2.11 -4.3	±1.4	+5.5 -6.1
Landing	±4.0	±1.0	+6.6 -4.0
Emergency Landing	+4.5 -1.5	±1.5	+4.5 -2.0

2) Random - Pallet   8.72 g RMS

3) Sine

Frequency Range   5-35 Hz
Level   ±0.25 g (0 to peak)
Sweep Rate   1 oct./min.

On-Orbit

1) Drag (g)

-3.0×10^{-6} axial (0° angle of attack)
-1.6×10^{-5} lateral (90° angle of attack)

2) RCS - Omnidirectional - 0.04g

3) OMS - Settling Acceleration - 0.077g

Figure II-1   Random Vibration Environment for Spacelab
             Pallet-Mounted Payload

An additional requirement in the SPAH is that the natural frequency of the tank assembly mounted with support structure to the Standard Spacelab pallet hardpoints must be greater than 35 Hz. This was found to be a significant weight driver for the CFME, particularly the increased size of the vacuum jacket girth ring web and thickness. These stringent environments imposed on payloads greatly influence the structural design, and result in significant weight and thermal penalties over tanks designed to environments representative of those specified for the basic Shuttle Orbiter hardware. It should be noted that the Orbiter tank systems (OMS, RCS and PRSA), which have a design goal of 100-mission life, are being qualified to less severe dynamic environments than that imposed on pallet-mounted structure.

For the larger tanks, the environments are those specified in the Space Shuttle Payload Accommodations Handbook, Reference 11. The conceptual designs of these larger tanks assume the tanks are mounted to the Orbiter keel and main longeron trunnion fittings. A 5-point payload retention system is defined for supporting large payloads within the cargo bay, as shown in Figure II-2. A 4-point retention system, with only one longeron stabilizing fitting, is also possible. For purposes of this study it was assumed that the tank support struts tie-in directly to these fittings. The support system for the tank essentially becomes a truss network, which could be used as a basic frame structure for the entire payload package. The acceleration/vibration environment for these larger tanks is summarized in Table II-4, and the acceleration spectral densities at the two trunnion mounting points (longeron and keel) are presented in Figures II-3 and II-4.

The thermal environment used for design and analysis was similar to that being used on the CFME, and is summarized in Table II-5. It was assumed that the tank assemblies are exposed to a hard vacuum and when in the payload bay are located centrally with an unobstructed view of the door. If the tank assemblies are removed from the orbiter as part of a spacecraft, stage, etc., the extreme hot and cold conditions to which the tanks are exposed are still assumed to be those in Table II-5.

C. Fluid Properties

Fluid properties were compiled from References 12 through 17 for each of the fluids in the study. The saturation temperature, surface tension, density, kinematic surface tension and heat of vaporization for liquid saturation pressures of 138 KN/m^2 (20 psia) and 414 KN/m^2 (60 psia) are presented in Tables II-6 and II-7 for each of the cryogens. (Table II-6 is in International Units and Table II-7 is in English Units.) Thermophysical property data are fairly well established for hydrogen, oxygen, methane and argon. Liquid helium thermophysical data are not as well characterized because of the difficulties of measuring the particular parameters at liquid helium temperature. Because this study is directed to liquid helium storage and supply and not the so-called "superfluid", which has received considerable interest over the past decade, a brief summary of helium properties is included in the following paragraphs.
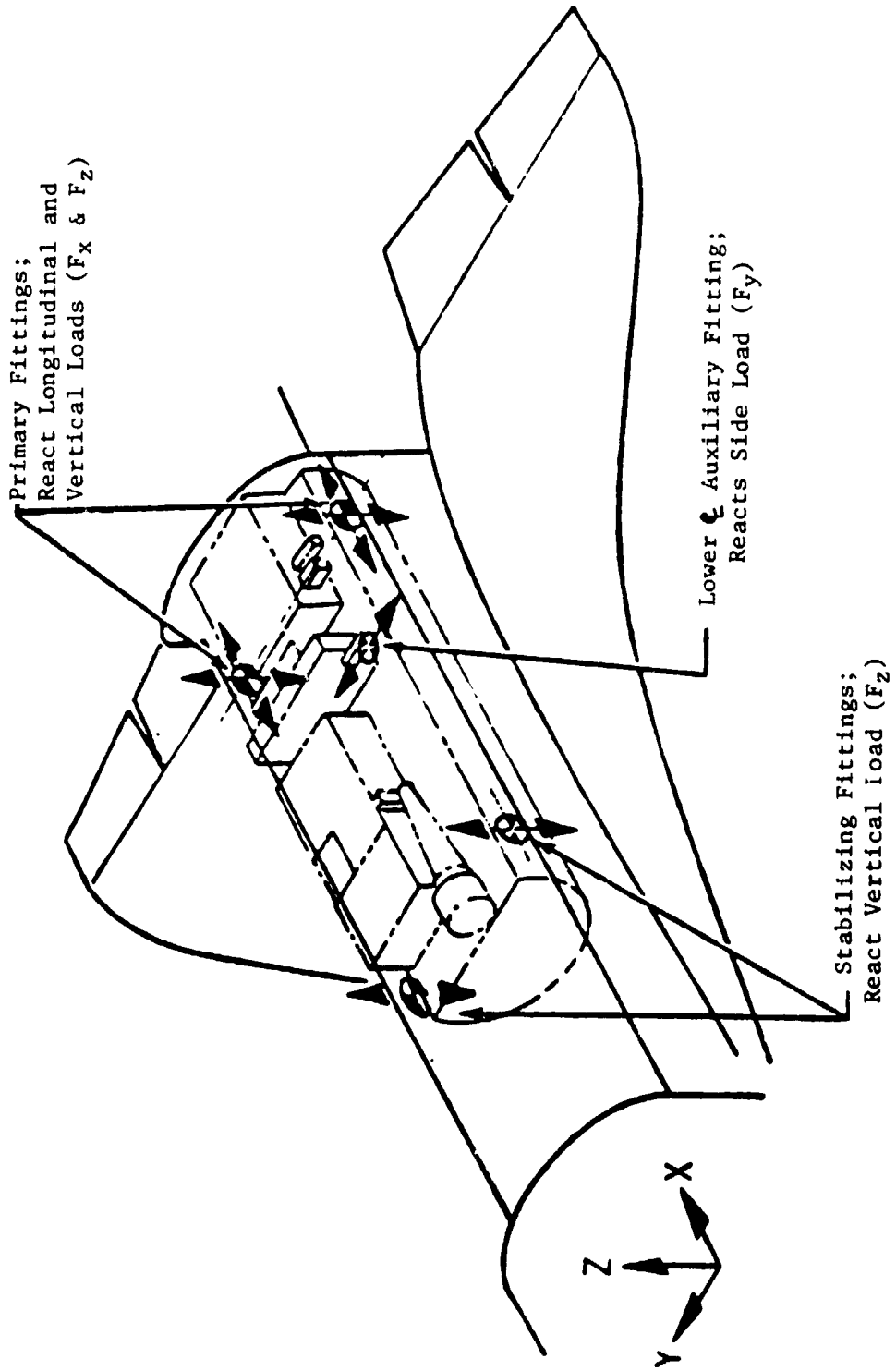
Figure II-2   5-Point Payload Retention System (Indeterminate)

Table II-4 Acceleration/Vibration Environment for Orbiter-
Mounted Tank Assemblies

Boost/Ascent ar.d Landing

1) Quasi-Static Accelerations (g)

Event	$\ddot{X}$	$\ddot{Y}$	$\ddot{Z}$
Lift-Off	-3.2	±1.4	±2.5
Landing	+1.8 / -2.0	±1.5	+4.2 / -1.0
Emergency Landing	+4.5 / -1.5	±1.5	+4.5 / -2.0

2) Random - Keel Trunnion Fitting - 9.71 g RMS

3) Random - Main Longeron Trunnion Fitting - 2.42 g RMS

4) Sine

Frequency Range	5-35 Hz
Level	+0.25 g (0 to peak)
Sweep Rate	1 oct./min.

On-Orbit

1) Drag (g)

-3.0×10^{-6} axial (0° angle of attack)
-1.6×10^{-5} lateral (90° angle of attack)

2) RCS - Omnidirectional - 0.04g

3) OMS - Settling Acceleration - 0.077g

Figure II-3   Unloaded Keel Trunnion Fitting Vibration
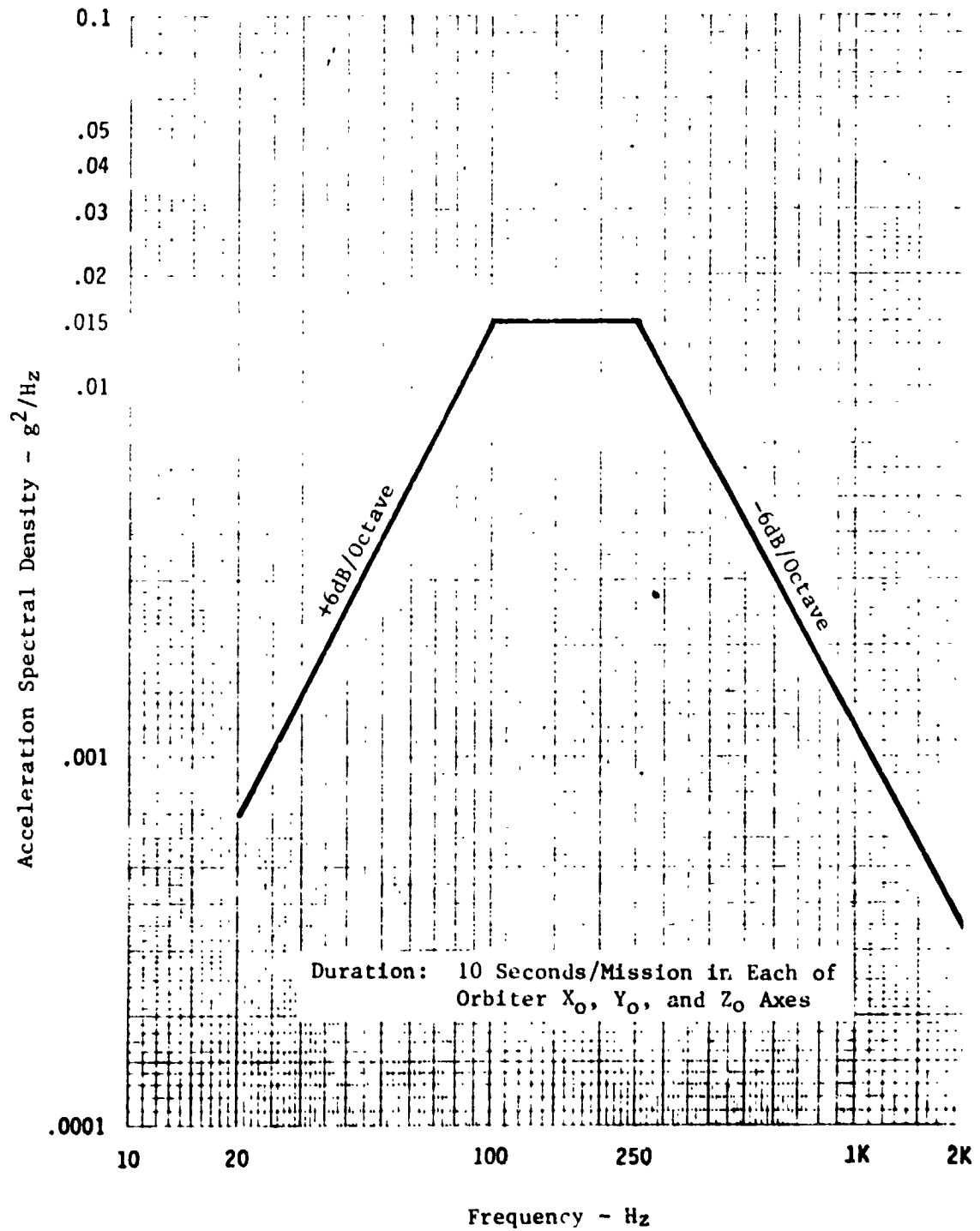
Figure II-4   Unloaded Main Longeron Trunnion Fitting Vibration

Table II-5   Thermal Environment Inside Cargo Bay

Worst Case Hot Environment

o   All surfaces inside cargo bay which can be viewed by tank assembly are at 393°K (708°R), and are effectively black.

o   Cargo doors are open and sun is viewed directly overhead with solar radiation flux of 1400 W/m² (444 Btu/hr-ft²). At the same time deep space is viewed with a sink temperature of absolute zero.

Worst Case Cold Environment

o   All surfaces inside cargo bay which can be viewed by tank assembly are at 123°K (222°R), and are effectively black.

o   Cargo bay doors are open and deep space is viewed with a sink temperature of absolute zero.

Worst Case Transient, Cold to Hot

o   All surfaces inside cargo bay which can be viewed by the tank assembly or to which the assembly is mounted, go from 123°K (222°R) to 393°K (708°R) following an exponential curve such that 95 percent of the change occurs in 23 min. The remaining 5 percent of the change is linear, reaching maximum temperature in 30 minutes. The environment then remains at hot condition for a maximum of 2 hours.

Worst Case Transient, Hot to Cold

o   All surfaces go from 708°R to 222°R following an exponential curve such that 95 percent of change occurs in approximately 68 minutes. The remaining 5 percent of the change is linear, reaching minimum temperature in 90 minutes. The environment then remains at the cold condition for a maximum of 2 hours.

Maximum Time at Extreme Conditions

o   Maximum time extreme conditions will exist is 2 hours. The environmental temperature will then cycle toward the other condition. This gives the maximum cycle time:

Hot condition	2.0 Hours
Hot to cold	1.5 Hours
Cold conditions	2.0 Hours
Cold to hot	0.5 Hours
Total max cycle time	6.0 Hours

Table II-6 Cryogenic Fluid Properties (International Units)

Liquid	Saturation Temperature (°K)	Surface Tension (Dyne/cm)	Density (kg/m³)	Kinematic Surface Tension (m³/s²)	Heat of Vaporization (joule/gm)
Saturation @ 138 KN/m²					
Hydrogen	21	1.8	0.27	2.5×10^{-5}	439
Helium	4	0.1	0.49	0.079×10^{-5}	21
Methane	116	13.4	1.64	3.2×10^{-5}	490
Oxygen	93	12.7	4.40	1.1×10^{-5}	209
Argon	88	11.2	5.38	0.82×10^{-5}	157
Saturation @ 414 KN/m²					
Hydrogen	26	0.9	0.24	1.5×10^{-5}	386
Helium*	--	--	--	--	--
Methane	132	9.8	1.52	2.5×10^{-5}	477
Oxygen	106	9.5	4.10	0.90×10^{-5}	195
Argon	103	8.0	5.02	0.62×10^{-5}	146

*Critical point for Helium is P_c = 228 KN/m², T_c = 5.22°K

Table II-7 Cryogenic Fluid Properties (English Units)

Liquid	Saturation Temperature (°R)	Surface Tension (lb/ft)	Density (lb/ft³)	Kinematic Surface Tension (ft³/sec²)	Heat of Vaporization (Btu/lb)
Saturation at 20 psia					
Hydrogen	38	1.2×10^{-4}	4.3	9.0×10^{-4}	189
Helium	8	6.9×10^{-6}	7.8	0.28×10^{-4}	9
Methane	208	9.2×10^{-4}	26.3	11.2×10^{-4}	211
Oxygen	168	8.7×10^{-4}	70.5	4.0×10^{-4}	90
Argon	159	7.7×10^{-4}	86.3	2.9×10^{-4}	68
Saturation at 60 psia					
Hydrogen	47	0.64×10^{-4}	3.9	5.28×10^{-4}	166
Helium*	--	--	--	--	--
Methane	238	6.7×10^{-4}	24.4	8.83×10^{-4}	205
Oxygen	191	6.5×10^{-4}	65.7	3.18×10^{-4}	84
Argon	186	5.5×10^{-4}	80.5	2.20×10^{-4}	63

*Critical point for Helium is P_c = 33.0 psia, T_c = 9.4°R

Helium exists as one of three isotopes: ^{3}He, ^{4}He and ^{6}He. The latter has a half-life of only 0.82 sec (Ref. 18) and is, therefore, unstable and not of interest in this study. The ratio of ^{3}He to ^{4}He as it is found naturally, is only about $1:10^7$ (Ref. 18) and is also therefore not pertinent to this study. The study is thus directed at the storage and supply of ^{4}He (alternately He-4), the properties of which are listed in Table II-8.

He-4 is characterized by its so-called "lambda-point" parameters. The liquid has a very drastic change in specific heat at a temperature of 2.17°K (3.9°R), the "lambda-transition" as seen in Figure II-5. The specific heat rises to a very high value at the lambda temperature and has the shape of lambda over the temperature range shown. The liquid exhibits a marked difference in behavior and properties above and below this temperature. The difference is great enough to give the regions separate labels. Normally they are referred to as He-1 and He-2, as pictured in the PT Plane in Figure II-6. The lambda transition is a straight line, as shown. The difference between He-1 and He-2 is reflected in all of the thermodynamic functions but is most apparent in the kinetic properties. Liquid He-2 is the "superfluid", known for its unique properties, e.g., a near-zero viscosity which yields its most distinctive quality of superfluidity.

As seen in Figure II-6, He-4 is considerably different when compared to a normal fluid in the PT plane. For the He-1 state, the viscosity of the saturated liquid is nearly a constant value of about 35 micropoise (Ref. 19), except near the lambda line. Absolute or dynamic viscosity is presented in Figure II-7. These viscosity data were obtained from NBS Technical Note 631, pp. 27 and 29, at saturation (Ref. 20). (The viscosity of He-2 as determined by its rate of flow through narrow slits, is extremely small, at least 10^6 times less than the viscosity of He-1.)

The mass density of He-4 is presented in Figure II-8 (Ref. 19, p. 9). It decreases with increased temperature from the lambda point. Surface tension of He-4 also decreases with increased temperature, Figure II-9. The dashed line (Ref. 20) compares closely to the solid line values obtained from Reference 19, p. 422. As seen from Figures II-8 and II-9, surface tension decreases with increased temperature at a greater rate than does mass density; therefore, kinematic surface tension decreases with increased temperature.

The problems of liquid helium storage and supply are evident from a review of these data. The critical point is only 1.0°K (1.8°R) above the normal boiling point, and the heat of vaporization is only 21 joule/8gm (9 Btu/lb). For a stored quantity of 74 kg (163 lb), only 1.55×10^6 joules (1467 Btu) will vaporize all the liquid. A mission duration of 180 days corresponds to an average heating rate of 0.10 watt (0.34 Btu/hr) to vaporize all the liquid. The net heat input for retaining liquid within the storage vessel therefore has to be less than this limiting condition. The preliminary conceptual design of the 0.62 m^3 (22 ft^3) helium tank assembly defined during Task I was influenced by these considerations.

Table II-8 Helium-4 Physical Property Data (Ref 18)

Condition	Pressure	Temperature	Mass Density
Critical Point	228 KN/m^2 (33.0 psia)	5.20°K (9.36°R)	69.7 kg/m^3 (4.35 lbm/ft^3)
Normal Boiling Point	101 KN/m^2 (14.7 psia)	4.22°K (7.60°R)	Gas: 16.8 kg/m^3 (1.05 lbm/ft^3) Liquid: 125 kg/m^3 (7.80 lbm/ft^3)
Lower Lambda Point	5.0 KN/m^2 (0.730 psia)	2.18°K (3.92°R)	146 kg/m^3 (9.13 lbm/ft^3)
Upper Lambda Point	3014 KN/m^2 (437.1 psia)	1.76°K (3.17°R)	180 kg/m^3 (11.26 lbm/ft^3)
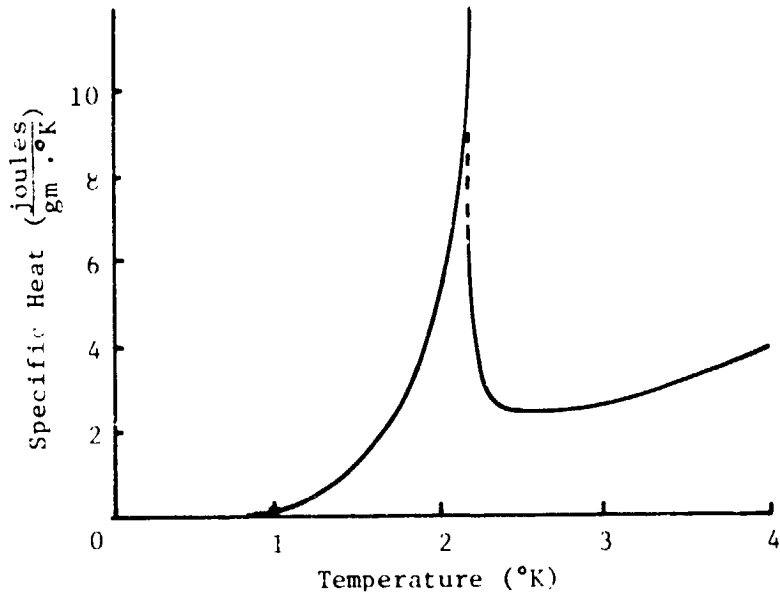
Figure II-5 Specific Heat of Liquid Helium-4 Under
Saturated Vapor Pressure
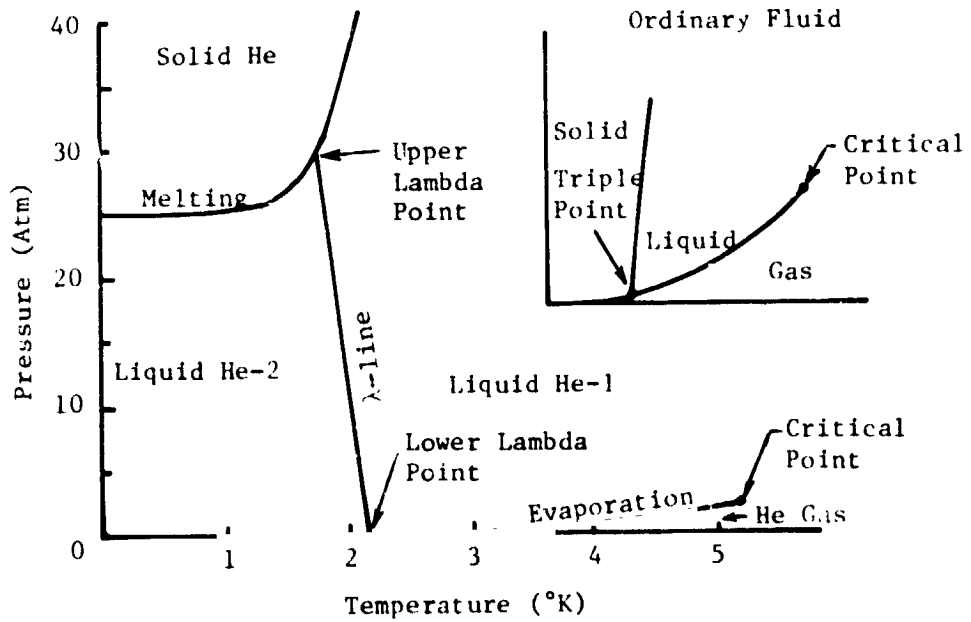
Figure II-6 The Four States of Helium-4
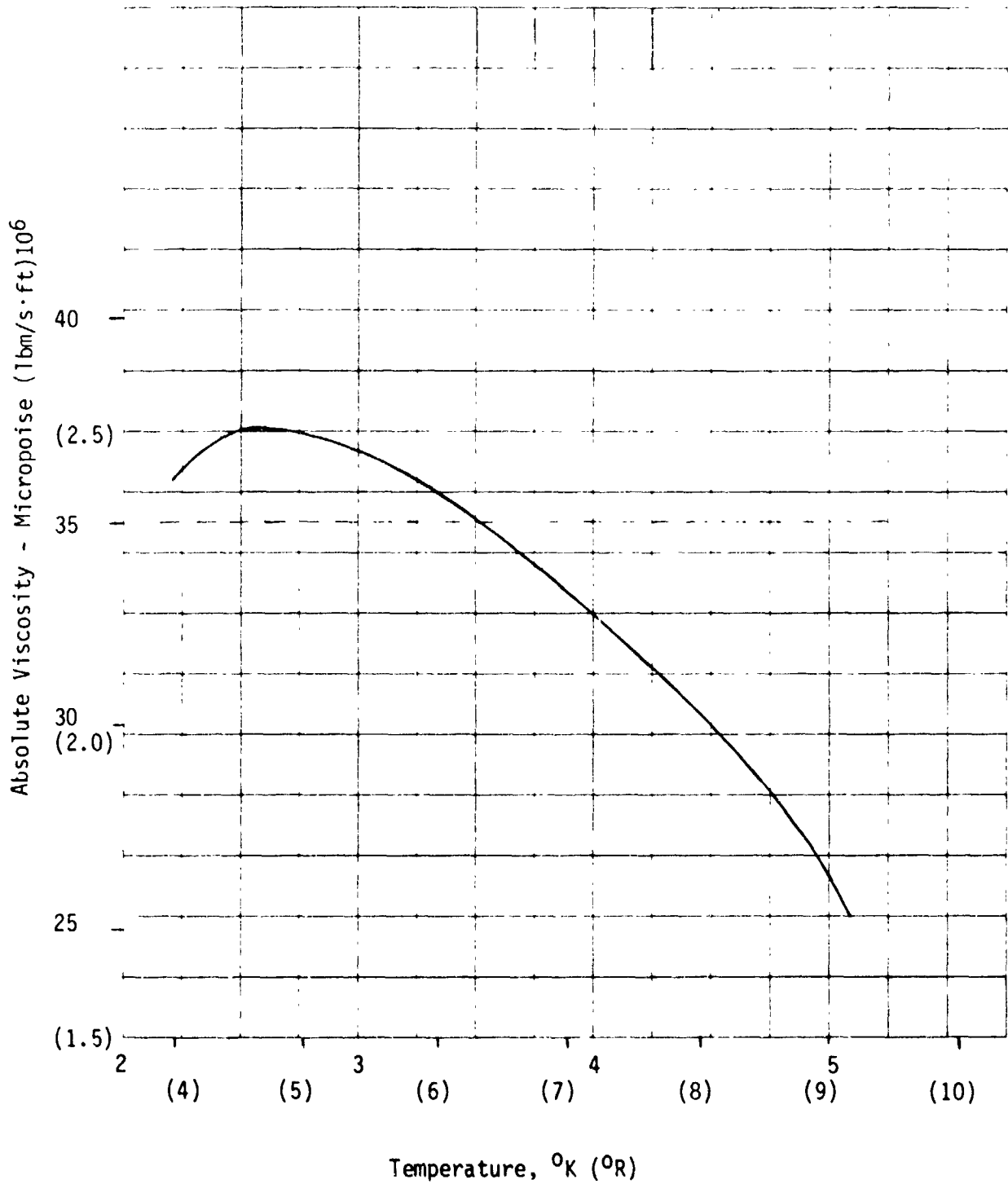
Figure II-7 Liquid Helium Viscosity at Saturated Conditions
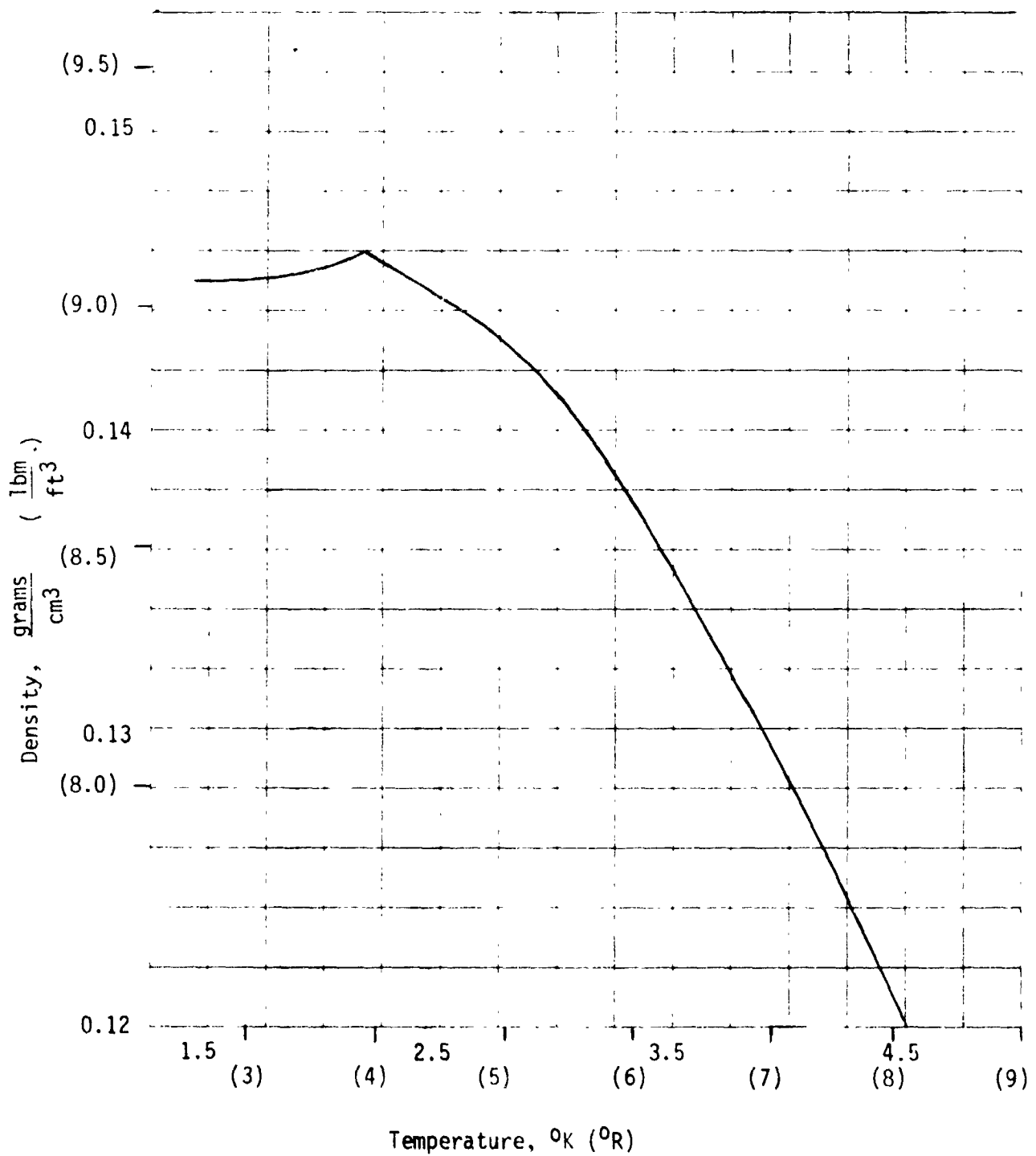
Figure II-8 Density of Liquid Helium-4 Under Saturated Conditions
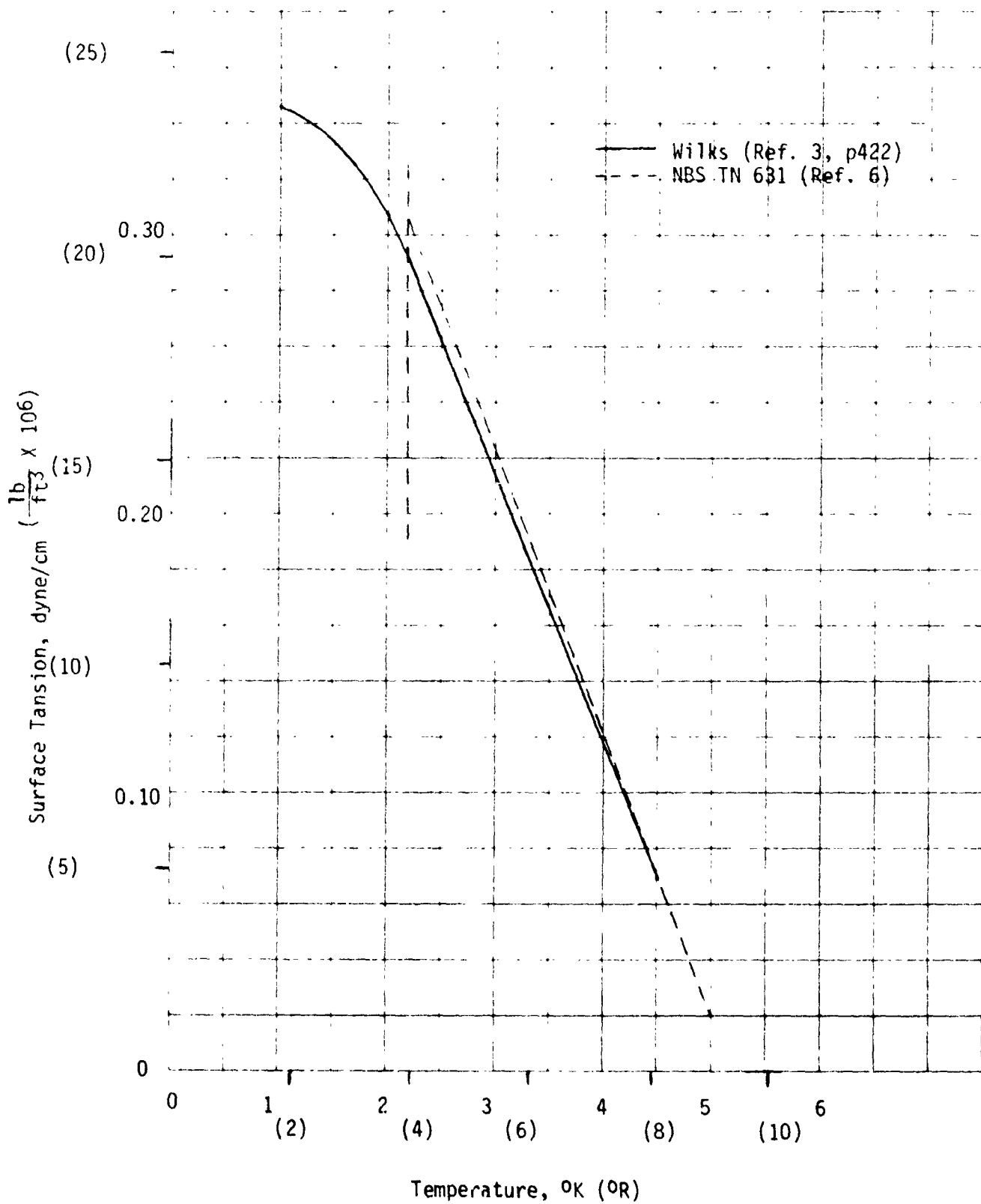
Figure II-9   Surface Tension of Liquid Helium-4

D. Material Properties

Primary materials of construction considered for this study were those employed in the baseline CFME design. These were aluminum for tankage materials, stainless steel for the liquid acquisition device, and S-glass/E-glass composites for structural supports. Properties of the metals were obtained from Reference 21 while those for the composites were obtained from References 22 through 25.

Tensile strength and good weldability are of prime importance to a vessel designed for burst. The higher tensile strength of 2014-T6 or 2219-T62, compared to 6061-T6, can be used to advantage in this application, resulting in reduced shell thicknesses and weights.

A comparison of the different aluminum alloys, Table II-9 for room temperature properties and Table II-10 for properties at liquid hydrogen temperature, shows the advantage of using a 2014-T6 or a 2219-T62 alloy. Martin Marietta has developed techniques for welding both alloys. Titan launch vehicle tanks are constructed of 2014-T6 and the External Tank for the Shuttle Space Transportation System is made from 2219-T62. However, neither of these alloys is as easy to weld as 6061 aluminum..

The critical material property when sizing the tank for collapse is the modulus of elasticity (E). All three materials considered have a similar E and therefore the better weldability of 6061-T6 makes it the preferred approach for the vacuum jackets.

Stainless steel was chosen for the channels and other elements of the liquid acquisition device because of its high strength and stiffness as well as its compatibility/weldability with the screen being used. The 325x2300 mesh Dutch twill woven wire cloth, constructed of 304L stainless steel, is preferred for fine-mesh screen acquisition devices because of its high capillary retention capability (high bubble point) and its excellent fabricability characteristics.

Composites are attractive as structural attachment members because of their low thermal conductivity and because they have relatively high strength. Properties of composites used in this study are included as Table II-11. The main problem with using these materials is the relatively small amount of data available on allowables at cryogenic temperatures. Also, practically no information is available on fatigue life expectancy, especially at cryogenic temperature. These problems, or shortcomings, are further amplified by the uncertainties resulting from incorporation of the basic materials into a composite lay-up, which is an art, at best. Further evaluation and classification of lay-up techniques to arrive at required properties, design specifications and manufacturing processes for the composites are required. These issues will be addressed in greater detail in Chapter VI - Technology Evaluation.

Table II-9 Typical Mechanical Properties of Metallic
Materials at 293°K (528°R)

Alloy	Condition	Modulus GPa (10^6 psi)	Parent Metal			As Welded		Weldability	Fabricability
			Ultimate Tensile Strength MPa (10^3 psi)	Tensile Yield Strength MPa (10^3 psi)	Elongation %	Ultimate Tensile Strength MPa (10^3 psi)	Tensile Yield Strength MPa (10^3 psi)		
2014	T6	69 (10)	490 (71)	440 (64)	10	GTAW, 4043 filler 350 (51)	240 (35)	Weldable by Special Practices	Fair
2219	T62	69 (10)	415 (60)	290 (42)	10	GTAW, 2319 filler 315 (45)	210 (31)	Readily Weldable	Good
6061	T6	69 (10)	320 (46)	290 (42)	12	GMAW, 4043 filler 220 (32)	160 (23)	Very Readily Weldable	Very Good
304L Cres.	Annealed (sheet)	--	660 (96)	295 (43)	56	430 (63)	159 (23)	Excellent	Good
321 Cres.	Annealed	180 (26)	620 (90)	225 (32)	55	520 (75)	210 (30)	Very Good	Good

Legend:

GTAW = Gas Tungsten Arc Welding
GMAW = Gas Metal Arc Welding

Table II-10 Typical Mechanical Properties of Metallic
Materials at 20°K (36°R)

Alloy	Condition	GPa Modulus (10⁶ psi)	Parent Metal Ultimate Tensile Strength MPa (10³psi)	Parent Metal Tensile Yield Strength MPa (10³psi)	Elongation %	As Welded Ultimate Tensile Strength MPa (10³psi)	As Welded Tensile Yield Strength MPa (10³psi)
2014	T6	83 (12)	685 (100)	565 (82)	12	GTAW, 4043 filler 480 (69)	
2219	T62	81 (12)	650 (95)	390 (56)	23	GTAW, 2319 filler 435 (63)	345 (50)
6061	T6	87 (13)	495 (72)	365 (53)	26	GMAW, 4043 filler 450 (66)	220 (32)
304L	Annealed (sheet)		1750 (254)	305 (45)	33		
321	Annealed	210 (31)	1650 (239)	375 (55)	36		

Legend:
GTAW = Gas Tungsten Arc Welding
GMAW = Gas Metal Arc Welding

Table II-11 Mechanical Properties of Composite Materials At
293°K (528°R)

	Ultimate Tensile Strength MPa $(10^3$ psi)	Modules of Elasticity 10^6 KPa $(10^6$ psi)
S-Glass SP-250-52	1,680 (243)	46.2 (6.7)
181 E-Glass	827 (120)	41.4 (6.0)
Optimum Composite Lay-up of S-Glass/E-Glass	334 (48.5)	42.8 (6.2)

The Task I effort involved conceptual design of the 0.62 m^3 (22 ft^3), 12.5 m^3 (440 ft^3), and 37.4 m^3 (1320 ft^3) cryogenic orbital storage and supply systems previously identified in Table I-1. With the CFME as the baseline system, emphasis was placed on selecting components and subsystems that would be suitable for more than one cryogenic liquid. Changes to the CFME baseline were therefore only defined if required to satisfy the mission and operational requirements. Two subsystem elements were to be retained for each tank assembly, a total liquid retention device fabricated from fine mesh screen material for liquid acquisition and expulsion, and an external thermodynamic vent system for pressure control. The candidate storage and supply systems are discussed in Section A and preliminary conceptual designs for these systems are presented in Section B.

A. Candidate Storage and Supply Systems

A total of 13 configurations were identified as candidate concepts during Task I iterations for the eight size/fluid combinations in the study. These candidate configurations are listed in Table III-1, where the eight size/fluid combinations are designated as Categories I through VIII. The basic mounting approach for each is defined, whether on a Spacelab pallet or directly in the Orbiter bay. The small 0.62 m^3 (22 ft^3) tanks are all considered mounted on a Spacelab pallet, even though mission durations of 180 days or longer are defined.

One of the groundrules for the study was to use the CFME baseline configuration to assess performance (fluid dynamic, thermal and structural), and to identify modifications, as required. All of the 0.62 m^3 (22 ft^3) systems are configured with a vapor-cooled shield and vacuum jacket (Configurations 1-4). Our preliminary look at these tank systems indicated that all fluids but helium could be accommodated with a CFME tank configuration with changes in structure thickness, thermal performance (percent of loaded volume vented to maintain tank pressure), and expulsion performance (residual remaining at depletion). A tank schematic of the oxygen, methane and argon systems is presented in Figure III-1. The helium system is somewhat different in the arrangement of the vaper-cooled shield and thermodynamic vent elements, and the method of controlling heat flux into these elements. The allowable heat input into the liquid helium tank is very small, and a much improved thermal control system is required. The critical point is only 1.0° K (1.8° R) above the normal boiling point and the heat of vaporization is only 21 joule/gm (9 Btu/lb). For a stored quantity of 74 kg (163 lb), only 1546 x 10^3 joules (1467 Btu) will vaporize all the liquid, and a mission duration of 180 days corresponds to an average heating rate of 0.1 watt (0.34 Btu/hr) to vaporize all the liquid. The net heat input for retaining liquid within the storage vessel therefore has to be less than this limiting condition.

The baseline CFME configuration with a vapor-cooled shield (VCS) and thermodynamic vent system (TVS) contained within a vacuum annulus with 75 layers of multilayer insulation is clearly inadequate for liquid helium storage for 180 days. The heat inputs through the MLI, structural supports

Table III-1 – Preliminary Candidate Configurations

Config.	Category	Size	Fluid/Mounting (CFME)	Vacuum Jacket (VJ)	Vapor Cooled Shield (VCS)	No VJ No VCS
	Baseline	0.62 m³ (22 ft³)	Hydrogen	X	X	
1	I	0.62 m³ (22 ft³)	Methane/Spacelab	X	X	
2	II	0.62 m³ (22 ft³)	Argon/Spacelab	X	X	
3	III	0.62 m³ (22 ft³)	Oxygen/Spacelab	X	X	
4	IV	0.62 m³ (22 ft³)	Helium/Spacelab	X	X	
5	V	12.5 m³ (440 ft³)	Argon/Orbiter	X	X	
6		12.5 m³ (440 ft³)	Argon/Orbiter			X
7		12.5 m³ (440 ft³)	Argon/Spacelab			X
8	VI	12.5 m³ (440 ft³)	Methane/Orbiter	X	X	
9		12.5 m³ (440 ft³)	Methane/Orbiter			X
10	VII	12.5 m³ (440 ft³)	Oxygen/Orbiter	X	X	
11		12.5 m³ (440 ft³)	Oxygen/Orbiter			X
12	VIII	37.4 m³ (1320 ft³)	Cylindrical/Hydrogen/Orbiter		X	
13		37.4 m³ (1320 ft³)	Spherical/Hydrogen/Orbiter		X	
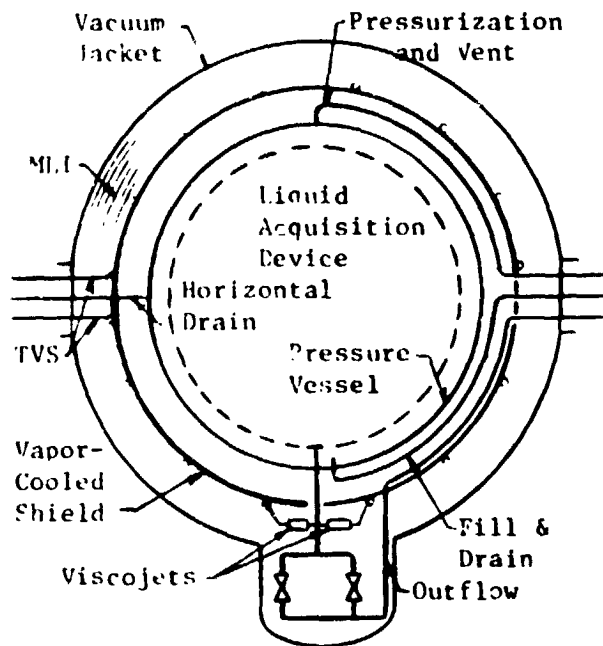
Figure III-1   Tank Schematic for Oxygen, Methane and Argon
(CFME Size-Configuration 1-3)

and plumbing must be reduced considerably. An approach was selected which
uses a liquid hydrogen-cooled outer shield to control the boundary temperature
and minimize the temperature difference and heat input into the inner storage
and supply tank. A schematic of the concept selected for further analysis is
illustrated in Figure III-2. The design of the hydrogen outer shield and heat
exchanger is such that the trunnion support members are at liquid hydrogen
temperature at a location where the hydrogen VCS intercepts the trunnion. The
width of the outer annulus is thus sized for the optimum MLI thickness and
trunnion length to minimize hydrogen requirements to maintain this desired
boundary condition.

The helium thermodynamic vents are used to intercept heat coming through
the trunnions that attach directly to the helium storage tank. The fluid for
these heat exchangers is extracted from the liquid acquisition device at two
locations on the channels which are in the plane of the trunnion attachment
points. The two-phase fluid, which is at a temperature below the tank
saturation temperature, is then routed through a manifold around each trunnion
to minimize the heating through the trunnion. This fluid is subsequently
routed through a heat exchanger attached to a shield embedded in the MLI
between the storage tank and the hydrogen-cooled shield.

The 12.5 m³ (440 ft³) vacuum-jacketed tanks designed like the CFME are
Configurations 5, 8 and 10. A schematic representation of these systems is
shown in Figure III-3. Because system weight is highly dependent on the
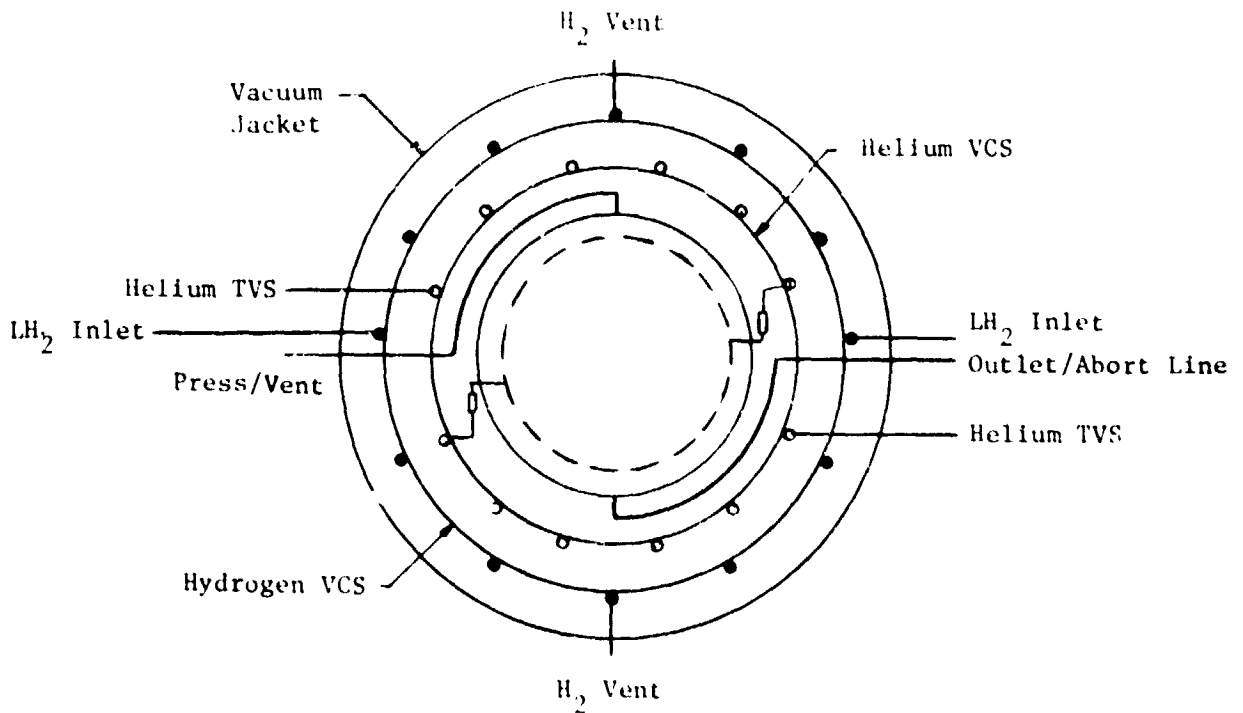
III-3

Figure III-2 Tank Schematic for Helium (CFME Size-Configuration 4)
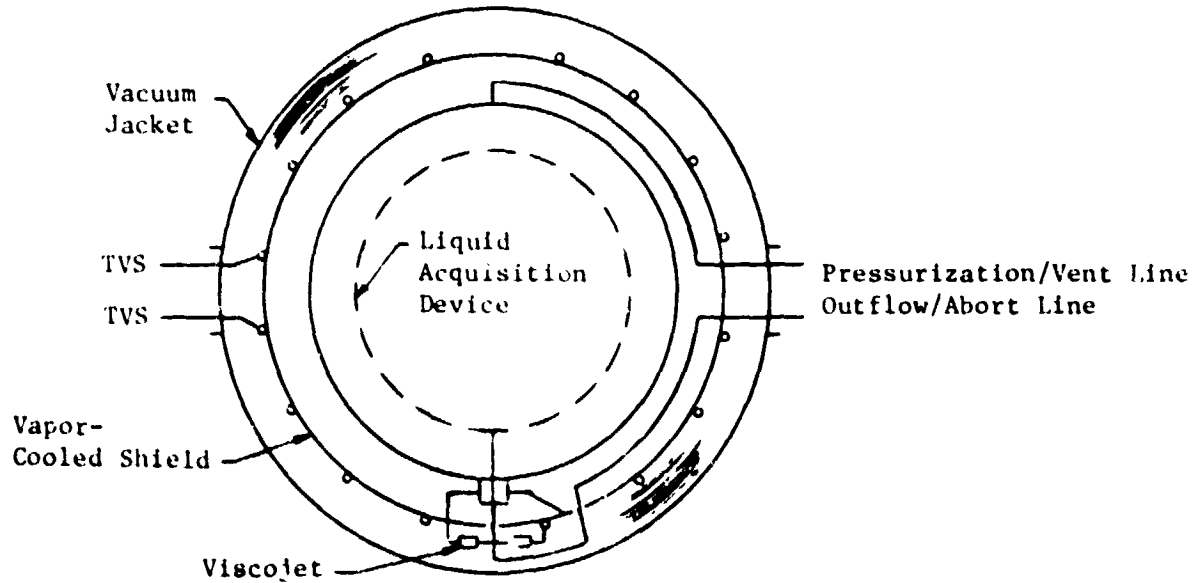
Figure III-3 Schematic for 12.5 m^3 (440 ft^3) Vacuum-Jacketed
Tanks (Configurations, 5, 8 and 10)

support structure and the tank shell design as it is driven by the dynamic launch environments, comparisons with non-vacuum-jacketed designs are valid only if the same groundrules and environments are used for sizing. A non-vacuum-jacketed tank design was therefore also included in the study for each of the 12.5 m^3 (440 ft^3) configurations. A direct comparison of weights c'n therefore be obtained for tanks designed to the same loading conditions.

One 12.5 m^3 (440 ft^3) (Configuration 7) was considered for mounting on a Spacelab pallet. The argon tank assembly was chosen because it represented the greatest mass concentration to be supported, and therefore would permit a determination of maximum potential weight penalty associated with an alternate mounting approach. It was recognized that this would not be the likely support and mounting arrangement for this application, and so thermal performance (Task II) was not evaluated; the main consideration was weight differential between Configurations 6 and 7.

Two configurations were identified for the 37.4 m^3 (1320 ft^3) hydrogen tank, one spherical and one cylindrical, neither with a vacuum jacket. A vacuum jacket for this tank size is unrealistic because a shell designed to withstand buckling would weigh in excess of 1000 kg (2200 lb), which corresponds to a significant percentage of the total hydrogen loaded within the tank. A conceptual design similar to the 12.5 m^3 (440 ft^3) tanks was thus defined for the remaining study effort. A flow schematic for the large, non-vacuum-jacketed tanks is shown in Figure III-4.

TVS · TVS · Structural Support · TVS Line · Liquid Acquisition Device · Press/Vent Line · Structural Support · Outflow/Abort Line · TVS Line · N$_2$-purged MLI · Viscojet · SOFI
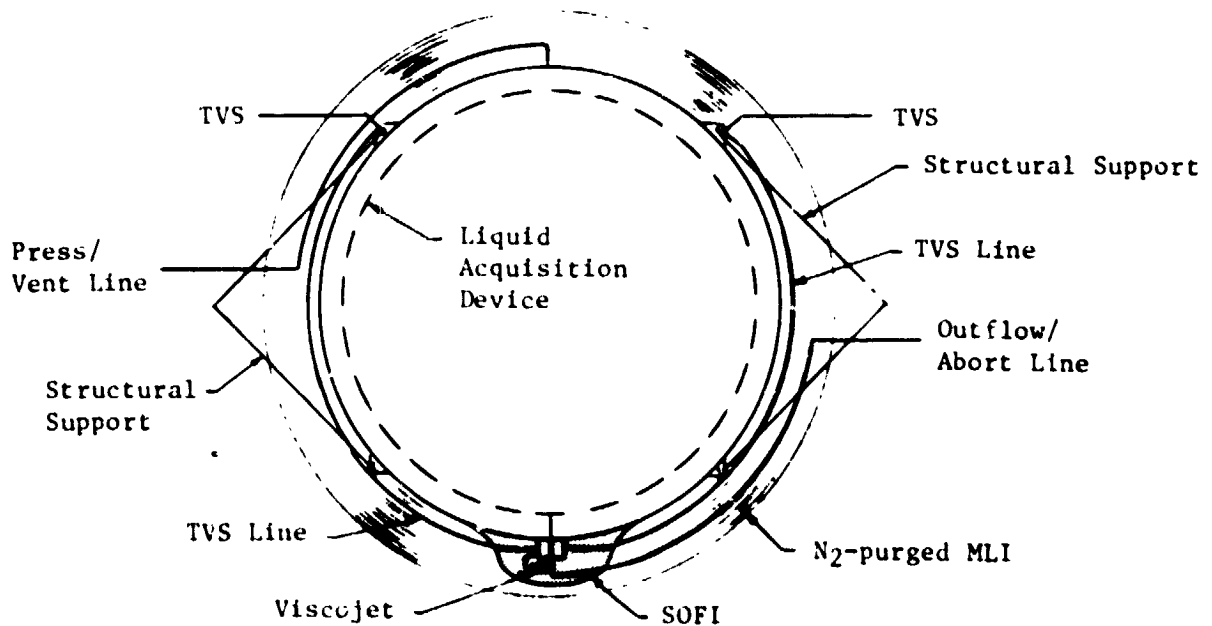
Note: For Configurations 12 and 13 (Hydrogen), a thin layer of SOFI is included under the N$_2$-Purged MLI

Figure III-4 Schematic for Large Non-Vacuum-Jacketed Tanks
(Configurations 6, 7, 9, 11, 12 and 13)

B. Preliminary Conceptual Designs

Preliminary conceptual designs were defined to form the basis for the analysis conducted during Task II. The design and analysis efforts were performed concurrently with design iterations leading to an acceptable system that could meet the structural and operational performance requirements. Chapter V presents the conceptual designs that derive from these preliminary concepts. Arriving at an acceptable design that met the structural and thermal requirements was also an iterative process that tended to drive the particular design element size in opposing directions (e.g., thicker to handle loads, thinner to cut down heat leak). Particular attention was therefore directed at defining the dynamic loads that the structural elements had to withstand. These are addressed in Section 2 below. The resulting structural concepts and approaches were then carried into the analytical efforts described in Chapter IV.

1. Liquid Acquisition Devices

The liquid acquisition device must be capable of expelling gas-free liquid in the low-g, on-orbit environment. Single phase liquid is supplied to both the liquid outflow line and to feed the thermodynamic vent system. Because the orientation of the liquid in the low-g environment tends to be arbitrary, a concept that can maintain communication with the liquid regardless of its location is required. A device composed of individual flow channels is the most effective method of providing this total communication. A total communication device was therefore selected as the CFME baseline, as previously described in Chapter I.

The use of this four-channel acquisition device for the 0.62 m^3 (22 ft^3) tank size as the preliminary concept for the other fluids is fairly straight-forward. A study groundrule specified that a total communication device be analyzed for the larger tanks. It is recognized that a total communication device may not be optimum for these tank sizes; a refillable trap with some type of communication channels feeding the bulk fluid region, or a non-refillable trap which is configured to handle multiple settling burns, such as the 12.5 m^3 (440 ft^3) methane mission, may be preferred under certain mission and operational requirements. Trade studies directed at selecting the best acquisition device configuration for each application were not a part of this study effort. The total communication device was assumed for each tank/fluid combination. It should be recognized that this may introduce a weight penalty over other concepts when appropriate acquisition device support structure is included to guarantee integrity in the launch environment. On the other hand, the total communication device does provide the greatest degree of flexibility in terms of mission duty cycle and residuals at depletion.

Because of the relatively low surface tensions of the cryogens in this study, the 325 x 2300 mesh screen was determined to be preferred for all cases. This screen mesh only comes in stainless steel screen, and the entire screen channel assembly is therefore made of stainless steel. A bimetallic transition is required where the acquisition device exits the pressure vessel, which is made of aluminum for all cases in this study. In all cases, the channels were assumed to be truncated such that the enclosed flow passage does

not extend into the ullage. This is required because of the low probability that the screens can retain their pressure retention capability under the boost environment. This approach gives a high degree of confidence that the liquid acquisition device will arrive on-orbit completely full of liquid and ready to perform liquid outflow.

Truncating the channels by this amount does not degrade the ability of the channels to communicate with the liquid. The sheet metal of the channels extends to the top of the tank, so capillary pumping of the liquid in that region will still provide indirect communication with the screen channels. An added advantage of the truncation is that it improves thermal isolation of the device. Heat conduction through the pressurization/vent line at the top of the tank will not be directly transmitted to the liquid in the channels.

Acquisition device channel cross sections are a function of the flowrate requirements for the particular mission. The sizes for the large tanks were determined as part of the fluid dynamic analysis of Task II (Chapter IV, Section A). The channels were assumed bolted to the tank wall, with a non-metalic spacer (e.g., Teflon) used to thermally isolate the flow region of the channel as much as possible. Slotted tabs were included on the channel structure to allow for differential contraction and expansion.

The screen surface of the channels has been shown to be relatively insensitive to effects of warm gas on its outer surface, as long as its inner surface is in contact with liquid. Screen components have been tested using LH_2 in extreme thermal environments and the influence on the screen retention capability measured (Ref 26 and 27). Maximum degradation in the retention capability of 12 percent was measured at a heat flux of 9450 w/m^2 (3000 Btu/hr ft^2), more than three orders of magnitude greater than any determined in this study. This points up another advantage of the total communication device in that some portion of the total channel network is in contact with the bulk liquid, so a supply is always available to replace any liquid evaporated at the screen surface. Vaporization-induced emptying of an all-liquid region may not be as great a problem as for a partial acquisition device that is not in direct contact with the bulk liquid.

2. Structural Support Concepts

The 0.62 m^3 (22 ft^3) tank assembly structural supports were assumed to be identical to the CFME, except for liquid helium. In the CFME concept, the internal storage vessel is supported within the vacuum jacket by composite supports. The vacuum jacket is supported on the Spacelab pallet by a 6061-T62 aluminium bipod arrangement. For the helium tank, the external support of the vacuum jacket was assumed to be identical to the CFME approach, but the internal arrangement was modified to decrease heat input to the helium.

Composite struts were assumed for the preliminary conceptual supports for the larger tanks. Preliminary dynamic assessments were made on the various tank/liquid configurations in order to derive reasonable design loads. The design loads were based on the FME dynamic analysis (Ref 7), the Space Transportation System Core Interface Control Document (STS Core ICD, Ref 11, Attachment 1) and the Spacelab Payload Accommodations Handbook (SPAH, Ref 10). The STS Core ICD defines the static and dynamic environments for payloads mounted directly to the Orbiter keel and trunnion fittings. The SPAH defines the static and dynamic environments for payloads mounted directly on a Spacelab pallet. Emphasis was placed on design loads for supporting structure (e.g., trunnions, struts, etc). Detailed modal loads analyses were beyond the scope of this study. Support concepts for the 0.62 m^3 (22 ft^3) and larger tanks are discussed separately in the following paragraphs.

0.62 m^3 (22 ft^3) Tank Supports

The liquid storage vessels for this tank size are supported from the vacuum jacket girth ring by two diametrically opposed composite trunnions which are bolted to the pressure vessel, as shown in Figure III-5. The trunnions are supported from the vacuum jacket girth ring by external tubes. One post is fixed to this supporting tube by a threaded and vented fitting to provide a radial load path from the pressure vessel (this mount is shown in Figure III-5). The opposing post is allowed to slide, accounting for differential thermal and pressure expansion and contraction between the pressure vessel and vacuum jacket. A third restraining support is provided between the pressure vessel outlet and the vacuum jacket valve enclosure for taking out torsion and supporting the valve assembly.
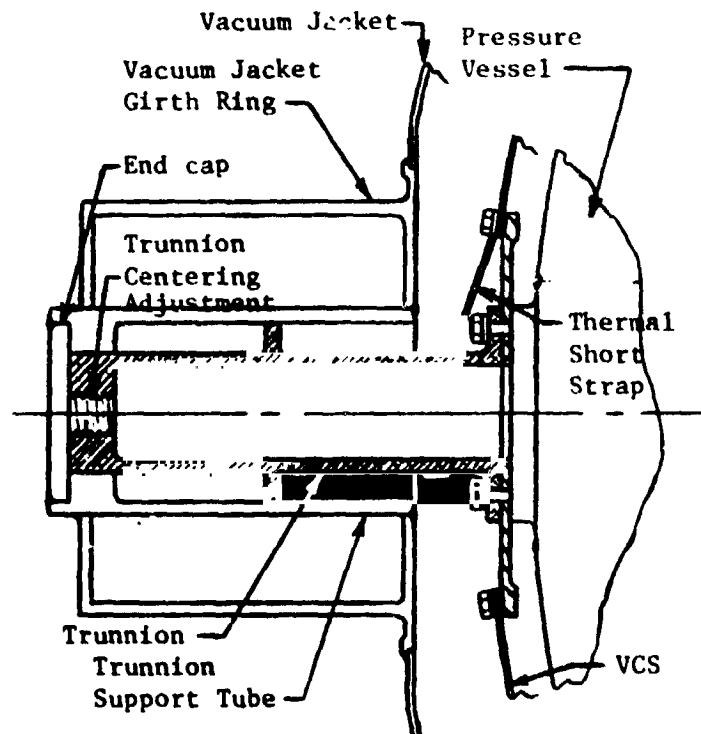
Figure III-5 Trunnion Mount Configuration

Calculations were made to determine the tank design load factors for each of the fluids using the CFME random vibration spectrum (Fig II-1). The random vibration load factors (LF) were based on Miles equation

$$LF = \sigma \sqrt{\frac{\pi}{2} \; PSD_f \; F_N \; Q}$$

where PSD_f is the power spectral density at the natural frequency, F_N the natural frequency and Q the amplification factor. Table III-2 summarizes the 2σ random vibration load factors for the various configurations.

All the configurations have supported frequencies greater than 35 Hz. Therefore, the quasi-static load factors for Reference 10 apply:

$X_o = 4.3$ g

$Y_o = 1.4$ g

$Z_o = 10.6$ g

Superimposing these quasi-static load factors with the random load factors of Table III-2 results in the design limit load factors for the various 0.62 m^3 (22 ft^3) configurations. Table III-3 summarizes these design limit loads. From these design loads, variations in trunnion sizing from the baseline CFME configuration were determined and these are shown in Table III-4, along with the effective bending stiffnesses. These preliminary sizes were used as the starting point for the Task II thermal performance analysis.

Table III-2 Random Vibration Load Factor Summary (CFME Size Tank)

Liquid	Total Supported Weight Liquid & Structure		Trunnion Support Frequency (Hz)	Limit Load Factor*(g) Based on Q = 15 (2σ)
Hydrogen	102 kg	(224 lb)	68.2	7.8
Argon	880 kg	(1934 lb)	47.8	3.7
Methane	313 kg	(689 lb)	52.5	4.6
Oxygen	733 kg	(1612 lb)	49.1	4.0
Helium	137 kg	(302 lb)	65.3	7.1

* From Miles Equation

Table III-3. Tank Design Limit Load Factor Summary
(CFME Size Tank)

Liquid	Design Limit Load Factors (g's)*		
	$\pm X_o$	$\pm Y_o$	$\pm Z_o$
Hydrogen	12.1	9.2	18.4
Argon	8.0	5.1	14.3
Methane	8.9	6.0	15.2
Oxygen	8.3	5.4	14.6
Helium	11.4	8.5	17.7

*Orbiter Coordinate System

Table III-4   Trunnion Size and Effective Trunnion Stiffness
(CFME Size Tank)

Liquid	Trunnion Sizing						Effective Bending Stiffness	
	Diameter		Thickness		Moment			
	cm	(in)	cm	(in)	cm^4	(in^4)	10^3N/cm	$(10^3 lb/in)$
Hydrogen	5.0	(2.0)	0.4	(0.15)	15.4	(0.37)	93	(53)
Argon	6.4	(2.5)	1.1	(0.45)	66.6	(1.60)	396	(226)
Methane	5.0	(2.0)	1.0	(0.40)	28.3	(0.68)	170	(97)
Oxygen	6.4	(2.5)	1.0	(0.40)	58.3	(1.40)	350	(200)
Helium	5.0	(2.0)	0.5	(0.20)	19.1	(0.46)	116	(66)

The support of the tank assembly on the Spacelab pallet is accomplished by two bipods and a base frame, as was shown in Figure I-2. The vacuum jacket girth ring has three support attachment points which are picked up in such a way as to minimize radial loads into the vacuum jacket. One attach point is to the base frame, directly adjacent to the pallet hard point. This is a shear support on the Z-axis (Orbiter coordinate system). The other two points are picked up by bipods which mount to the base frame.

For the helium system, the support of the helium storage tank, helium VCS, hydrogen VCS and MLI within the vacuum jacket by composite trunnions is not as straightforward as the CFME design. As previously mentioned, controlling heat leak into the inner helium storage vessel is crucial. One conceptual approach which requires a minimum modification to the CFME approach is shown in Figure III-6. Two supports carry the load of the helium storage vessel through attachments to the vacuum jacket. They are cooled by helium from the thermodynamic vents which flow through manifolds near their attach points to the pressure vessel. Two additional trunnions are provided to support the MLI and vapor-cooled shields within the vacuum jacket. The thermal design approach is to cool each of these trunnions to liquid hydrogen temperature, 20° K (36° R), at the location where the hydrogen VCS interfaces with the trunnions. An arrangement of "fixed" and "sliding" trunnions must also be applied here to allow for thermal and pressurization contractions and expansions.

An alternate support approach for the liquid helium tank is shown in Figure III-7. This approach is configured to obtain greater load carrying capability while still trying to minimize thermal input by lengthening the supports. This approach looks somewhat similar to the CFME in that two trunnions and a third torsional restraint are in direct contact with the inner vessel. The use of composite straps, which have been investigated by others for similar applications (e.g., Orbiter PRSA tanks for LO_2 and LH_2 storage), are not considered to be appropriate for this application and environment because of the high loads and relatively severe dynamic environment associated with Spacelab pallet mounting in the payload bay. Other more innovative techniques being investigated for storing liquid helium were not considered because they depart considerably from the basic CFME concept.

12.5 m³ (440 ft³) and 37.4 m³ (1320 ft³) Tank Supports

The preliminary conceptual designs for the larger tank supports differ greatly from the CFME-size tank design. The support members that hold the tank within the payload bay include struts that extend from the Orbiter trunnion and keel fittings to the pickups on the vacuum jacket shell, or tank itself if a vacuum jacket is not used. The large masses of liquid and size of the tanks, as listed in Table III-5, are indicative of fairly low frequency structure.

Discussions with both NASA-JSC and NASA-MSFC indicated that comparative loads data for supported masses this large do not exist. Consequently, the published load factors from the Volume XIV Shuttle ICD (Ref 11) were used with a 50 percent amplification factor applied to account for dynamic amplification and random vibration loads. The resulting limit load factors are tabulated in Table III-6. (Sign notations on the load factors indicate the direction of

MLI — Vacuum Jacket

Tank Assembly Bipod Supports

Four Channel Liquid-Acquisition Device

Composite Support Members

Helium TVS

LH$_2$ Inlet

Helium VCS

LHe outflow line

LH$_2$ Inlet

Hydrogen VCS
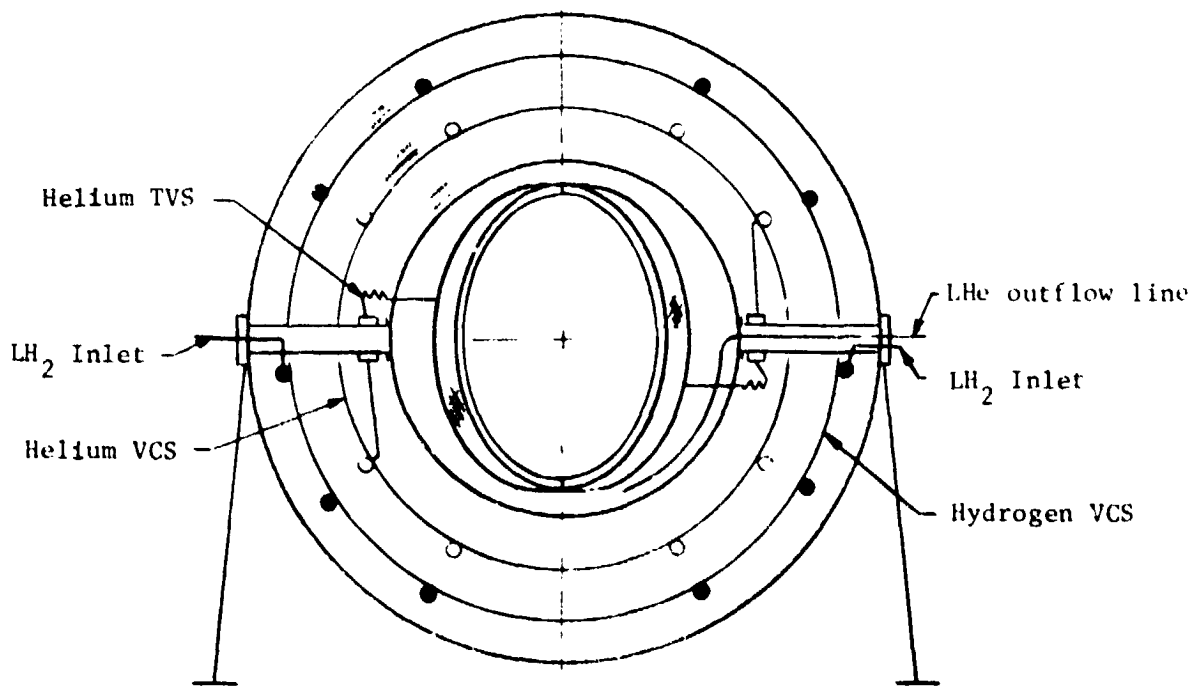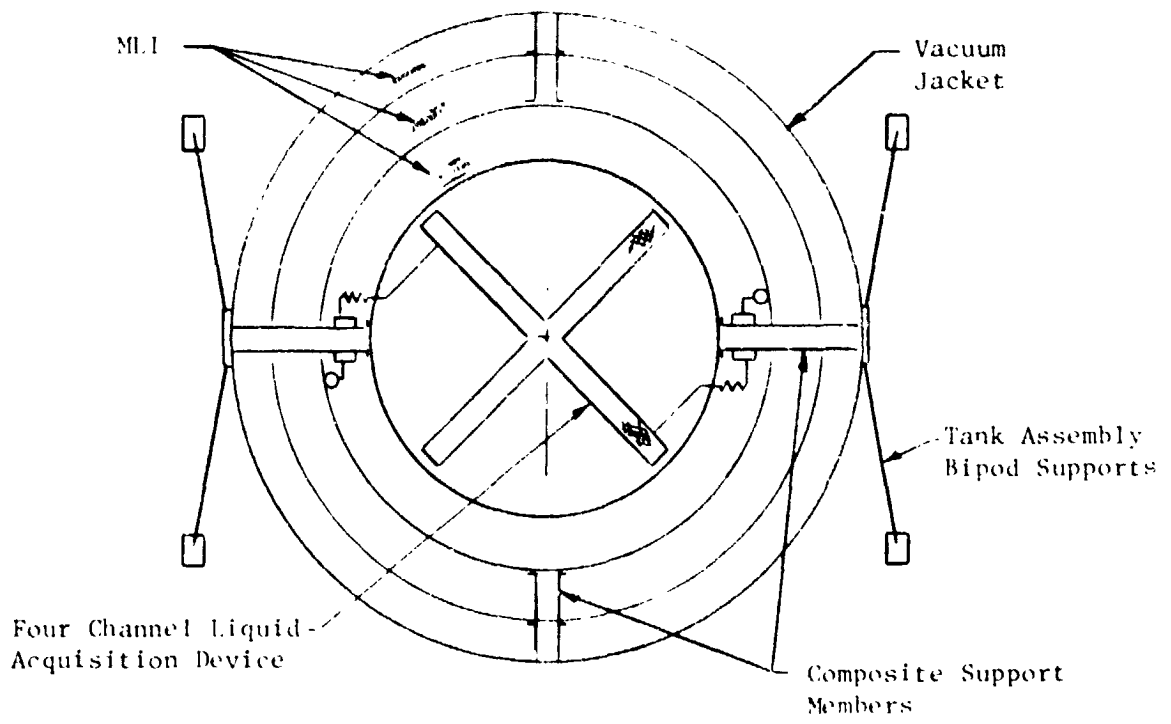
Figure III-6   Conceptual Design of Liquid Helium Storage
and supply Tank (Configuration 4)
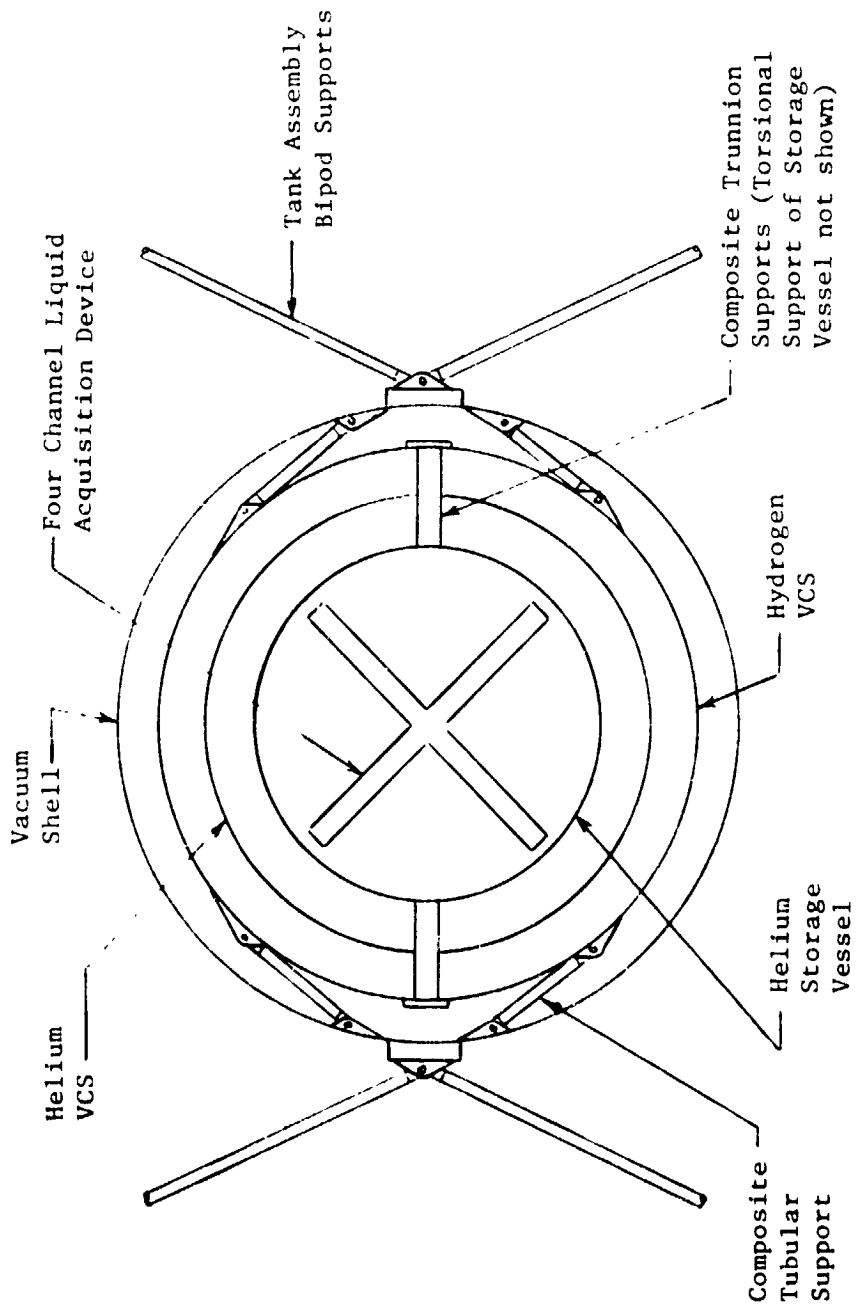
Figure III-7   Conceptual Design of Alternate Liquid Helium Storage
and Supply Tank (Configuration 4)

Table III-5 Liquid Mass Loads for Large Tanks

Tank Volume	Cryogen	Liquid Mass Loaded
12.5 m³ (440 ft³)	Argon	16,301 kg (35,906 lb)
	Methane	4,787 kg (10,545 lb)
	Oxygen	13,380 kg (29,470 lb)
37.4 m³ (1320 ft³)	Hydrogen	2,447 kg (5,390 lb)

Table III-6 Limit Load Factors for Large Tanks

Event	Limit Load Factor, g's*		
	x	y	z
Liftoff	+4.5 −6.5	±2.5	+6.0
Landing	±3.0	±2.0	±6.0
Emergency Landing (Factors are Ultimate)	+4.5 −1.5	±1.5	+4.5 −2.0

* These loads are applied simultaneously in x,y,z directions (worst sense)

load application in the STS coordinate reference frame.) Local structure may see increased loads due to STS interface random vibration environments, but in general these should be local effects due to the large tank masses. A transient loads analysis would be required to support a detailed structural design, but that is beyond the scope of this study. The values given in Table III-6 were therefore considered adequate for conceptual design and analysis purposes.

Composite struts were selected as the preferred approach for attaching the tank assembly to the cargo bay support fittings, and also attaching the pressure vessels to the vacuum jackets for those tanks configured in this manner. The general configuration selected was similar to those previously evaluated for this type of application (Ref 28 and 29). A typical S-glass/epoxy tube with aluminum end fittings is shown in Figure III-8. The particular arrangement of the struts in the preliminary conceptual designs was influenced by the desire to minimize stresses into the tank shells due to differential thermal and pressure expansion and contraction.

Hoop Wrapped
Graphite Filament (Typ)

S-Glass Composite Tube
934 Resin System

Ti-6Al-4V
End Fitting
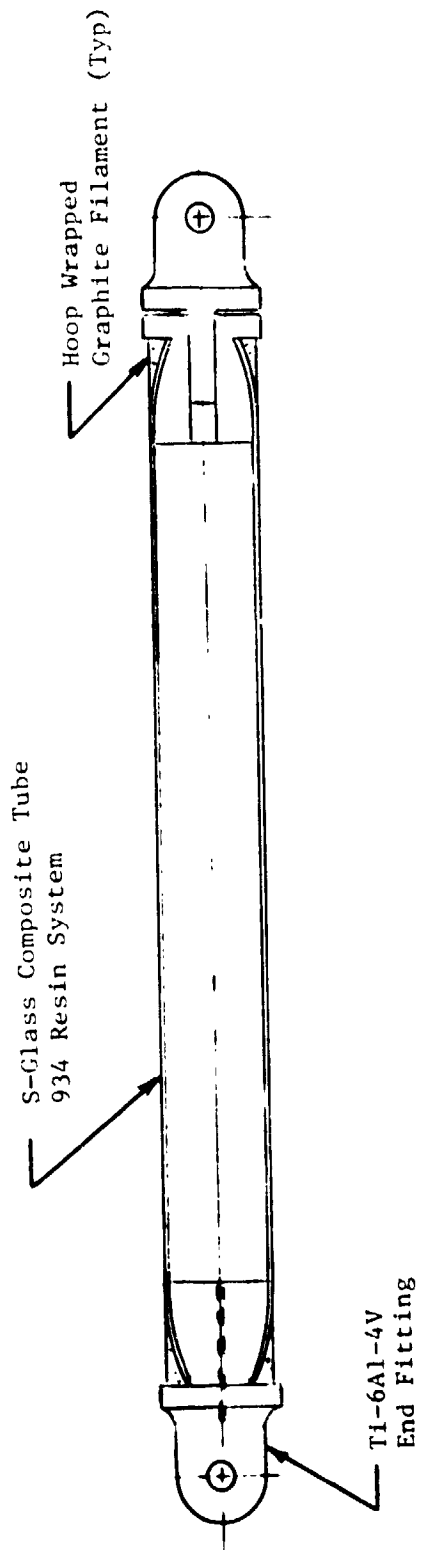
Figure III-8 Representative Composite Trunnion Support Concept for Large Tanks

The preliminary concepts for supporting the 12.5 m^3 (440 ft^3) vacuum-jacketed and non-vacuum-jacketed tanks from the Orbiter fittings are shown in Figures III-9 and III-10, respectively. Aluminum channel members are provided to tie the structure together between the longeron trunnion fittings. The composite struts tie into these channels and attach to the tank girth rings in bipod arrangements. An alternate approach to mounting directly to the Shuttle Orbiter fittings is to mount on a Spacelab pallet, as sketched in Figure III-11. The tank support structure attaches to the Spacelab sill hardpoints and the Spacelab keel hardpoints. The attachment of the tank to the support structure occurs at the tank girth ring.

Preliminary concepts for supporting the 37.4 m^3 (1320 ft^3) spherical and cylindrical tanks within the payload bay are presented in Figures III-12 and III-13. Aluminum channel members are similarly used for these designs to tie the structure to the Orbiter fittings, with composite struts tying the tank assembly to this framework.

3. Insulation Concepts

The insulation previously selected for the CFME baseline consisted of 1/4-mil double aluminized Mylar with two B4A Dacron net spacers per reflector, assembled to about 60 layers per inch (60 reflectors, 120 spacers per inch). This assembly corresponds to a density of approximately 56 kg/m^3 (3.5 lb/ft^3). For the preliminary conceptual designs of each of the vacuum-jacketed tank configurations, this same insulation was assumed. We assumed an installed thermal conductivity of 8.6 x 10^{-5} W/m°K (5X10^{-5} Btu/hr-ft°R) when the boundary temperatures are 20 and 255°K (36 and 460°R), with the thermal conductivity proportional to $T^{0.6}$. This yields the following relationship:

$$k_{eff} = 3.26 \times 10^{-6} \, T^{0.6} \text{ (International Units)}$$

$$k_{eff} = 1.88 \times 10^{-6} \, T^{0.6} \text{ (English units)}$$

This relationship for conductivity agrees with the data in Reference 31, but is conservative with respect to the data presented in References 32 and 33.

The following approach was assumed for the configuration and installation of MLI for the large tank sizes (12.5 m^3 and 37.4 m^3). Figure III-14 shows a sketch of the concept. The insulation is fabricated in gore sections over a mandrel of the proper size and shape. It is assembled with closely spaced threads tied between the structural nets or between plastic disks attached to the structural net. Thickness of the blanket is controlled by mechanically gaging the length of the thread. A small preload helps to improve dimensional stability. Diagonal threads are installed in the direction of the primary load on the blanket to limit slippage and compression of the blanket during boost loads. A hot needle is used to penetrate the Mylar foils through which the threads pass. This technique provides a reinforced hole with much greater strength than the torn opening made by a cold needle.

III-16
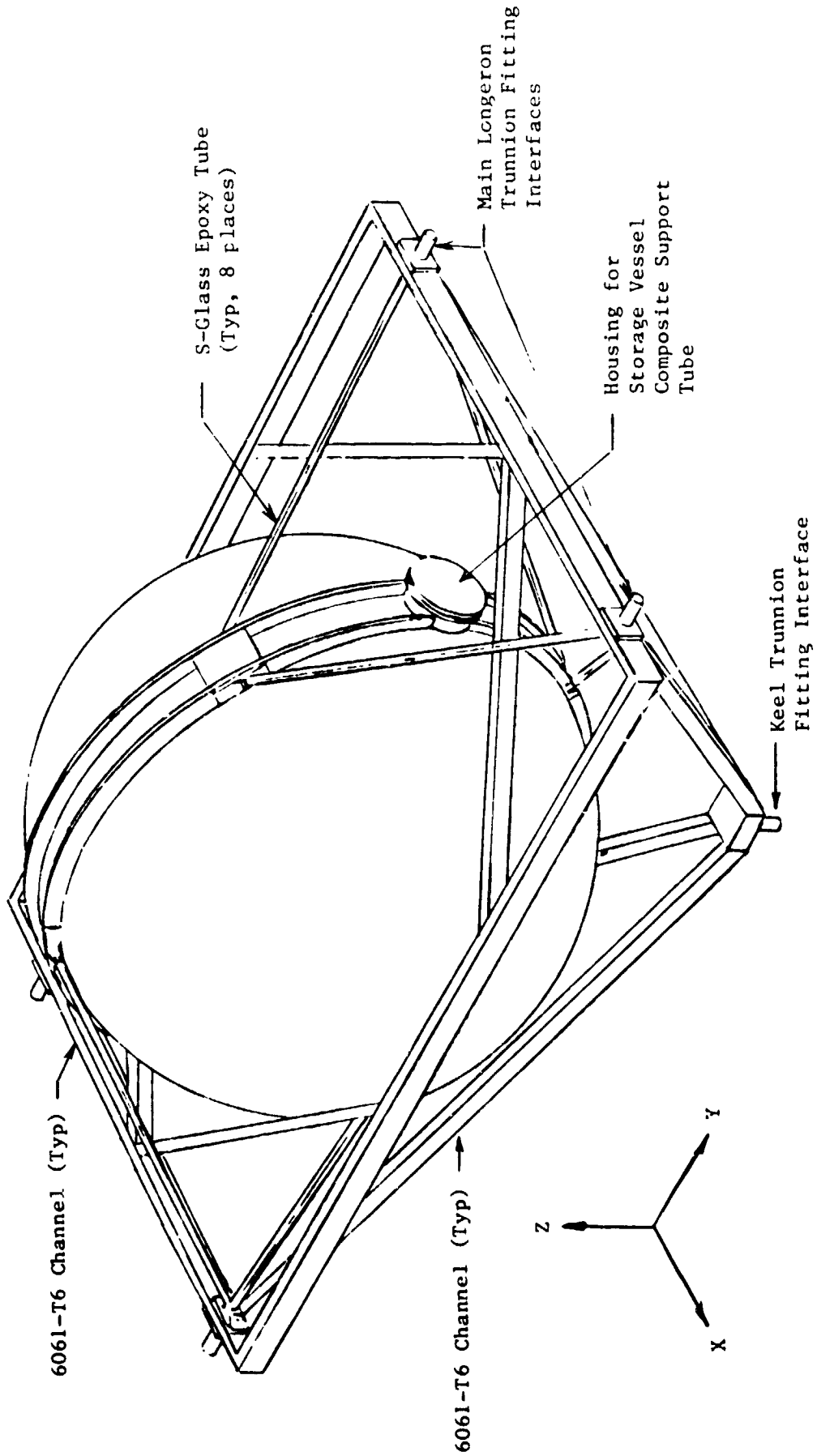
Figure III-9 Vacuum-Jacketed 12.5m³ (440 ft³) Tank Support Concept

S-Glass Epoxy Tube (Typ, 8 places)

Main Longeron Trunnion Fitting Interfaces

Housing for Storage Vessel Composite Support Tube

Keel Trunnion Fitting Interface

6061-T6 Channel (Typ)

6061-T6 Channel (Typ)

Z

Y

X

S-glass Epoxy Tube
(Typ. 8 places)

Main Longeron
Trunnion Fitting
Interfaces

6061-T6 Channel (Typ)

6061-T6 Channel
(Typ. 4 places)

Keel Trunnion
Fitting Interface

Figure III-10 Non-Vacuum-Jacketed 12.5m^3 (440 ft^3) Tank Support Concept

6061-T6 Ring
Support Channels
(Typ, 3 places)

6061-T6 Channel (Typ)

Spacelab Pallet
Sill Hardpoint
Attachment

Spacelab
Pallet

Spacelab
Pallet
Keel
Hardpoints

Figure III-11 Spherical 12.5 m^3 (440 ft^3) Tank Mounted on Spacelab Pallet

III-19

Main Longeron
Trunnion Fitting
Interfaces
(Typ. 4 places)

S-glass Epoxy Tube (Typ. 4 places)

S-glass Epoxy Tube
(Typ. 24 places)

Keel Trunnion
Fitting Interface
(Typ. 3 places)
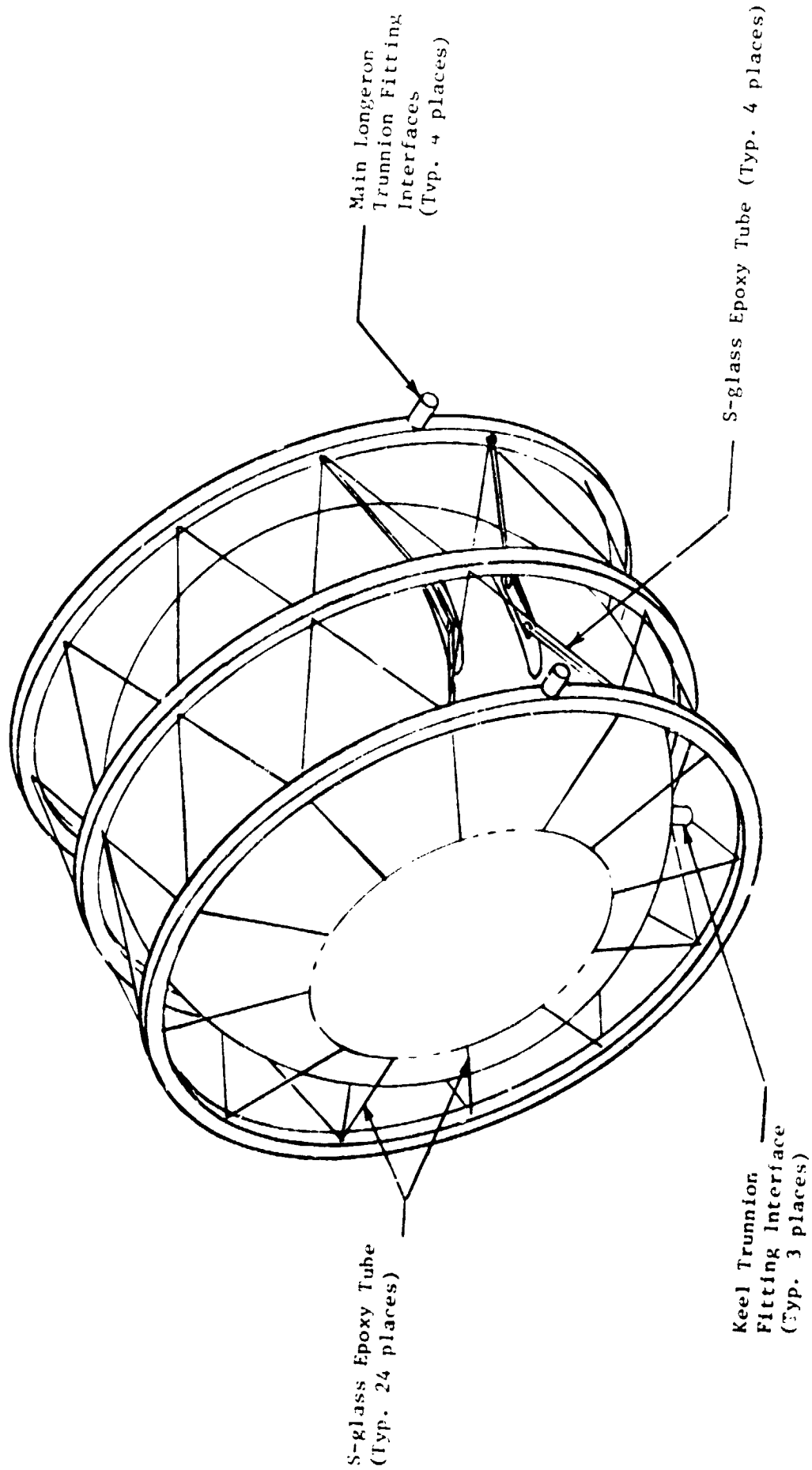
Figure III-12 Spherical 37.4m^3 (1320 ft^3) Tank Support Concept

III-20

Tank Girth
Rings

S-Glass Epoxy Tube

6061-T6 Ring
Support Channels
(Typ, 3 places)

Main Longeron Trunnion
Fitting Interfaces

Keel Trunnion
Fitting Interface
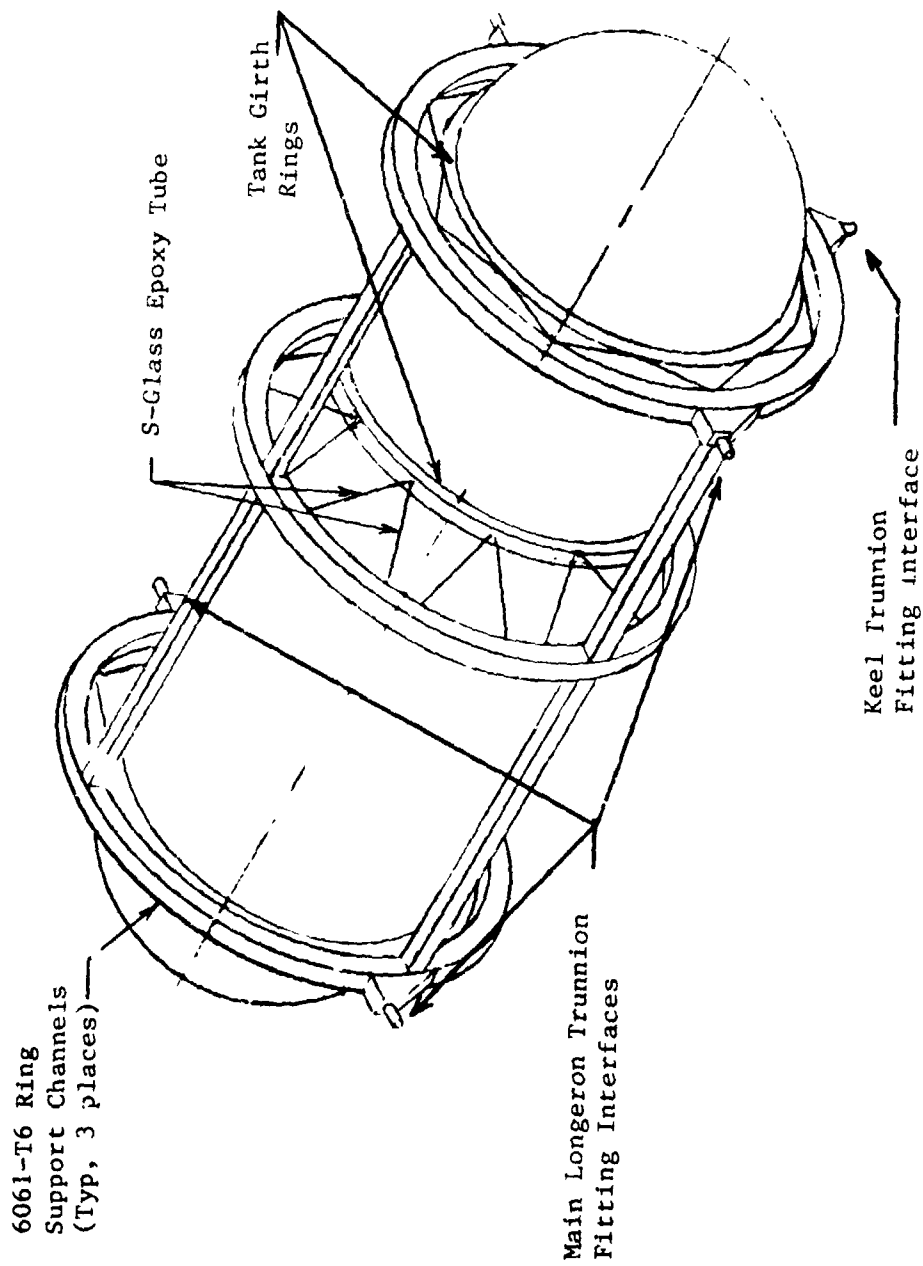
Figure III-13 Cylindrical 37.4m^3 (1320 ft^3) Tank Support Concept

Gore section butted together with foil
strip between layers

Insulation gore segment
installed in layers. Offset
joint on succeeding layers.

Cap

Girth ring
(Tank support pickups
located on ring)
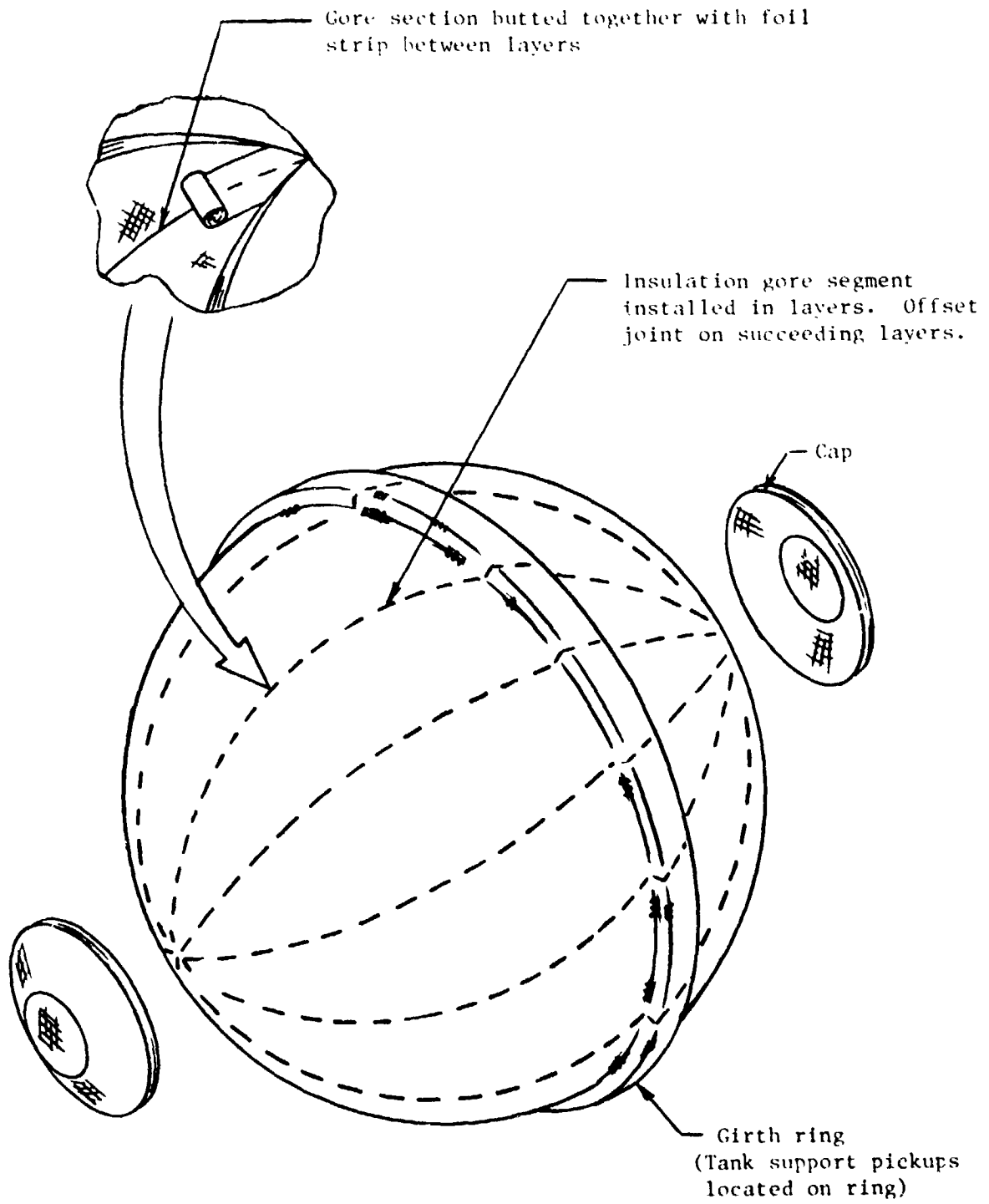
Figure III-14 MLI Concept for 12.5 m³ and 37.4 m³ Tanks

The aluminized Mylar reflector material must be perforated for purging and to assure evacuation in space. The perforated area must be adequate to allow flow of purge gas and to permit evacuation in a reasonable time without stressing the panels due to contained gas. On the other hand, the perforated area should be no greater than necessary while the spacing between perforations should be kept large.

Attachment of the insulation blankets is by means of snap and curtain fasteners attached to Dacron ribbons which, in turn, are fastened across the full length or breadth of the panel. These fasteners are located on all sides of each blanket, with mating pins bonded to the tank or shroud. At frequent intervals (approximately 0.3 m) over the surface of the blanket, Velcro pile strips are bonded. Velcro hook strips are mounted on the tank or shroud at right angles to permit engagement with small alignment errors.

These strips are secured in place with small strips of Mylar tape at appropriate intervals. Inner and outer structural nets of adjacent panels are stitched together over the full length of the butt joints. This method of fabrication and installation was used in insulation of a 1.2-m (4-ft) diameter, 1.8-m (6-ft) long cylindrical tank under contract NAS8-21330, Development of Advanced Materials for Integrated Tank Insulation System for the Long Term Storage of Cryogens in Space (Ref 28). The method of fabrication, installation and close out proved practical and the system was satisfactorily tested with liquid hydrogen.

For the relatively large, non-vacuum-jacketed tanks, the type of insulation (helium-purged MLI, spray-on-foam-insulation (SOFI), or combinations of the two), and the number of layers were variables to be addressed in the Task II-Thermal Analysis (See Chapter IV, Section B). Because of the relatively longer storage times addressed in this study, calculated optimum MLI thicknesses become quite large. A determination of the largest practical thickness was made during Task I.

Several different approaches have been used in the past to calculate MLI performance as a function of number of layers. Either semi-emperical equations for the MLI heat flux (which contain empirical terms related to number of MLI layers) or an effective thermal conductivity (assumed to vary linearly with number of layers) are used to predict the MLI thermal performance. The effective thermal conductivity defined previously (used for CFME baseline) has been verified up to 40 layers (Ref 28) and semi-emperical equations have been verified up to 112 layers (Ref 34). Stochl (Ref 34) reported on an experimental investigation to obtain heat transfer data on a particular insulation system containing a large number of MLI layers, determined whether a semi-emperical equation could be used to predict the heat transfer through a large number of layers, and determined whether an effective thermal conductivity based on a few layers could be used to predict the thermal performance of large numbers of layers.

The insulation system tested by Stochl consisted of from 20 to 160 layers of double alumized mylar with silk net spacers at an average density of 52 layers/inch. The insulation was spirally wrapped around a 76-cm (30-in) diameter cylindrical calorimeter (the spiral wrapping was intended to

eliminate the discontinuities associated with blankets). Five tests were run with 160, 100, 60, 40 and 20 layers, respectively. A hot boundary temperature of 294°K (530°R) was maintained, with the cold boundary temperature at 21°K (37.6°R) (liquid hydrogen). The tests were conducted at a pressure of 10^{-6} torr to minimize gaseous heat conduction. The normal heat flux was the parameter used to evaluate the MLI thermal performance, and was obtained by boiloff calorimetry, corrected for non-normal heat inputs and penetration heat inputs.

Steady state test data for the five insulation thicknesses are given in Table III-7. Also shown in Table III-7 are effective thermal conductivities. These data indicate an exponentially decreasing heat flux for increasing numbers of layers. Adding 80 layers to the 20-layer baseline reduced the heat flux by 78 percent. An additional 60 layers of MLI produced only an additional 11 percent reduction in the 20-layer heat flux.

Other MLI thermal performance data comes from laboratory tests on small samples (References 35 and 36). DeWitt and Boyle (Ref 37) present thermal performance results for a simulated spacecraft on a long duration mission. Both shielded and non-shielded tanks are considered. A review of all of this data suggests that both a semi-emperical heat flux correlation and an effective thermal conductivity of a small number of layers (20) adequately predict the thermal performance of many layers of MLI, having predicted heat flux to within 10% of that obtained experimentally. However, as Stochl points out, when an effective thermal conductivity is used, the layer density, boundary temperatures, and interstitial pressure should be the same as those for which it was originally evaluated.

Table III-7 Steady State Test Results on Effect of
Number of Layers of MLI (from Stochl, Ref 34)

No. of Layers	Average Density Layers/cm (Layers/inch)	Normal Heat Flux W/m² (Btu/hr ft²)	Effective Thermal Cond. W/m°K (Btu/hr ft°R)
20	20.2 (51.3)	0.8728 (0.2767)	3.22×10^{-5} (1.861×10^{-5})
40	20.5 (52.0)	0.4952 (0.1570)	3.406×10^{-5} (2.003×10^{-5})
60	20.5 (52.0)	0.3186 (0.1010)	3.834×10^{-5} (1.914×10^{-5})
100	20.5 (52.0)	0.1889 (0.0599)	3.229×10^{-5} (1.866×10^{-5})
160	20.5 (52.0)	0.0931 (0.0295)	2.430×10^{-5} (1.404×10^{-5})

A comparison of test data with the conductivity predicted by equation (1) indicates that it is generally conservative by about a factor of 6 for small layer thicknesses (up to 60 layers). Based on the data from Stochl, the reduction in heat flux is expected to decrease with the increasing thickness in an exponential manner. Therefore, calculations made using equation (1) would be expected to be less conservative for thicker MLI blankets. Since the assumption of a linear temperature gradient predicts a linearly decreasing heat flux with MLI thickness, while the actual heat flux decreases in an exponential manner, the difference between the two heat fluxes decreases with thickness. Using the data from Table III-7, the conservatism in MLI thermal conductivity used in this study is about a factor of 6 at 34 layers, and about a factor of 4 at 160 layers. A maximum insulation thickness of 10-cm (4-in) was assumed. This thickness may only be attainable if better installation techniques became available and layer density is better controlled to prevent compression in the one-g ground launch environments. Considering the relatively large factors on performance at the thinner blanket thicknesses, it was considered reasonable for this study to use the conductivity given by equation (1), assuming some improvements in technology for thicker blankets.

A new concept was considered for the large hydrogen tank, in which MLI is used in conjunction with spray-on-foam-insulation (SOFI). The SOFI can be applied under the MLI to eliminate the helium purge requirement for the non-vacuum-jacketed hydrogen tank. The SOFI is applied in a thick-enough layer to raise the SOFI-MLI interface temperature above the liquifaction temperature for nitrogen, 78°K (140°R).

During ground hold, the moderately high heat flux through the combined insulation results in an interface temperature above the condensation temperature of air or nitrogen. In the case of a Shuttle payload (groundruled for this study), a nitrogen purge is available for cryogenic payloads, and a separate purge system for the insulation is not required. The only requirement is that the MLI must be purged of moisture prior to installation in the payload bay.

The thermal conductivity of SOFI at a mean temperature between the nitrogen liquifaction temperature and liquid hydrogen temperature is 6.7×10^{-3} W/m°K (3.9×10^{-3} Btu/hr ft°R) (Ref 38). However, a wide variation in conductivity results for "as applied" insulation. A range of ± 75 percent covers 95 percent of the data scatter (95% confidence limit). The maximum value of 1.2×10^{-2} W/m°K (6.8×10^{-3} Btu/hr ft°R) at the 95 percent confidence limit was selected to determine SOFI thickness to preclude nitrogen liquifaction for any worst case condition. We are thus 95 percent certain that no nitrogen liquifaction (and increased heat flux) will occur due to increased conductivity.

Existing technology for application of SOFI to the Space Shuttle External Tank indicates that the machine application thickness tolerance is about ± 0.64-cm (± 0.25-in). In addition, with today's technology, the minimum thickness that can be applied, and still obtain the required SOFI performance is about 1.3-cm (0.5-in). This value was used in the thermal performance analysis, Task II.

Fluid dynamic, steady-state thermal and preliminary structural analyses were performed for each of the 13 configurations which make up the eight tank/fluid combinations in the study. Refinements were made in the preliminary conceptual designs as iterations occurred between efficient thermal and structural approaches. In general, these analyses were directed at a relatively conservative approach when design changes to the CFME baseline were identified. Unverified design concepts and significant improvements in the state-of-the-art were not used for the larger tank sizes and the helium tank; rather, a realistic approach in terms of fabricability, reliability, reusability and cost was followed. Analysis techniques used were those previously used for the CFME baseline.

A. Fluid Dynamic Analysis

The fluid dynamic analysis involved establishing the fluid behavior in each cryogenic storage and supply system conceptual design. The major system elements considered were the liquid acquisition devices and the various lines connected to the tank. The lines included the inflow and outflow lines, the pressurization/vent line and the thermodynamic vent lines. The desired output of this anlaysis included an estimate of performance in terms of maximum outflow rates and residuals following loss of acquisition device capability at tank depletion on-orbit.

1. Liquid Acquisition Devices

The operation of liquid acquisition devices depends on the interaction of the liquid/gas interface with the device. Liquid surface tension and ullage pressure support are used to passively provide near-instantaneous, gas-free liquid expulsion on demand. The devices are configured within the tank to position liquid at the outlet and stabilize the liquid/gas interface at the surface of the device to assure gas-free liquid expulsion under periods of low-g or adverse-g. Capillary configurations differ because of the varied system/mission requirements; however, the operational principle for each system relies on the relatively small pressure differential that exists across any curved gas/liquid interface due to intermolecular forces. This capillary pressure difference, ΔP_c, may be expressed at any point across the interface as

$$\Delta P_c = \sigma\left[\frac{1}{R_1} + \frac{1}{R_2}\right] \qquad (2)$$

where σ is the liquid/gas surface tension and R_1 and R_2 are the principal radii of curvature of the interface.

For a spherical interface, R_1 equals R_2 and the pressure difference is

$$\Delta P_c = \frac{2\sigma}{R_s} \tag{3}$$

where R_s is the radius of curvature. The capillary pressure difference can be related to a dimension (other than the radius of curvature) such as the pore radius R and a second parameter, the liquid-to-solid contact angle θ. Using the relationship between R, θ, and R_s, results in

$$\Delta P_c = \frac{2\sigma \cos\theta}{R} \tag{4}$$

The cryogenic propellants of interest are totally wetting with liquid-to-solid contact angles from zero to two degrees.

The capillary pressure difference for a circular pore, as in a perforated plate, can be determined from this equation. Capillary pressure retention for pore geometries other than circular, as in fine-mesh screen, is more accurately determined empirically. The accepted technique is the so-called "bubble point" method used by the filter industry. The screen material is covered by a thin layer of liquid, usually alcohol, and its underside is pressurized slowly with air or gaseous nitrogen. The pressure difference at which the first bubble passes through the material is termed the bubble point (BP). The pressure retention for perforated material can be predicted for other liquids from:

$$(BP)_1 = \frac{\sigma_1}{\sigma_m} (BP)_m \tag{5}$$

This assumes the θ's are equal. The subscripts refer to the second liquid (liquid hydrogen, for example) and to a test liquid, such as methanol(m).

The maximum capillary pressure retention for 325 x 2300 fine mesh Dutch twill screen with the cryogenic fluids of this study, except for helium, is presented in Table IV-1. The values in the table were calculated based on a value of 66-cm (26-inches) of water as measured in methanol. The calculated values agree well with measured values for liquids hydrogen (Ref 26, 27) and oxygen (Ref 26). Pressure retention values have not been measured for 325 x 2300 screen in methane or argon, but it is felt that these fluids are similar enough to liquid oxygen that the standard surface tension scaling approach applies.

Because of the narrow temperature range for liquid helium-4 from the normal boiling point to the critical point, and because the surface tension of a liquid goes to zero at the critical point, the variation of surface tension with saturation temperature (Fig II-9) over this range provides a good indication of how the pressure retention capability will vary. The pressure retention capability of liquid helium-4 for a single layer of 325 x 2300 mesh screen is shown in Table IV-2, where equation (5) was used for the calculation.

Table IV-1   Pressure Retention Capability of 325 x 2300 Mesh Screen

Fluid	Pressure Retention Capability	
	Saturation at 138 KN/m^2 (20 psia)	Saturation at 414 KN/m^2 (60 psia)
Hydrogen	0.48 KN/m^2 (0.07 psi)	0.28 KN/m^2 (0.04 psi)
Methane	3.86 KN/m^2 (0.56 psi)	2.83 KN/m^2 (0.41 psi)
Oxygen	3.65 KN/m^2 (0.53 psi)	2.76 KN/m^2 (0.40 psi)
Argon	3.24 KN/m^2 (0.47 psi)	2.34 KN/m^2 (0.34 psi)

Table IV-2   Pressure Retention Capability of
325 x 2300 Mesh Screen with Helium-4

Temperature		Surface Tension		Pressure Retention Capability	
$^{\circ}$K	$^{\circ}$R	Dyne/cm	lb$_f$/ft (10^5)	KN/m^2 (10^3)	psi (10^3)
2.2	4.0	0.3063	2.098	80.9	11.74
3.0	5.4	0.2247	1.539	59.4	8.62
4.0	7.2	0.1226	0.840	32.4	4.70
5.0	9.0	0.0206	0.141	5.4	0.79
5.2	9.4	0	0	0	0

The small capillary pressure difference or pressure retention capability of the screen must balance or exceed the sum of other pressure differences tending to break down the passively-controlled liquid-gas interface. Premature interface breakdown reduces expulsion efficiency due to gas ingestion. During storage with no liquid outflow

$$BP = \Delta P_c \geq \Delta P_h \quad \text{or} \quad \frac{2\sigma}{R} \cos\theta \geq \rho a h \tag{6}$$

where ΔP_h is the hydrostatic head supported by the screen, ρ is the liquid mass density, a is the acceleration, and h is the hydrostatic head. Equation (6) shows that the pore size required decreases with increasing acceleration. The maximum hydrostatic head which can be supported by the 325 x 2300 mesh screen is presented in Figure IV-1. Hydrostatic head capability for single-layer 325 x 2300 mesh screen in helium-4 is shown in Figure IV-2 as a function of storage temperature. Two on-orbit conditions, OMS settling (a = 0.077g) and RCS omnidirectional acceleration (a = 0.04g) are shown. A hydrostatic head equal to the tank diameter can be provided up to 2.9° K (5.3° R) for the RCS condition. Since the screen channels for the CFME baseline are truncated at about a 10% ullage, this height is also shown on the figure. Liquid-vapor interface stability can be provided over the entire length of the truncated channels for the RCS acceleration at 2.2-to-3.4° K (4.0-to-6.1° R).

Additional losses are introduced in a flowing system, and

$$BP \geq \Delta P_h + \Delta P_e + \Delta P_v + \Delta P_f + \Delta P_t \tag{7}$$

where ΔP_e is the pressure loss due to flow through screen, ΔP_v is the change in pressure head to velocity head, ΔP_f is the viscous loss due to flow in the device, and ΔP_t is the loss due to transients, such as pulsed flow, vibration, etc.

An additional criterion for determining hydrostatic interface stability is the Bond number, Bo, a dimensionless ratio of acceleration-to-capillary forces (Ref 39).

$$Bo = \frac{\rho a L^2}{\sigma} \tag{8}$$

where L is the characteristic system dimension. The liquid/gas interface is stable in a cylindrical container (tank, line, etc.) or circular pore when Bo $\leq$ 0.84. The Bond Number will be referenced later in the discussion of two-phase flow in the thermodynamic vent lines.
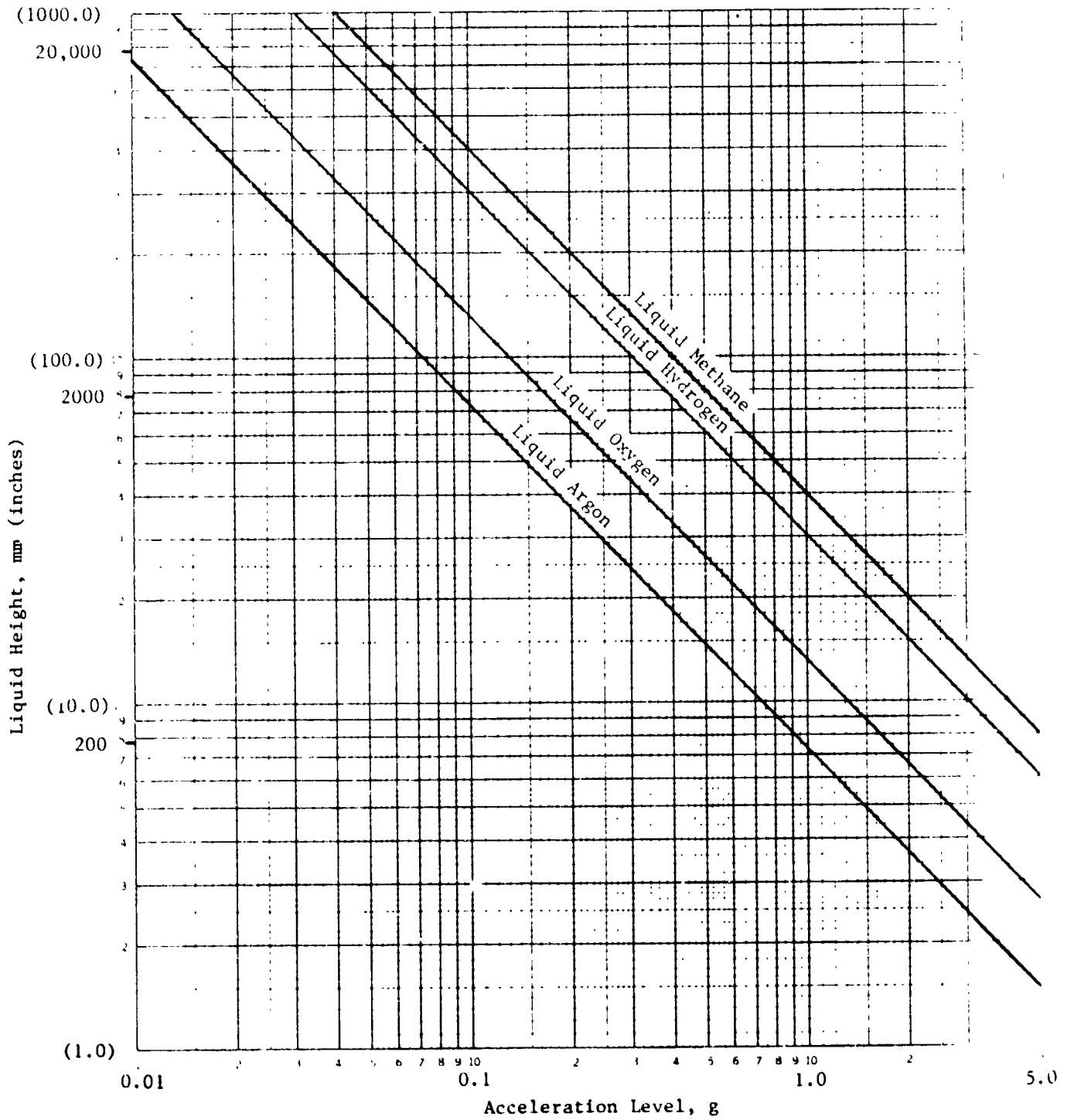
Figure IV-1 Maximum Liquid Hydrostatic Head vs Acceleration Level for Various Liquids Using 325 X 2300 Mesh Screen

IV-5
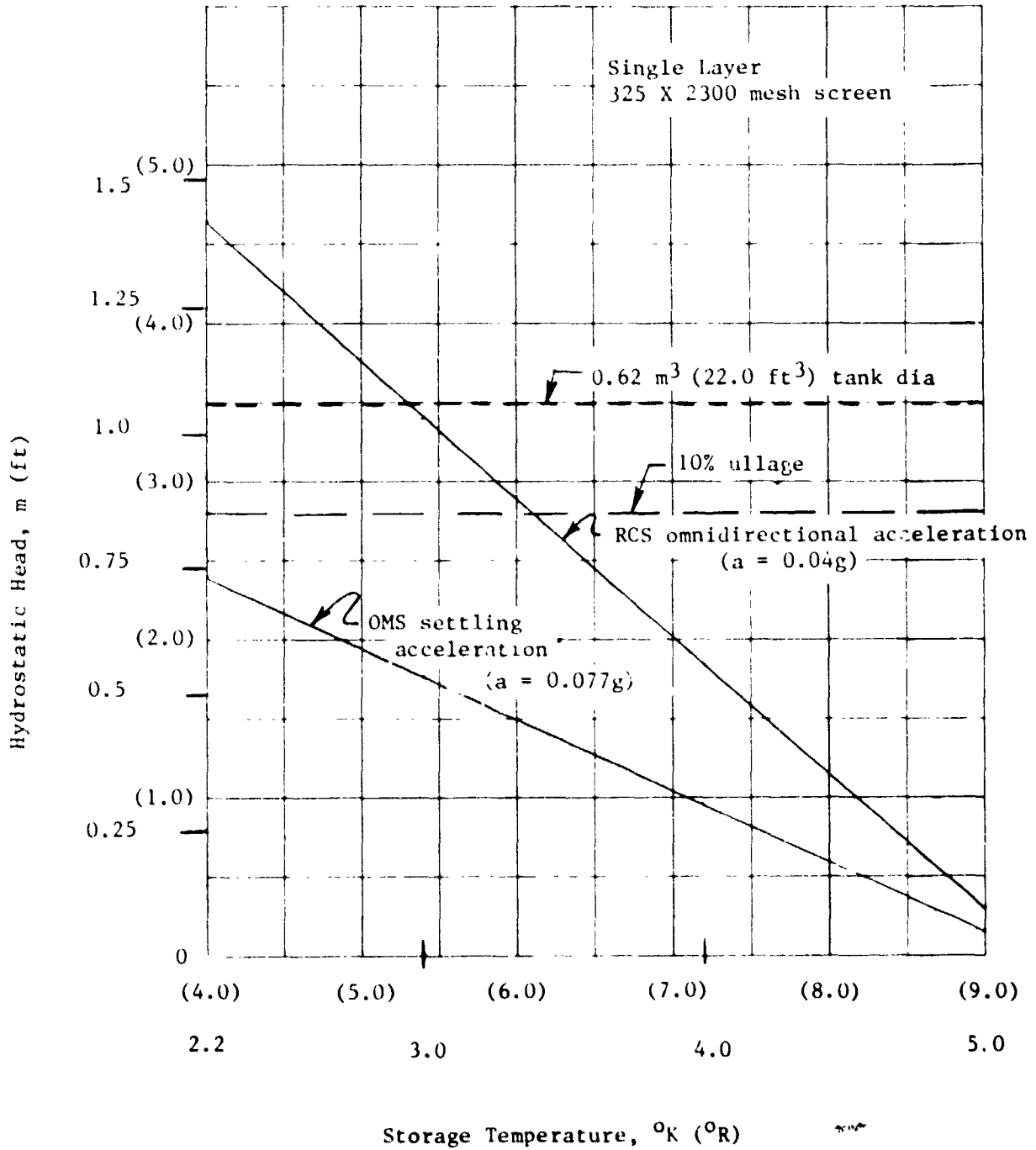
Figure IV-2 Helium-4 Hydrostatic Head Capability

Acquisition device performance involves the determi... .ion of screen breakdown for each liquid/tank case. Screen breakdown occurs when gas is ingested with liquid draining of the tank. At this poin single phase liquid expulsion is interrupted and liquid remaining in the tank at screen breakdown is considered outage or residual.

For analysis purposes, it was assumed that draining of the tank on orbit may occur at any one of three accelerations.

a) OMS (Orbital Maneuvering System) - settling acceleration of 0.077g. Liquid is settled over the tank outlet.

b) A lateral acceleration of 1.6 x 10^{-5} g due to drag acting on the Orbiter at an angle of attack of 90°.

c) An axial acceleration of 3.0 x 10^{-6} g due to drag acting on the Orbiter at an angle of attack of zero degrees.

Depletion during orbital maneuvering system firing was the worst case because of the hydrostatic heads imposed on the channels, particularly for the larger tank sizes. For the case of a Return-to-Launch-Site (RTLS) abort, which has the highest flowrate requirements, it was assumed that a Shuttle Reaction Control System (RCS) settling environment was present.

A summary of acquisition device residuals for all 13 configurations is tabulated in Table IV-3, for International units, and Table IV-4 for English units. Both the volume and percent of loaded quantity remaining inside the channels of the acquisition device at depletion are listed in the tables. Residuals are tabulated for both on-orbit depletion and RTLS abort depletion. or all cases except liquid helium, the temperature in the tank was assumed ' be saturated at the maximum pressure of 414 KN/m^2 (60 psia). (The helium performance will be discussed in greater detail later in this subsection.) It was determined that the CFME channel size was adequate for all the 0.62 m^3 (22 ft^3) cases. The channel size for the 12.5 m^3 (440 ft^3) argon and methane tanks had to be increased to 11.7-cm x 3.0-cm (4.6-in x 1.2-in). The total volume of the four channels is 0.04 m^3 (1.47 ft^3), or about 0.4 percent of the total tank volume. This size results in an abort residual of about 10 percent for argon, but this was considered acceptable since argon is an inert fluid.

The abc ᵔ flowrate for the 12.5 m^3 (440 ft^3) oxygen tank dictates a different channel size than for the methane or argon tanks. Iterations on channel size versus residual resulted in channel cross-sectional dimensions of 28.4-cm x 7.4-cm (11.2-in. x 2.9-in.). This gives a 5 pe .ent residual for the abort condition, and a 3 percent residual for on-orbit depletion.

The calculated channel dimensions for the spherical hydrogen tank (Configuration 13) are 27.0-cm x 6.9-cm (10.6-in. x 2.7-in.), which gives an internal volume of about 0.37 m^3 (13 ft^3). ᵔor this spherical configuration, on-orbit and abort residuals are 2 and 3 percent,

Table IV-3 Liquid Acquisition Device Residuals (International Units)

Config.	Category	Size	Fluid	Vol. in LAD	% in LAD	Total Liquid Loaded (kg)	Residuals			
							On-Orbit (%)	Coast (kg)	Abort* (%)	Abort* (kg)
	CFME	0.62 m³	Hydrogen	2.5x10⁻³m³	0.4%	39	2.5	1.0	2.5	1.0
1	I	0.62 m³	Methane	"	"	250	0.6	1.5	0.6	1.5
2	II	0.62 m³	Argon	"	"	816	0.6	4.9	0.6	4.9
3	III	0.62 m³	Oxygen	"	"	670	0.6	4.0	4.0	27
4	IV	0.62 m³	Helium	"	"	74	0.6+	0.5	8.0+	5.9
5-7	V	12.5 m³	Argon	0.04 m³	"	16320	0.8	130	10.0	1652
8,9	VI	12.5 m³	Methane	"	"	4794	2.0	96	2.5	120
10,11	VII	12.5 m³	Oxygen	0.21 m³	2.0%	13395	3.0	402	5.0	670
12	VIII	37.4 m³ (Cyl)	Hydrogen	0.52 m³	1.4%	2450	2.5	61	5.0	123
12(Alt)	VIII	37.4 m³ (Cyl)	Hydrogen	0.18 m³	0.5%	2450	1.0	24	**	**
13	VIII	37.4 m³ (Sph)	Hydrogen	0.37 m³	1.0%	2450	2.0	49	3.0	74

+   Assuming depletion with liquid temperature of 3.33° K
*   Abort with settling RCS maneuver
** Alternate channel configuration, 14.7-cm x 3.8-cm, designed for on-orbit coast depletion

Table IV-4 Liquid Acquisition Device Residuals (English Units)

Config.	Category	Size	Fluid	Vol. in LAD	% in LAD	Total Liquid Loaded (lb)	Residuals			
							On-Orbit (%)	Coast (lb)	Abort* (%)	Abort* (lb)
	CFME	22 ft³	Hydrogen	0.09 ft³	0.4%	85	2.5	2.1	2.5	2.1
1	I	22 ft³	Methane	"	"	550	0.6	3.3	0.6	3.3
2	II	22 ft³	Argon	"	"	1795	0.6	10.8	0.6	10.8
3	III	22 ft³	Oxygen	"	"	1473	0.6	8.8	4.0	58.9
4	IV	22 ft³	Helium	"	"	163	0.6+	1.0	8.0+	13.0
5-7	V	440 ft³	Argon	1.47 ft³	"	35,906	0.8	287	10.0	3591
8,9	VI	440 ft³	Methane	"	"	10,545	2.0	211	2.5	264
10,11	VII	440 ft³	Oxygen	7.53 ft³	2.0%	29,470	3.0	884	5.0	1474
12	VIII	1320 ft³ (Cyl)	Hydrogen	18.3 ft³	1.4%	5,390	2.5	135	5.0	270
12(Alt)	VIII	1320 ft³ (Cyl)	Hydrogen	6.5 ft³	0.5%	5,390	1.0	54	**	**
13	VIII	1320 ft³ (Sph)	Hydrogen	13.0 ft³	1.0%	5,390	2.0	108	3.0	162

+   Assuming depletion with liquid temperature of 60R

*   Abort with settling RCS maneuver

**   Alternate channel configuration, .8-in x 1.5-in, designed for on-orbit coast depletion

respectively. If these same dimensions are used for the cylindrical geometry (Configuration 12), the increased channel volume results in residuals of 2.5 and 5 percent for the on-orbit depletion and abort conditions. These relatively significant residuals are driven by the abort requirements; if the channels were sized specifically to minimize on-orbit residuals, a 1 percent residual is obtained, as indicated for Configuration 12 (Alt). A channel dimension of 14.7-cm x 2.8-cm (5.8-in. x 1.5-in.) is adequate to obtain this low, on-orbit residual.

The performance of the liquid helium tank requires some additional discussion. The pressure retention, ΔP_c, must satisfy pressure differences due to hydrostatic and hydrodynamic considerations, as indicated previously. The results of the analysis at both the abort flowrate of 0.014 kg/sec (0.03 lb/sec) and the mission flowrate of 0.02 kg/hr (0.04 lb/hr) are presented in Tables IV-5 and IV-6 for depletion in the low-g (drag) environment. The expulsion performance is highly dependent on storage temperature. The expulsion efficiency approaches 100 percent except for the higher abort outflow condition at a storage temperature of 5.0°K (9.0°R) and storage pressure of 200 KN/m^2 (29 psia) for the saturated helium.

At the 5.0°K abort condition, the sum of adverse pressure differences is greater than the capillary retention as provided by the 325 x 2300 mesh. A negative value results for screen entrance loss, as shown. Thus, at the 5°K (9°R) condition, it is not possible to flow through the LAD at the abort flowrate without getting gas ingestion into the screen channels, even with a nearly full tank. For the other conditions in the tables, a relatively small screen flow area, Ae, is required to prevent screen breakdown. The figures in the bottom row in the tables are the minimum flow areas, i.e., below this area, vapor is ingested and single-phase liquid draining is interrupted. The liquid expulsion efficiency is determined at this point.

The upper limit for expulsion efficiency (no flow losses) in the OMS and RCS environments is pictured in Figure IV-3 as a function of storage temperature. The solid lines are based upon interface stability over channels configured through the entire tank. The OMS acceleration condition, as mentioned, settles liquid over the tank outlet. The channels are truncated which tends to improve expulsion efficiency by reducing the hydrostatic head retention requirement. The dashed line shows this improvement for the RCS condition. The near-100% expulsion can be provided from 2.2 to 3.4°K (4.0 to 6.1°R) for the 0.04 g omnidirectional state, as shown.

The subcritical storage of liquid helium with capillary devices to provide control for liquid draining represents a new challenge. The results show that the capillary configuration in the CFME tank tends to present rather stringent thermal control requirements. The desired liquid control using the single-layer 325 x 2300 screen shows preferential storage of the saturated helium-4 near the lower lambda conditions of 2.2°K (3.9°R) and 5.0 KN/m^2 (0.730 psia). Additional layers of screen, rather than a single layer, would tend to relax this narrow temperature requirement of storage by providing greater retention.

Table IV-5 Low-G (Drag) Channel Flow Analysis (Saturated He-4, International Units)

Helium Flowrate	0.014 kg/sec				0.018 kg/hr			
Storage Conditions								
Temperature, °K	2.2	3.0	4.0	5.0	2.2	4.0	4.0	5.0
Pressure, KN/m²	5.0	24.3	82.2	195	5.0	24.3	82.2	195
Screen Retention, ΔP_c *	0.08	0.06	0.03	0.0054	0.08	0.06	0.03	0.0054
Pressure Diff*								
Hydrostatic	negligible	negligible	negligible	negligible	3.67×10^{-6}	3.54×10^{-6}	3.23×10^{-6}	2.54×10^{-6}
Dynamic	0.0029	0.0030	0.0033	0.0042	3.99×10^{-6}	4.1×10^{-10}	4.6×10^{-10}	5.8×10^{-10}
Friction	0.0086	0.0089	0.0097	0.0114	3.8×10^{-8}	4.0×10^{-8}	3.9×10^{-8}	4.0×10^{-8}
Total of Pressure Differences, ΔP_r *	0.0115	0.0119	0.0130	0.0185	3.7×10^{-6}	3.6×10^{-6}	3.3×10^{-6}	2.6×10^{-6}
Pressure Difference Available for Flow thru Screen (ΔP_e)*	0.0694	0.0475	0.0194	-0.0131	0.0809	0.0594	0.0324	0.0054
Screen Flow Area** Req'd for ΔP_e, i.e., Breakdown	6.5	9.8	22.8	None	2.1×10^{-3}	2.9×10^{-3}	5.2×10^{-3}	2.9×10^{-3}

*All pressures are kN/m²
**Screen Area is cm²

Table IV-6 Low-G (Drag) Channel Flow Analysis (Saturated He-4, English Units)

Helium Flowrate	0.03 lb/sec				0.04 lb/hr			
Storage Conditions								
Temperature, °R	4.0	5.4	7.2	9.0	4.0	5.4	7.2	9.0
Pressure, psia	0.73	3.52	11.92	28.35	0.73	3.52	11.92	28.35
Screen Retention, ΔP_c *	0.01174	0.00862	0.00470	0.00079	0.01174	0.0086.2	0.00470	0.00079
Pressure Diff*								
Hydrostatic	negligible	negligible	negligible	negligible	5.32×10^{-7}	5.14×10^{-7}	4.68×10^{-7}	3.68×10^{-7}
Dynamic	0.000422	0.000437	0.000481	0.000611	5.79×10^{-11}	6.00×10^{-11}	6.60×10^{-11}	8.38×10^{-11}
Friction	0.001250	0.001294	0.001406	0.001659	5.51×10^{-9}	5.83×10^{-9}	5.71×10^{-9}	5.83×10^{-9}
Total of Pressure Differences, ΔP_t *	0.001672	0.001731	0.001887	0.00269	5.38×10^{-7}	5.20×10^{-7}	4.74×10^{-7}	3.74×10^{-7}
Pressure Difference Available for Flow thru Screen (ΔP_e)*	0.010068	0.006889	0.002813	-0.00190	0.01174	0.00862	0.00470	0.00079
Screen Flow Area** Req'd for ΔP_e, i.e., Breakdown	1.01	1.52	3.53	None	3.23×10^{-4}	4.56×10^{-4}	8.02×10^{-4}	4.53×10^{-3}

*All pressures are psia
**Screen Area is in^2
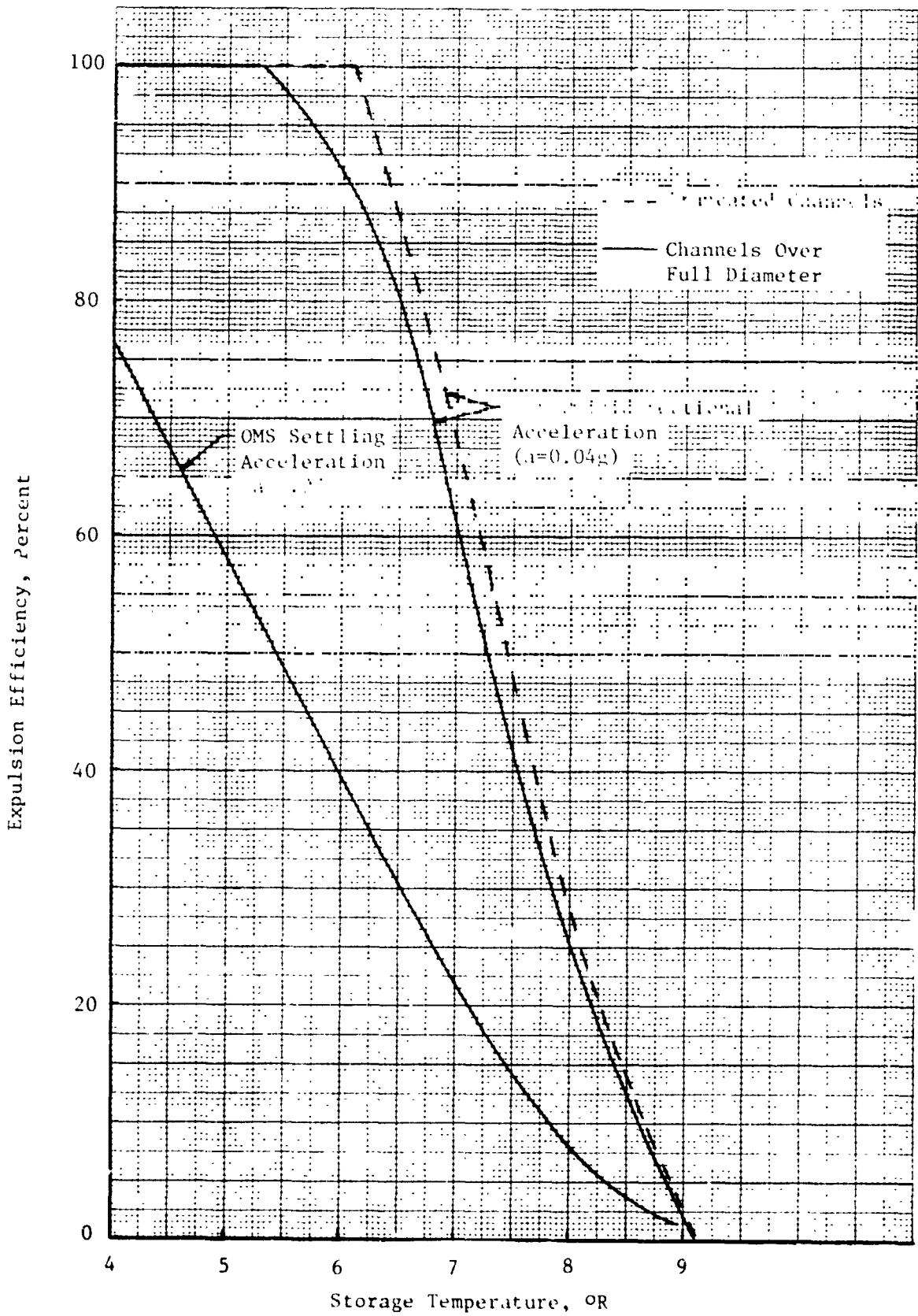
Figure IV-3   Helium Tank Expulsion Efficiency Based on
Hydrostatic Head Retention Only

2. Fluid Lines

Four different line types were sized for each cryogenic storage and supply tank. They are: (a) the outflow/abort line, (b) the inflow line, (c) the pressurization/vent line, and (d) the thermodynamic vent system lines. The characteristics of the fluid flow in each line vary greatly with the particular fluid and mission requirements. Several general assumptions were made in the analysis. The external piping, valves, and other flow or flow-metering components were assumed analogous to the baseline CFME for all tanks. Also, the lines were only sized for each category, not for each configuration, as previously defined in Table III-1. This ensured that the line sizes for the maximum conditions encountered in the mission for each category were applicable to all the configurations in that category. For example, the pressurization/vent line for the non-vacuum-jacketed 12.5 m^3 (440 ft^3) argon tank was sized to handle a higher flowrate during ground hold than the corresponding vacuum-jacketed tank. The line was sized for the former case and was assumed applicable, albeit conservative, for the latter configuration.

The flow analysis for the outflow/abort line, the inflow line, and the pressurization/vent line is identical. A friction factor, f, is defined as:

$$f = \frac{d}{L} \left[\frac{\Delta P}{1/2 \, \rho \, g_c \, \bar{\mathcal{V}}^2} \right] \qquad (9)$$

where d is the tube diameter, L is the tube length, ΔP is the pressure drop, ρ is the fluid density, and $\bar{\mathcal{V}}$ is the average velocity of the fluid. The data is only valid for incompressible flow (constant density) of Newtonian fluids. For the range of flowrates and fluids considered in this study, these criteria are met (Mach number less than unity, all fluids considered Newtonian).

To account for friction due to roughness of the pipe, a roughness factor, e, of 1.52 X 10^{-6}m (5.0 X 10^{-6} ft) was used for drawn tubing. A relative roughness, e/d, was then determined. To account for friction due to elbows, valves, flowmeters, and other flow apparatus, an equivalent length of straight pipe required to produce the same amount of friction was determined as:

$$L^* = nL$$

$$(10)$$

where L is the actual length of tubing, L* is the equivalent length, and n is a friction multiple which accounts for all the frictional losses due to the flow apparatus.

Substituting L* for L in Equation (9), an expression for tube diameter is obtained:

$$ d = \left[\frac{8 \; L^* \; \dot{m}^2}{\pi^2 \; g_c \; \rho} \; \frac{f}{\Delta P} \right]^{1/5} \tag{11} $$

where m is the mass flowrate and f is a function of the Reynolds number and the relative roughness. An iteration between tube diameter, Reynolds Number and relative roughness was made to determine the correct line size for the required flow rate.

Outflow/Abort Line

In all tank categories the abort flow conditions yielded a larger line diameter than the maximum outflow conditions, so the abort conditions sized the line. The large number of elbows, valves, flowmeters, and other flow apparatus increased the equivalent length, L*, considerably. The estimate used for this line was generally about 50L. The outflow/abort line sizes are shown in Table IV-7. The analysis is conservative in that the values for ρ, f, etc., are chosen at their limits which give the largest diameter. The pressure drop, ΔP, is chosen as the allowable drop in pressure to maintain subcooled or saturated liquid conditions. The temperature used to determine the state of the liquid at the inlet to the outflow/abort line is based on the results of mission simulations using CSAM (as discussed later in Section B of this chapter)

The results of Table IV-7 show that the CFME outflow/abort line diameter of 1.27-cm (0.50-in) must be modified for operation with the other fluids in the 0.62 m^3 (22.0 ft^3) tanks. The 12.5 m^3 (440 ft^3) oxygen tank (Category VII) has the largest diameter because of the large mass to be aborted in only 0.5 hr.

Inflow Line

The ground rule used for the inflow line analysis was that the 0.62 m^3 (22.0 ft^3) tanks are filled in 0.5 hr and the larger tanks are filled in 1.0 hr. It was assumed that tank cooldown must also be accomplished within this time constraint but that tank pre-chill had been performed previously. Estimates were made of the amount of fluid vaporized during cooldown. Two times the loaded mass was required to accomplish cooldown and loading for saturated hydrogen liquid at 101 kN/m^2 (14.7 psia), and proportionally less was required for the other liquids. The maximum inflow rates shown on Table IV-8 correspond to these conditions.

The inflow line diameters given in Table IV-8 were determined using an equivalent length, L*, 20 times the actual length of the inflow tubing. The allowable pressure drop, ΔP, used in sizing the inflow line is based on an inflow pressure of approximately 207 KN/m^2 (30.0 psia) and an internal tank pressure of 101 KN/m^2 (14.7 psia). The liquid at the entrance of the inflow line is assumed to be subcooled with a saturation pressure of 101 kN/m^2 (14.7 psia).

Table IV-7 Outflow/Abort Line Sizing

Category	Size	Fluid	Maximum Outflow Rate				Line Diameter	
			Mission		Abort			
			kg/hr	(lb/hr)	kg/hr	(lb/hr)	cm	(in)
Baseline	0.62 m³	H₂	1.50	(3.3)	82	(180)	1.3	(0.5)
I	0.62 m³	CH₄	0.016	(0.035)	249	(548)	2.6	(1.0)
II	0.62 m³	Ar	*	*	543	(1192)	2.7	(1.0)
III	0.62 m³	O₂	0.16	(0.35)	1340	(2948)	3.9	(1.5)
IV	0.62 m³	He	0.017	(0.037)	49	(108)	1.5	(0.6)
V	12.5 m³	Ar	2.5	(5.6)	10900	(23980)	7.7	(3.0)
VI	12.5 m³	CH₄	103	(227)	4780	(10516)	7.7	(3.0)
VII	12.5 m³	O₂	4460	(9812)	26700	(58740)	11.4	(4.5)
VIII	37.4 m³	H₂	815	(1793)	2440	(5368)	7.7	(3.0)

*Mission outflow through thermodynamic vent lines.

Table IV-8 Inflow Line Sizing

Category	Size	Fluid	Maximum Inflow Rate		Inflow Line Diameter	
			(kg/hr)	(lb/hr)	cm	(in)
Baseline	0.62 m³	H₂	154	(339)	1.3	(0.5)
I	0.62 m³	CH₄	828	(1822)	1.9	(0.75)
II	0.62 m³	Ar	2840	(6248)	1.9	(0.75)
III	0.62 m³	O₂	2310	(5082)	1.9	(0.75)
IV	0.62 m³	He	303	(660)	1.3	(0.5)
V	12.5 m³	Ar	28400	(62480)	6.3	(2.5)
VI	12.5 m³	CH₄	7940	(17470)	5.0	(2.0)
VII	12.5 m³	O₂	23200	(51040)	5.7	(2.25)
VIII	37.4 m³	H₂	4890	(10760)	5.7	(2.25)

The inflow line for the 0.62 m² (22.0 ft³) storage tanks is 1.9-cm (0.75-in) except for liquid helium, which is the same as the CFME inflow line. The larger tanks have larger inflow line diameters. A comparison with the outflow/abort line sizes of Table IV-7 indicates that the inflow lines are smaller in diameter for all cases, indicating that a single tank penetration can be used for both the filling and draining functions.

Pressurization/Vent Line

The fluid dynamic analysis approach used for the outflow/abort lines and the inflow lines is also applicable to the pressurization/vent line.

There are four conditions which can determine the pressurization/vent line diameter:

(1) The maximum flowrate of helium for pressurization, which occurs during draining of the tank at abort conditions.

(2) The flowrate of evaporating fluid within the tank which must be vented due to increased heat flux if air, or the storage fluid diffuses into the volume between the tank wall and the outermost surface on the storage vessel while the tank is on the ground.

(3) The liquid venting flowrate required to preclude excessive pressure buildup, assuming liquid covers the vent port in the low-g, on-orbit case.

(4) The vapor flowrate resulting from initial liquid filling of the tank when the entire tank and inflow lines are at ambient conditions. The flashing of vapor continues until the tank is sufficiently chilled.

It has been determined that for all fluids the first case is not a determining factor. Vapor venting during chilldown is not critical if adequate pre-chill is performed. It was assumed that sufficient time was available to pre-chill, precluding rapid vapor flashing on the walls of the tank and large gas venting rates. The most critical condition is likely Case (2), where condensed air or storage fluid in the vacuum annulus (or alternately, an ineffective purged insulation for the non-vacuum-jacketed cases) causes a significant increase in the heat flux into the stored cryogen. The pressurization/vent line was therefore sized for this condition. A heating rate of 1580 W/m² (500 Btu/hr-ft²) was assumed for the helium and hydrogen tanks and 474 W/m² (150 Btu/hr-ft²) was used for the other tanks. The higher heat flux is due to air condensation while the latter heat flux results from gaseous heat transfer. The equivalent length, L*, used in the analysis was 20 times the actual length, L. The results are presented in Table IV-9. The allowable pressure drop, ΔP, used in sizing this line is based on the ground vent operating at 345 KN/m² (50.0 psia), with exit conditions maintained above the highest attainable melting point of the fluid to prevent line freezing.

Table IV-9 Pressurization/Vent Line Sizing

Category	Size	Fluid	Maximum Vent Rate		Line Diameter	
			kg/hr	(lb/hr)	cm	(in)
Baseline	0.62 m^3	H$_2$	52	(116)	1.3	(0.5)
I	0.62 m^3	CH$_4$	12	(27)	1.3	(0.5)
II	0.62 m^3	Ar	40	(89)	1.3	(0.5)
III	0.62 m^3	O$_2$	30	(67)	1.3	(0.5)
IV	0.62 m^3	He	1870	(4130)	3.2	(1.25)
V	12.5 m^3	Ar	296	(653)	2.5	(1.00)
VI	12.5 m^3	CH$_4$	91	(201)	1.9	(0.75)
VII	12.5 m^3	O$_2$	224	(494)	1.9	(0.75)
VIII	37.4 m^3	H$_2$	900	(1980)	4.3	(1.75)

Thermodynamic Vent System Line Analysis

The major consideration in analyzing the two-phase fluid dynamics in the lines of the thermodynamic vent system (TVS) is the interaction of the various forces acting on the fluid--surface tension, gravitational, viscous and inertial. Since the heat exchangers near the exit of the Viscojets contain two-phase fluid, the flow patterns and the heat tra.sfer mechanisms between the fluid and tank wall are important in the overall thermal efficiency of design. The predominant one-g and low-g flow patterns of the vapor and liquid are a matter of opinion, although capillary effects appear to strongly overpower viscous effects. The critical parameters for sizing the heat exchangers are the Weber number (We, ratio of inertia force-to-surface tension force), the Capillary number (Ca, ratio of viscous force-to-surface tension force), and the Bond number (Bo, ratio of gravitational force-to-surface tension force). If these dimensionless groups have values on the order of one or less over the region of two-phase flow, then the line diameter is acceptable. (A more thorough discussion of TVS operation is contained in Appendix A.)

Table IV-10 gives the results of the TVS line sizing analysis. The maximum allowable pressure drop after the fluid has exited the flow restrictor (Viscojet) is set at 34 KN/m^2 (5.0 psia). The viscous and inertial forces are small due to the low mass flowrates, yielding Weber numbers and Capillary numbers on the order of 10^{-3} or less. The gravitational forces are important prior to orbit, so the maximum Bond number (when the tank is at one-g) is tabulated for each category.

Table IV-10 Thermodynamic Vent System Line Sizing

Category	Fluid	Maximum Vent Rate		Maximum Bond Number (Dimensionless)	Line Diameter	
		kg/hr	(lb/hr)		mm	(in)
Baseline	H_2	0.04	(0.09)	0.21	4.8	(0.19)
I	CH_4	0.02	(0.04)	0.22	4.8	(0.19)
II	Ar	0.05	(0.11)	0.73	4.8	(0.19)
III	D_2	0.05	(0.11)	0.60	4.8	(0.19)
IV	He	0.001	(0.002)	0.80	1.6	(0.063)
V	Ar	0.05	(0.11)	0.73	4.8	(0.19)
VI	CH_4	0.20	(0.44)	0.22	4.8	(0.19)
VII	O_2	0.05	(0.11)	0.60	4.8	(0.19)
VIII	H_2	0.20	(0.44)	0.21	4.8	(0.19)

B. **Steady State Thermal Analysis**

A steady state thermal analysis was performed for each preliminary conceptual design identified in Task I. The analysis for each configuration involved insulation selection, structural support thermal evaluations and thermal performance of the total tankage for the specified missions. The rate of heat addition to each storage tank, vent rates, and helium pressurant requirements were established for cryogenic liquid expulsion under orbital conditions.

1. Insulation Selection

Parametric insulation performance data were generated for each of the 12.5 m^3 (440 ft^3) tanks and the 37.4 m^3 (1320 ft^3) hydrogen tank. The optimum insulation thickness, (Δt^*), is that thickness which minimizes the mass of vented fluid (M_{vf}) plus the mass of insulation on the tank (M_{MLI}). Mathematically, this reads

$$\Delta t \rightarrow \Delta t^* \text{ when } \frac{d(M_{vf} + M_{MLI})}{d(\Delta t)} = 0 \tag{12}$$

A fluid value factor (a) was added to this equation to "weigh" the relative importance of the fluid.

$$\Delta t \rightarrow \Delta t^* \text{ when } \frac{d(a\ M_{vf} + M_{MLI})}{d(\Delta t)} = 0 \tag{13}$$

This increases the optimum insulation thickness for higher values of a. For this study a was set equal to two for hydrogen (analogous to the CFME baseline); a was set equal to one for all other fluids.

For a spherical tank, the mass of MLI is given by:

$$M_{MLI} = \frac{4}{3}\pi \rho \left[(r_1 + \Delta t)^3 - r_1^3 \right] \tag{14}$$

where

ρ = density of MLI
r_1 = radius to inner boundary of MLI
Δt = thickness of MLI

The mass of fluid vented to maintain tank pressure is

$$M_{vf} = \frac{\dot{q}_{tot}\theta}{h_{fg}} \tag{15}$$

where
θ = length of mission
h_{fg} = heat of vaporization of fluid
$\dot{q}_{tot}$ = total heat transfer into fluid

The term $\dot{q}_{tot}$ is broken down into four heat leaks, giving:

$$\dot{q}_{supt} = k_{supt} A_{supt} \Delta T / L_{supt} \qquad \text{(Supports)}$$

$$\dot{q}_{top} = k_{top} A_{top} \Delta T / L_{top} \qquad \text{(Top Penetrations)}$$

$$\dot{q}_{bot} = k_{bot} A_{bot} \Delta T / L_{bot} \qquad \text{(Bottom Penetrations)}$$

$$\dot{q}_{MLI} = k_{MLI} \frac{4\pi r_1 (r_1 + \Delta t)\Delta T}{\Delta t} \qquad \text{(Multi-layer Insulation)}$$

so that

$$M_{vf} = \frac{\Delta t\, \theta}{h_{fg}} \left[\frac{k_{supt} A_{supt}}{L_{supt}} + \frac{k_{top} A_{top}}{L_{top}} + \frac{k_{bot} A_{bot}}{L_{bot}} + 4\pi k_{MLI} r_1 (1 + \frac{r_1}{\Delta t}) \right] \tag{16}$$

Substituting Equations (16) and (14) into (13) and solving, gives:

$$\Delta t^* = \frac{1}{2}\left[\left(r_1^2 + 4\sqrt{\frac{k_{MLI}\, r_1^2\, a\, \theta \Delta T}{\rho\, h_{fg}}} \right)^{\frac{1}{2}} - r_1 \right] \tag{17}$$

For the cylindrical tank a similar analysis can be done by changing the volume and area in Equations (14) and (16) and differentiating $aM_{vf} + M_{MLI}$ using different values for Δt.

Parametric MLI optimization curves for the 12.5 m³ (440 ft³) oxygen and methane tanks are presented in Figures IV-4 and IV-5. Optimization for the 37.4 m³ (1320 ft³) spherical hydrogen tank is shown in Figure IV-6. A comparable curve is not presented for the 12.5 m³ (440 ft³) argon tank because the calculated MLI thickness was in excess of the maximum 10-cm (4-in) considered in this study.

The determination of the optimum thickness for helium-purged or nitrogen-purged MLI used a modified version of Equation (17). For the time in which the non-vacuum-jacketed tank is operating on the ground, (θ_g), the thermal conductivity of the MLI purged with helium is given by a value, k_{gp}, almost three orders of magnitude greater than k_{MLI}. After the tank is transferred to orbit, the remainder of the mission (θ_s) is modelled with the MLI in a perfect vacuum. This analysis modified Equations (15) and (16), and yielded an optimum insulation thickness given by:

$$\Delta t^* = \frac{1}{2}\left[\left(r_i^2 + 4\sqrt{\frac{(k_{MLI}\,\theta_s + k_{gp}\,\theta_g)\,r_1^2\,a\,\Delta t}{\rho\,h_{fg}}}\right)^{\frac{1}{2}} - r_1\right] \tag{18}$$

For example, the 12.5 m³ (440 ft³) argon tank mission calls for a 4-hour ground hold (θ_g = 4 hr) and 7-year stationkeeping (θ_s = 61360 hr), the sum $k_{MLI}\,\theta_s + k_{gp}\,\theta_g$ is very close to $k_{MLI}\,\theta_s$.

A combination of nitrogen-purged MLI on top of SOFI was considered as an attractive alternative insulation concept to eliminate the helium purge requirement for ground hold. The MLI thickness is sized by the orbit requirements, since evacuated MLI is about 3 orders of magnitude better in thermal performance then SOFI. The SOFI thickness is determined such that the interface temperature is above the liquifaction temperature for nitrogen. Since the tanks considered are typically large in diameter compared to the MLI and SOFI thicknesses, the problem can be analyzed using planar surfaces:
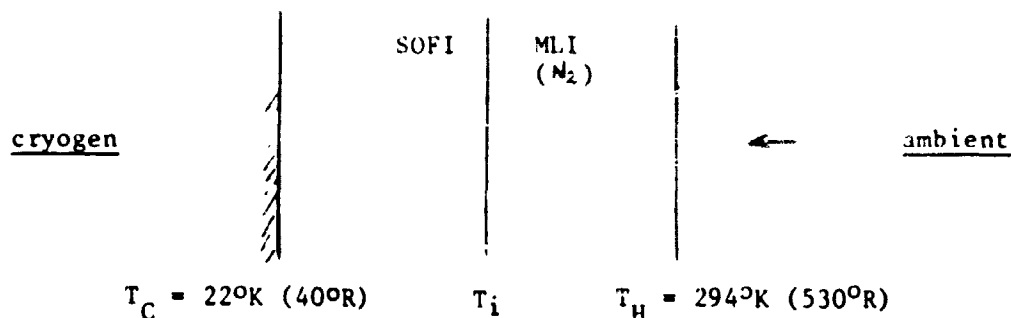
During ground hold the MLI is filled with nitrogen gas. The system energy balance yields

$$\dot{q} = \frac{k_{SOFI}\,A\,(T_i - T_c)}{t_{SOFI}} = \frac{k_{N_2}\,A\,(T_H - T_i)}{t_{MLI}}$$
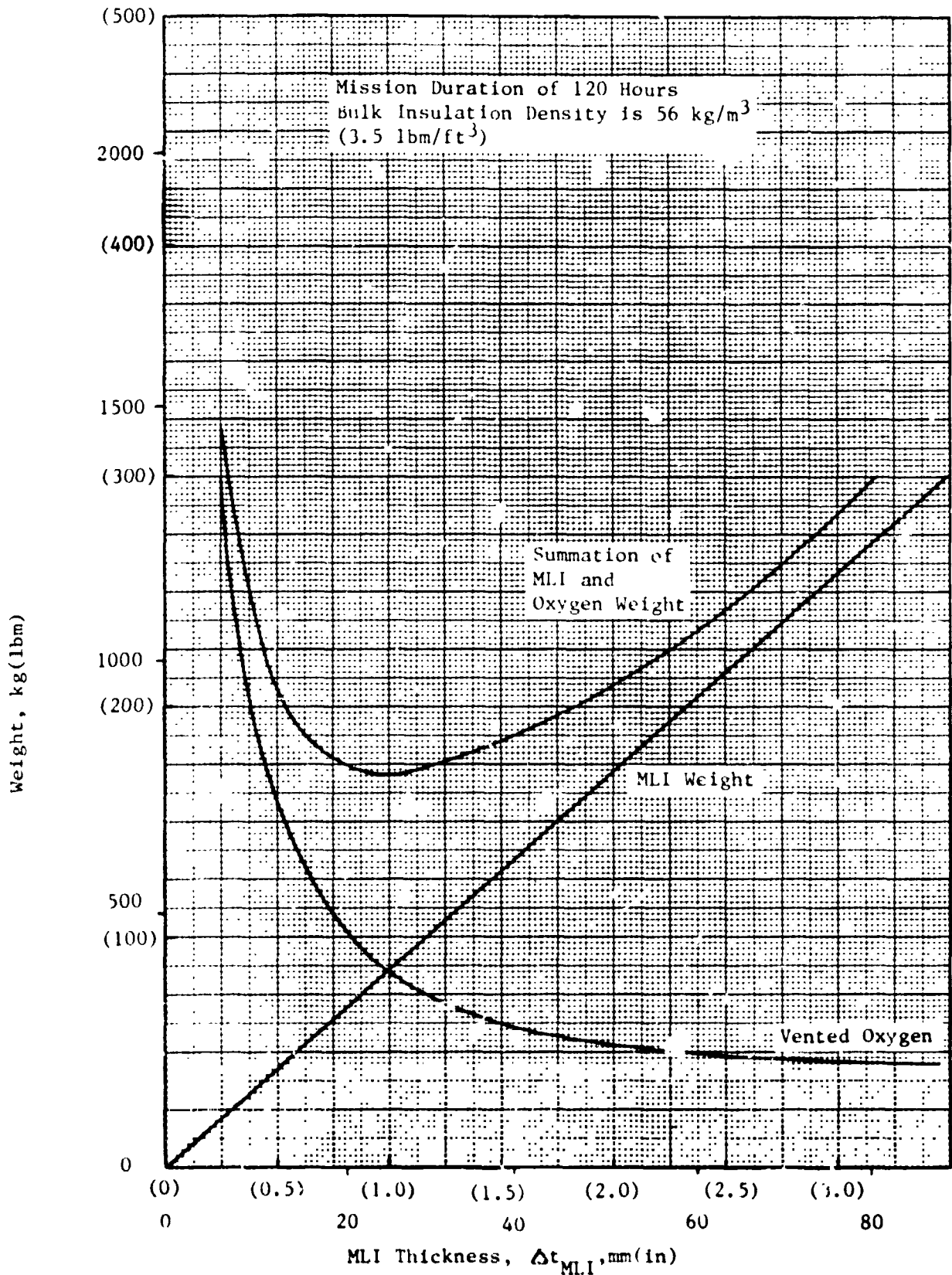
Figure IV-4 Optimization of 12.46 m³ (440 ft³) Spherical
Oxygen Tank Multilayer Insulation Thickness
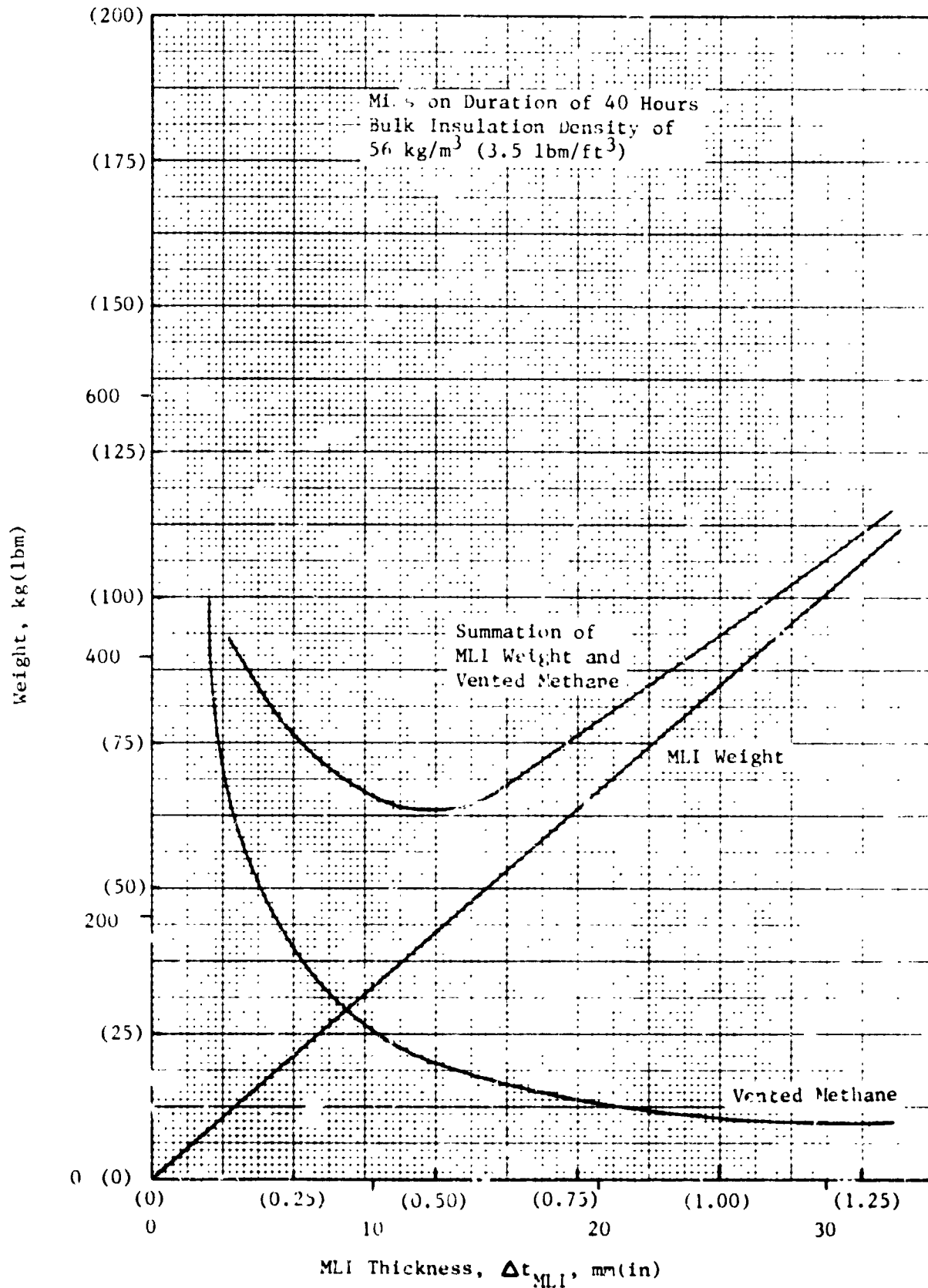
Figure IV-5   Optimization of 12.46 m³ (440 ft³) Spherical
Methane Tank Multilayer Insulation Thickness

IV-23
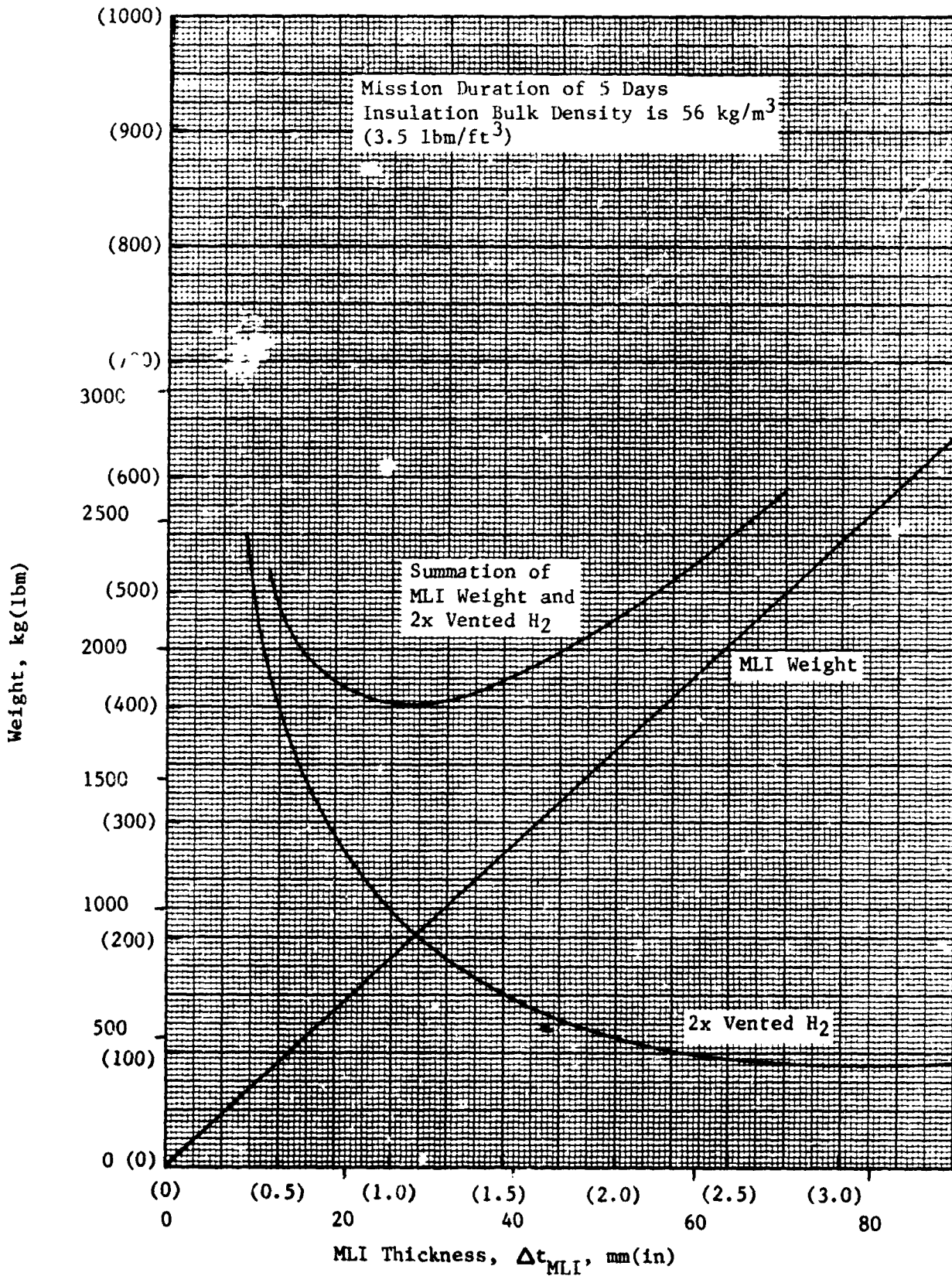
Figure IV-6 Optimization of 37.4 m³ (1320 ft³) Spherical
Hydrogen Tank Multilayer Insulation Thickness

IV-24

or

$$\frac{t_{SOFI}}{t_{MLI}} = \left(\frac{k_{SOFI}}{k_{N_2}}\right)\left(\frac{T_i - T_c}{T_H - T_i}\right)$$

The nitrogen thermal conductivity is given by $k(T) = 1.65 \times 10^{-2} + .148 \times 10^{-3} T^{.75}$ (from CSAM). Using this in the above energy balance, the N_2 thermal conductivity can be integrated from T_i to T_H to yield

$$k_{N_2} = -0.165 \times 10^{-2} + 0.845 \times 10^{-4} \left(\frac{T_H^{1.75} - T_i^{1.75}}{T_H - T_i}\right)$$

The nominal SOFI thermal conductivity is given by

$$k_{SOFI} = 0.0017 + 2.45 \times 10^{-5} T_m$$

and the plus 2σ (95% confidence) SOFI thermal conductivity is given by

$$k_{SOFI} = .0046 + .00002452 T_m, \text{ (Ref 38)}$$

T_m is the median temperature between T_c and T_i. Both of these expressions were used in the energy balance to compute the SOFI thickness.

The ratio of SOFI to MLI thickness was determined for several interface temperatures, using both the nominal and plus 2σ SOFI thermal conductivities. The results are plotted in Figure IV-7. Once the MLI thickness was determined using the orbital requirements, Figure IV-7 was used to determine the required SOFI thickness to yield a desired interface temperature. For example, the MLI thickness required for the 37.4 m^3 (1320 ft^3) spherical hydrogen tank was 1.75-cm (0.69-in) for a 5 day mission. Nitrogen liquifaction temperature at one atmosphere is 77°K (139°R). Using 78°K (140°R) and t_{MLI} = 1.75-cm (0.69-in), Figure IV-7 indicates that

$$\frac{t_{SOFI}}{t_{MLI}} = 0.1 \text{ (nominal)}$$

and

$$\frac{t_{SOFI}}{t_{MLI}} = 0.18 \text{ (plus } 2\sigma)$$
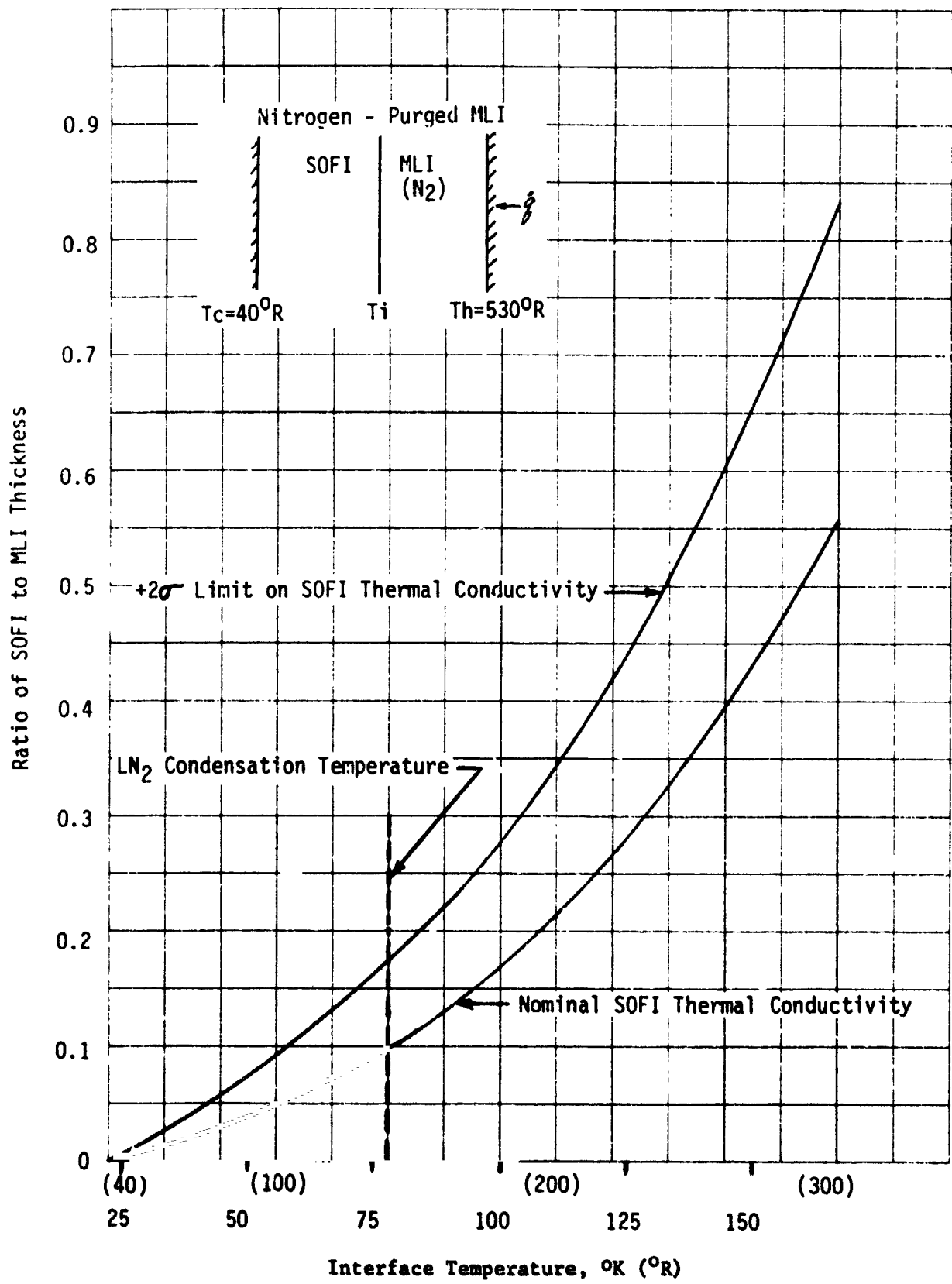
Figure IV-7 Variation of Ratio of SOFI Thickness to MLI Thickness with
Interface Temperature

IV-26

so that

$$t_{SOFI} = 0.18 \text{ cm } (0.069 \text{ in}) \text{ (nominal)}$$

and

$$t_{SOFI} = 0.32 \text{ cm } (0.12 \text{ in}) \text{ (plus } 2\sigma)$$

Discussions with Martin Marietta personnel working the External Tank indicated that the minimum application thickness using current technology is 1.3-cm (0.5-in). This is addressed in greater detail in Chapter VI.

A plot of MLI thickness for both nominal and +2σ SOFI thermal conductivities is presented in Figure IV-8 for various SOFI/MLI interface temperatures. For example, in the case of the previously mentioned MLI thickness of 1.75-cm (0.69-in), the interface temperature would be about 178°K (320°R), for the nominal SOFI, and about 156°K (280°R) for the +2σ SOFI thermal conductivity. In both cases the interface would be far above the liquifaction temperature of nitrogen at one atmosphere pressure.

A comparison was made between helium-purged MLI and the nitrogen-purged MLI/SOFI combination. For a given MLI thickness, the heat flux to the tank is about an order of magnitude greater for the helium-purged system than the nitrogen-purged combination. Figure IV-9 is a plot of heat flux versus MLI thickness for helium-purged and nitrogen-purged/SOFI insulations, with an interface temperature of 78°K (140°R). Note that for both systems the MLI thickness requirements are identical, since the MLI is sized for orbital requirements. For a 37.4 m³ (1320 ft³) spherical hydrogen tank with 1.75-cm (0.69-in) of MLI and a 4-hour ground hold, the helium-purged MLI would boiloff 2150 kg (4740 lb) more than the nitrogen purged MLI (2230 kg versus 73 kg), (4900 lb versus 160 lbm), or the helium-purged system would lose 84 percent of the original loaded hydrogen while the combination would lose 3 percent.

The insulation systems selected for the thermal performance studies are listed in Table IV-11 for each of the 13 configurations evaluated. Ground hold requirements varied from 28-hours to topping immediately prior to lift-off; lower final tank pressures and/or reduction in vented fluid are available in all cases if the latter ground hold situation is followed. For the shorter orbital missions, weight is quite sensitive to the ground hold condition and this must be adequately accounted for in comparing these designs with other study results.

Purged MLI systems allow larger heat inputs to the cryogens during ground hold. This can result in reductions of liquid density due to vigorous boiling. A new bulk density can be determined by calculating the volume change due to bubble formation in the saturated cryogen. The bulk density can be expressed as

$$\bar{\rho} = \frac{m_l}{V + \Delta V}$$
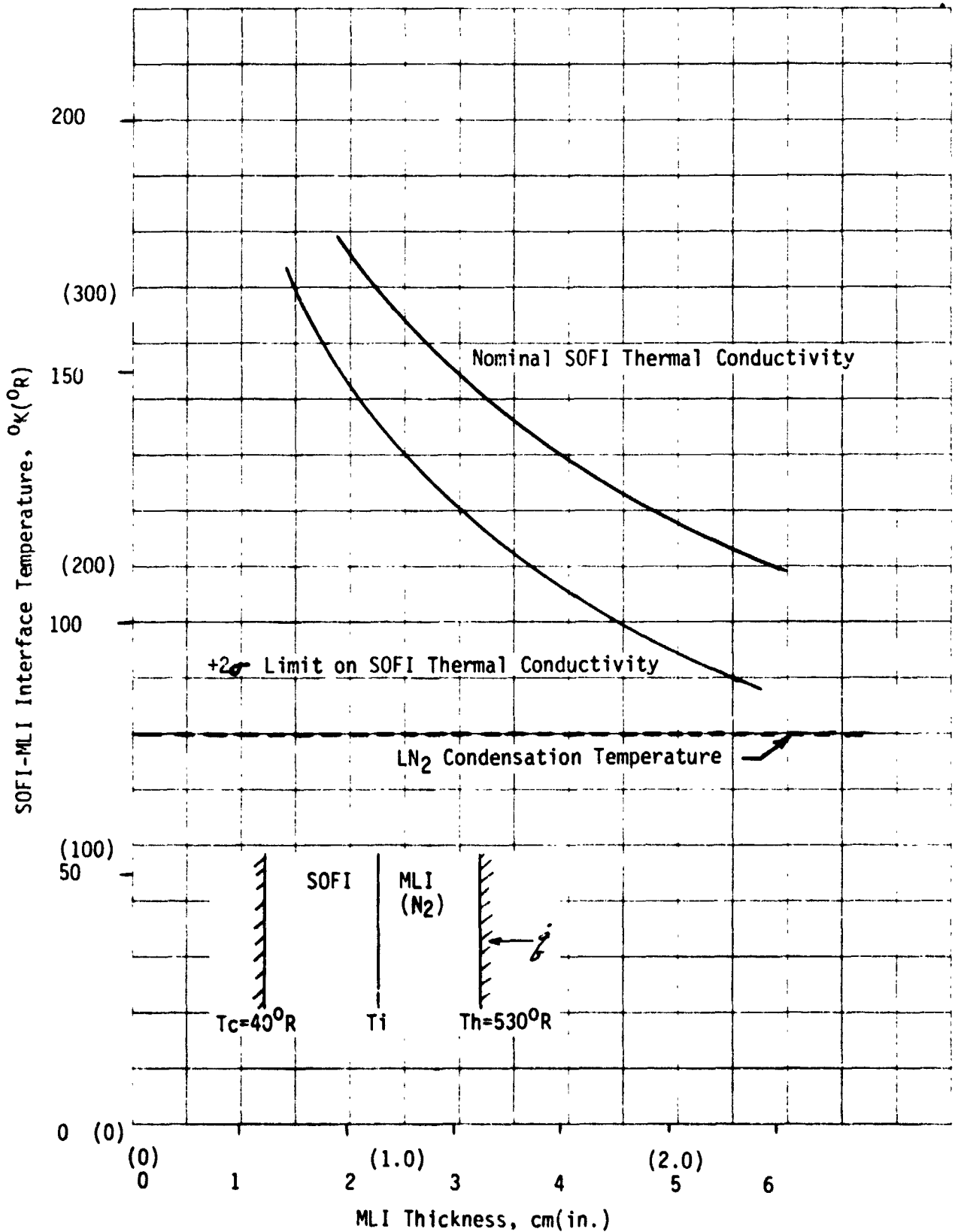
Figure IV-8 Variation of SOFI/MLI Interface Temperature with MLI Thickness

IV-28
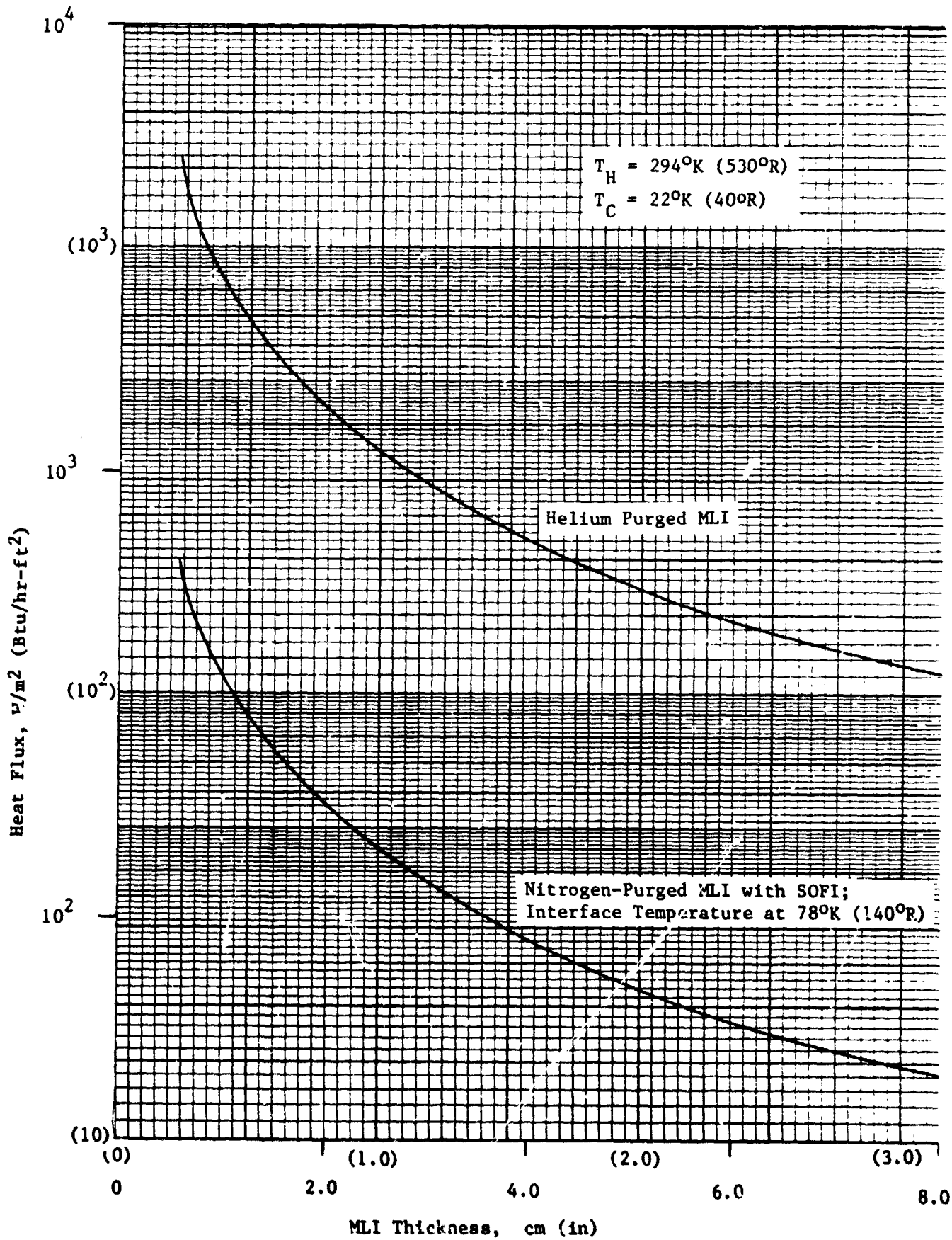
Figure IV-9 Comparison of Helium-Purged MLI Heat Flux with Nitrogen-Purged
MLI/SOFI Heat Flux

Table IV-11 Selected Insulation for the Study Configurations

Config- uration	Size	Fluid	Ground Hold Time	Insulation	Description
CFME	0.62 m^3	H$_2$	28-hr	3.2-cm (1.25-in)	MLI/vacuum jacket
1	0.62 m^3	CH$_4$	28-hr	4.7-cm (1.85-in)	MLI/vacuum jacket
2	0.62 m^3	Ar	28-hr	10-cm (4.0-in)	MLI/vacuum jacket
3	0.62 m^3	O$_2$	28-hr	3.2-cm (1.25-in)	MLI/vacuum jacket
4	0.62 m^3	He	28-hr	3.2-cm (1.25-in)	MLI inside & outside He VCS/vacuum jacket
5	12.5 m^3	Ar	4-hr	10-cm (4.0in)	MLI/vacuum jacket
6	12.5 m^3	Ar	4-hr	10-cm (4.0-in)	MLI/Nitrogen purged
7	12.5 m^3	Ar	4-hr	10-cm (4.0-in)	MLI/Nitrogen purged
8	12.5 m^3	CH$_4$	28-hr	1.2-cm (0.5-in)	MLI/vacuum jacket
9	12.5 m^3	CH$_4$	*	1.2-cm (0.5-in)	MLI/Nitrogen purged
10	12.5 m^3	O$_2$	28-hr	2.0-cm (0.8-in)	MLI/vacuum jacket
11	12.5 m^3	O$_2$	4-hr	6.1-cm (2.4-in)	MLI/Nitrogen purged
12	37.4 m^3	H$_2$	*	1.2-cm (0.5-in)SOFI 1.5-cm (0.57-in)MLI	Nitrogen-purged
13	37.4 m^3	H$_2$	*	1.2-cm (0.5-in)SOFI 1.8-cm (0.69-in)MLI	Nitrogen-purged

* Topping just prior to lift-off

where m_v is the liquid mass, V it's volume and ΔV the volume change due to vaporization. The term ΔV can be written as

$$\Delta V = m_v \left(\frac{\rho_1 - \rho_v}{\rho_1 \rho_v} \right)$$

where m_v is the mass of liquid vaporized.

The time interval to determine how much vaporized liquid is instantaneously entrained in the bulk liquid is the rise time for a bubble (i.e. the tank depth divided by bubble velocity). The assumption is that initially a bubble forms on the bottom of the tank and then rises to the surface. A column of bubbles rises and continuous boiling occurs. A change in liquid density occurs, remaining relatively constant with time. The bubble velocity is given in Reference 30 as:

$$v = \left(\frac{4 \sigma g}{\rho_1} \right)^{\frac{1}{4}}$$

so that

$$m_v = \frac{\dot{q}}{h_{fg}} \left(\frac{\rho_1 d^4}{4 \sigma g} \right)^{\frac{1}{4}}$$

where d is the liquid depth, and σ the surface tension.

The resulting bulk liquid densities for the 12.5 m^3 (440 ft^3) and 37.4 m^3 (1320 ft^3) tanks are given in Table IV-12. Oxygen is reduced in density by less than 1%. The methane density is reduced by 2.5%. The argon density is also reduced by less than 1%. Finally the hydrogen density in the large tank is reduced by 5%. For a given tank size, the bulk density change is most sensitive to the mass of liquid vaporized (i.e. heat input to the tank). Also tank depth affects bubble rise time, so that deeper tanks have a greater density change. Pressure also has a minor effect on the bulk density change. Although increasing pressure slightly increases the amount of liquid vaporized, the density increase of both phases reduces the density ratio term significantly, so that the bulk density is not reduced as much. These density changes should be considered in more detailed mission studies where purged insulation systems are defined.

Table IV-12   Effect of Purged Insulation Heat Input on Liquid Density

	P = 100 KN/m² (15 psia)			
	(440 ft³) Oxygen	(440 ft³) Methane	(440 ft³) Argon	(1320 ft³) Hydrogen
Density (kg/m³) (1bm/ft³)	1140 (71.23)	22.30 (26.36)	1394.50 (87.05)	70.80 (4.42)
Heat Input (W) (Btu/hr)	1500 (5145)	6775 (23120)	915 (3120)	13930 (47550)
Tank Depth(m) (ft)	2.9 (9.4)	2.9 (9.4)	2.9 (9.4)	12.0 (39.2)
New Bulk Density (kg/m³) (1bm/ft³)	1138 (71.04)	418.4 (26.12)	1392 (86.91)	67.9 (4.24)
Density Ratio	0.997	0.991	0.998	0.959

2. Structural Support Thermal Evaluation

Thermal analysis of the structural supports for the preliminary conceptual designs was accomplished with the CSAM program. The analysis is straight-forward, using nodal networks and accepted computational techniques to determine the temperature distributions and heat leaks of the tank assemblies and their support structures. The internal composite trunnions for the 0.62 m³ (22 ft³) tanks and the external composite struts for the larger tanks deserve special attention because of the pertinence of the results to overall thermal performance.

Internal Trunnions - CFME Size Tanks

A steady-state analysis of the heat leak through the trunnion supports was made, and the temperature distributions within the trunnion calculated. This analysis used a three-dimensional nodal model of the trunnion and the CSAM program. A diagram of the trunnion supports showing how the geometry was divided into nodes for conducting the analysis is presented in Figure IV-10.

The tank pressure for the cases analyzed was 276 KN/m² (40 psia) and the low temperature heat sink was considered to be the same as the saturation temperature for the fluid in the tank. Both the fixed and sliding-end trunnion configurations were analyzed for each of the fluids. Wall thicknesses and outer diameter of the trunnion vary with fluid and are listed along with
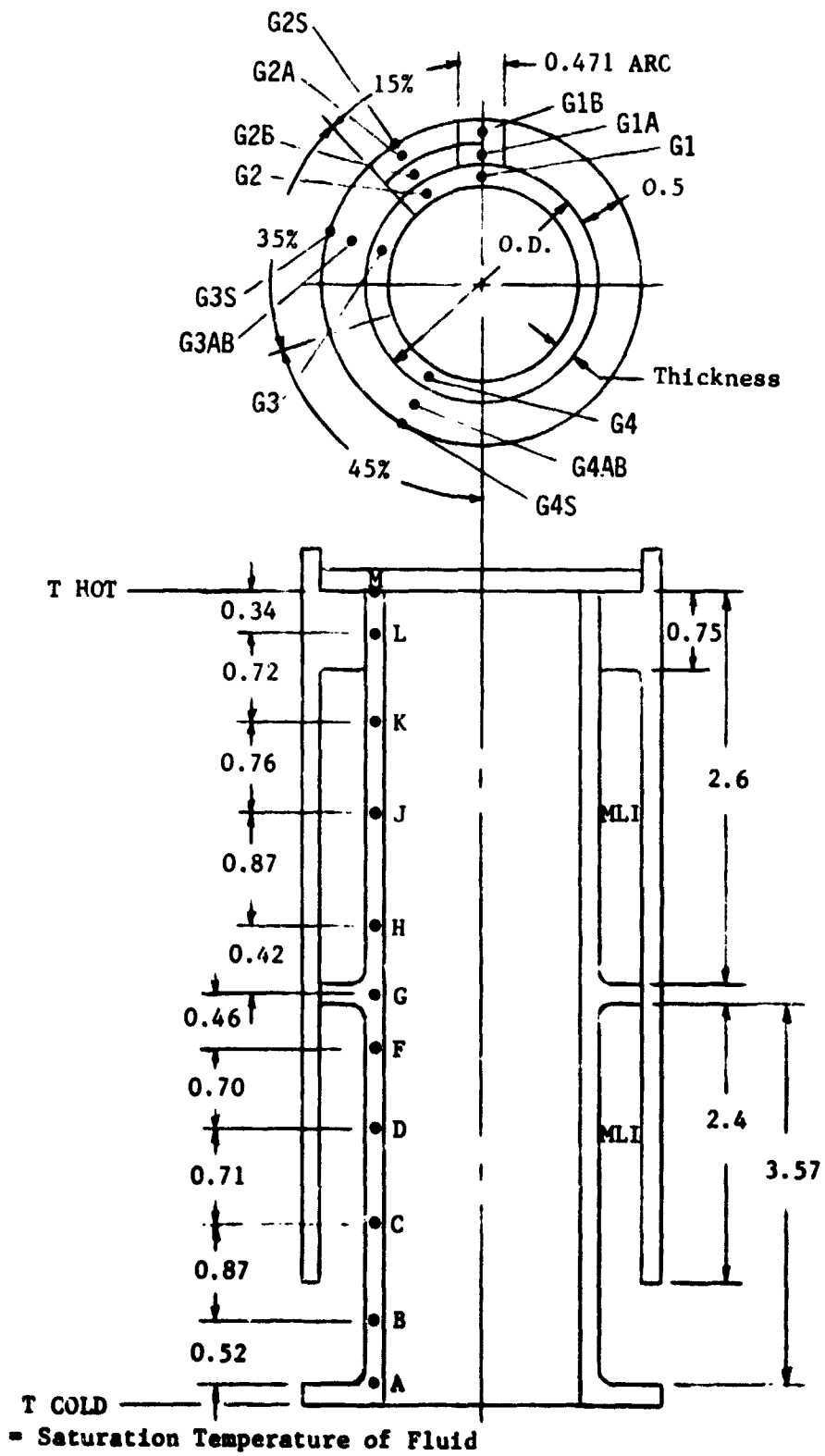
Figure IV-10   Trunnion Support Node Diagram

saturation temperature of the fluid and steady state heat leak for the trunnions in Table IV-13. The heat leak through both the fixed and sliding trunnions is nearly identical (within 2-3 percent) and so only a single value is given in Table IV-13 for each fluid. Steady-state temperatures at various locations along the length of the trunnion (corresponding to the points noted in Figure IV-10) are listed in Table IV-14.

Table IV-13 Typical Trunnion Thermal Characteristics for 0.62 m³ (22 ft³) Storage Tank Assemblies

Trunnion Geometry	Para-Hydrogen	Argon	Methane	Oxygen	Helium
Trunnion O.D., cm. (in)	5.0 (2.0)	6.4 (2.5)	5.0 (2.0)	6.4 (2.5)	5.0 (2.0)
Trunnion Thickness, cm (in)	0.38 (0.15)	1.14 (0.45)	1.02 (0.40)	0.89 (0.35)	0.51 (0.20)
Tsat at 276 KN/m²,°K (40 psia), (°R)	22 (40)	98 (176)	126 (226)	101 (182)	8.3 (15)
Trunnion Heat Leak,* Watt (Btu/hr) (fixed and sliding)	1.0 (3.37)	2.53 (8.62)	1.64 (5.61)	2.03 (6.92)	1.22 (4.17)

*External Temp = 393° K (708° P)

An evaluation was made of the reduction in heat leak through the trunnion obtained by intercepting a portion of the incoming heat flux with vent fluid in the VCS lines (a thermal short between the trunnion and VCS is built into each support). A plot of heat leak versus temperature drop between the storage tank and node D on the trunnion is presented in Figure IV-11. The amount of heat intercepted by the VCS line versus temperature drop between node D and the VCS line is presented in Figure IV-12. This data was used to optimize the reduction of heat leak through the trunnions as a function of VCS operations as determined by the thermal performance model (CSAM).

Reductions in trunnion heat leak from the zero intercept condition (no VCS connection), as a function of the amount of heat intercepted at node D are shown in Figure IV-13. The relationship for each fluid is linear and varies little from fluid to fluid. Similarly, reductions in trunnion heat leak as a function of the temperatures at node D are shown in Figure IV-14. The endpoints of the curves represent the idealized conditions where the temperatures at node D are equal to the fluid saturation temperatures and the reduction in heat leak is equal to the maximum heat leak through the trunnions, as indicated previously in Table IV-13.

Table IV-14 Steady-State Temperatures for Composite Trunnions Designed for 0.62 m^3 (22 ft^3) Tank Assemblies*

Location on Trunnion	Parahydrogen Tsat = 22° K (40° R)	Argon Tsat = 98° K (176° R)	Methane Tsat = 126° K (226° R)	Oxygen Tsat = 101° K (182° R)	Helium 4 Tsat = 8.3° K (15° R)
A	97 (54)	194 (108)	239 (133)	199 (111)	82 (46)
B	235 (131)	272 (151)	302 (168)	273 (152)	224 (124)
C	367 (204)	369 (205)	387 (215)	368 (204)	354 (19/)
D	451 (251)	436 (242)	447 (248)	433 (241)	436 (242)
F1	537 (298)	501 (278)	509 (283)	⁻01 (278)	514 (286)
G1	598 (332)	550 (306)	555 (308)	549 (305)	577 (321)
G2A	619 (344)	590 (328)	595 (331)	586 (326)	605 (336)
G3AB	598 (332)	569 (316)	571 (317)	562 (312)	581 (323)
G4S	604 (336)	577 (321)	574 (319)	571 (317)	589 (327)
H	594 (330)	558 (310)	556 (309)	549 (305)	575 (319)
J	626 (348)	601 (334)	589 (327)	584 (324)	609 (338)
K	657 (365)	646 (359)	622 (346)	619 (344)	643 (357)
L	687 (382)	693 (385)	655 (364)	655 (364)	678 (377)
M	694 (386)	695 (386)	667 (371)	665 (369)	686 (381)

* Tank Pressure = 276 KN/m^2 (40 psia)
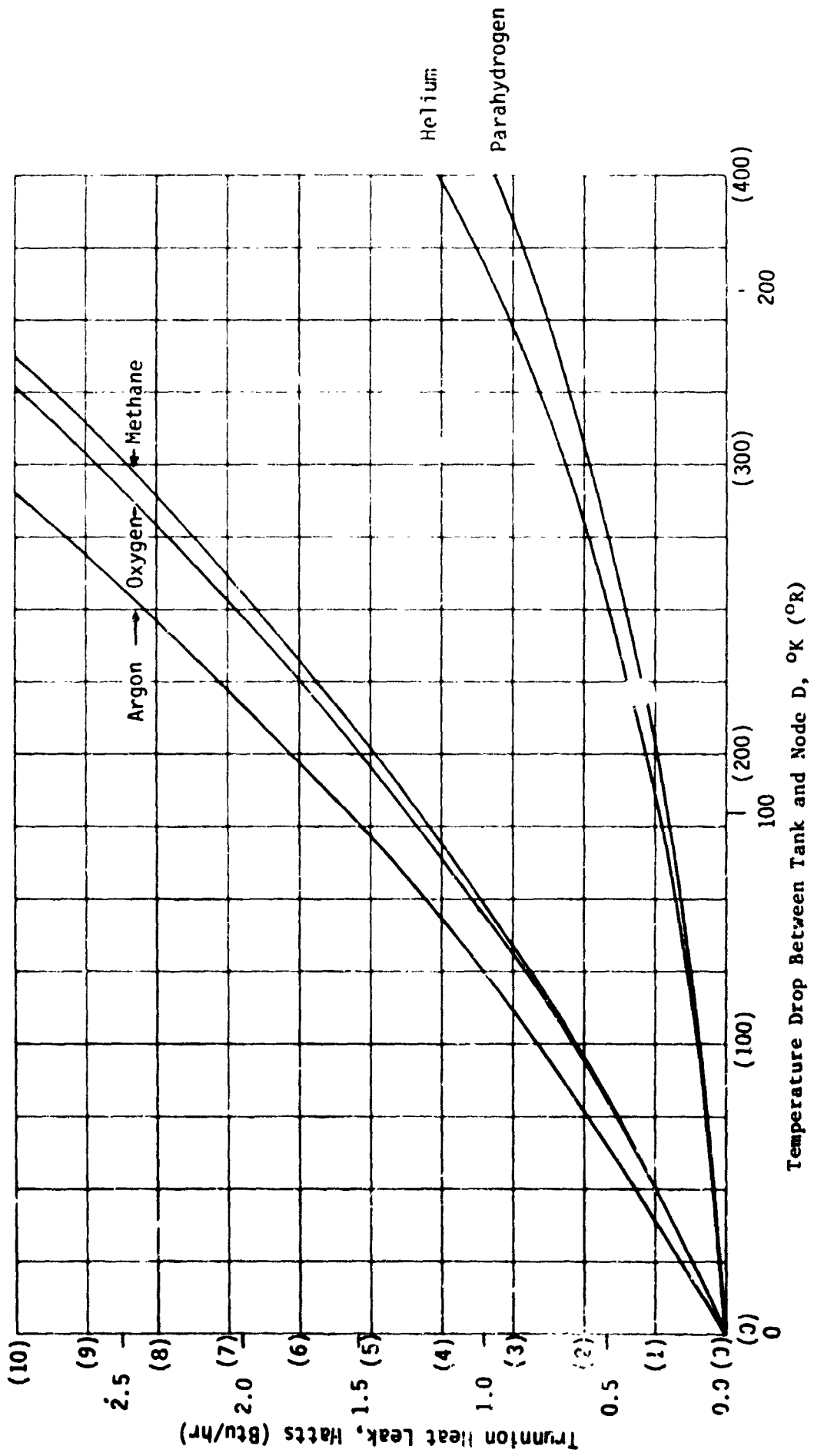
Figure IV-11 Trunnion Heat Leak versus Temperature Drop Between Tank and Node D

IV-36
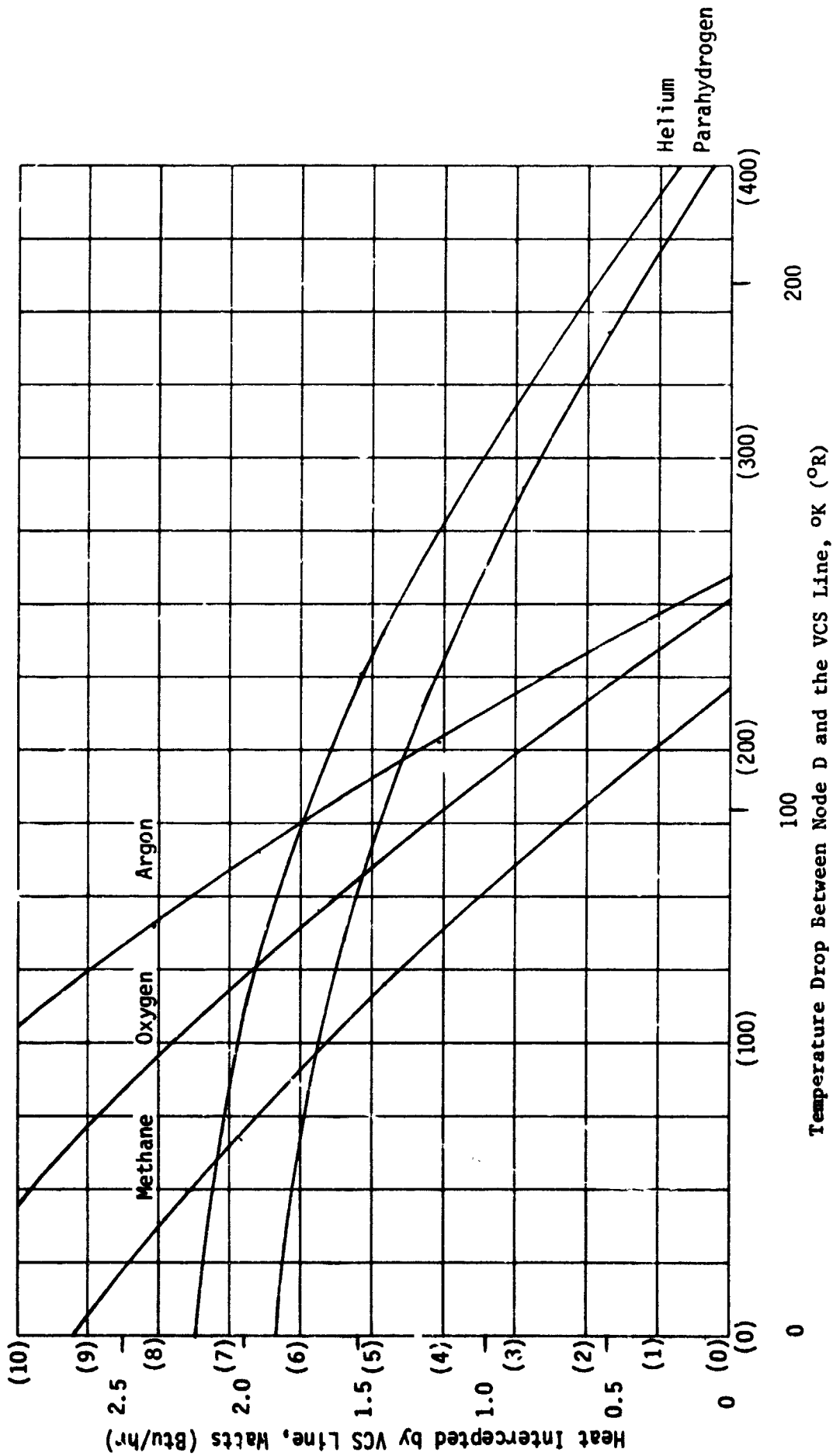
Figure IV-12 Heat Intercepted by VCS Line versus Temperature Drop Between VCS Line and Trunnion

IV-37
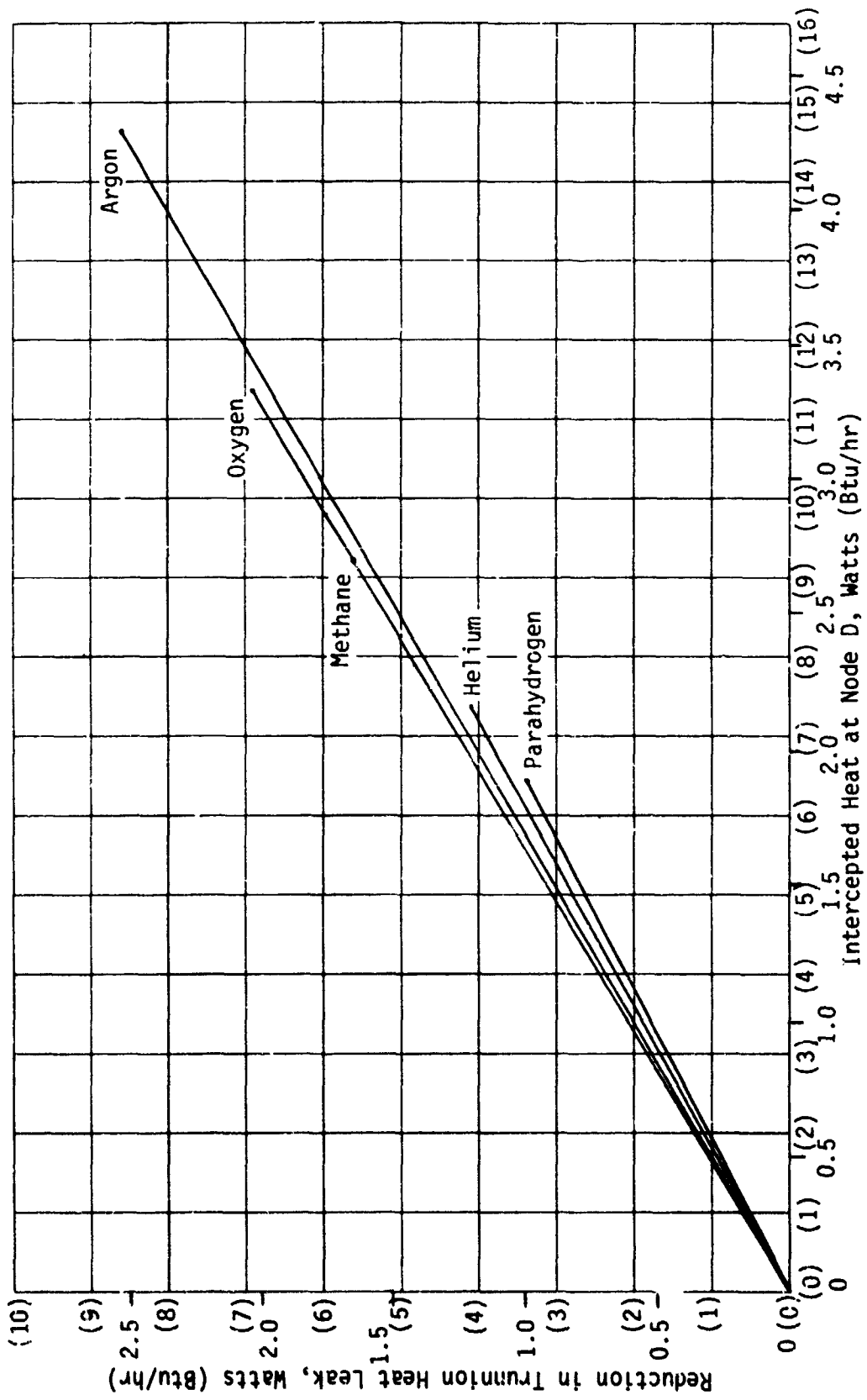
Figure IV-13 Trunnion Heat Leak Reduction versus Intercepted Heat Leak at Node D
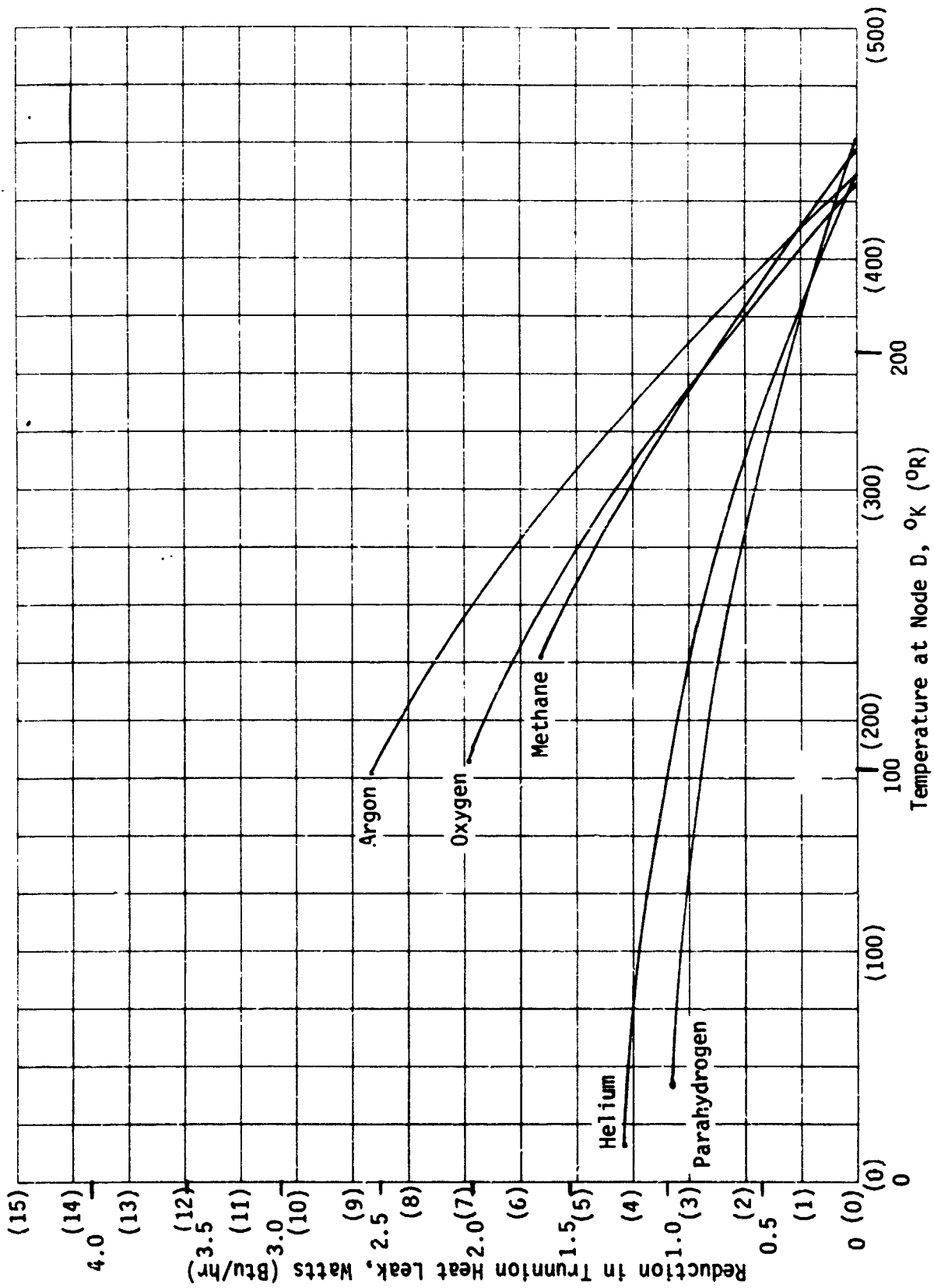
Figure IV-14   Reduction in Trunnion Heat Leak versus Node D Temperature

External Support Struts-Large Tanks

The structural support heat inputs for each of the 12.5 m^3 (440 ft^3) argon, methane and oxygen tanks and the 37.4 m^3 (1320 ft^3) cylindrical hydrogen tank were calculated by two methods. First each support was assumed to be perfectly insulated, except for the ends, and to have a linear temperature gradient along it's length. One end was assumed fixed at 294°K (530°R), with the other fixed at the cryogen saturation temperature. For the second case each support was assumed to be viewing the sun (absorptivity of 0.2) and to be radiating to space (emissivity of 0.8). The end temperatures were fixed, as for the first case. The heat input to the support from the sun was determined by using the value of the solar flux at the edge of the earth's atmosphere. The sink was assumed to be a black body at 4°K (7°R). A 10 node energy balance gave the support temperature gradient, from which the heat input was obtained.

The support geometries are listed in Table IV-15. All 12.5 m^3 (440 ft^3) tanks have the same number and size of tubular supports, having been sized for the heaviest fluid (i.e. argon). Both the end and center supports

Table IV-15 Structural Support Heat Inputs
for Large Tanks

Volume	Tubular Support Geometry	Fluid	Support Heat Inputs			
			Non-Sun Viewing		Sun Viewing	
			Watt	(Btu/hr)	Watt	(Btu/hr)
12.5 m^3 (440 ft^3)	Number - 8 Radius 6.4-cm (2.5-in)	LAr	1.6	(5.6)	3.0	(10.4)
	Length 114-cm (45-in)	LCH$_4$	1.4	(4.8)	7.0	(24.0)
	Thickness 0.5-cm (0.2-in)	LO$_2$	1.6	(5.6)	8.4	(28.8)
37.4 m^3 (1320 ft^3) Cylindrical	End Supports Number - 48 Radius 3.8-cm (1.5-in) Length 41-cm (16-in) Thickness 0.32-cm (0.13-in) Center Support Number - 24 Radius 3.8-cm (1.5-in) Length 61-cm (24-in) Thickness 0.32-cm (0.13-in)	LH$_2$	17	(58)	84	(288)

for the 37.4m³ (1320 ft³) cylindrical tank were analyzed. All of the supports are S-glass epoxy. The heat input from the sun was obtained by assuming the solar flux at the edge of the earth's atmosphere to be 1400 W/m² (444 Btu/hr ft²), and using the support projected area. Using a very high source temperature of $5.5 \times 10^{4}°K$ ($10^{5}°R$) and a fictitious conductance, the appropriate heat input was calculated. The sink was assumed to be a black body at 4°K (7°R). The total strut circumferential surface area was used, and a view factor of 1.0 was assumed. Even at hydrogen saturation temperature, the radiation from space was found to be negligible, so that the support-to-space conductance could be simplified. In evaluating the conductance in the support, an average thermal conductivity taken from Reference 39 was used.

A typical temperature distribution in the support for the 12.5 m³ (440 ft³) tank is shown in Figure IV-15 for oxygen. The dashed line represents a linear temperature gradient (and is considered, therefore, to be an insulated, non-sun-viewing condition). The sun-viewing support has a temperature gradient at the tank end that is about 5 times as steep as the linear gradient. Similar temperature distributions in the supports for the 37.4 m³ (1320 ft³) cylindrical hydrogen tank are shown in Figure IV-16.

Structural support heat inputs for the larger tanks are listed in Table IV-15 for both sun-viewing and non-sun-viewing cases. The support heat inputs for the oxygen and argon tanks are the same for the non-sun-viewing case, due to the assumption of a linear temperature gradient and almost identical fluid saturation temperatures. Methane has a higher saturation temperature, so the support heat input is lower.

For the sun-viewing supports argon has the lowest heat input, with methane higher, and oxygen slightly higher than the methane. The argon is lowest because roughly a third of the support is insulated (by tank MLI), reducing the value of the temperature gradient at the tank. The relative difference between oxygen and methane support heat inputs is about the same for both cases, due to the saturation temperatures. Note that the heat input listed for the non-sun viewing case is probably high, since the thick layer of MLI (about 1/3 the length of the support) would tend to reduce the tank end temperature gradient somewhat, from the linear gradient assumed, but the effect would probably not be as severe as for the sun-viewing case.

Comparison of support heat input between sun-viewing and non-sun-viewing cases shows that the sun-viewing heat inputs are about 400% greater for the hydrogen case than the non-sun-viewing heat inputs. The increase from the non-sun-viewing to sun-viewing for argon is only about 86%.
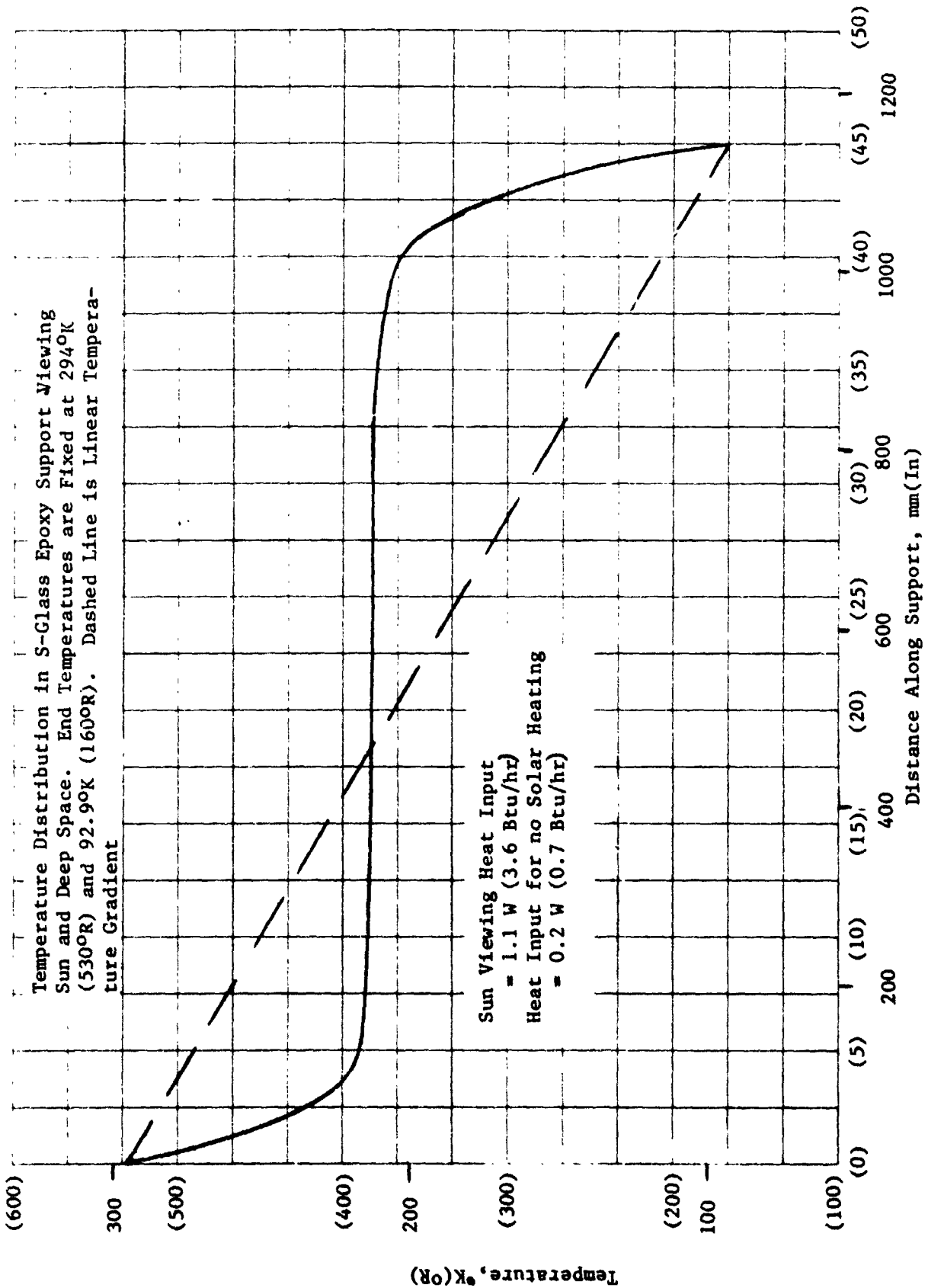
Figure IV-15 Temperature Distribution in Sun-Viewing Supports, 12.5 m³ (440 ft³) Liquid Oxygen Tank

Temperature Distribution in S-Glass Epoxy Support Viewing Sun and Deep Space. End Temperatures are Fixed at 294°K (530°R) and 92.9°K (160°R). Dashed Line is Linear Temperature Gradient

Sun Viewing Heat Input = 1.1 W (3.6 Btu/hr)
Heat Input for no Solar Heating = 0.2 W (0.7 Btu/hr)

Distance Along Support, mm(In)
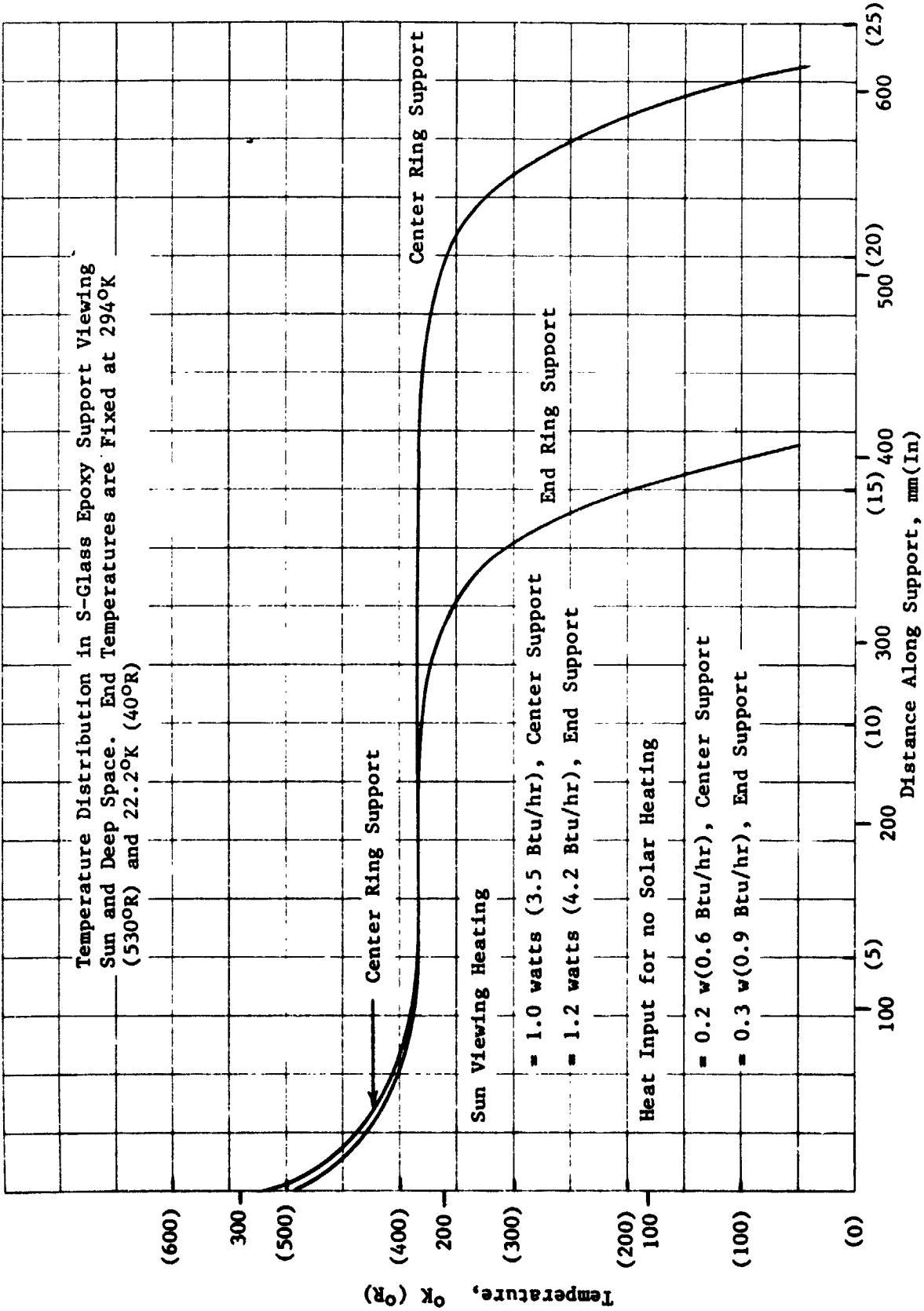
Temperature, °K(°R)

Figure IV-16 Temperature Distribution in Sun-Viewing Supports, 37.4 m³ (1320 ft³) Cylindrical Liquid Hydrogen Tank

IV-43

3. Thermal Performance

The Cryogenic Storage Analysis Model (CSAM) was used to determine the thermal performance of each tank configuration. The programmed inputs to CSAM allow quite complex missions to be simulated without interrupting the program. The Thermodynamic Vent System (TVS) rates and set points, the pressurization rate and set point, the outflow rate, and the variations in gravitational acceleration can all be changed at preset times during the mission simulation. This capability allows all of the missions to be modelled by CSAM, yielding a mission profile which includes the tank pressure, the mass of fluid in the tank, the amount of fluid vented through the TVS, and the amount of pressurant used, each as a function of mission time. Data from CSAM can also be compiled to determine the "quasi" steady-state heat inputs for each fluid/tank configuration.

The heat leaks into the tanks are through the supports, the MLI, the top penetration (pressurization/vent line), and the bottom penetration (the outflow line, which also functions as the abort line and inflow line). The structural supports and penetrations described previously were modelled thermally by CSAM using comparable diameters, lengths, and wall thicknesses. The optimum MLI thicknesses previously determined were used for simulation of each configuration.

Ground rules used in the analysis for the large tanks were: 1) Liquid initially saturated at one atmosphere; 2) Outer boundary temperature of 293°K (530°R) on the vacuum jacket or outer layer of MLI; 3) Gravity level changes from one g to 10^{-3} at liftoff (8-10 min boost phase neglected), 4) In most cases, the tank was pressurized to 3 psia above the storage pressure prior to outflow to preclude vaporization in the liquid outflow line.

A summary compilation of the results of the thermal analysis using CSAM is shown in Tables IV-16 and IV-17. These tables show for each configuration evaluated the MLI thickness, the total steady-state heat input (with and without the TVS operative), the TVS flowrate, the total amount of fluid vented through the TVS, and the total helium pressurant used. Each of the 13 configurations will be discussed separately; the CFME baseline steady-state heat leaks were presented previously in Table I-2.

Configuration 1

The thermal performance of the 0.62 m³ (22.0 ft³) methane storage and supply tank is presented in Figure IV-17. The requirement for this tank was a 180-day mission consisting of a 28-hour ground hold (in which no venting was required), followed by a constant liquid outflow for the remaining time on orbit. The optimum thickness of MLI for this mission and configuration was 4.7-cm (1.85-in).

The pressure in the tank rises rapidly until it reaches 138 KN/m² (20 psia) even though the convection in the tank has decreased (in the model, "g" changes from 1.0 to 0.0001 at 28 hours) and liquid outflow has begun. The combined effect does not greatly reduce the pressure rise rate and so heat

Table IV-16 Thermal Analysis Summary (International Units)

Configuration Number

	Base-line	1	2	3	4	5	6	7	8	9	10	11	12	13
MLI Thickness (cm)	3.2	4.7	10.2	3.2	3.2/3/2	No Anal.	10.2	No Anal.	1.2	No Anal.	2.0	6.1	1.5	1.8
Heat Leak:														
(a)TVS Inoperative (Watts)	7.1	7.2	6.9	7.7	0.069		6.8		65.		33.	13.	170.	84.
(Watts/m²)	2.0	2.0	2.0	2.2	0.020		0.26		2.5		1.3	0.49	3.2	1.5
(b)TVS Operative (Watts)	1.8	0.055	0.015	0.16	0.012		0.14		in-active		in-active	in-active	120.	63.
(Watts/m²)	0.51	0.016	0.0043	0.044	0.0034		0.001		in-active		in-active	in-active	2.2	1.2
Thermodynamic Vent Flowrate (kg/hr)	0.023	0.041	0.11	0.10	0.0023		0.11		0.0		0.0	0.0	0.45	0.15
Total Fluid Vented through TVS (kg)	3.8	180.	810.	500.	8.6		12000.		0.0		0.0	0.0	59.	18.
Helium Pressurant Requirement (kg)	1.7	0.029	0.0	0.0	0.0		0.0		3.4		4.1	4.6	26.	20.

IV-45

Table IV-17 Thermal Analysis Summary (English Units)

Configuration Number

	Base-line	1	2	3	4	5	6	7	8	9	10	11	12	13
MLI Thickness (in)	1.25	1.85	4.02	1.25	1.25/1.25	No Anal.	4.02	No Anal.	0.47	No Anal.	0.80	2.40	0.57	0.69
Heat Leak: (a)TVS Inoperative (Btu/hr)	24.	25.	24.	26.	0.24		23.		220		110.	44.	580.	290.
(Btu/hr ft^2)	0.63	0.63	0.63	0.70	0.0063		0.082		0.79		0.41	0.16	1.0	0.48
(b)TVS Operative (Btu/hr)	6.1	0.19	0.051	0.55	0.041		0.48		in-active		in-active	in-active	410	220
(Btu/hr)	0.16	0.0051	0.0014	0.014	0.0011		0.00032		in-active		in-active	in-active	0.70	0.38
Thermodynamic Vent Flowrate (lbm/hr)	0.050	0.090	0.25	0.22	0.0051		0.24		0.0		0.0	0.0	0.99	0.30
Total Fluid Vented through TVS (lbm)	8.4	400.	1800.	1100.	19.		26,000.		0.0		0.0	0.0	130.	40.
Helium Pressurant Requirement (lbm)	3.7	0.064	0.0	0.0	0.0		0.0		7.5		9.0	10.	57.	44.
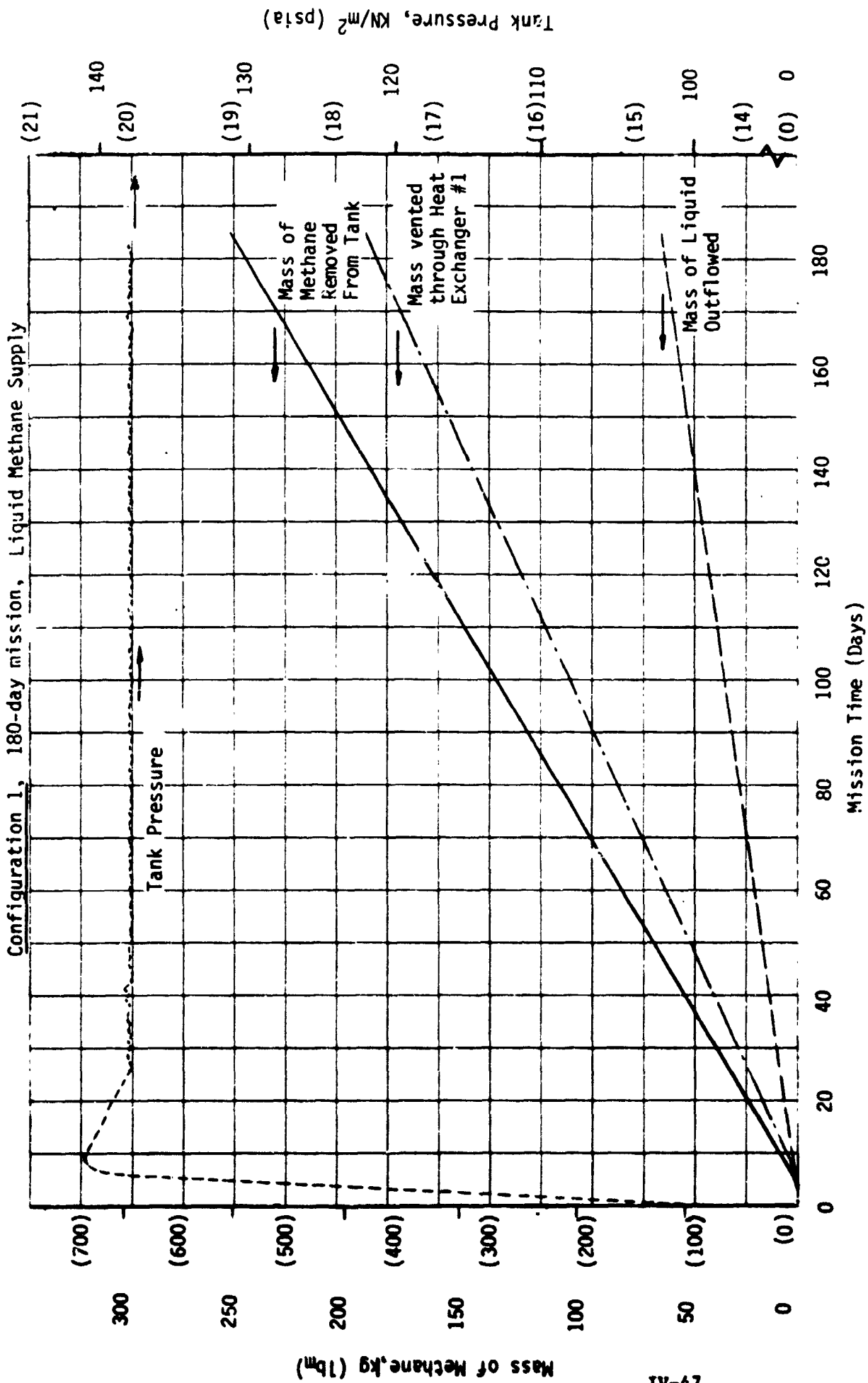
Figure IV-17 Methane 0.62 m^3 (22 ft^3) Storage Tank Performance

exchanger 1 of the TVS is enabled when the pressure reaches the 138 KN/m^2 (20 psia) set point at about 6 days. The flowrate of heat exchanger 1 is 0.041 kg/hr (0.090 lb/hr), which is enough to keep the pressure rise in check and slowly bring it down to 138 KN/m^2 (20 psia). Even when the TVS is operative, there is still a slight heat input into the tank. The pressure in the tank drops because the outflow process from the tank itself reduces the tank pressure and temperature enough to overcome the small heat leak.

In Figure IV-17 it is observed that only 59.0 kg (130 lb) of the total stored quantity of 249 kg (550 lb) can be delivered as gas-free liquid at a constant flowrate of 0.3 kg/hr (0.7 lb/hr) over the 180-day storage and supply period. The remaining 190 kg (420 lb) is vented through the TVS to maintain thermal control as described above. Table IV-18 shows the steady state heat leak for this configuration. Because of the relatively large quantity of methane vented, compared to liquid supplied, it is helpful in understanding the thermal performance to compare this table with that for the CFME tank, which was designed for a 7-day mission. Although the heat input through the MLI is less for Configuration 1 due to a greater thickness and a smaller temperature difference, the overall heat input is comparable to the CFME due to the much larger cross-sectional area of the trunnions in the methane tank.

Table IV-18   Steady State Heat Leak - 0.62 m^3 (22 ft^3)
Methane Tank - Config. 1

Conductor	TVS Inoperative Heat Input		% of Total	TVS Operative Heat Input	
	Watts (Btu/hr)	Watts/m^2 (Btu/hr ft^2)		Watts (Btu/hr)	Watts/m^2 (Btu/hr ft^2)
MLI Thickness 4.7-cm (1.85-in)	2.0 (6.8)	0.57 (.18)	28	1.7 (5.8)	0.48 (0.15)
Supports	3.5 (11.9)	0.99 (.31)	49	3.1 (10.6)	0.88 (0.28)
Penetrations	1.5 (5.1)	0.43 (.14)	20	1.3 (4.4)	0.37 (0.12)
Thermodynamic Vent System (Flowrate = 0.041kg/hr) (0.090 lbm/hr)	0.2 (0.7)	0.06 (0.2)	3	6.0* (2v.5)*	1.71* (0.54)*
Total	7.2 (24.6)	2.0 (.65)	100	0.1 (0.3)	0.02 (0.01)

* indicates heat flow from tank to conductor

If the user system only required gaseous supply, the combined heat
exchanger and liquid outflow rate of 0.059 kg/hr (0.13 lb/hr) could be
supplied on a continuous basis over the 180-day mission. Another way of
evaluating the thermal performance is to compare these results with fluid
venting only to maintain a constant pressure of 138 KN/m^2 (20 psia). If
saturated liquid is converted to saturated vapor and vented overboard, all the
liquid in the tank will be depleted in 190 days. Thus the CFME thermal
control approach provides a significant thermal advantage; a heat input of
7.2 W (24.6 Btu/hr) and a flux of 2.0 W/m^2 (0.65 Btu/hr-ft^2) are
reasonably good levels for a tank this size mounted to survive the launch
environment on a Spacelab pallet.

Configuration 2

The small tank size, 0.62 m^3 (22 ft^3), and corresponding load of argon
precludes being able to approach anywhere near 7-year storage and supply for
this electric propulsion application. If the entire quantity of argon were
used for venting, a heat leak as low as 0.6 W (2 Btu/hr) would be required to
obtain 7-year storage. An MLI thickness of 10.2-cm (4.0-in), considered to be
a maximum limit on insulation capability as discussed previously, was used for
this case. The heat flux through the insulation alone contributes 1.9 W (6.5
Btu/hr). When the TVS is inoperative, the major heat input is through the
trunnions, and operation of the heat exchanger, modified to reduce the support
heat input, can only stretch the mission to about 300 days. A summary of the
heat input is listed in Table IV-19.

Table IV-19   Steady State Heat Leak - 0.62 m^3 (22 ft^3)
Oxygen Tank - Config. 2

Conductor	TVS Inoperative Heat Input		% of Total	TVS Operative Heat Input	
	Watts (Btu/hr)	Watts/m^2 (Btu/hr ft^2)		Watts (Btu/hr)	Watts/m^2 (Btu/hr ft^2)
MLI Thickness 10.2-cm (4-in)	1.9 (6.5)	0.55 (0.17)	28	1.00 (3.41)	0.28 (0.089)
Supports	4.0 (13.7)	1.14 (0.36)	58	0.29 (0.99)	0.08 (0.025)
Penetrations	0.9 (3.1)	0.26 (0.08)	13	0.70 (2.39)	0.19 (0.060)
Thermodynamic Vent System (Flowrate = 0.11 kg/hr) (.25 lb/hr)	0.1 (0.3)	0.05 (0.02)	1	1.97* (6.72)*	0.55* (0.174)*
Total	6.9 (23.5)	2.0 (0.63)	100	0.02 (0.07)	0.01 (0.003)

* indicates heat flow from tank to conductor.

The thermal performance is presented in Figure IV-18. The pressure in the tank rises to approximately 114 KN/m² (16.5 psia), even though both heat exchangers are enabled at 103 KN/m² (15 psia). This is primarily due to the assumption of a 28-hour ground hold prior to lift-off. Heat exchanger 2 is set to operate for a period of 24 hours to aid in cool-down of penetrations and supports. After about 2 days into the mission, heat exchanger 2 is turned off. At this point in time, 5.4 kg (12 lb) have been vented through heat exchanger 2, and heat exchanger 1 continues to operate at an average flowrate of 0.1¹ kg/hr (0.25 lb/hr). This mode of operation is enough to stop the rise in pressure after about 6 days and actually causes the pressure to drop slightly, where it remains essentially constant for the remainder of the mission. Again referring to Table IV-19, the net heat leak into the fluid is still slightly positive; the pressure drop due to expansion of the ullage upon venting compensates for this and thus the tank pressure decreases, relatively quickly at first, as the percentage of ullage volume increases, then slower as the ullage volume increases.

Because the usage requirement is for a flowrate of 0.14 Kg/hr (0.30 lb/hr) with a 25-percent "on cycle", venting losses to keep the pressure nearly constant are 0.08 Kg/hr (.175 lb/hr) average over the mission duration. This is a total of 573 Kg (1260 lb) for thermal control.

Configuration 3

Results for the 0.62 m³ (22.0 ft³) oxygen storage tank are presented in Figure IV-19 and Table IV-20. The optimum MLI thickness for this configuration and a 180-day mission is small since all of the vented fluid is utilized for gaseous supply at a constant flowrate. The baseline (CFME) thickness of 3.2-cm (1.25-in) was used for this simulation to supply the user requirement of 0.15 kg/hr (0.34 lb/hr), some of which is liquid supply, converted to vapor, and the remainder vapor supply from the TVS. (A more optimum design approach would be to use fewer layers of MLI, increasing the vent rate through the TVS to match the required outflow and maintain tank pressure nearly constant.)

The tank pressure rises during the 28-hour ground hold but stabilizes within ± 7 KN/m² (1 psia) following launch. As the pressure rises beyond 138 KN/m² (20 psia), the TVS is enabled. At this point, both heat exchanger 1 and 2 are operative and the rate of gaseous plus liquid supply is slightly greater than the user requirement. At a time of 20 days into the mission, the pressure has stabilized around 138 KN/m² (20 psia) and heat exchanger 2 is turned off until the pressure rises by 0.7 KN/m² (0.1 psi). This mode of operation runs heat exchanger 2 intermittantly, but on the average the flowrate leaving the oxygen tank is 0.15 kg/hr (0.34 lb/hr). Using a microprocessor to control the flow through the liquid outflow valve and deliver the required flowrate results in a thermally efficient design that optimizes the use of fluid flowing through the TVS. Operation of the TVS in this manner also eliminates the need for helium pressurant.
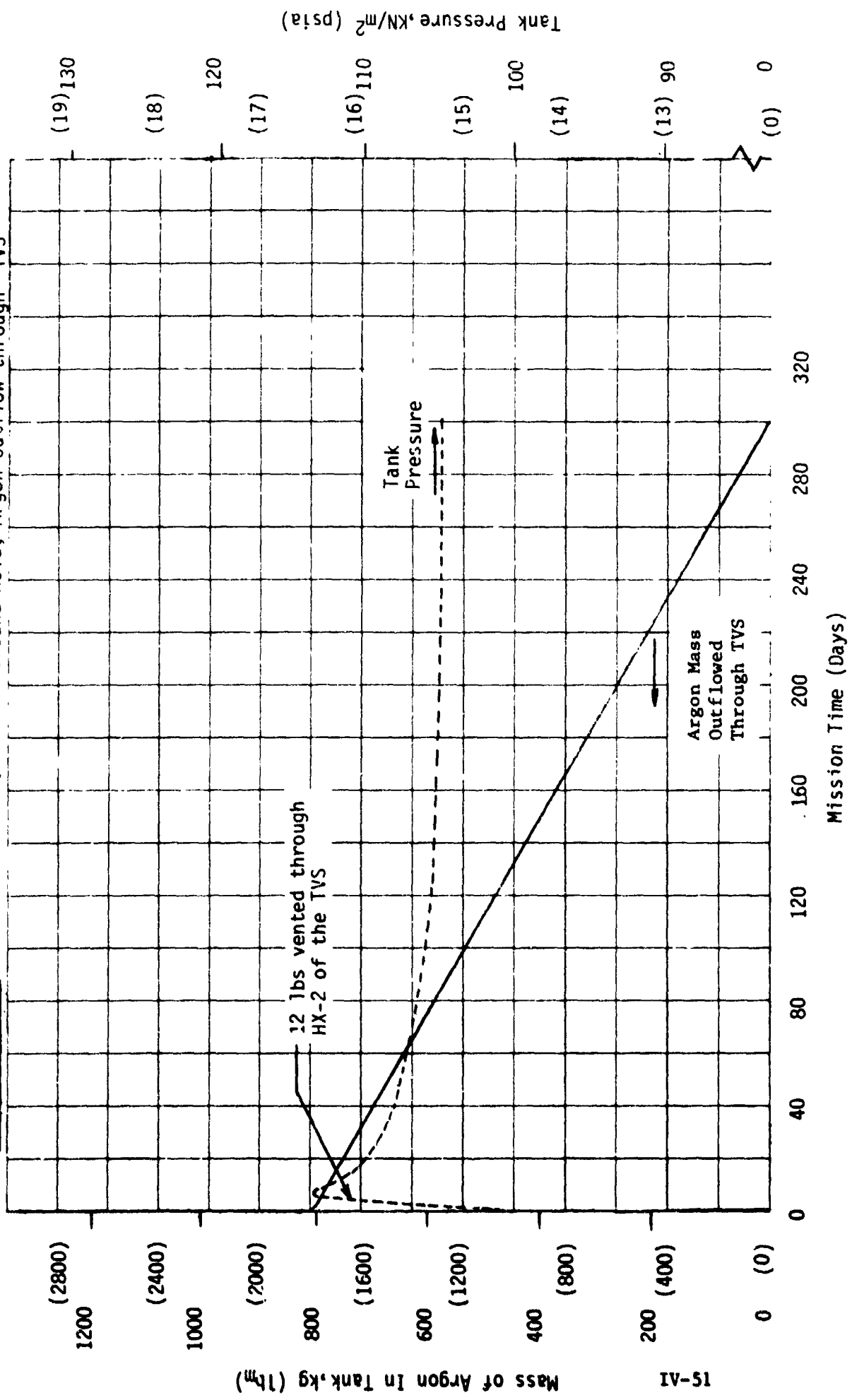
Figure IV-18 Argon 0.62 m³ (22 ft³) Storage Tank Performance

IV-51

Configuration 3, 180-day Mission, Gaseous Oxygen Supply

Total Oxygen Removed From Tank

Mass Vented through Heat Exchanger #1

Mass of Liquid Outflowed

Mass Vented through Heat Exchanger #2

Tank Pressure

Tank Pressure, KN/m² (psia)

Mass of Oxygen, kg (lb_m)

Mission Time (Days)

(21) 140
(20)
(19) 130
(18) 120
(17)
(16) 110
(15) 100
(14)
(0) 0

700
600 (1400)
(1200)
500 (1000)
400 (800)
300 (600)
200 (400)
100 (200)
0 (0)

Figure IV-19 Oxygen 0.62 m³ (22 ft³) Storage Tank Performance

Table IV-20 Steady State Heat Leak - 0.62 m^3 (22 ft^3)
Oxygen Tank - Config. 3

Conductor	TVS Inoperative Heat Input		% of Total	TVS Operative Heat Input	
	Watts (Btu/hr)	Watts/m^2 (Btu/hr ft^2)		Watts (Btu/hr)	Watts/m^2 (Btu/hr ft^2)
MLI Thickness 3.2-cm (1.25-in)	2.5 (8.5)	0.71 (0.23)	32	2.2 7.5)	0.62 (0.20)
Supports	3.8 (13.0)	1.09 (0.35)	49	2.9 (9.9)	0.82 (0.26)
Penetrations	1.1 (3.8)	0.31 (0.10)	15	0.9 (3.1)	0.26 (0.08)
Thermodynamic Vent System (Flowrate = 0.10 kg/hr) (0.22 lb/hr)	0.3 (1.0)	0.09 (0.03)	4	5.8* (19.8)*	1.66* (0.53)*
Total	7.7 (26.3)	2.2 (0.70)	100	0.2 (0.7)	0.04 (0.01)

* indicates heat flow from tank to conductor.

Configuration 4

The 0.62 m^3 (22.0 ft^3) helium storage system is a unique case due to
the constraints that are imposed by the thermophysical properties. The
requirements for this system call for 74 kg (163 lb) of liquid helium to be
supplied at a constant flowrate of 0.017 kg/hr (0.038 lb/hr) over a 180-day
period. A brief review of the configuration is helpful in understanding the
performance. The tank is surrounded by 3.2-cm (1.25-in) of MLI, a VCS which
is cooled with helium through two thermodynamic vent system heat exchangers,
another 3.2-cm (1.25-in) MLI, and a second VCS. This second VCS is cooled
with hydrogen supplied from a separate tank. There is a third region of
3.2-cm (1.25-in) MLI between the hydrogen VCS and the outer vacuum jacket.
The support system is configured to prevent a direct heat "short" from the
vacuum jacket to the helium tank.

Figure IV-20 and Table IV-21 present the results for this 180-day mission
simulation, the first 28 hours of which are ground hold with no liquid
outflow. At the onset of liquid outflow, the pressure begins to drop due to
expansion of the ullage. The pressure turns back up after 20 days as the
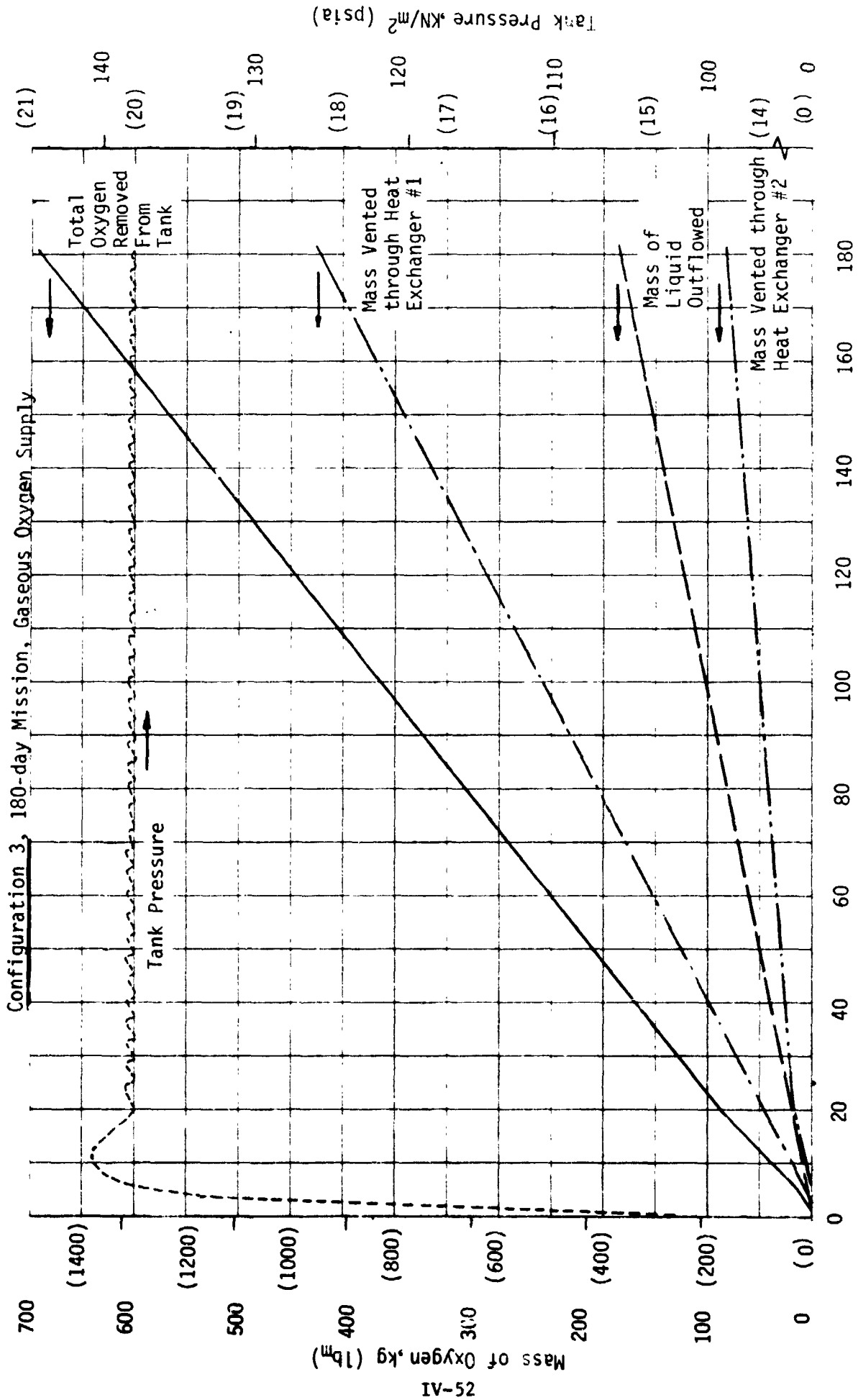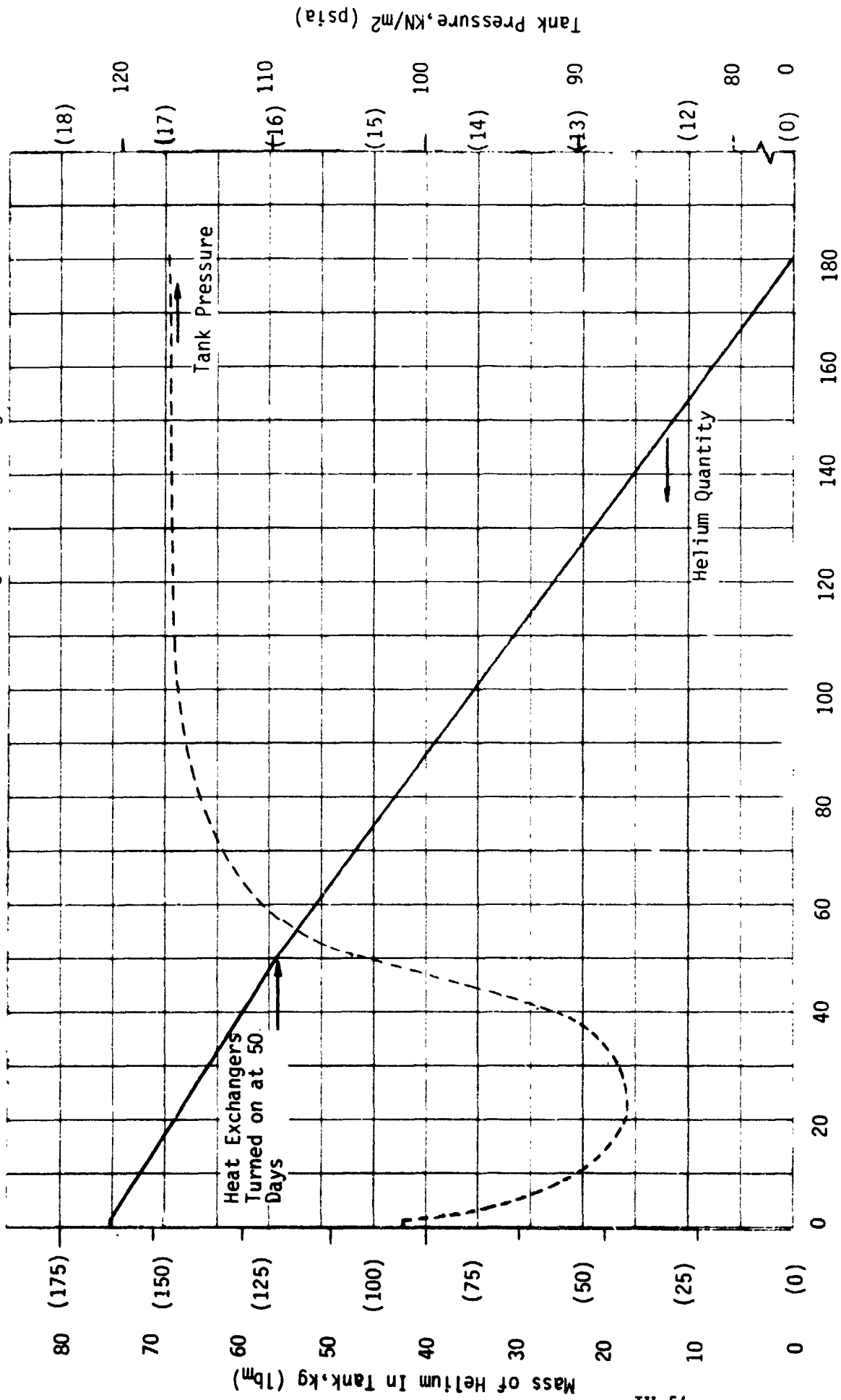
Figure IV-20 Helium 0.62 m³ (22 ft³) Storage Tank Performance

Table IV-21   Steady State Heat Leak - 0.62 m³ (22 ft³)
Helium Tank - Config. 4

Conductor	Helium TVS Inoperative Heat Input		% of Total	Helium TVS Operative Heat Input	
	Watts (Btu/hr)	Watts/m² (Btu/hr ft²)		Watts (Btu/hr)	Watts/m² (Btu/hr ft²)
MLI Thickness 3.2-cm (1.25-in)	0.024 (0.082)	0.007 (0.0022)	35	0.017 (0.058)	0.0048 (0.0015)
Supports	0.029 (0.099)	0.008 (0.0025)	42	0.023 (0.078)	0.0065 (0.0021)
Penetrations	0.012 (0.041)	0.004 (0.0013)	17	0.006 (0.020)	0.0017 (0.0005)
Thermodynamic Vent System (Flowrate = 0.0023 kg/hr) (0.05 lb/hr)	0.004 (0.014)	0.001 (0.0003)	6	0.034* (0.116)*	0.0096* (0.0030)*
Total	0.069 (0.235)	0.020 (0.0063)	100	0.012 (0.041)	0.0034 (0.0011)

* indicates heat flow from tank to conductor.

initial conditions slowly develop into a steady-state profile; the steady-state heat input is not fully developed until after 60 days. For other fluids, the thermal conductivity is high enough that a transient phenomenon such as this is dissipated quickly with small perturbations in tank pressure. However, the relatively low thermal conductivity of helium and low heat of vaporization lead to long transition periods to establish steady state with considerable fluctuations in pressure.

When the pressure in the tank reaches 103 KN/m² (15 psia), the helium TVS is activated with both heat exchangers operational. The total flowrate through the helium TVS is 0.0023 kg/hr (0.005 lb/hr), enough to reduce the heat input to 0.012 W (0.040 Btu/hr) and minimize the pressure rise. A total of 8.6 kg (19 lb) of helium is vented through the helium TVS, leaving 65.3 kg (144 lb) available for liquid supply. Assuming that the storage system is at steady state when the mission begins, it is conservative to estimate that the tank pressure reaches 103 KN/m² (15 psia) after 2-3 days. Activating the TVS at this time required that 12 kg (26 lb) of helium be vented, leaving 62.0 kg (137 lb) for liquid supply.

The heat leak through the hydrogen VCS into the helium VCS was 0.088 W (0.30 Btu/hr). The hydrogen heat exchanger was modelled to remove a small amount of heat from the hydrogen VCS, a large amount from the supports (by designing the hydrogen to flow in an annulus around each support), and the ramainder from just inside the vacuum jacket. This highly efficient design requires a hydrogen flowrate of 0.035 kg/hr (0.078 lb/hr), or a total of 152 kg (335 lb) of hydrogen for the 180-day mission.

Configurations 5 & 6

The 12.5 m^3 (440 ft^3) argon storage system was analyzed both with and without a vacuum jacket. Because the insulation thickness for this long-term storage application is determined by the 7-year operating requirement, the vacuum-jacketed (configuration 5) and non-vacuum-jacketed (configuration 6) argon tanks have the same insulation thickness. The 4-hour ground hold raises the tank pressure of the non-vacuum-jacketed tank by less than 1% over the vacuum-jacketed tank. The results clearly point out the minimal gain in performance obtained from adding a bulky vacuum jacket. Therefore, Configuration 5 was not modelled separately using CSAM.

The mission for Configuration 6 requires a loaded mass of 16,287 kg (35,906 lb) providing a flowrate of 2.54 kg/hr (5.61 lb/hr) during a 200-day LEO-to-GEO transfer, followed by a flowrate of 0.14 kg/hr (0.30 lb/hr) for 12 hours out of every 24-hour period (for stationkeeping). As previously explained for the 0.62 m^3 (22.0 ft^3) argon tank, a maximum limit of 10.2-cm (4.0-in) of MLI was considered in this study, and was therefore used for this system. The results of this mission simulation are presented in Figure IV-21 and Table IV-22.

The pressure in the argon tank rises despite the liquid outflow rate. Heat exchanger 1 of the TVS is set to operate at or above 193 KN/m^2 (28 psia). It is necessary to vent 172 kg (380 lb) of argon through the TVS to halt the pressure rise at the end of LEO-to-GEO transfer. Optimizing the heat exchanger performance to maintain a nearly constant tank pressure during the GEO stationkeeping requires a TVS flowrate of 0.11 kg/hr (0.25 lb/hr). However, the average flowrate required for the 7-year stationkeeping, is only 0.07 kg/hr (0.15 lb/hr), resulting in 0.05 kg/hr (0.10 lb/hr) vented overboard. As a result, the tank is depleted after about 1630 days or 4-1/2 years.

It is evident from Table IV-22 that a large amount of heat (53%) enters the tank through the supports. Disconnecting some supports after transfer to orbit would significantly extend the on-orbit stay time since the fluid vent requirements would more nearly match the total heat input to the argon. Improvement in support heat leak is discussed in more detail in Chapter VI-Technology Evaluation.

Configuration 5 & 6, LEO-to-GEO Transfer Followed by Stationkeeping
102mm (4-inches)MLI, Non-Vacuum Jacketed Tank

LEO-to-GEO Transfer (Liquid Outflow plus 173 kg (380 lbs) through HX1 of TVS)

Stationkeeping (Outflow through HX1 of TVS)

Tank Pressure

Argon Quantity
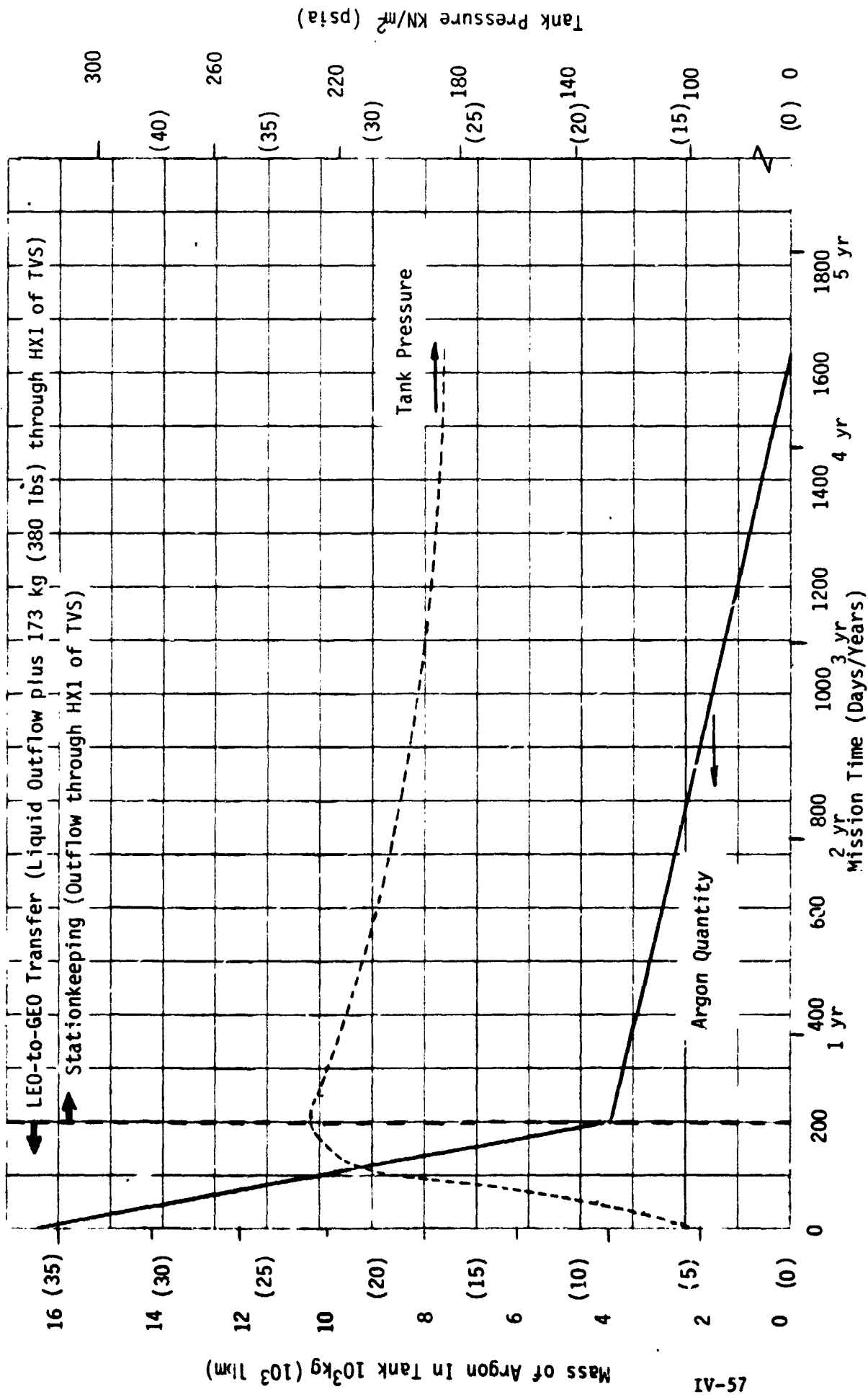
Figure IV-21 Argon 12.5 m³ (440 ft³) Storage Tank Performance

Table IV-22 Steady State Heat Leaks - 12.5 m^3 (440 ft^3)
Argon Tank - Config. 6

Conductor	TVS Inoperative Heat Input		% of Total	TVS Operative Heat Input	
	Watts (Btu/hr)	Watts/m^2 (Btu/hr ft^2)		Watts (Btu/hr)	Watts/m^2 (Btu/hr ft^2)
MLI Thickness 10.2-cm (4-in)	2.4 (8.2)	0.09 (0.029)	35	1.8 (6.1)	0.07 (0.022)
Supports	3.6 (12.3)	0.14 (0.044)	53	2.9 (9.9)	0.11 (0.035)
Penetrations	0.6 (2.0)	0.02 (0.006)	9	0.3 (1.0)	0.01 (0.003)
Thermodynamic Vent System (Flowrate = 0.11 kg/hr) (.25 lb/hr)	0.2 (0.7)	0.01 (0.003)	3	4.9* (16.6)*	0.19* (0.060)*
Total	6.8 (23.2)	0.26 (0.082)	100	0.14 (0.48)	0.001 (0.003)

* indicates heat flow from tank to conductor.

Configuration 7

The 12.5 m^3 (440 ft^3) argon tank without a vacuum jacket and designed
for compatibility with the Spacelab pallet was not modelled using CSAM. The
only difference between this configuration and configuration 6 is the support
structure. As mentioned for Configuration 6, 53 percent of the heat leak is
through the support structure. It was felt that the support structure between
the tank assembly and tne Spacelab pallet hardpoints would yield an increased
heat leak over that of Configuration 6. The increased heat flux would come
from reduced support length available between the tank and nardpoints.
Conceptual designs of this support structure were not generated. The larger
heat flux results in a greater vent rate and a shorter mission duration.

Configuration 8

The 12.5 m³ (440 ft³) methane storage tank corresponds to a 445 N (100 lb) thrust, 9 burn mission scenario for a Large Space Systems application. A total loaded liquid mass of 4783 kg (10,545 lb) is used to accomplish the 66.7 hour LEO-to-GEO transfer. A 40-hour, on-orbit storage period was assumed prior to the transfer. The results for this mission are presented in Figure IV-22. Both the tank pressure history and the mass of methane in the tank are presented as a function of mission time. The storage tank configuration for this simulation was a vacuum-jacketed storage tank assembly, and non-vented operation was evaluated. A tank pressure level of 124 KN/m² (18 psia) was seleted for the burns. A 28-hour ground hold period was assumed prior to launch, with liquid initially loaded at 101 KN/m² (14.7 psia) saturation. For this simulation, the helium pressurization was terminated just prior to the end of each burn, resulting in a drop in tank pressure as liquid outflow continued. For each burn, however, the partial pressure of methane remained above the saturation pressure to preclude vaporization within the acquisition device and outflow line of the tank. It should be noted that an NPSH less than 7 KN/m² (1 psia) is available after the third burn with this operational technique at this pressure level. As indicated in the figure, a margin of approximately 205 kg (450 lb) of liquid remains after the conclusion of the last circularization burn.

Control of tank pressure by allowing the pressure to blowdown near the end of each burn may be a difficult operational technique to follow. Because of the relatively high thermal heat input into the storage vessel due to structural supports and plumbing penetrations, the tank pressure rise rate is fairly rapid. An alternate approach to blowdown pressure control is to pressurize with helium at a preset delta pressure above the saturation level prior to each burn. This type of operation is illustrated in Figure IV-23. The delta pressure level for each burn is 21 KN/m² (3 psia). The configuration and ground hold duration is the same as that previously used in the Figure IV-22 simulation. For this case, however, the TVS is activated for pressure control prior to launch and during each coast period. The vent rate is 0.2 kg/hr (0.5 lb/hr) when the vent is activated, and the pressure is maintained at the same level used for the preceding burn. A total of 5.5 kg (12 lb) is vented prior to the first transfer burn to maintain pressure below 15 psia. A total of 15 kg (33 lb) is vented during transfer. Liquid margin is therefore 21 kg (45 lb) less at depletion as compared to the previous non-vented case. A NPSH of 21 KN/m² (3 psia) is provided during each burn; however, the tank pressure has risen to 290 KN/m² (42 psia). Variations of these two approaches to thermal conditioning and expulsion can be defined and further optimizations performed. In any case, the 12.5 m³ (440 ft³) tank conceptually defined and analyzed in this study can meet the mission requirements defined for this application. The thermal summary for this case is presented in Table IV-23.

Configuration 9

The 12.5 m³ (440 ft³) methane tank without a vacuum jacket was not modelled using CSAM. The optimum MLI thickness is almost identical to that for the vacuum-jacketed case, assuming a minimum ground hold time is possible (i.e. topping just prior to lift-off). Since 89% of the heat input in the previous case is through the MLI and only 7% through the supports, the orbital thermal performance for the non-vacuum-jacketed case will closely follow that of Configuration 8.

Figure IV-22 Methane 12.5 m³ (440 ft3) Storage Tank Performance (Blowdown Pressure Control)
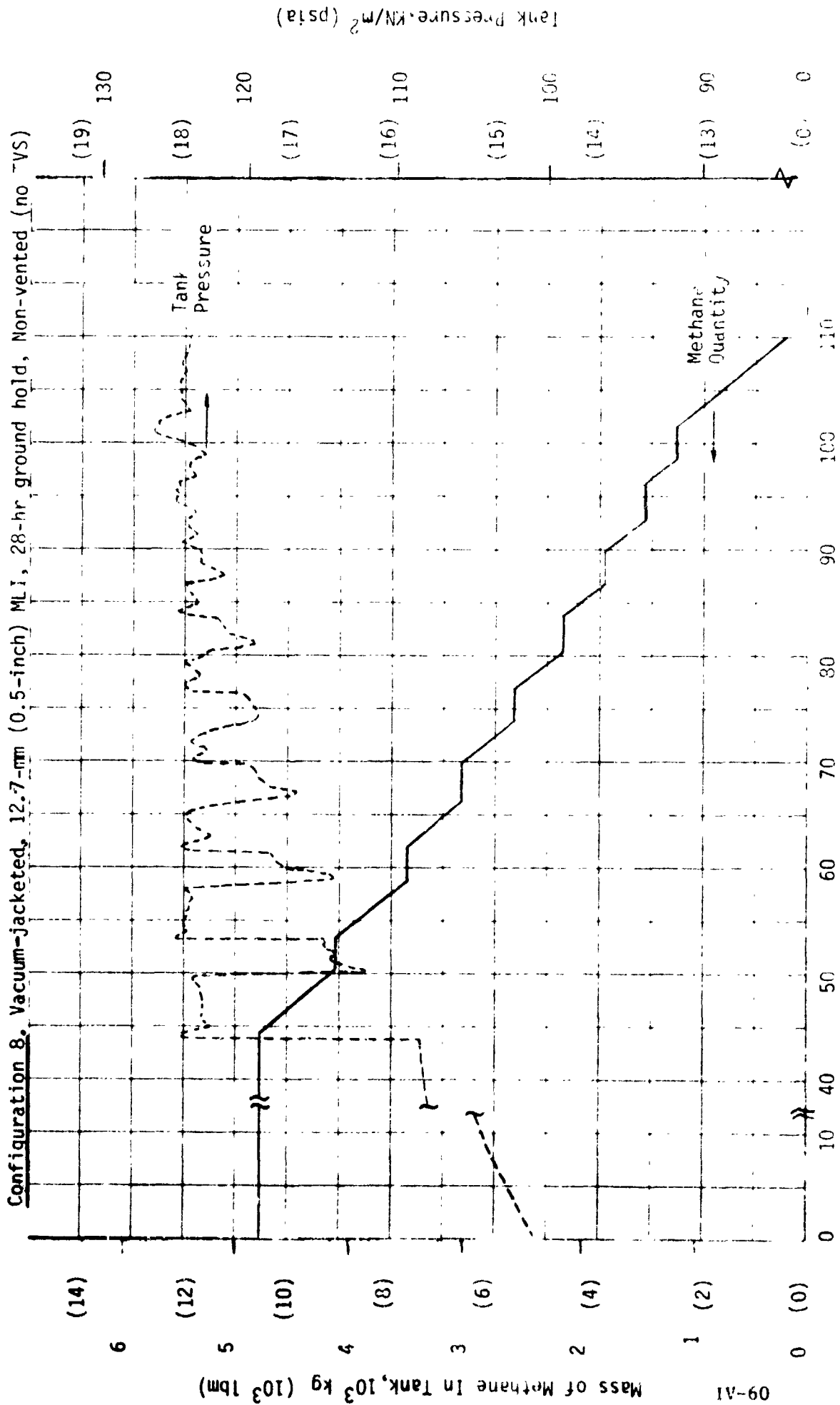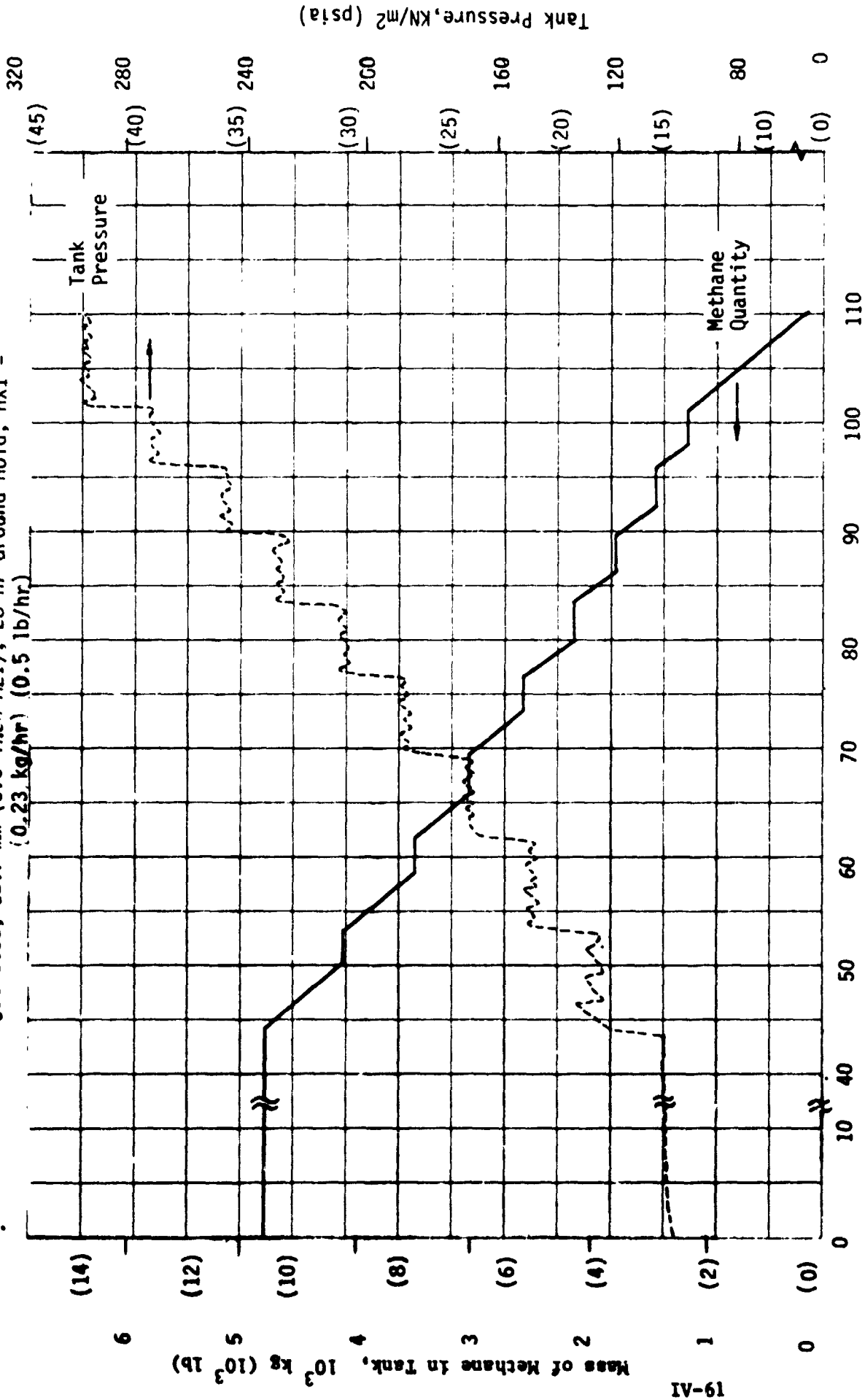
Figure IV-23 Methane 12.5 m³ (440 ft³) Storage Tank Performance (NPSH Pressure Control)

Table IV-23 Steady State Heat Leak - 12.5 m^3 (440 ft^3)
Methane Tank - Config. 8

| Conductor | TVS Inoperative Heat Input | | % of Total |
	Watts (Btu/hr)	(Watts/m^2) (Btu/hr ft^2)	
MLI Thickness 1.2-cm (0.47-in)	58 (198)	2.2 (0.70)	89
Supports	5 (17)	0.2 (0.06)	7
Penetrations	1 (3)	0.1 (0.03)	2
Thermodynamic Vent System (Flowrate = 0.0 kg/hr) (0.0 lb/hr)	1 (3)	0.1 (0.03)	2
Total	65 (222)	2.5 (0.79)	100

Configuration 10

The 12.5 m^3 (440 ft^3) vacuum-jacketed oxygen tank is specified for a 3-hour orbital resupply function at the end of a 5-day mission. An optimum MLI thickness of 2.0-cm (0.80-in) was determined. The results are presented in Figure IV-24 and Table IV-24.

The tank pressure rises slowly throughout the 28-hour ground hold and the 89-hour on-orbit coast. Heat exchanger 1 of the TVS is set at 138 KN/m^2 (20 psia) and is not activated since the pressure only rises to 111 KN/m^2 (16.1 psia) at the end of self-pressurization. The tank pressure is increased to 124 KN/m^2 (18 psia) just prior to outflow and maintained during outflow. (The average pressure rise rate i. 0.083 KN/m^2 (0.012 psi/hr); there is no oxygen vent loss.) For this system, a total of 4.1 kg (9.0 lb) of helium pressurant is required to accomplish the liquid outflow. A total of 86% of the heat input is through the MLI. However, the total steady state heat leak is only 33 W (113 Btu/hr) and therefore does not pose any significant storage problems over the 5-day mission.
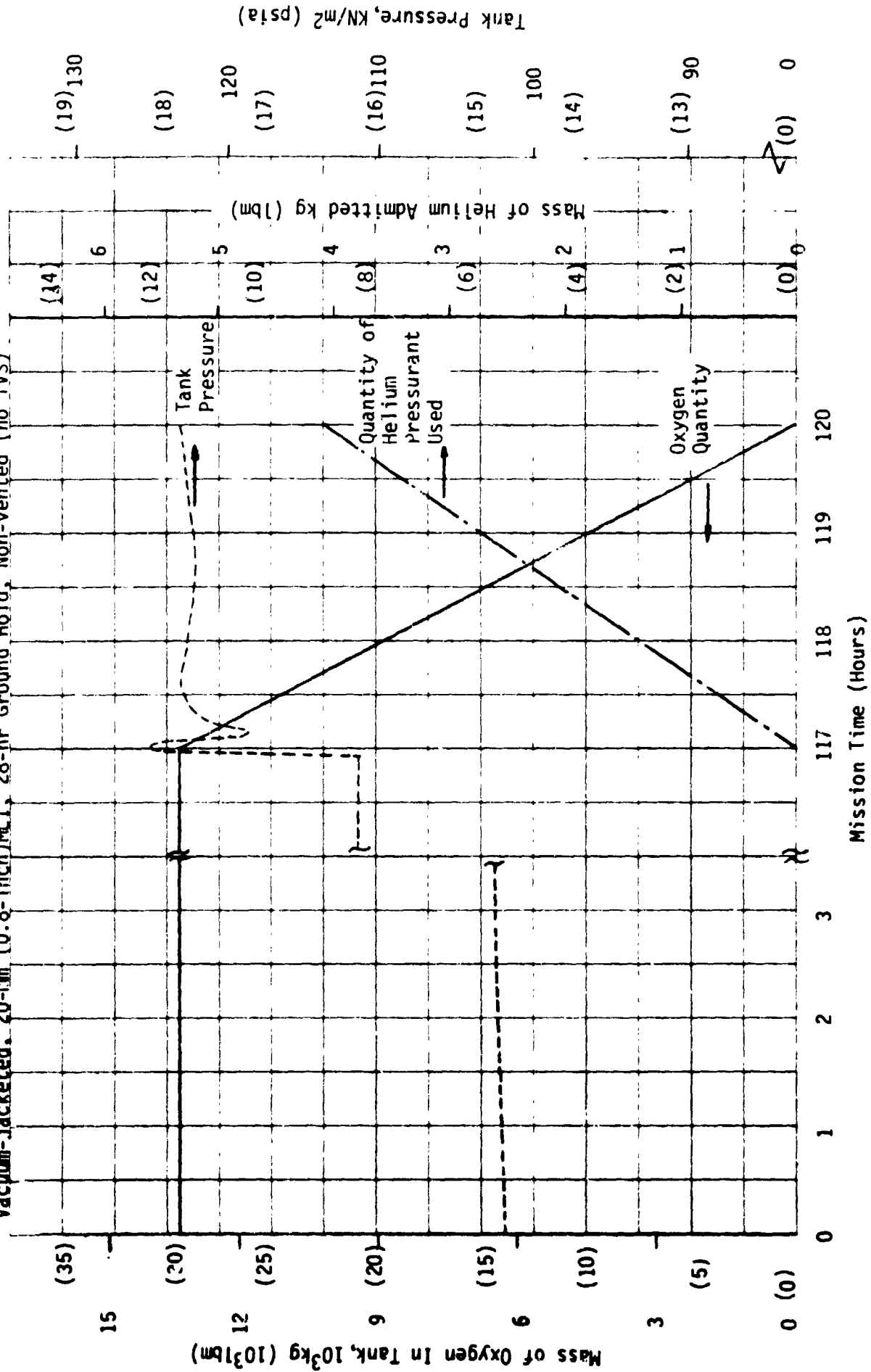
Figure IV-24 Vacuum-Jacketed Oxygen 12.5 m³ (440 ft³) Storage and Supply Tank for On-Orbit Resupply

Table IV-24 Steady State Heat Leak - 12.5 m³ (440 ft³)
Oxygen Tank (Vacuum-Jacketed) - Config. 10

| Conductor | TVS Inoperative Heat Input | | % of Total |
	Watts (Btu/hr)	Watts/m² (Btu/hr ft²)	
MLI Thickness 2.0-cm (0.80-in)	28.3 (96.5)	1.1 (0.35)	86
Supports	4.2 (14.3)	0.2 (0.06)	13
Penetrations	0.3 (1.0)	0.1 (0.03)	< 1
Thermodynamic Vent System (Flowrate = 0.0 kg/hr) (0.0 lb/hr)	0.2 (0.7)	0.1 (0.03)	< 1
Total	33 (112.5)	1.3 (0.41)	100

Configuration 11

The 12.5 m³ (440 ft³) oxygen tank without a vacuum jacket was evaluated for both a 28-hour ground hold and a 4-hour ground hold. The 28-hour ground hold case would require an optimum insulation thickness greater than practical or would result in unacceptable venting losses. The 4-hour case was analyzed, resulting in an optimum insulation thickness of 6.1-cm (2.4-in). The results are presented in Figure IV-25 and Table IV-25.

The tank pressure rise rate during the four-hour ground hold is 5.0 KN/m² (0.73 psi/hr). During on-orbit coast the heat leak is quite small, resulting in a pressure rise rate of 0.032 KN/m² (0.0047 psi/hr). Because this heating rate is small, there is no need to vent the oxygen tank for this mission. The on-orbit pressure rise rate for configuration 11 is less than for configuration 10 because the greater thickness of MLI (added to improve ground performance of the non-vacuum jacketed tank) results in a lower net heat flux to the liquid oxygen.

The tank is pressurized with helium to 138 KN/m² (20 psia) just prior to outflow and maintained until depletion of liquid oxygen. The weight advantage of the non-vacuum-jacketed approach is clearly obvious. A 6061-T6 aluminum vacuum jacket weight of about 450 kg (1000 lb) is much greater than the weight of approximately 61 kg (135 lb) of additional MLI plus 136 kg (300 lb) for the purge bag and closeout fairings.
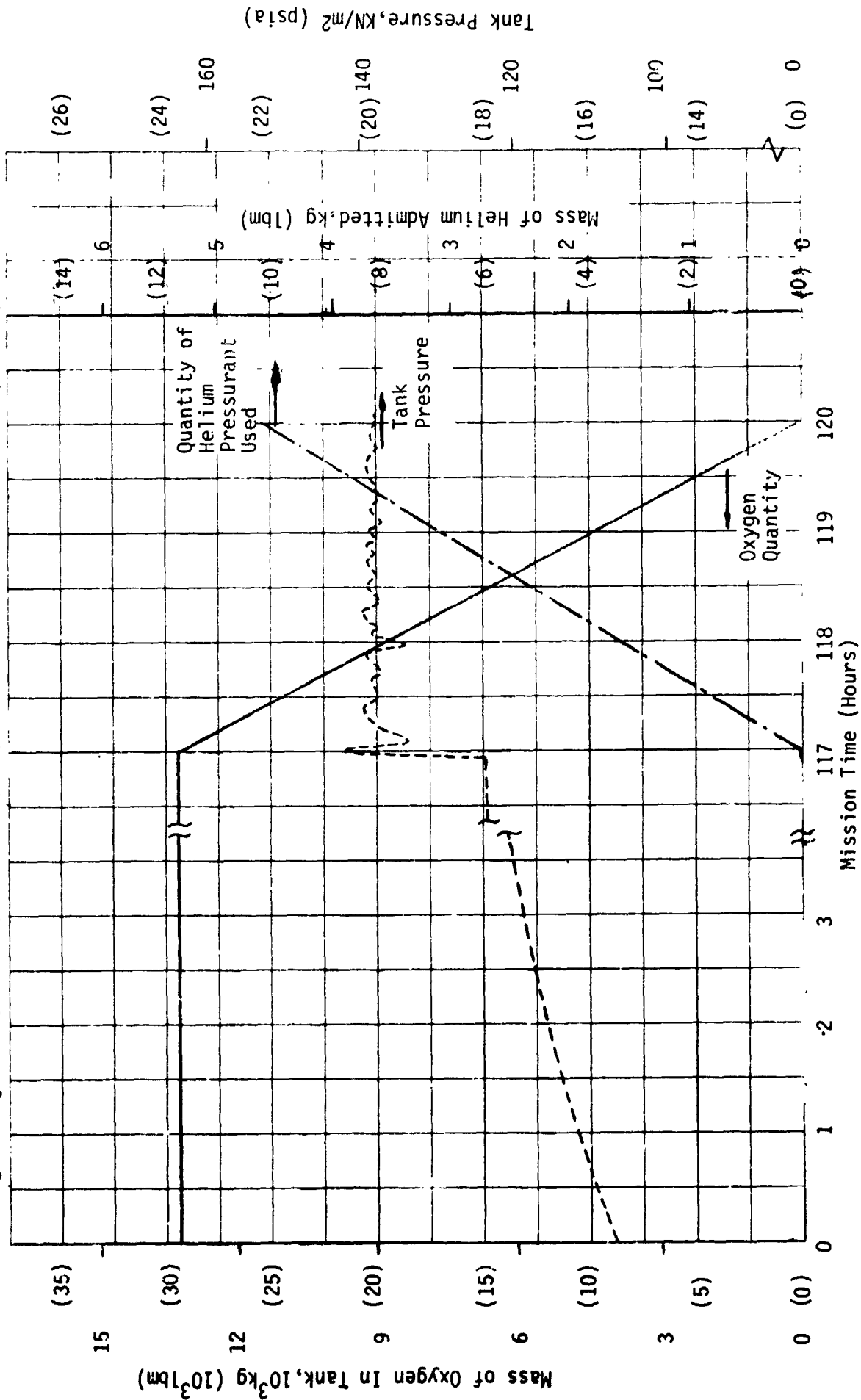
Figure IV-25 Oxygen 12.5 m³ (440 ft³) Storage and Supply Tank for
On-Orbit Resupply (4-Hour Ground Hold)

Table IV-25 Steady State Heat Leak - 12.5 m^3 (440 ft^3)
Oxygen Tank (No Vacuum Jacket) - Config. 11

| Conductor | TVS Inoperative Heat Input | | % of Total |
	Watts (Btu/hr)	Watts/m^2 (Btu/hr ft^2)	
MLI Thickness 6.1-cm (2.4-in)	9.3 (31.7)	0.36 (0.114)	72
Supports	3.1 (10.6)	0.12 (0.038)	23
Penetrations	0.4 (1.4)	0.01 (0.003)	3
Thermodynamic Vent System (Flowrate = 0.0 kg/hr) (0.0 lb/hr)	0.2 (0.7)	0.01 (0.003)	2
Total	13 (44.4)	0.49 (0.158)	100

Configuration 12

The 37.4 m^3 (1320 ft^3) cylindrical hydrogen storage tank is modelled with a TVS to cool the penetrations under the SOFI insulation to intercept the heat leak. A 5-day mission is simulated, the final 3 hours of which are used to outflow for resupply. To show the sensitivity to ground heat leak, a 4-hour ground hold case, and a case where topping of the tank occurs immediately prior to liftoff, were evaluated.

The results for the 37.4 m^3 (1320 ft^3) cylindrical hydrogen tank with a 4-hour ground hold and with no ground hold appear in Figures IV-26 and IV-27, respectively. Table IV-26 gives the steady-state heat inputs for the no-ground-hold case. The optimum MLI thickness for the cylindrical tank with 4 hours of ground hold is 5.0-cm (1.95-in). The tank pressure rises from 103 KN/m^2 to 228 KN/m^2 (15 to 33 psia) during the 4 hours of nitrogen-purge prior to liftoff, despite the fact that 186 kg (410 lb) of hydrogen is vented
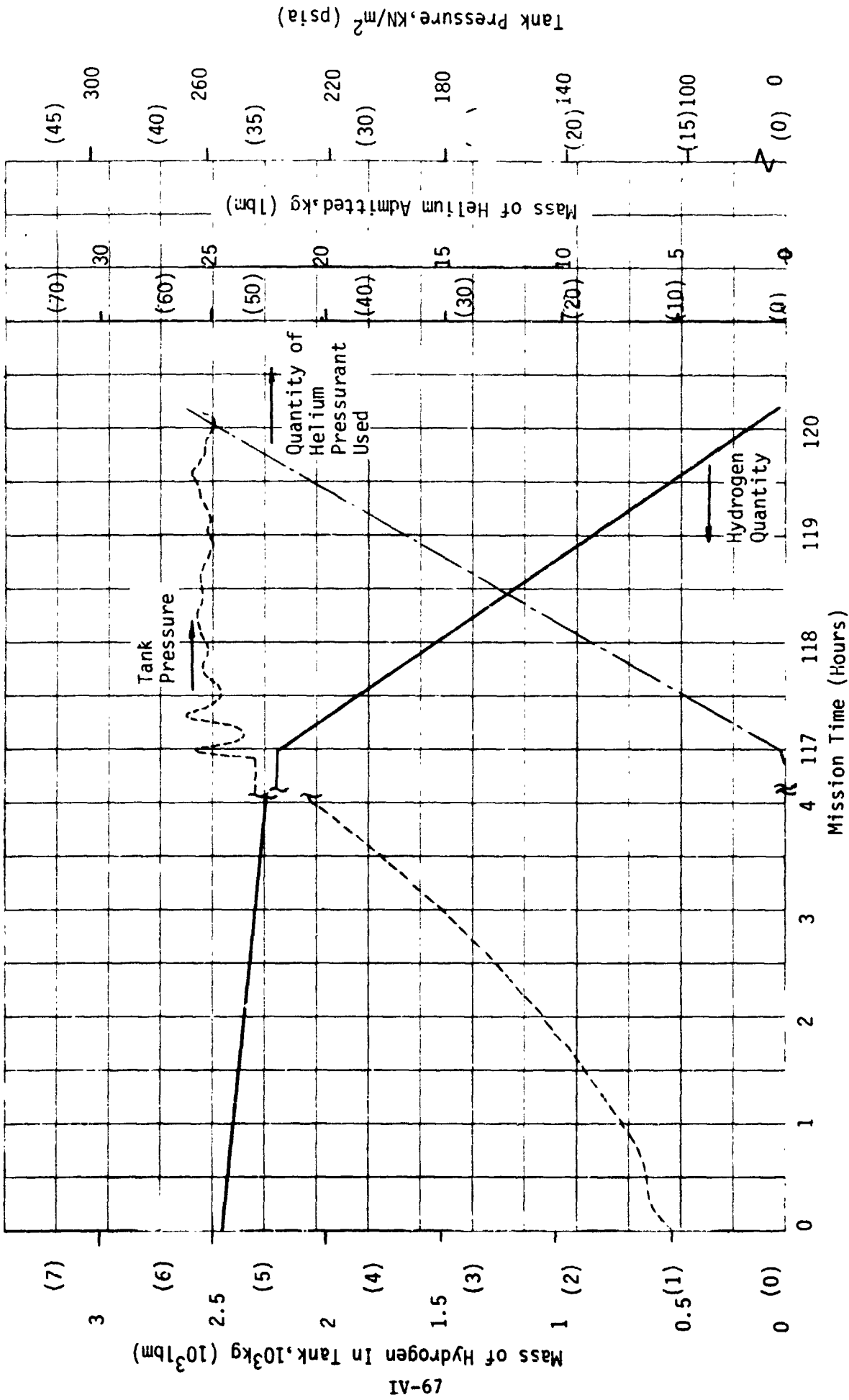
Figure IV-26 Cylindrical Hydrogen 37.4 m³ (1320 ft³) Storage and Supply Tank for On-Orbit Resupply (4-Hour Ground Hold)

IV-67
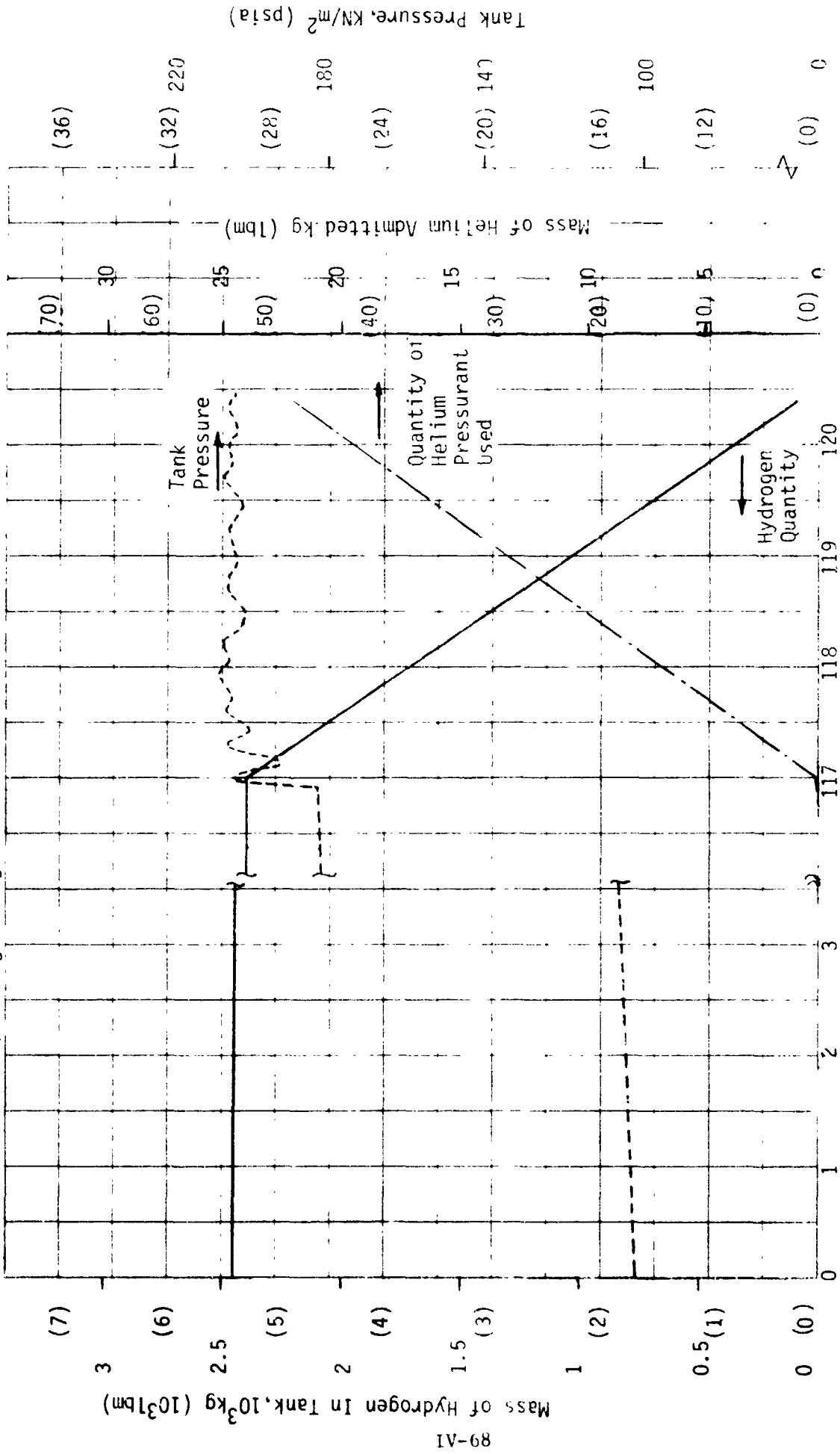
Figure IV-27 Cylindrical Hydrogen 37.4 m³ (1320 ft³) Storage and Supply Tank for On-Orbit
Resupply (Topping Immediately Prior to Lift-off)

at a rate of 46.6 kg/hr (103 lb/hr). During the 113-hour on-orbit coast the pressure only rises another 15 KN/m^2 (2.2 psi), which is a pressure rise rate of 0.13 KN/m^2 (0.019 psi/hr). A TVS flowrate of 0.42 kg/hr (0.93 lb/hr) is utilized, resulting in 48 kg (105 lb) of hydrogen vented while on-orbit. A total of 2211 kg (4875 lb) of liquid hydrogen is available for transfer. A total of 26 kg (58 lb) of helium is required to accomplish the outflow while maintaining a tank pressure of 262 KN/m^2 (38 psia).

The optimum MLI thickness for the cylindrical tank with no ground hold is 1.5-cm (0.57-in). In Figure IV-27, the on-orbit tank pressure rise rate is 0.70 KN/m^2 (0.10 psi/hr) with only 59 kg (130 lb) of hydrogen vented through the TVS at a rate of 0.51 kg/hr (1.11 lb/hr). Since the pressure is lower in this case than in the 4-hour ground hold condition, only 22 kg (49 lb) of helium pressurant is required for outflow to maintain a pressure of 203 KN/m^2 (29.5 psia). Also, 2386 kg (5260 lb) of hydrogen is available for transfer, an increase of 175 kg (385 lb) over the previous case.

Table IV-26 Steady-State Heat Leak - 37.4 m^3 (1320 ft^3)
Cylindrical Hydrogen Tank - Config. 12

Conductor	TVS Inoperative Heat Input		% of Total	TVS Operative Heat Input	
	Watts (Btu/hr)	Watts/m^2 (Btu/hr ft^2)		Watts (Btu/hr)	Watts/m^2 (Btu/hr ft^2)
MLI Thickness 1.5-cm (0.57-in)	108 (369)	2.0 (0.63)	64	106 (362)	2.0 (0.63)
Supports	61 (208)	1.2 (0.38)	36	59 (201)	1.1 (0.35)
Penetrations	1 (3)	0.1 (0.03)	<1	1 (3)	0.1 (0.03)
Thermodynamic Vent System (Flowrate = 0.45 kg/hr) (1.0 lbm/hr)	1 (3)	0.1 (0.03)	<1	45* (154)*	0.9* (0.29)*
Total	171 (583)	3.4 (1.04)	100	121 (412)	2.3 (0.72)

* indicates heat flow from tank to conductor.

Configuration 13

The results for the 37.4 m³ (1320 ft³) spherical hydrogen tank with topping immediately prior to liftoff are presented in Table IV-27 and Figure IV-28. The optimum MLI thickness for this configuration is 1.75-cm (0.69-in), compared to 1.5-cm (0.57-in) of MLI for the comparable cylindrical tank case (configuration 12). The reason more MLI was utilized for this configuration was because it has a smaller surface area, resulting in less weight of MLI per layer. (The relative weighting of MLI weight and vented hydrogen weight was identical to that of the cylindrical tank; i.e. each pound of MLI weight considered equivalent to two pounds of vented hydrogen weight.)

The tank pressure rises to 183 KN/m² (26.5 psia) in the 117 hours prior to lift-off. This corresponds to a pressure rise rate of 0.67 KN/m² (0.096 psi/hr), which is slightly less than the cylindrical tank with a slightly thinner insulation blanket. The quantity of hydrogen vented through the TVS at a rate of 0.15 kg/hr (0.33 lb/hr) results in a total of 18 kg (39 lb) vented, which is also less than the 59 kg (130 lb) vented for the cylinrical case.

As with the cylindrical tank, the pressure is increased to 203 KN/m² (29.5 psia) with helium just prior to outflow and is maintained until the tank is depleted. A total of 20 kg (44 lb) of helium pressurant is required to accomplish outflow.

Table IV-27   Steady-State Heat Leak - 37.4 m³ (1320 ft³)
Spherical Hydrogen Tank - Config. 13

Conductor	TVS Inoperative Heat Input		% of Total	TVS Operative Heat Input	
	Watts (Btu/hr)	Watts/m² (Btu/hr ft²)		Watts (Btu/hr)	Watts/m² (Btu/hr ft²)
MLI Thickness 1.8-cm (0.69-in)	79 (270)	1.4 (0.44)	94	76 (259)	1.4 (0.44)
Supports	4 (14)	0.1 (0.03)	5	4 (14)	0.1 (0.03)
Penetrations	1 (3)	0.1 (0.03)	< 1	1 (3)	0.1 (0.03)
Thermodynamic Vent System (Flowrate = 0.15 kg/hr) (.33 lb/hr)	1 (3)	0.1 (0.03)	< 1	17* (58)*	0.3* (0.10)
Total	85 (290)	1.7 (0.53)	100	64 (218)	1.3 (0.40)

* indicates heat flow from tank to conductor.
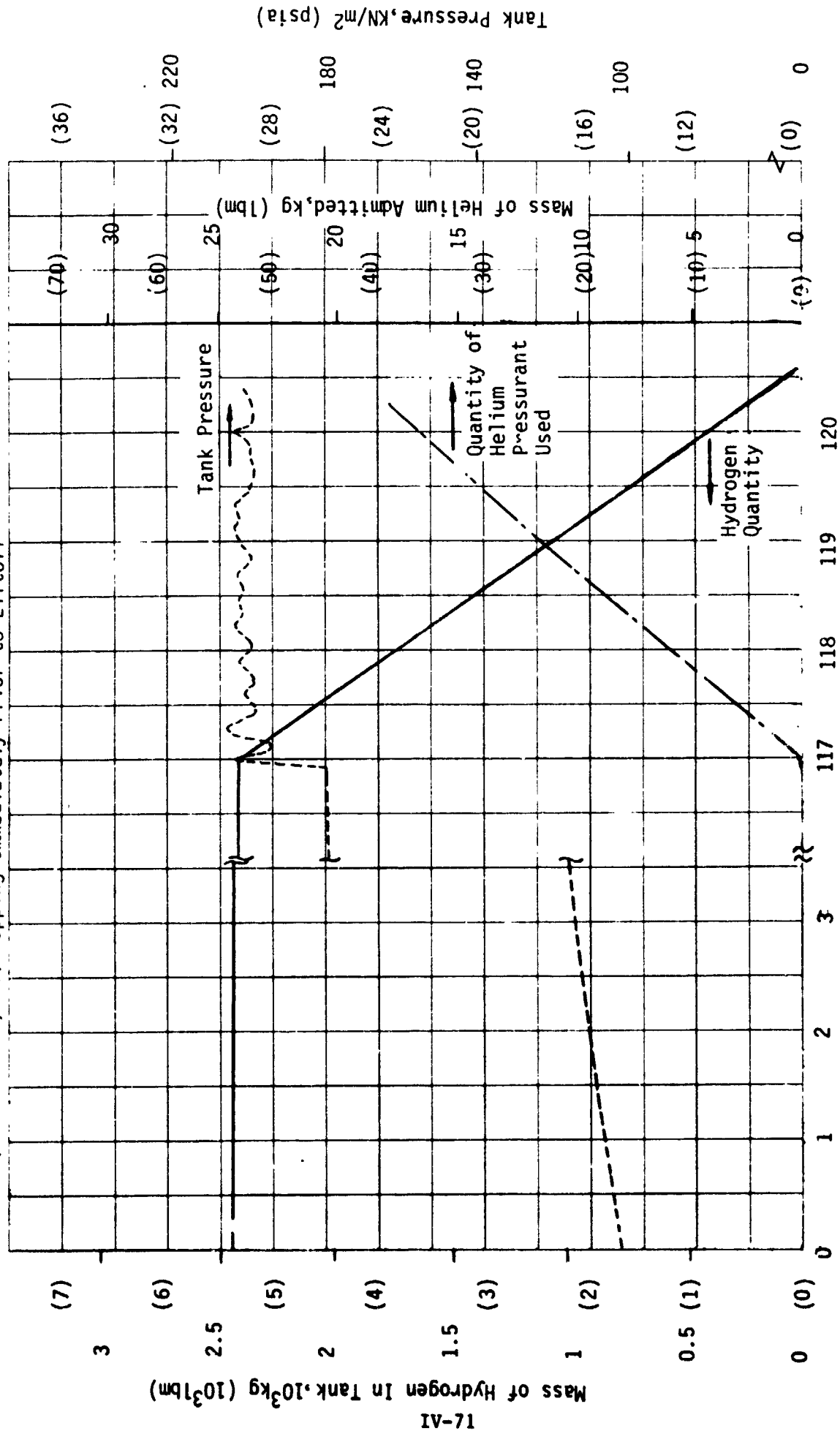
Figure IV-28 Spherical 37.4 m^3 (1320 ft^3) Hydrogen Storage and Supply Tank for On-Orbit Resupply

A comparison of Table IV-27 with the previous table for the cylindrical tank reveals that the total heat leak with the TVS inoperative is 84 W (287 Btu/hr) for the spherical tank and 170 W (580 Btu/hr) for the cylindrical tank. The largest difference between these tanks is not the MLI heat input, but rather the support heat input. This is understandable when the supports of the two configurations are compared, as will be discussed in Section C and Chapter V. The cylindrical tank has supports of a much greater cross-sectional area, and the average length of the supports is about one-third the length of those for the spherical tank. Both of these factors greatly increase the support heat leak.

C. Preliminary Structural Analysis

The structural analysis was primarily concerned with assuring that the structural integrity of each storage and supply system was maintained during transport to low-earth-orbit within the Shuttle payload bay. The specific elements evaluated for each system were the acquisition device, pressure vessel, vacuum jacket, and supports.

1. Liquid Acquisition Device Structural Evaluation

For the 0.62 m^3 (22 ft^3) tanks, the LAD designed for the CFME was adequate to meet all performance requirements. The concept of the LAD structure is a polar mounted design, attached to the inner pressure vessel at two locations. One end is welded to the tank at the attachment of the outlet tube, and the other end is restrained only in the lateral direction. The primary elements of the LAD are the two complete fluid carrying ring structures in mutually perpendicular planes to each other. They join at the two main support points to the pressure vessel in a manifold structure. Special proprietary provisions are included in the design to handle the rather severe dynamic loads occurring during launch. Primary structural material is annealed 321 stainless steel. Structural joints are accomplished using fusion welding, and resistance spot and seam welding.

The random vibration environment produces inertial responses of the structural mass plus effective fluid mass. Since structural design is an iterative process, a value of 50 g's limit was used for the preliminary sizing. The effective fluid loading was taken as twice the mass on the circular cross-sectional area, with a diameter equal to the maximum width of the structure in the direction of loading.

The four major loading conditions considered were:

1) Torsion
2) Lateral
3) Longitudinal
4) Egging

The configuration and support of the LAD for the larger tanks vary from concepts used on the 0.62 m³ (22 ft³) tanks. The initial concept here is to bolt the channels to the tank wall. The channels are bolted every 66-cm (26-in) to meet an estimated maximum deflection requirement of 0.25-cm (0.10-in). Slotted holes are provided in the support flanges (Figure IV-29) to allow for differential expansion and contraction under cryogenic conditions. This prevents the introduction of additional stresses into the basic channel structure.

For these larger tank sizes, the primary elements of the LAD are still the two complete fluid carrying ring structures in mutually perpendicular planes. Structural material and joints are similar to 0.62 m³ (22 ft³) tanks. The random vibration environment is less severe on the larger tanks due to the larger size and mass. The level used in preliminary sizing was 6.5 g's.

2. Pressure Vessel Sizing

The 0.62 m³ (22 ft³) tank was sized to an ultimate pressure of 3.75 times the maximum operating pressure of 414 KN/m² (60 psia) or 1551 KN/m² (225 psia). A factor of 2.5 was applied to the maximum operating pressure to obtain the limit pressure load. A factor of 1.5 was then applied to limit to obtain the ultimate pressure load. This high ultimate factor was used due to the experimental nature of the CFME, and the fact that the storage tank contains liquid hydrogen in the Shuttle cargo bay. The pressure vessel is 6061-T6 aluminum, with a wall thickness of 0.15-cm (0.057-in). A detailed BOSOR 4 (Buckling of shells of Revolution - Ref 41) model was run to determine local thickening due to bending at the supports and to inertial G loads.

The maximum operating pressure for sizing the larger pressure vessels was 414 KN/m² (60 psia). A design factor of 1.5 was applied to obtain the ultimate pressure. This criteria was used to determine shell thicknesses, which are listed in Table IV-28. Aluminum alloys used for comparison were 2014-T6, 2219-T62, and 6061-T6. The thicknesses for the hemispheres that serve as end caps for the 37.4 m³ cylindrical pressure vessel are identical to those of the 12.5 m³ tanks since the diameters are the same. A sufficient taper in the hemispheres of the cylindrical tank is needed to match the additional thickness required by the cylinder.
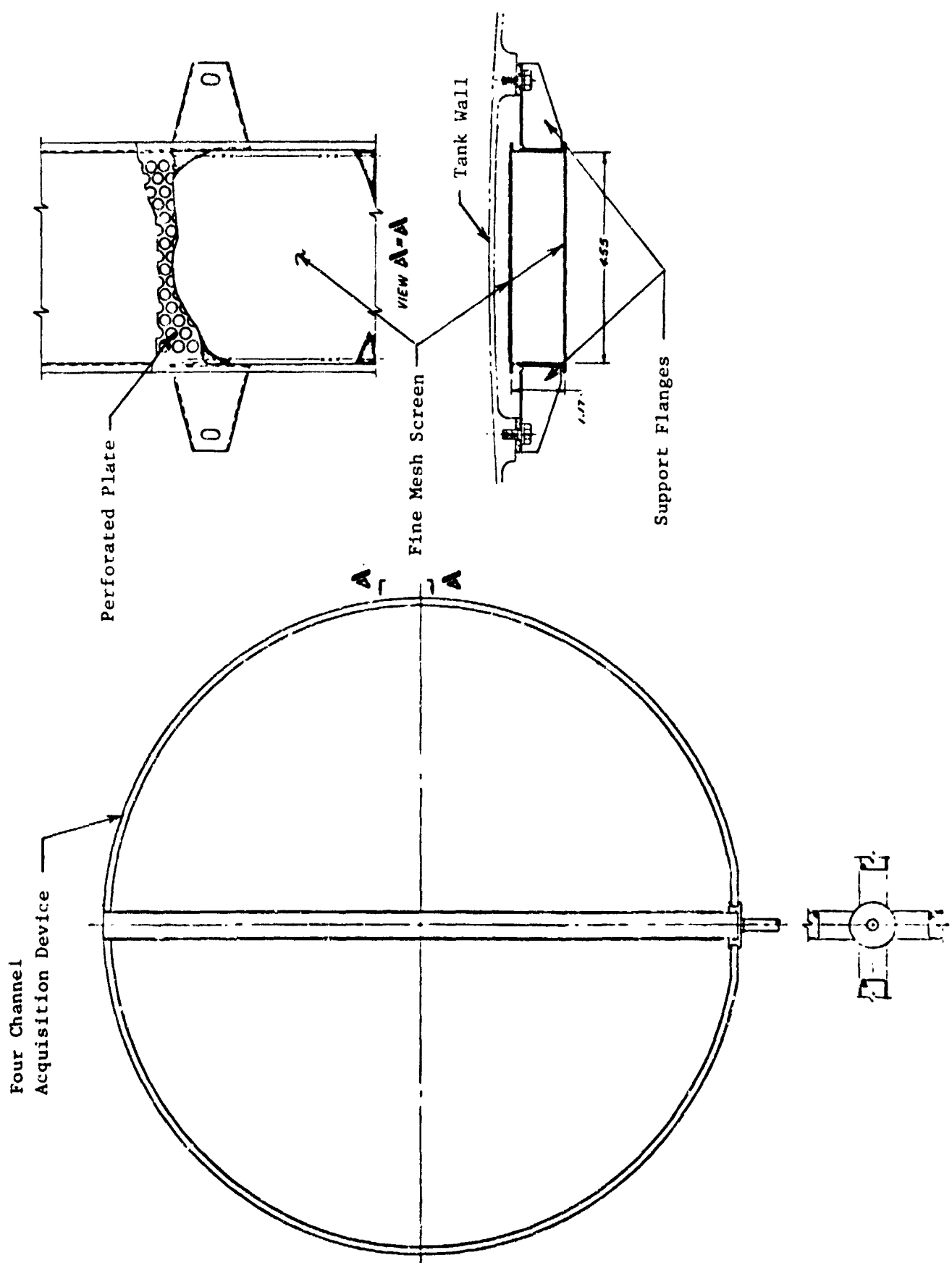
Figure IV-29 Acquisition Device Channel Support Concept

Table IV-28 Pressure Vessel Shell Thicknesses

Tank Size	Wall Thickness cm (in)		
	6061-T6	2219-T62	2014-T6
0.62 m^3 (22 ft^3)	0.14 (0.057)	0.10 (0.041)	0.08 (0.033)
12.5 m^3 (440 ft^3)	0.17 (0.067)	0.12 (0.048)	0.10 (0.039)
37.4 m^3 (1320 ft^3) cylindrical {dome configuration {barrel	0.17 (0.067) 0.34 (0.134)	0.12 (0.048) 0.24 (0.096)	0.10 (0.039) 0.20 (0.078)
spherical configuration	0.25 (0.097)	0.18 (0.069)	0.14 (0.056)

A simplified BOSOR 4 model was run for the 12.5 m^3 (440 ft^3) pressure vessel to verify shell thicknesses. The 37.4 m^3 (1320 ft^3) spherical tank is very similar, so this BOSOR run was used to verify both tanks. Due to the complexity of the support structure on the 37.4 m^3 (1320 ft^3) cylindrical tank, a BOSOR model was not generated for this configuration. A complex BOSOR 4 model (or alternate) is needed for all the larger tanks to determine thicknesses for areas with discontinuity stresses, weld areas with low allowables, and local thickening where supports are attached.

Comparison of the different aluminum alloys shows the advantage of using a 2014-T6 or a 2219-T62 alloy. Neither of these alloys is as easy to weld as 6061 but Martin Marietta has developed techniques for welding both alloys. Alloy 2014-T6 is used in construction of large propellant tanks on the Titan program and 2219-T62 is being used on the Shuttle External Tank.

3. Vacuum Jacket Sizing

A finite element model (NASTRAN) of the CFME vacuum jacket structure, including girth ring and external supporting tube, was generated. The model consisted of about 500 node points which described the geometric configurations of the two hemispherical pieces with connecting girth ring and supporting tube. A total of 450 plate elements were used for the vacuum jacket and girth ring while about 60 plate elements were used to model the supporting tubes. All plate elements in the model were capable of carrying in-plane forces as well as out-of-plane moments.

A factor of 1.5 was used on a collapse pressure of 101 KN/m^2 (14.7 psi) for ultimate collapse pressure. A shell wall thickness of 0.28 cm (0.11 in) on the jacket was selected assuming spun hemispherical domes, with local thicknesses added for support pickups and line penetrations. This provided a design margin of +0.63.

Vacuum jackets for the larger tanks were sized by hand analysis using the knock down factors in the Astronautic Structures Manual (Ref 42). Table IV-29 lists vacuum jacket shell thicknesses for each tank size and the three aluminum alloys, 6061-T6, 2219-T62 and 2014-T6. Here ultimate collapse pressure was taken to be 1.25 times a collapse pressure of 101 KN/m^2 (14.7 psi).

One way to reduce vacuum jacket weight for these larger tank sizes is to go to some type of honeycomb structure, such as an isogrid pattern. Potential weight savings of this method would be about 20 percent, although this does not represent a significant enough improvement to make the vacuum-jacketed approach the preferred design.

Table IV-29   Vacuum Jacket Shell Thicknesses

Tank Size	Wall Thickness cm (in)		
	6061-T6	2219-T62	2014-T6
0.62 m^3 (22 ft^3)	0.28 (0.11)	0.25 (0.10)	0.25 (0.10)
12.5 m^3 (440 ft^3)	0.64 (0.25)	0.61 (0.24)	0.61 (0.24)
37.4 m^3 (1320 ft^3) cylindrical {dome configuration {barrel	0.64 (0.25) 1.18 (0.47)	0.60 (0.24) 1.16 (0.46)	0.60 (0.24) 1.16 (0.46)
spherical configuration	0.94 (0.37)	0.91 (0.36)	0.91 (0.36)

4. Structural Supports for Larger Tanks

The material selected for the struts that attach the tank assembly to the Orbiter supports was S-glass epoxy. This material was selected due to its low thermal conductivity and low coefficient of expansion. The critical loading condition on the struts was during liftoff when the tank is subjected to -4.5, +6.5 g in the X direction, +2.5 in the Y direction and +6.0 g in the Z direction. These are limit load factors and can be applied singly or in combination. The struts are pin ended and are critical in compression. The thermal effects due to the contents of the tanks (e.g. liquid hydrogen) were also taken into account in analyzing the struts. Allowables for the S-glass epoxy were generated using the SQ5 computer program.

All tanks (except for the one mounted on the Spacelab pallet) were attached to five hardpoints in the Shuttle cargo bay, four on the side longerons and one (keel fitting) in the center floor of the cargo bay. All four longeron hardpoints are capable of reacting vertical loads (Z), two can react fore & aft loads (X) and the keel fitting hardpoint can react side loads (Y). Reactions at these five hardpoints did not exceed the load capability of the hardpoints. The specific sizes of each of the S-glass struts and aluminum channel members are identified on the design sketches in Chapter V.

V. ORBITAL STORAGE AND SUPPLY SYSTEM CONCEPTUAL DESIGN (TASK I UPDATE)

Following the Task II fluid dynamic, thermal and structural analysis, the preliminary conceptual designs were updated to reflect specific lengths, diameters and thicknesses of the various elements that make up the tank assemblies. Weight estimates were then generated for each of the 13 configurations.

A. Conceptual Design Update

A sketch of the 12.5 m^3 (440 ft^3) vacuum-jacketed tank is shown in Figure V-1. S-glass epoxy support struts were used to support the storage tank inside the vacuum jacket. The relatively severe environment during launch, and the need to take out torsion dictated the specific arrangement of the struts. It was also desirable to get as much length as possible for thermal considerations. The 12.5 m^3 (440 ft^3) non-vacuum-jacketed tank support concept is presented in Figure V-2. This tank is attached to an aluminum framework by eight S-glass epoxy struts. The aluminum frame distributes the loads to four hardpoints on the payload bay side longerons. The tank is attached directly to the Shuttle floor to take out side loads.

The 12.5 m^3 (440 ft^3) non-vacuum-jacketed tank mounted on a Spacelab pallet is shown in Figure V-3. Attachment to the pallet is by ten struts. With this configuration, the pallet redistributes the loads to the payload bay hardpoints. The struts for this case are relatively long, and therefore large in diameter and thickness to support the loaded argon tank assembly.

The 37.4 m^3 (1320 ft^3) cylindrical hydrogen tank, shown in Figure V-4, is supported in a rigid framework consisting of three aluminum rings connected to each other by struts. Loads are transmitted to the rings through the S-glass epoxy struts, and the rings connect to the cargo bay hardpoints. The rings are statically indeterminate, so a finite element model was generated of the rings and struts. Shears, bending moments and axial loads were used to size the rings.

The 37.4 m^3 (1320 ft^3) spherical hydrogen tank mounting approach is shown in Figure V-5. Because there is very little clearance in the cargo bay for this size spherical tank (even without a vacuum jacket), the support members are relatively short-coupled. Twenty-four struts connect the tank to two aluminum rings which form a rigid support structure by means of braces and attaching beams. The rings pick up 5 cargo bay attach points, four longeron hardpoints and a keel hardpoint. These rings were also analyzed using a finite element model.

B. Weight Estimates

Calculated weights for each of the cryogenic storage and supply systems are presented in Table V-1. The weights of the storage tank, acquisition device and vacuum jacket have been increased by 10 percent to account for local thickening, fittings, etc. The storage tank and vacuum jacket were assumed to be 6061-T6 aluminum, and the acquisition device stainless steel. The weights of the composite support trunnions and struts contain a 15 percent allowance for local thickening, end fittings and couplings.

TORSIONAL RESTRAINT
6.0-CM OD, 0.64-CM WALL
(2.4-IN OD, 0.25-IN WALL)

NOTE: ALL STRUTS
S-GLASS/EPOXY TUBE

ALUMINUM TUBE
9.5CM OD, .64CM WALL
(3.75IN OD, X .25IN WALL)

5.1-CM OD, 0.56-CM WALL
(2.0-IN OD, 0.22-IN WALL)

5.1-CM OD, 0.56-CM WALL
(2.0-IN OD, 0.22-IN WALL)

3.8-CM OD, 0.32-CM WALL
(1.5-IN OD, 0.13-IN WALL)

VACUUM JACKET

STRUT 7.62-CM OD, 0.64-CM WALL
(3.0-IN OD, 0.25-IN WALL) MS = +.07

STORAGE TANK

RECT. ALUM. TUBE
15.2CM X 10.2CM X 1.3CM
(6.0IN X 4.0IN X .5IN)

Figure V-1 Vacuum-Jacketed 12.5 m³ (440 ft³) Tank Support Concept

V-2

NOTE: ALL STRUTS
S-GLASS/EPOXY TUBE

15.2-CM OD, 0.95-CM WALL
(6.0-IN OD, 0.38-IN WALL)

STORAGE TANK

11.4-CM OD, 0.95-CM WALL
(4.5-IN OD, 0.38-IN WALL)

PAYLOAD BAY
ENVELOPE

RECT. TUBE
15.2CM X 10.2CM X 1.3CM
(6.0IN X 4.0IN X.5IN)
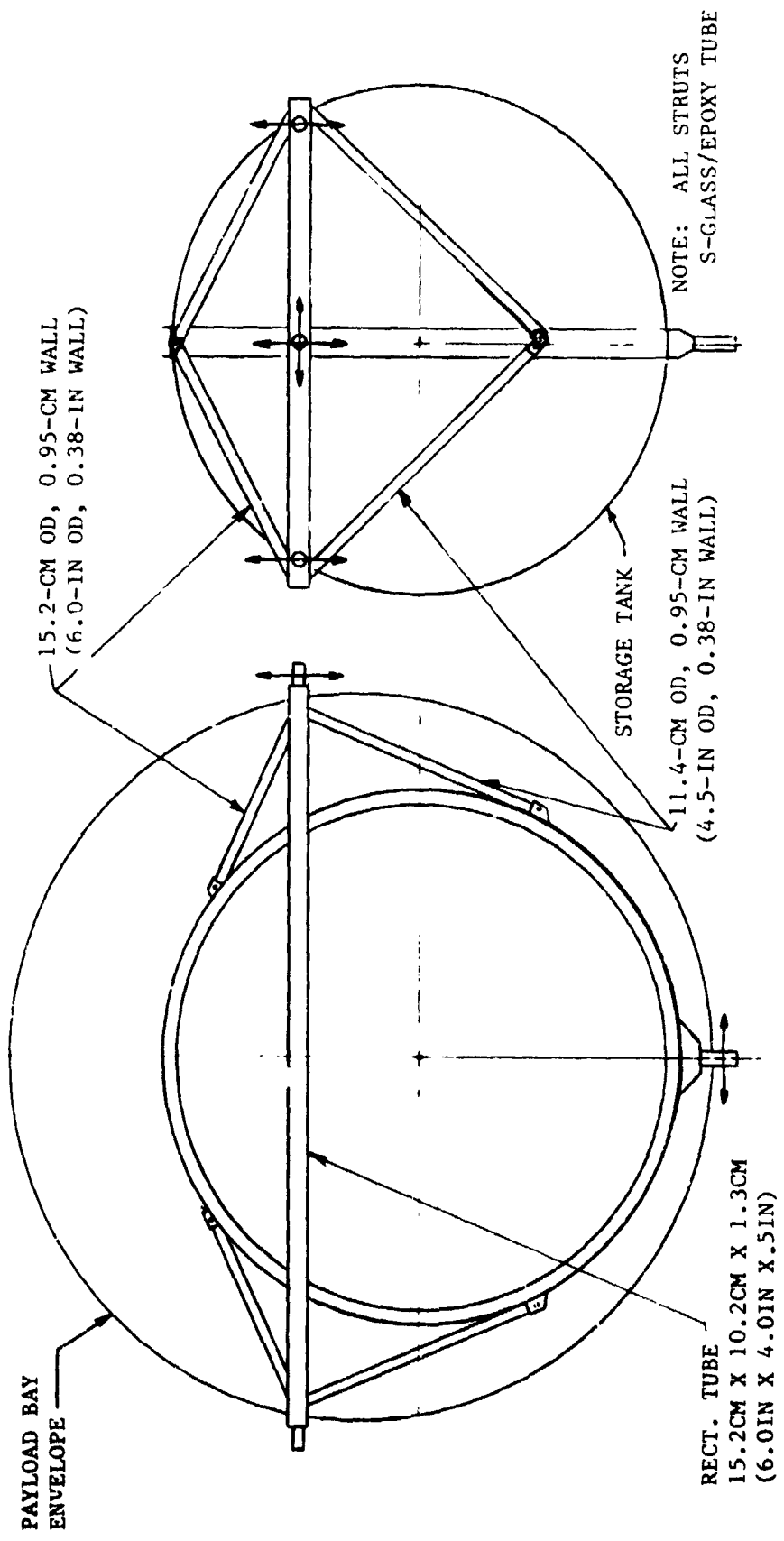
Figure V-2 Non-Vacuum-Jacketed 12.5 m³ (440 ft³) Tank Support Concept

NOTE: ALL STRUTS S-GLASS/EPOXY TUBE

STORAGE TANK

STRUTS
10.2-CM OD, 1.3-CM
WALL (4.0-IN OD, 0.50-IN
WALL)   MS = + .13

SPACELAB PALLET

PAYLOAD BAY
ENVELOPE

8.26CM OD, 0.64-CM WALL
(3.25-IN OD, 0.25-IN WALL)
MS = 0.0 +
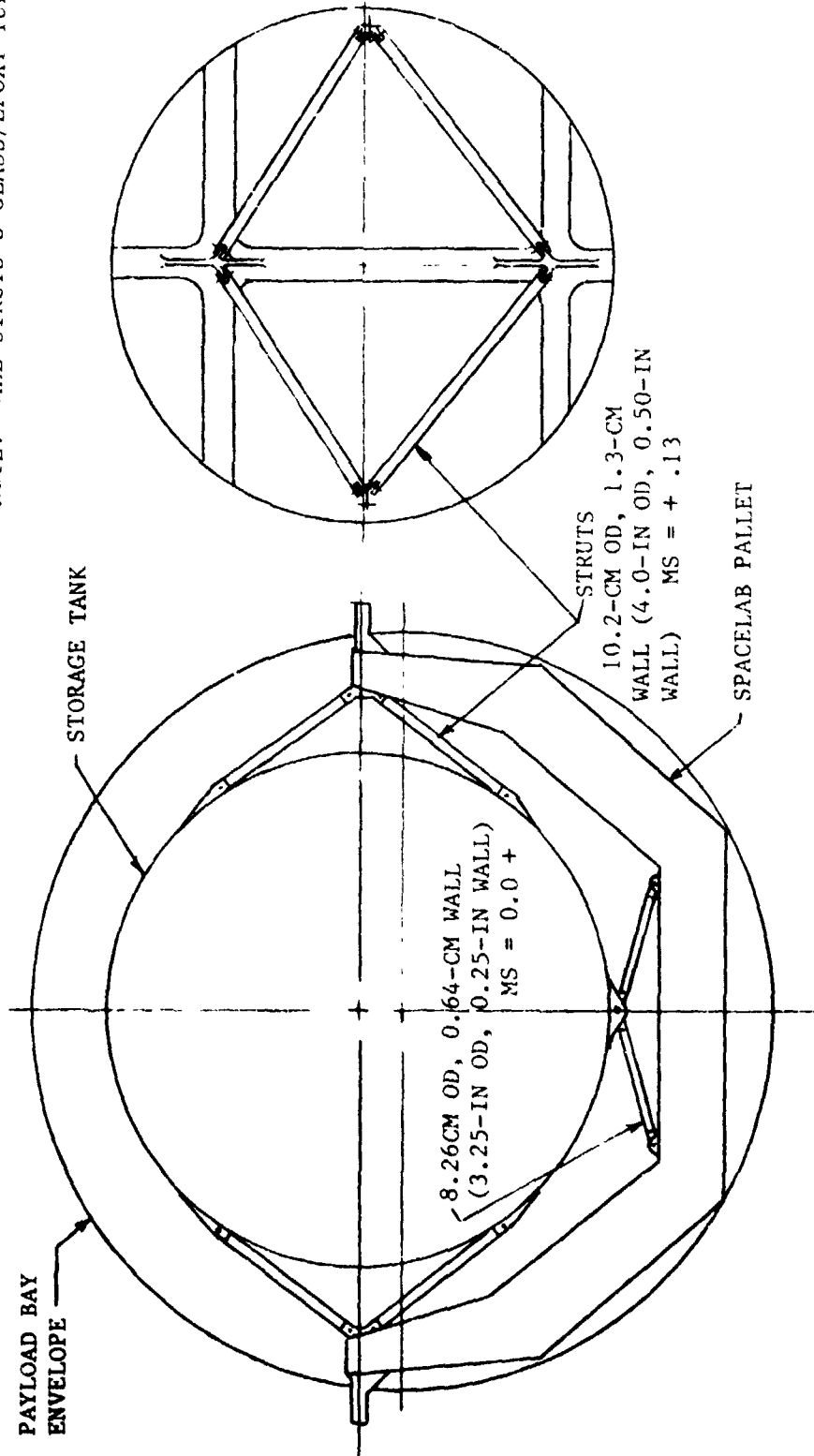
Figure V-3   Non-Vacuum-Jacketed 12.5 m^3 (440 ft^3) Tank Mounted on
Spacelab Pallet

I BEAM (ALUMINUM)
15.2CM X 10.2CM X .64CM
(6.0IN X 4.0IN X .25IN)

STORAGE TANK

7.6-CM OD, 0.48-CM
WALL (3.0-IN OD,
0.19-IN WALL)

8.3-CM OD, 0.48-CM WALL
(3.25-IN OD, 0.19-IN WALL)

7.0-CM OD, 0.40-CM WALL
(2.75-IN OD, 0.16-IN WALL)

5.1-CM OD, 0.32-CM WALL
(2.0-IN OD, 0.13-IN WALL)
TOP & BOTTOM MEMBERS

4.44-CM OD, 0.40-CM WALL
(1.75-IN OD, 0.16-IN
WALL)

3.2-CM OD
0.3-CM WALL
(1.25-IN OD,
0.12-IN WALL)
TOP & BOTTOM-
BOTH ENDS

3.8-CM OD,
0.3-CM WALL
(1.5-IN OD,
0.12-IN WALL)
EACH SIDE

NOTE:
ALL STRUTS S-GLASS/EPOXY
TUBE
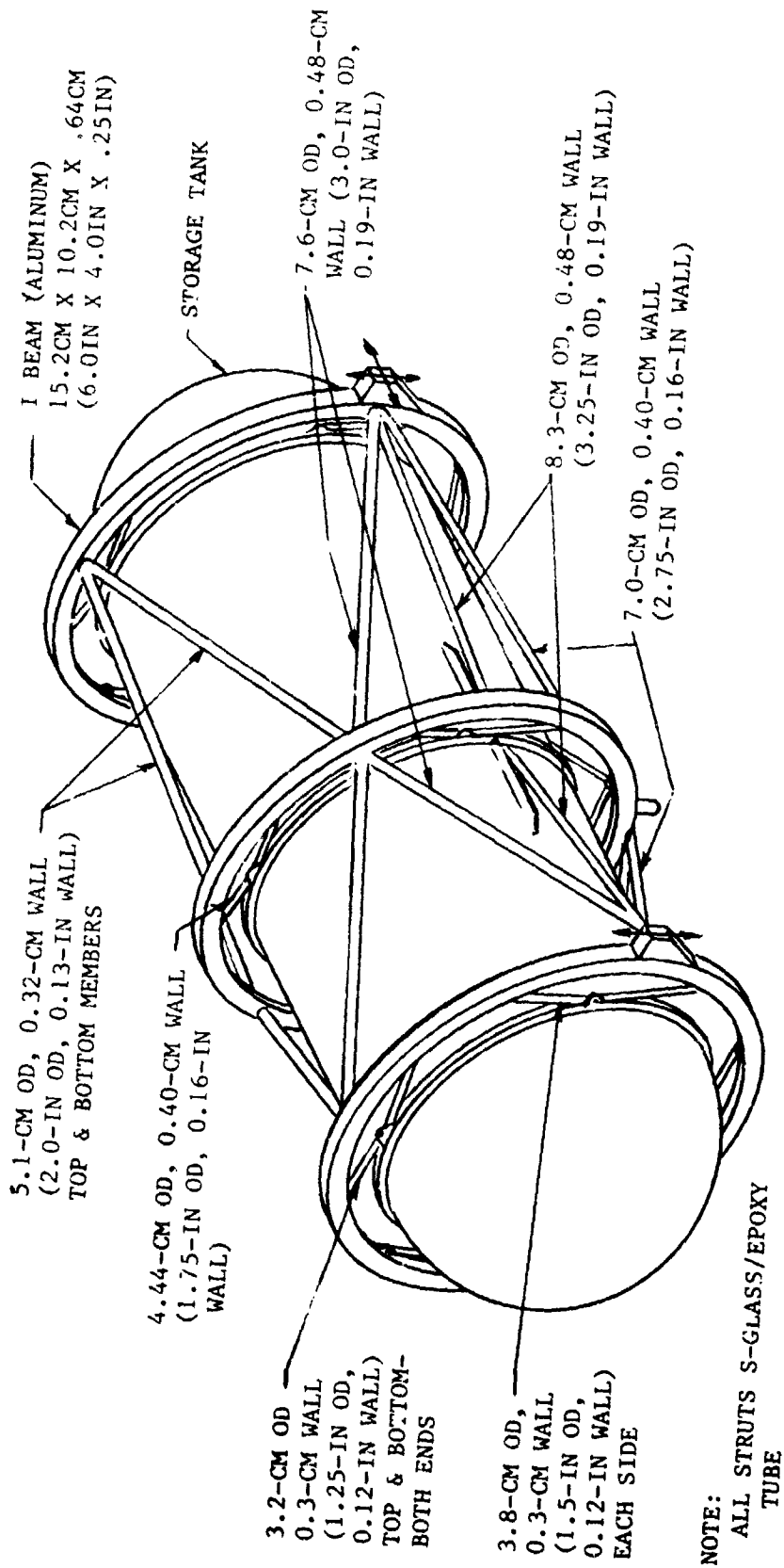
Figure V-4 Cylindrical 37.4 m^3 (1320 ft^3) Tank Support Concept

I BEAM (ALUMINUM)
15.2CM X 10.2CM X .64CM
(6.0IN X 4.0IN X .25IN)

SECTION B-B
(4 PLACES)

STORAGE TANK

4.45-CM OD, 0.32-CM
WALL

(1.75-IN OD, 0.13-IN
WALL)

MS = + .16

3.8-CM OD, 0.32-CM WALL
(1.5-IN OD, 0.13-IN WALL)
MS = + .17

4.45-CM OD, 0.40-CM WALL
(1.75-IN OD, 0.16-IN WALL.)
MS = + .11

3.8-CM OD, 0.40-CM WALL
(1.5-IN OD, 0.16-IN WALL)
MS = + .05

TOP & BOTTOM

NOTE:
ALL STRUTS S-GLASS/EPOXY TUBE

Figure V-5 Spherical 37.4 m^3 (1320 ft^3) Tank Support Concept

Table V-1 Cryogenic Storage and Supply System Weight Comparison

Weights, kg (lb)

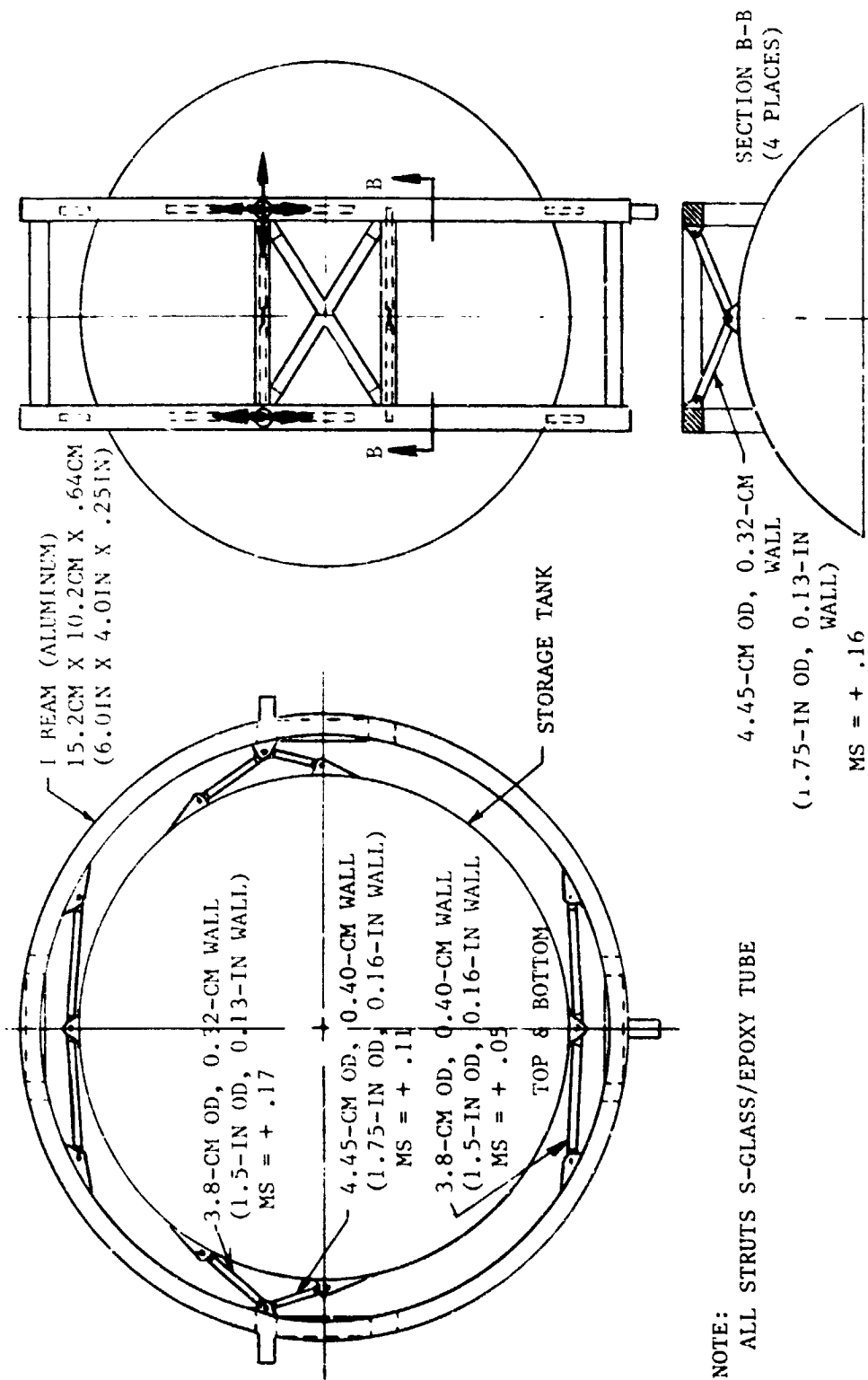| Config.	Category	Size	Fluid	Storage* Tank	Acquisition* Device	Structural△ Supports	Insulation†	Thermal TVS/VCS	Purge System	Vacuum* Jacket	Total
CPME	Baseline	0.62 m³	H₂	22 (49)	10 (23)	3 (7)	8 (18)	21 (47)	--	61 (133)	125 (277)
1	I	0.62 m³	CH₄	22 (49)	10 (23)	4 (8)	10 (22)	21 (47)	--	64 (140)	131 (289)
2	II	0.62 m³	Ar	22 (49)	10 (23)	7 (16)	25 (54)	21 (47)	--	104 (228)	189 (417)
3	III	0.62 m³	O₂	22 (49)	10 (23)	4 (8)	8 (18)	21 (47)	--	61 (133)	126 (278)
4	IV	0.62 m³	He	22 (49)	10 (23)	8 (18)	25 (54)	41 (90)	--	104 (228)	210 (462)
5	V	12.5 m³	Ar	132 (290)	31 (69)	252 (555)	160 (351)	156 (343)	--	515 (1132)	1248 (2740)
6		12.5 m³	Ar	132 (290)	31 (69)	302 (665)	160 (351)	16 (35)	80 (176)	--	721 (1586)
7		12.5 m³	Ar	132 (290)	31 (69)	110 (242)**	160 (351)	16 (35)	80 (176)	--	529 (1163)
8	VI	12.5 m³	CH₄	132 (290)	31 (69)	252 (555)	18 (39)	156 (343)	--	515 (1132)	1104 (2458)
9		12.5 m³	CH₄	132 (290)	31 (69)	302 (665)	18 (39)	16 (35)	80 (176)	--	579 (1304)
10	VII	12.5 m³	O₂	132 (290)	31 (69)	252 (555)	30 (66)	156 (343)	--	515 (1132)	1116 (2487)
11		12.5 m³	O₂	132 (290)	31 (69)	302 (665)	93 (204)	16 (35)	80 (176)	--	655 (1439)
12	VIII	37.4 m³ (CYL)	H₂	425 (936)	43 (95)	295 (650)	72 (159)	35 (76)	184 (405)	--	1054 (2321)
13		37.4 m³ (SPH)	H₂	397 (873)	43 (95)	174 (382)	76 (167)	23 (51)	160 (352)	--	873 (1920)

* weights have been increased (except for CPME Baseline) by 10 percent to account for local thickening, fittings, etc. Storage Tank and Vacuum Jacket are 6061-T6 Aluminum, Acquisition Device is Stainless Steel.

** Does not include any weight for spacelab pallet.

△ weights have been increased (except 0.62 m³ tanks) by 15 percent to account for local thickening, fitting, etc.

† MLI, except for category VIII, which is MLI over SOFI

The weights for the 0.62 m³ (22 ft³) oxygen and methane tanks are close to that of the baseline CFME and reflect the minimum modifications required to handle the added fluid mass and the increased outlet line size. The 0.62 m³ (22 ft³) argon tank is heavier due to the thicker MLI blanket required and the larger vacuum jacket needed to accommodate the thicker MLI. The liquid helium tank assembly is substantially heavier than the CFME baseline due to the added hydrogen-cooled VCS and additional MLI.

A comparison of the 12.5 m³ (440 ft³) vacuum-jacketed tanks and the nitrogen-purged MLI (non-vacuum-jacketed) tanks shows at least a 455 kg (1000 lb) improvement for all cases, even with an estimated weight of 80 kg (176 lb) for a nitrogen-purge system, including purge bag, closeout fairings, and the purge gas distribution network. This purge system weight may be reduced if a bag arrangement can be developed to keep the insulation dry until the tank is enclosed in the payload bay, the doors are closed, and the cargo bay nitrogen purge system is activated.

The 37.4 m³ (1320 ft³) spherical hydrogen tank is approximately 159 kg (350 lb) lighter than the cylindrical tank, and both are significantly lighter than a vacuum-jacketed tank construction. A vacuum jacket is not possible for the spherical tank due to the maximum dynamic envelope available in the cargo bay. The spherical storage vessel size is 4.14 m (13.6 ft) and the Shuttle limitation is 4.57 m (15 ft), which is insufficient space for a vacuum jacket and structural supports. A vacuum jacket for the cylindrical tank would weight 1830 kg (4035 lb), which is more than a factor of 2 greater than the current concept design. If 2014-T6 were used for the storage tank instead of 6061-T6, a weight reduction of 106 kg (233 lb) is possible for the cylindrical tank, and 167 kg (368 lb) for the spherical tank.

The technology status for each cryogenic storage and supply system was evaluated and the results are presented in Table VI-1. A summary of both technology status and adequacy, and deficiencies, are listed in the Table. Additional descriptions of technology status in some of these areas are presented below and recommendations for analytical and experimental efforts itemized in Section B.

A. Technology Status

1. Liquid Acquisition Device (LAD)

Areas of technology deficiency for the LAD include all analytical and experimental aspects of performance with liquid helium, and adequate design information for evaluating and designing thermal isolation of the fine-mesh screen covered channels for all the fluids in the 12.5 m^3 (440 ft^3) and 37.4 m^3 (1320 ft^3) tanks.

In 1972 and 1973, a ground test program was conducted to verify several LAD design techniques for use with cryogenic fluids. Several bench models were tested in plus and minus 1-g, using LN$_2$, LO$_2$ and LH$_2$. A 63.5-cm (25-in) diameter LAD was successfully ground tested with LH$_2$. Gas-free liquid hydrogen expulsion was demonstrated under minus 1-g with both GH$_2$ and GHe pressurization (Ref 26).

Very little technology exists for application of a LAD to liquid helium. A study of passive low-gravity storage of liquid helium looked at applications, physical properties of helium I and II and some capillary system design ideas. Applications identified were cooling of I. R. telescopes, super-conducting magnets, a maser receiver for long distance communications, magnetometers, accelerometers and gravity wave detectors. System design ideas in this study centered around a dual screen liner with porous plugs in place of screen (Ref 43). Considerably more experimental data are needed to permit design extrapolation of current technology to liquid helium.

2. Viscojets*

Viscojets are used to produce a pressure drop, and a resulting temperature drop, in the upstream portion of the TVS tubing. The characterization of Viscojet performance from a pressure drop (and flowrate) standpoint is not completely understood for cryogenic fluids. Martin Marietta has conducted Internal Research and Development (IRAD) work with liquids nitrogen, hydrogen and argon, but this work needs to be extended to the other croyogens, particulary liquid helium.

---

*Devices manufactured by the Lee Company

Table VI-1 Technology Status and Deficiencies for Each
Cryogenic Storage and Supply System Category

Category	Tank Size	Fluid	Technology Status	Deficiencies
I	0.62 m³ (22 ft³)	CH₄	o Acquisition device technology available although bubble point not measured in methane o Design concepts and technology from CFME available for detailed design and development	o Viscojet performance with methane o Low-g performance of TVS o Allowables of composite layups for trunnions, including fatigue data at cryo. temp. o Structural capability of fabricated trunnion
II	0.62 m³ (22 ft³)	Ar	o Acquisition device technology available although bubble point not measured in argon o Some Viscojet data available from Martin Marietta IRAD tests o Effectiveness of 10.2-cm (4.0-in) of MLI may not be feasible, even with improvements; this impacts on-orbit storage time capability	o Low-g performance of TVS o Improvements in layer density control (e.g. compression during launch) and outgassing of thick layers needed o Allowables of composite layups for trunnions, including fatigue data at cryo. temp. o Structural capability of fabricated trunnion.

Table VI-1 (Continued)

Category	Tank Size	Fluid	Technology Status	Deficiencies
III	0.62 m^3 (22 ft^3)	O$_2$	o Acquisition device technology available; bubble point measurements in oxygen confirm calculated values o Design concepts and technology from CFME available for detailed design and development	o Viscojet performance with oxygen o Low-g performance of TVS o Allowables of composite layups for trunnions, including fatigue data at cryo. temp. o Structural capability of fabricated trunnion
IV	0.62 m^3 (22 ft^3)	He	o Design concepts and technology from CFME available for detailed design and development of LH$_2$ vapor-cooled shield; limited Viscojet and one-g TVS performance data from Martin Marietta IRAD tests for LH$_2$ o Only limited amount of conceptual design studies for passive storage concepts of liquid helium (Ref 41)	o 325X2300 Dutch Twill screen performance in liquid helium o Acquisition device design and performance data in liquid helium – verification that empirically derived analytical tools are valid for liquid helium o Viscojet performance with liquid helium o TVS performance (both one-g and low-g) with liquid helium

Table VI-1 (Continued)

Category	Tank Size	Fluid	Technology Status	Deficiencies
IV	0.62 m³ (22 ft³) (continued)	He	o A more detailed conceptual design effort is needed just to try to identify all technology needs	o Composite properties, including fatigue, at liquid helium temperatures very limited; (more in-depth look at design concepts of support members for helium storage vessel required) o Valves that can be located at the tank outlet and operate at helium temp.
V	12.5 m³ (440 ft³)	Ar	o Acquisition device technology is available; thermal isolation of the LAD for larger tanks not totally resolved o Acquisition device channels for large tanks have been fabricated up to 178-cm (70-in) diameter o Effectiveness of 10.2-cm (4.0-in) of MLI may not be feasible, even with improvements; this translates into on-orbit storage time capability o Technology for helium-purged insulation exists, but not for this large tank size or thickness of insulation; Technology for nitrogen-purged insulation does not exist	o Techniques for acquisition device checkout in one-g (outflow or bubble point tests are complicated for large tanks) o Adequate data on maximum insulation thicknesses, considering layer density control, outgassing, and impact of Shuttle dynamic launch environment for large tank sizes o Structural supports that can withstand the launch loads, and then be uncoupled from the tank to cut down heat leak for long-term storage

Table VI-1 (Continued)

Category	Tank Size	Fluid	Technology Status	Deficiencies
V	12.5 m³ (440 ft³) (continued)	Ar	o Composite technology exists to fabricate the large support struts, although a new bonding adhesive for end fittings must be verified o Structural models (NASTRAN, BOSOR, etc.) exist for sizing pressure vessels and vacuum jackets; these models should be used in a more detailed analysis to verify support point loads, which size local wall thickness o A coupled loads analysis of the payload supports and the Orbiter pickups is required for all payloads of this size prior to STS safety approval	o Heat flux levels that can dry-out wetted screen on a channel with and without a large bubble in the all-liquid region of the channel o Effect of start transients on the LAD due to the many valve openings and closings o Sufficient detail of configuration and routing of external TVS lines to provide a more accurate value of net heat leak into the stored cryogen. (Design details can significantly alter total heat leak)
VI	12.5 m³ (440 ft³)	CH₄	o Comments for Argon tank apply except for those addressing large insulation thicknesses, which aren't required for this mission	o Comments for Argon tank apply except for MLI thickness

Table VI-1 (Continued)

Category	Tank Size	Fluid	Technology Status	Deficiencies
VII	12.5 m³ (440 ft³)	O₂	o Comments for Argon tank apply except for those addressing large insulation thicknesses, which aren't required for this mission	o Comments for Argon tank apply except for MLI thickness
VIII	37.4 m³ (1320 ft³)	H₂	o Acquisition device technology is available; thermal isolation of the LAD for this size tank without a vacuum jacket is not totally resolved o Fabrication of cryogenic tanks of this size has been accomplished. Incorporation of an integral acquisition device should be evaluated in greater detail, particularly with regard to the dynamic loads. A sufficient data base exists to perform this more detailed analysis o Structural models (NASTRAN, BOSOR, etc) exist for sizing pressure vessels and vacuum jackets; these models should be used in a more detailed analysis to verify support point loads, which size local wall thicknesses o A coupled loads analysis of the payload supports and the Orbiter pickups is required for all payloads of this size prior to STS safety approval. This may change details of the structural design o A sufficient technology base exists for preparing a more detailed design of the SOFI/MLI insulation concept. A more thorough review of the nitrogen purge requirements, and the purge capability within the Shuttle payload bay should be pursued	o Low-g performance of TVS o Sufficient detail of configuration and routing of external TVS lines to provide a more accurate value of net heat leak into the stored cryogen (Design details can significantly alter total heat leak) o Technique needed for installed acquisition device checkout in one-g for this large tank size o Heat flux levels that can dry out wetted screen on a channel with and without a large bubble in the all liquid region of the channel (concern is increased heat flux level for non-vacuum jacketed tank) o Demonstration of feasibility and performance of SOFI/MLI insulation concept

Data from our IRAD program was used to select the appropriate Viscojets for the CFME (Ref 44). The objective of the test program was to establish the relationship between the two-phase cryogenic flow rate through the Viscojet and pertinent flow parameters, including pressure drop, outlet pressure, inlet and outlet temperature and fluid properties. Three Viscojets were tested with nitrogen and two of the Viscojets were also tested with Argon. A total of 151 valid data points were obtained, as follows:

Viscojet Size	Number of LN$_2$ Tests	Number of LAr Tests
313,000 Lohm*	24	
465,000 Lohm	47	41
700,000 Lohm	14	25

(* Manufacturer designation for flow resistance in the Viscojet. One Lohm represents a flow of 100 gallons per minute of water at a pressure drop of 172 KN/m^2 (25 psia) and a temperature of 300°K (540°R). Flowrate through the Viscojet is inversely proportional to the Lohm rating.)

The inlet pressure range varied between 138 and 414 KN/m^2 (20 and 60 psia) and the range of pressure differential across the Viscojets varied from 48 to 331 KN/m^2 (7 to 48 psid).

These tests were conducted using a test setup designed to minimize effects of heat leak and with provision to assure that 100 percent liquid was present at the Viscojet inlet. The liquid reservoir, Viscojet and connecting piping were mounted within a vacuum jacket, and the Viscojet test conditions were similar to the CFME application. Data recorded included temperature in the reservoir and at the Viscojet inlet and outlet, inlet pressure and pressure drop across the Viscojet, and flow rate. The test data were correlated and the flow rate was found to be dependent on the pressure drop, inlet and outlet properties of the fluid, and the Reynolds number based on the minimum passage dimension with the Viscojet. The expression found to best correlate the data is similar to that obtained in an earlier test program, as documented in Ref. 2.

Flow rate is specified as follows:

$$\dot{m} = \frac{F(Re)\sqrt{\Delta P \rho}}{L}$$

where $\dot{m}$ is flow rate, (lb/hr)

    ΔP is pressure drop across the Viscojet (lb_f/in^2)

    ρ is average of inlet and outlet fluid densities (lb_m/ft^3)

    L is Viscojet Lohm rating

$F(Re)$ is a function of Reynolds Number based on volumetric average of inlet and outlet conditions and minimum passage dimensions; $F(Re) = 45.23\sqrt{Re}$ for best data correlation. A plot of the test data showing the Reynolds number correlations for liquid nitrogen is presented in Figure VI-1. Based upon this data and adjusting the correlation for liquid hydrogen, Viscojets with a Lohm rating of 950,000 were selected for the CFMF design.

3. Insulation

Long duration missions require relatively large MLI thicknesses. However, the MLI performance diminishes in an exponential manner as thickness increases, for a given layer density. From the data of Stochl (Ref 34), it appears that technology exists for predicting MLI performance for blanket thickness up to 7.8-cm (3.1-in). Problems of layer density control and outgassing at thicknesses greater than this are unresolved. Outgassing time for MLI increases with increasing thickness. It is unknown at present how much additional outgassing time will be required for thicker blankets. This is particularly pertinent to the nitrogen-purged MLI blankets for the argon tanks. Current technology also appears to be inadequate for controlling MLI sag and compression during fabrication, and in the dynamic launch environment, without decreasing the MLI performance. The use of a VCS to support the insulation, including several shields for the thicker insulation blankets, is one approach to structural integrity, which also offers thermal performance advantages when coupled with a TVS.

Keller (Ref 33) discusses and presents results from an experimental program to measure tank installed layer density and heat flux for double goldized Mylar silk net insulation. An x-ray technique to measure layer density without physically disturbing the MLI, and a needle-probe technique were both used to determine MLI layer density. Although the needle-probe technique disturbs the MLI layer density locally, the results obtained using this technique show good agreement with the x-ray layer density measurements. A technique such as this would certainly be part of any fabrication and inspection program to verify the as-designed and as-assembled MLI thermal performance capability.

Current technology for spray-on-foam-insulation requires that a minimum layer of 1.3-cm (0.5-in) be installed to guarantee published design conductivity values. Elimination of the helium purge requirement for non-vacuum-jacketed tanks can be accomplished with 0.36-cm (0.14-in). Additional weight reductions are possible if improvements can be made in techniques of application. For machine applied foam, the minimum tolerance is currently +0.64-cm (+0.25-in). For hand applied foam the minimum tolerance is +2.5-cm (+1.0-in). Minimum SOFI application thickness is controlled by the properties of the foam itself. Development of an alternate spray-on insulation could allow application of thinner layers. Application tolerance could be reduced through development of improved spraying technology.
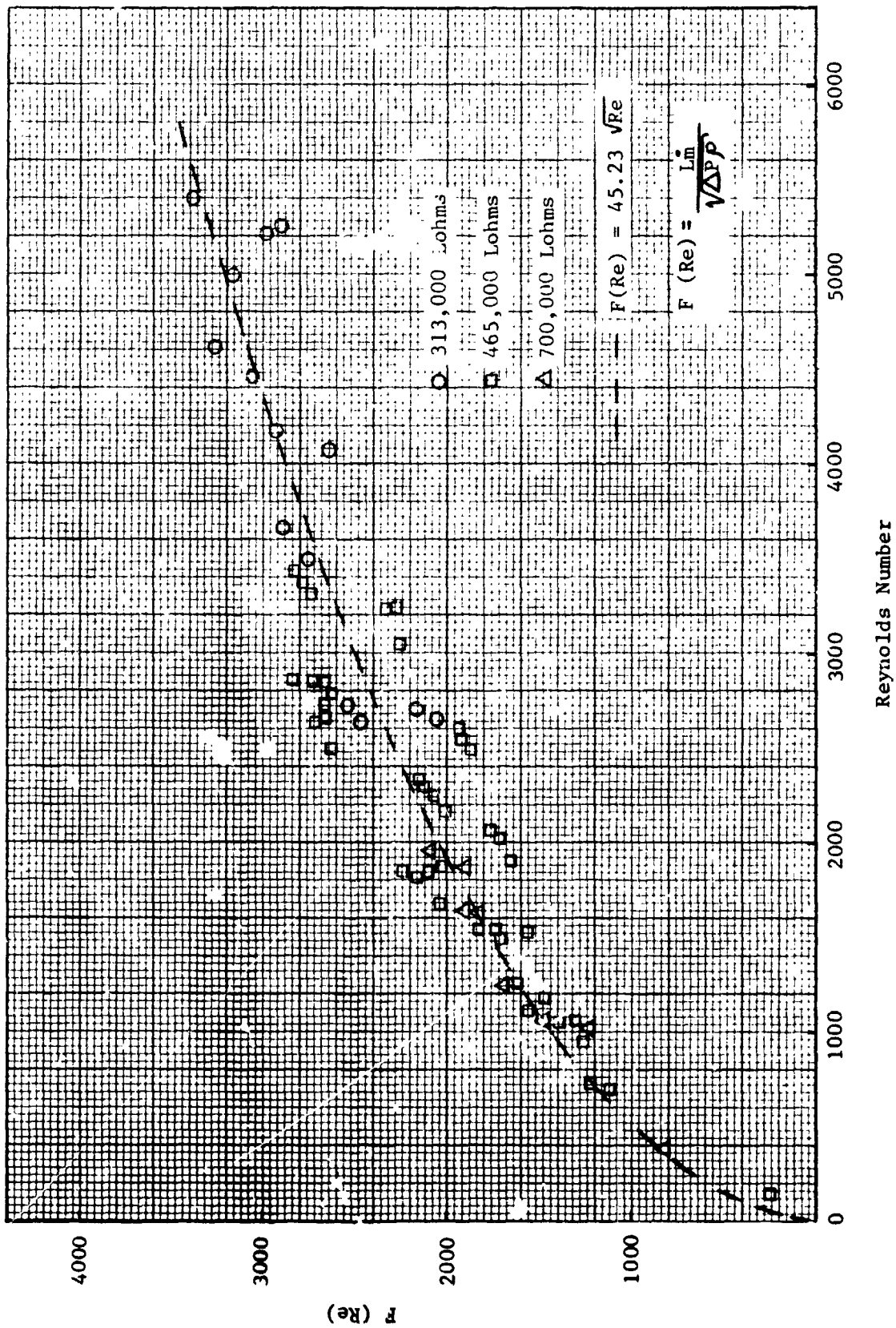
Figure VI-1 Viscojet Flow Correlation For Liquid Nitrogen Tests

Reynolds Number

F (Re)

○ 313,000 Lohms
□ 465,000 Lohms
△ 700,000 Lohms

$F(Re) = 45.23 \sqrt{Re}$

$$F(Re) = \frac{\dot{L}m}{\sqrt{\Delta P \rho}}$$

4. Composite Supports

The composite matrices defined in this study for the trunnions and support members are identical to those being used for the CFME. A CFME test plan has been prepared, recommending that mechanical property data be gathered for the multilayer lamina material to be used in the fabrication of the trunnion and for the laminate materials which approximate the layup configuration of the completed trunnion. If the recommended CFME tests are accomplished and the results agree with design allowables, no further composite testing would be necessary. The composite supports should be tested in fatigue since many applications will take advantage of the reflight capability of the Shuttle. Unfortunately there exists little data predicting crossply composite fatigue performance, especially under cryogenic conditions. When crossplied, the failure modes of composites become a complex function of the anisotropy of the particular layup, as well as of the constituent properties, composite quality, and other variables.

Another technology area involves the adhesive bonding of aluminum or titanium male fittings to the tubular composite members. In the past Crest 7343 was considered the best adhesive for these cryogenic applications. The use of 7343 has since been discontinued because the catalyst is on the list of carcinogenic materials issued by the government. Adhesive 810AB is a relatively new alternative to 7343. This resin system is recommended because of its reported excellent lap shear properties over a wide range of temperatures, with maximum strength at cryogenic temperatures (Table VI-2). Because of the lack of experience with this adhesive, and the lack of published mechanical properties data for S- and E-glass-to-aluminum, utilizing 810AB adhesive, it is recommended that lap shear tests be performed in tension and compression. In order to simulate the service temperature expected of the adhesive, these tests should be performed at 367°K (660°R), 294°K (530°R), 78°K (140°R) and 20°K (36°R). The support members, fabricated with end fittings, should be tested to failure in tension and compression at room temperature.

Table VI-2
Mechanical Properties Crest 810 AB Adhesive
(from Crest Products Bulletin)

Tensile Shear (Aluminum-to-Aluminum)			
Cure Cycle at 297°K (537°R)	Test Temperature	Shear Strength kPa	Psi
24 hours	297°K (535°R)	3930	570
24 hours	193°K (348°R)	32269	4680
48 hours	297°K (535°R)	7929	1150
72 hours	297°K (535°R)	10618	1540
72 hours	193°K (348°R)	34475	5000
7 days	297°K (535°R)	11308	1640
7 days	78°K (140°R)	48817	7080
7 days	373°K (672°R)	2758	400

5. Valves

The types of valves required by the various systems are ON/OFF valves controlled electrically or pneumatically, and relief-type valves that are controlled by the pressure sensed internally by the valve. Size requirements range from 6.4-mm (0.25-in) diameter to 115-mm (4.5-in) diameter, the largest size required for the Category VII liquid oxygen tank abort flowrate.

It is felt that adequate technology exists for all valves except the liquid helium valves for the Category IV system. This is not to imply that valves are available off the shelf, but rather that the technology exists to fabricate these valves with a minimal degree of uncertainty that major technical problems would surface. The basic problems with liquid helium valves relate to the extreme low temperature, and the very low heat of vaporization of liquid helium. The extremely low temperature causes problems with materials of construction and solenoid coils. The low heat of vaporization requires sophisticated designs to reduce heat leak into the liquid from conduction along tubing, the environment and solenoid coils.

The difficulty in obtaining relief valves for these systems is the requirement of a low cracking pressure at very low temperature combined with low allowable leakage. This requirement has been met in the past with complex, expensive relief valves.

6. Burst Discs

Although some difficult problems are presented to the burst disc designer, it is felt that adequate technology exists for their development except in the case of liquid helium. The most difficult design problem likely to occur for these systems is the requirement for low burst pressure with a small pressure margin above operating pressure, coupled with a wide temperature range.

7. Instrumentation

There are two areas of technology regarding instrumentation; cryogenic mass flow metering devices, and zero-g propellant mass gaging. Neither of these was directly addressed as part of this study but further work in developing this capability is required. Both of these areas are being addressed as part of the development of the CFME and associated low-g fluid transfer technology programs.

B. Recommendations

The following analytical and experimental activities are recommended to develop the required technology:

1. The CFME program should be continued as expeditiously as possible to obtain general design data and performance capability of the integrated liquid acquisition device/thermodynamic vent system in the low-g

on-orbit environment. For many of the fluid dynamic, thermal and structural aspects of on-orbit storage and supply, liquid hydrogen represents a worst-case design and performance situation; information from the CFME flights will provide a significant data base for extrapolation to the other fluids of this study, except for liquid helium. The CFME trunnion support concept will also be proved, lending credence to its use for tank sizes in the 0.62 m^3 (22 ft^3) range.

2. Long-term storage of cryogens in large tanks should be addressed in greater detail by performing a preliminary detailed design of a total storage and supply system, including the user system, storage tankage, structural suppports and ancillary equipment. For example, a design study looking at the integration of an argon storage tank with an electric propulsion subsystem would provide meaningful data on overall thermal performance, packaging, size, weight, and mission life capability for all of the large tank sizes and fluids of this study. An argon storage tank for a long orbital life presents several difficult design problems identified and briefly evaluated in this study; namely, structural support of a large, dense mass within the payload bay, and insulation and structural support thermal designs for extended (up to 7-year) storage.

A more detailed look at the support struts should be made, including possible methods for uncoupling following launch to reduce heat input to the inner vessel. It is believed that some weight reductions to the aluminum ring and truss frames, and the composite struts, can be obtained as the result of a more detailed design and analytical evaluation. Detailed BOSOR runs should be made of those areas of the tank shell which are beefed-up for attachment of the struts. These local areas of increased thickness add significant weight to shells of this size. At least a portion of the support channels and truss network in reality would be part of a spacecraft or platform structure to which other system elements and components can also be supported. Assigning the large weight penalty of this support structure only to the tank assembly improperly penalizes the liquid storage system in those cases where a basic structural framework holds together the entire payload package.

Since the argon application has a long-life storage requirement, a more detailed design will address the specifics of a large thickness of nitrogen-purged or helium-purged insulation. This would include details of how layer density control during fabrication and launch can be maintained, and details of a purge system, if required, including the purge bag, closeout fairings, and the purge gas distribution network.

3. Further analytical and experimental work is recommended in low-g convection, boiling and heat transfer; specifically, analytical and experimental efforts are needed to characterize low-g external and internal TVS performance for different fluids. The relative comparison should be made for a representative long-duration mission,

assuming the same sizes, environments and operational requirements. This study did not address an internal TVS configuration, but the attractiveness of such a system should be compared to that of an external system, particularly regarding pressure control of large volume, non-vacuum-jacketed tank configurations, with large localized heat inputs. The key technology evaluation would include the capability of the internal TVS to control temperature stratification, and the capability of the external TVS to significantly reduce the heat flux into the liquid. A combination of these two may be the preferred approach for large tanks requiring efficient thermal control for long-term storage.

4. The performance characterization of Viscojets for use with all the cryogens should be accomplished. This should include combining the Viscojet, heat exchanger and/or manifold arrangement that surrounds a penetration or support, and flow control valves.

5. Additional development and demonstration is recommended to ascertain the capability of the acquisition device to cope with environmental effects, i.e. vibration, pulsed flow (transients), shock and thermal inputs.

6. An analytical and experimental program should be pursued to confirm attractiveness of nitrogen-purged MLI for use in the Shuttle bay, and SOFI/nitrogen-purged MLI combination for hydrogen storage in the Shuttle. The experimental effort would include both calorimetric tests in a laboratory environment and large scale tank tests in a vacuum chamber.

7. The following component technology should be pursued:

   a. Flight-weight liquid helium valves which introduce a minimum of heat into the helium from either the environment or internal solenoid coils.

   b. Relief valves with relieving pressures of 34 - 103 KN/m^2 (5-15 psi) and maximum leak rates of 1 x 10^{-6} scc/sec which are operable from 20°K to 293°K (36°R to 528°R).

   c. Burst discs for use in liquid helium systems.

   d. A propellant mass guage for low-g cryogenic usage. A nucleonic gauge has been developed which appears attractive for space usage, but it is not flight-proven for cryogenic applications. Other approaches should be pursued to get gauging accuracy in low-g to within 1-2 percent.

   e. A liquid cryogen flowmeter for usage in low-g, qualified for Shuttle-designed payloads.

Cryogenic storage and supply systems were conceptually designed using the Cryogenic Fluid Mangement Experiment as a system baseline configuration with appropriate changes identified to satisfy the mission and operational requirements. Minimum modifications were required for the 0.62 m^3 (22 ft^3) tanks except for liquid helium. The only changes were increased diameter and thickness of the trunnions which support the inner pressure vessel, an increased outlet line size to handle the abort flowrate requirement, and increased MLI thickness for the methane and argon cases due to much longer mission time requirements. The 0.62 m^3 (22 ft^3) helium storage and supply system required substantial modifications to the basic configuration due to the very low temperature and low heat of vaporization. A conceptual design was selected which contained an outer hydrogen-cooled shield to control heat input into the inner storage assembly. The thermodynamic vent system was reconfigured with a separate Viscojet and heat exchanger manifold for heat interception at each trunnion support location.

The vacuum-jacketed tanks for the larger sizes were found not to be weight competitive with conceptual designs using helium-purged MLI and nitrogen-purged MLI with a layer of spray-on-foam insulation (SOFI) underneath. The MLI/SOFI combination appears attractive for liquid hydrogen application, and may be useful for other cryogens depending on mission and ground-hold requirements, which will dictate specific configurations. The desire for commonality to handle other cryogens with a single design influenced the decision to size the 12.5 m^3 (440 ft^3) tanks and supporting structure for liquid argon, due to its rather substantial mass. This resulted in an overdesigned situation for oxygen and methane, with excessive weight and heat leak due to the substantial structural supports required to handle the dynamic loads in the payload bay at launch.

Long-duration missions (on the order of years) with liquid supply requirements need additional development of insulation and structural supports. Development of support mechanisms that can withstand the launch loads and then be uncoupled from the storage vessels offer the advantage of extended life traded against added complexity. For long missions with the requirement of low pressure gas supply at low flow rates, an external TVS is a good approach, since the user system can be supplied with vent fluid through the heat exchanger line. This thermodynamic vent system design is particularly attractive if the user requirements correspond to near optimum conditions where the gaseous supply rate matches the withdrawal rate needed to maintain constant tank pressure.

A total communication liquid acquisition device was found to be suitable for the missions defined in the study. Thermal isolation of the device is a design problem for the large tank sizes, but this can be managed by judicious routing and thermal coupling of the TVS to control localized heating.

APPENDIX A

CSAM Description

The Cryogenic Storage Analysis Model (CSAM), is applicable to
the analysis of cryogenic systems of varied configurations and
features. It includes a transient heat transfer network analysis,
internal tank fluid thermodynamics and a heat exchanger routine
simulating a thermodynamic vent system. User-oriented input routines
provide flexibility in problem setup, and configurations are
completely determined from input data. Events and boundary
conditions are programmable, permitting simulation of an entire
mission with a single input.

A cryogenic storage or transfer system is defined by
conductor/node networks. Nodes are identified with alphanumeric
names, and conductor connections are defined by specifying the names
of nodes to be connected. Descriptive node names can be used; this
feature not only eliminates manual table setup, but also simplifies
interpretation of result printouts. Liquid and gas contained in a
pressure vessel are similarly described by nodes and conductors. A
convective conductor between liquid and gas is automatically
converted into the proper parameters for calculation of heat and mass
transfer across the liquid-gas interface. Within the tank both
liquid and gas can be represented by one or more nodes each. Since
the program assumes no orientation beyond that described by input,
arbitrary liquid-gas configurations can be represented, including gas
surrounded by liquid in a zero-g environment.

Heat exchangers are also described by node conductor input
parameters, representing the heat exchanger tube segments and thermal
connections to the elements to be cooled. Nodes representing the
fluid in the heat exchanger tube and conductors describing heat
transfer from fluid to tube wall are automatically set up. Multiple
heat exchangers can be described and each can have any (practical)
number of segments. One of the liquid nodes in the tank is
designated as the supply of fluid for the thermodynamic vent heat
exchangers.

The transient heat transfer analysis is accomplished numerically
using an exponential method of solution of the equation,

$$m_i C_i dT_i/dt = \sum Q_i$$

where

dT_i/dt = the time rate of change of temperature of node i

m_i = mass of node i

C_i = the specific heat of node i

Q_i = the net rate of heat flow into node i

This method assures stability and generally permits large time steps with acceptable loss of accuracy. Temperatures of neighboring nodes are projected for the current calculation from the past three time steps. The time step is periodically adjusted between input-specified limits on the basis of the maximum temperature change of any node to maintain accuracy while minimizing computer usage.

Thermal conductivity as a function of temperature is incorporated in the program for a large number of materials normally encountered in cryogenic systems, including metals, nonmetals, composites and fluids. These properties are in the form of polynomial curve fits and the effective thermal conductivity of any conductor is calculated as a function of end point temperatures as

$$K_{eff} = \frac{1}{T_2 - T_1} \int_{T_1}^{T_2} K(T)dT$$

K_{eff} = effective thermal conductivity

$K(T)$ = thermal conductivity as a function of temperature

T_1, T_2 = temperature at end points

Input data required to describe conductors therefore consist of the "from-to" node descriptors, a code indicating the type of conductor and the physical parameters, i.e., cross-sectional area and length. Heat flux is calculated from the basic equation

$$Q_{i \to j} = \bar{C}(T_i - T_j)$$

where

$Q_{i \to j}$ = heat transfer from node i to node j

T_i and T_j = the end point temperatures

$\bar{C}$ = the conductance, calculated as

$$\bar{C} = K_{eff} \frac{A}{X}$$

A = the effective cross-sectional area of the conductor

X = conductor length

K_{eff} = the effective thermal conductivity

For free convection within the storage vessel, heat transfer is computed from a Grashoff-Prandtl product (Rayleigh number) correlation

$$Q_{ij} = A \frac{ak}{L} \left[\frac{L^3 \rho^2 g \beta \Delta T Cp\mu}{\mu^2 \quad K} \right]^m \quad (T_i - T_j)$$

where

A = heat transfer area (such as tank wall area)

a = coefficient defined below

m = exponent defined below

K = thermal conductivity of fluid

L = characteristic length

ρ = fluid density

g = acceleration or gravity

β = coefficient of thermal expansion of fluid

T = temperature difference $(T_i - T_j)$

Cp = specific heat of fluid

μ = fluid viscosity

T_i, T_j = temperatures of nodes i, j

The factors a and m are taken from such published data as The Chemical Engineers Handbook, Fifth Edition. The value of (a) ranges from 0.13 to 1.36 and (m) varies from 0.2 to 0.333, depending on configuration and the Rayleigh number (the quantity in the above equation that is taken to the m power). In this correlation, heat transfer goes to zero for a zero-gravity environment. Provision is made in the program to limit the Rayleigh number to a minimum value of 1, resulting in pure conduction for that case.

In the case of radiation, the product of area and gray-body view factor describes the conductor characteristics and the equivalent linear conductor is found by

$$\bar{C}_{eq} = AF \sigma (T_i^4 + T_j^2) (T_i + T_j)$$

where

$\bar{C}_{eq}$ = equivalent conductor for use in the heat transfer network

AF = effective product of area and view factor

σ = Stefan-Boltzman constant

For nodes, the parameter of interest is the thermal mass, or the product of mass and specific heat. Therefore the input data for each node is initial temperature, mass and designator to specify the material type. Specific heat values for material are built into the program, and are calculated from curve fits as a function of current node temperature. The thermal conductivity and specific heat data are contained in a single subroutine and additional material properties can be easily added without disruption of other program routines.

The determination of tank pressure depends on all other parameters, and is a primary result (as are temperature distributions) of system simulation using the CSAM program. Other output data include heat flux for all conductors, mass and makeup of the ullage, ullage volume, liquid mass, heat and mass transfer at the liquid-gas interface and heat exchanger parameters.

The complexity involved in simulation of the internal tank thermal and thermodynamic processes of the liquid and ullage within the containment vessel is illustrated in Figure A-1. The CSAM program determines tank pressure, mass transfer and temperature distributions, considering all of the factors shown, for either a vapor-pressurized tank or for the case when the ullage contains both vapor and helium as a pressurant. The ullage and liquid can each be represented by one or more nodes, permitting more detailed analysis of temperature distributions.

At the heart of this analysis is the heat and mass transfer at the liquid-gas interface. For the single specie ullage case, the liquid-gas interface temperature is determined by tank pressure (i.e. the interface is at the saturated state). Heat transfer will occur to and/or from the interface due to temperature differences between the interface and the adjacent liquid and gas. Any excess of heat at the interface will result in evaporation of liquid and any deficiency in the heat transfer will cause condensation of vapor according to

$$\dot{m} = \frac{\dot{Q}_{GI} - \dot{Q}_{IL}}{H_{ev}}$$

where

$\dot{m}$ = rate of evaporation, if positive, or condensation, if negative

$\dot{Q}_{GI}$ = rate of heat transfer from the bulk gas to the interface

$\dot{Q}_{IL}$ = rate of heat transfer from the interface to the bulk liquid

H_{ev} = heat of vaporization

The resulting mass transfer will change the density of the ullage gas and the heat transfer will change its temperature, both of which will influence tank pressure. A change in tank pressure will, in turn, change the interface temperature and therefore the heat transfer rates.
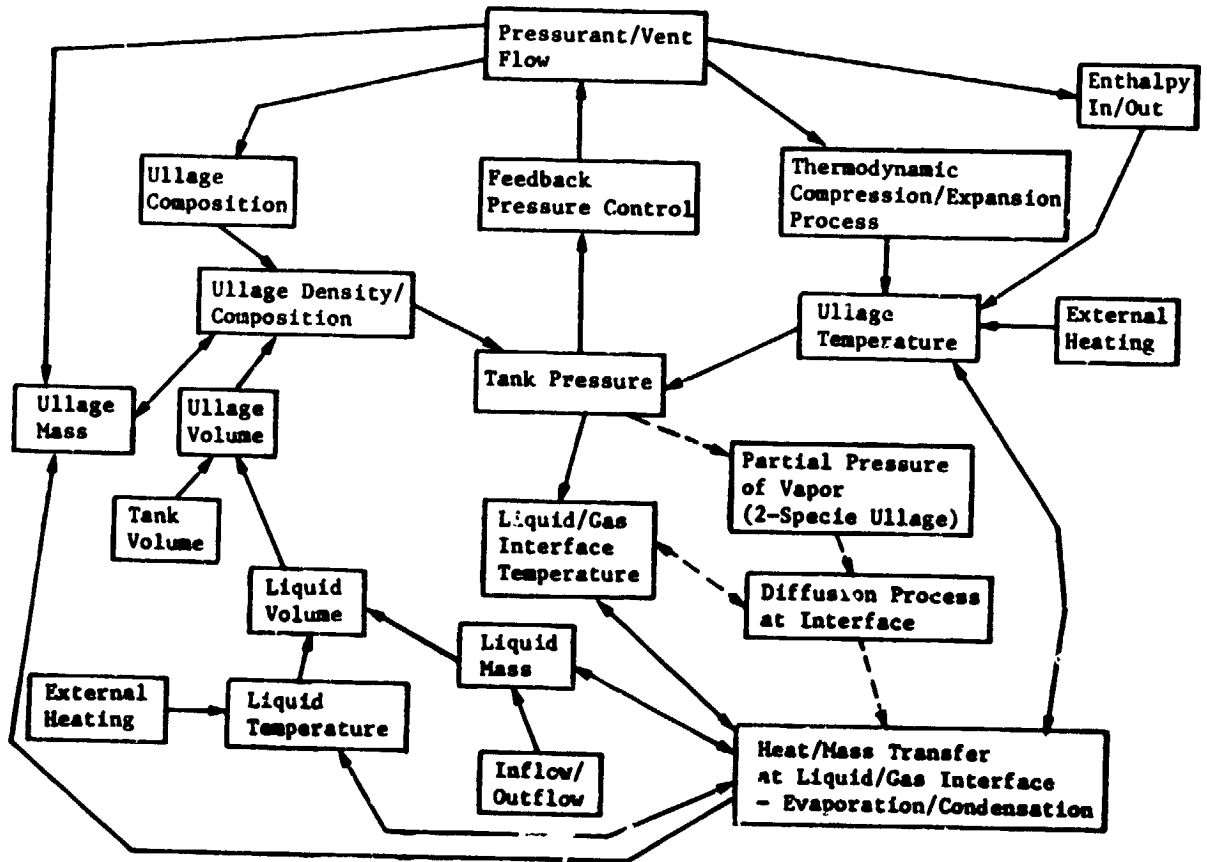

Figure A-1   Interactions Affecting Internal Tank Thermodynamics

When a noncondensible pressurant is included in the ullage, the process is complicated by the diffusion process in the two component gas mixture. This process largely determines the partial pressure of vapor adjacent to the interface, and therefore the interface temperature, and the heat and mass transfer rates.

For this process, Ring* gives the equation

$$\dot{m} = \frac{A_s \; C_{GS} \; \delta_v \; P_{TG} \; M_v}{D_t \; T_{GF} \; R_u} \left[\frac{P_{TG} - P_{VG}}{P_{TG} - P_{VL}}\right] \times \left[\frac{D_t^3 \; \delta_{GF} \; \rho_{GF} \; a \; |\Delta T|}{\mu_{GF} \; \delta_v}\right]^{1/4}$$

---

* Elliott Ring (Editor): Rocket Propellant and Pressurization Systems. Prentice Hall, New York, NY, 1964.

where

A_s = surface area

C_{GS} = a constant for convective heat transfer

δ_v = diffusion coefficient

P_{TG} = tank pressure

M_v = molecular weight of vapor

D_t = tank diameter

T_{GF} = temperature of film at interface

R_u = universal gas constant

P_{VL} = vapor pressure at interface temperature

P_{VG}' = partial pressure of vapor

ρ_{GF} = density of gas near interface

β_{GF} = coefficient of thermal expansion

a = acceleration

$\Delta 1$ = temperature difference

μ_{GF} = viscosity of film near interface

The CSAM program uses a numerical iteration routine that solves a simplified version of the above equation. This routine was taken from our pressurization model (computer program OD041), which has been successfully used to correlate test data for tankage systems using a noncondensible pressurant.

In the calculation of tank thermodynamic and thermal processes, some 25 properties of fluids are required (for the two specie ullage case). These properties are calculated in three subprograms, one for the stored fluid, one for the noncondensible pressurant, and one for determining the properties of the two component ullage as functions of temperature, pressure and mass fraction of pressurant gas in the mixture. The latter is independent of the fluids being used, calling on the first two for the single specie properties. Current capabilities include helium as the pressurant, and the following fluids as the stored cryogen:

1) Hydrogen;   4) Methane;

2) Nitrogen;   5) Argon;

3) Oxygen;   6) Helium.

The data are in the form of polynomial curve fits with real number exponents that vary with temperature and pressure. The data base includes the following properties:

Saturation temperature, $T_s(P)$;
Specific heat at constant pressure and volume for both liquid and vapor, $Cp(T)$, $Cv(T)$;
Heat of vaporization, $h_{vap}(P)$;
Enthalpy of liquid, $h_1(P,T)$;
Enthalpy of saturated liquid, $h_{sl}(P)$;
Enthalpy of saturated vapor, $h_{sv}(P)$;
Enthalpy of vapor. $h_v(T)$, $g_v(P,T)$;
Compressibility factor, $Z(P,T)$;
Density of vapor, $\rho(P,Z,T)$;
Viscosity of superheated vapor and subcooled liquid, $\mu(P,T)$;
Prandtl No. of vapor and liquid, $Pr(P,T)$;
Thermal conductivity of vapor and liquid, $k(P,T)$;
Thermal conductivity of saturated liquid, $k_{sl}(T)$;
Grashof-Prandtl product for superheated vapor and subcooled liquid, $(Pr)(Gr)$.

All functions of P and T generated for the data base use the form

$$F(P,T) = f(P)_T \; g(T)_P \; \frac{1}{F_o(P_o, T_o)}$$

where F_o is the value for a given property at a pressure and temperature typical for the phase of the substance, and which is chosen to yield the most accurate representation. The range of data for which the equations are valid is from the triple point to the critical point. In some instances a particular property, such as vapor enthalpy is figured for pressure and temperature over a wide range, but is modified for greater accuracy to be dependent only on temperature over a narrower range.

Mission events and boundary conditions that can be specified as functions of time include:

1) Set point pressure for thermodynamic vent system(s);

2) Set point pressure for direct gas vent;

3) Rate of liquid inflow and/or outflow;

4) Set point pressure for tank pressurization;

5) Gravity;

6) Temperature of external flux to/from boundary nodes.

In the thermodynamic vent, liquid is withdrawn from the tank where pressure reduction or control is required. This liquid flows through a flow-restricting device into a heat exchanger. The flow restrictor (along with the low-pressure sink of space) results in an internal heat exchanger pressure substantially below tank pressure. When the vent liquid undergoes a reduction in pressure, part of the liquid vaporizes and the two-phase mixture goes to the saturation temperature corresponding to the new pressure. At this point, the vent fluid is capable of absorbing heat from the tank contents (liquid and/or gas) as the fluid becomes totally vaporized and the vapor temperature increases to approach the temperature of the fluids being cooled. Therefore the heat exchanger is designed to utilize this refrigeration capability. Tank pressure is controlled by several processes, namely reduction of liquid volume, condensation of vapor at the liquid-gas interface and pressure reduction by lowering gas temperature at either constant or decreasing density. Having achieved these results, the vent vapor is capable of absorbing additional heat, and an optimal system may use this additional refrigerant capacity to intercept heat in the major heat leak paths such as tank insulation, supports and piping.

The CSAM computer program provides the capability for simulation of the thermodynamic vent system described above. One or more tubular heat exchangers can be configured. Each is separately controlled, and each can be arbitrarily routed to intercept heat from desired node points using any practical number of segments with various lengths. Heat transfer to the tube walls from the nodes being cooled is calculated in the basic heat transfer section of the program. Heat transfer from the fluid to the tube wall and determination of the thermodynamic state of the fluid is handled in a separate heat exchanger routine. The logic of this routine is shown in Figure A-2.

The inlet fluid quality is calculated from the assumption that the inlet fluid is all liquid at $T = T_1$ and that enthalpy remains constant through the pressure reduction process. It is assumed that both liquid and vapor at the discharge of the pressure reducing device are at the saturation temperature corresponding to the reduced pressure. The discharge quality is therefore found from

$$X_2 = \frac{H_{L1} - H_{L2}}{H_{SV2} - H_{L2}}$$

where

X_2 = quality

H_{L1} = enthalpy of liquid at entrance to device

H_{L2} = enthalpy of saturated liquid leaving device

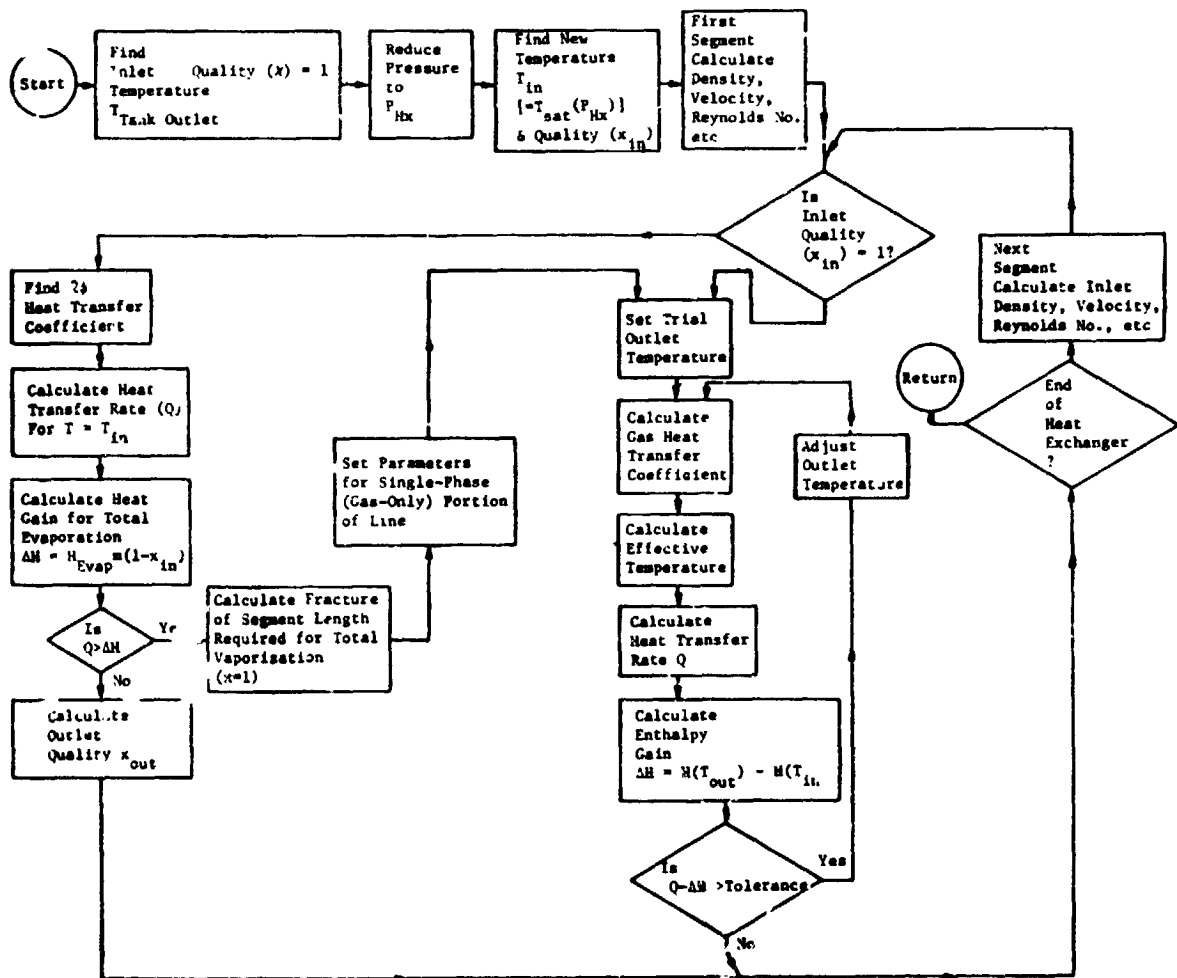H_{SV2} = enthalpy of saturated vapor leaving device

Figure A-2 Thermodynamic Vent Heat Exchanger Logic

Other assumptions that have been incorporated in the heat exchanger analysis are: (1) the pressure remains constant throughout the length of the heat exchanger, and (2) the temperature of vapor and liquid remain constant throughout the two-phase region (i.e., until the point where all liquid has been vaporized). In system simulations we have done in the past, the assumption of constant pressure, when compared with predicted pressure drop in the heat exchanger, results in negligible error. In fact, for such a system, internal heat exchanger pressure must be regulated by a backpressure-regulating device near the outlet and the requirement for optimal heat transfer tends to size the tube large compared to the fluid flow rate. However, the validity of this assumption is always checked and, if required, pressure loss in the system is calculated.

Heat transfer from the heat exchange fluid to the internal tube wall depends on the appropriate film heat transfer coefficient. For single-phase gas flow, the correlation given by Lauer* is

$$h_f = 0.0243 \ \frac{K}{D} \left(\frac{D \ V \rho}{\mu}\right)^{0.8} \left(\frac{Cp \mu}{K}\right)^{0.4}$$

where

h_f = film heat transfer coefficient

K = thermal conductivity of gas

D = internal diameter of tube

V = velocity in the tube

ρ = density of gas

μ = viscosity

Cp = specific heat of gas at constant pressure

For the two-phase flow before the point where all liquid has vaporized, many correlations are presented in the literature. Our analysis indictes that fluid flow in this region in a low gravity environment will be dominated by capillary forces. In addition, velocities will be small as will heat flux. We are presently using the correlation suggested by Dougall and Rohsenow** (similar to that given above) as

---

* B. E. Lauer: "How to Evaluate Film Coefficients for Heat-Transfer Calculations". Reprinted from the Oil and .as Journal, 1953.

** R. S. Dougall and W. M. Rohsenow: Film Boiling on the Inside of Vertical Tubes with Vertical Flow of the Fluid at Low Qualities. MIT Report 9079-26, 1963.

$$\dot{n}_f = \frac{0.023 \ Kv}{D} \ \left(\frac{\rho_v}{\mu_v} \ \frac{D}{A} \ \frac{Q_1 + Q_v}{A}\right)^{0.8} \ \left(\frac{Cp_v \ \mu_v}{Kv}\right)^{0.4}$$

where

Q_1, Q_v = volumetric flow rates of liquid and vapor, respectively

A = tube internal cross-sectional area and the other parameters are as previously given, the subscript v denoting that the parameter is evaluated for saturated vapor.

APPENDIX B

ACRONYMNS

BP	Bubble Point
CFME	Cryogenic Fluid Management Experiment
CSAM	Cryogenic Storage Analysis Model
DACS	Data Acquisition and Control System
GEO	Geosynchronous Orbit
HX1	Heat Exchanger 1
HX2	Heat Exchanger 2
ICD	Interface Control Document
LAD	Liquid Acquisition Device
LEO	Low Earth Orbit
LeRC	Lewis Research Center
LF	Load Factor
MLI	Multilayer Insulation
OMS	Orbital Maneuvering System
OTV	Orbit Transfer Vehicle
PSD	Power Spectral Density, g^2/Hz
RCS	Reaction Control System
RTLS	Return to Launch Site
SOFI	Spray-On-Foam-Insulation
SPAH	Spacelab Payload Accommodations Handbook
SQ5	Composites Computer Program
STS	Space Transportation System
TVS	Thermodynamic Vent System
VCS	Vapor-cooled Shield
VJ	Vacuum Jacket

REFERENCES

1. Eberhardt, R. N.. Fester, D. A. and Aydelott, J. C.: A Liquid Hydrogen
   Experiment as a Shuttle Payload. AIAA Paper No. 80-1096, Presented at
   AIAA/SAE/ASME 16th Joint Propulsion Conference, Hartford, Conn. June
   30-July 2, 1980.

2. Anderson, J. E. and Eberhardt, R. N.: Cryogenic Storage System
   Development for Long Term Space Missions, AIAA Paper No. 79-1261,
   AIAA/SAE/ASME 15th Joint Propulsion Conference, Las Vegas, Nevada, June
   18-20, 1979.

3. Cady, E. C.: Design and Evaluation of Thermodynamic Vent/Screen Baffle
   Cryogenic Storage System, NASA CR-134810, McDonnell Douglas Astronautics
   Company, June 1975.

4. Eberhardt, R. N. and Tegart, J. R.: Conceptual Design Report-Cryogenic
   Fluid Management Experiment, MCR-79-561, Martin Marietta Corporation,
   June 1979.

5. Tegart, J. R.: Hydrodynamic Analysis Report - Cryogenic Fluid Management
   Experiment, MCR-79-563, Martin Marietta Corporation, June 1979, (Contract
   NAS3-21591).

6. Gille, J. P.: Thermal Analysis Report - Cryogenic Fluid Management
   Experiment, MCR-79-564, Martin Marietta Corporation, June 1979, (Contract
   NAS3-21591).

7. Berry, R. L., Leang, L. T. and McCandless, J. R.: Structural Analysis
   Report - Cryogenic Fluid Management Experiment, MCR-79-567, Martin
   Marietta Corporation, June 1979, (Contract NAS3-21591).

8. "Low Thrust Chemical Orbit to Orbit Propulsion System Propellant
   Management Study," Fifth Monthly Progress Report, MCR-79-657, Issue 5,
   Martin Marietta Corporation, March 1980.

9. Orbital Propellant Handling and Storage Systems Definition Study Final
   Report - Volume II, Technical," GDC-ASP-79-002, General Dynamics Convair,
   August 1979 (Contract NAS9-15640).

10. "Spacelab Payload Accommodation Handbook," SLP/2104, Issue 1, Rev. 2, 31
    July 1979.

11. "Space Shuttle Payload Accommodations, Level II, Program Definition and
    Requirements" JSC 07700, Vol. XIV, Rev. F Change 30, 5 October 1979.

12. McCarty, R. D. and Weber, L. A.: Thermophysical Properties of
    Parahydrogen from the Freezing Liquid Line to 5000 R for Pressures to
    10,000 psia, NBS Tech. Note 617, National Bureau of Standards, April 1972.

13. McCarty, R. D.: Thermophysical Properties of Helium 4 from 4 to 3000 R with Pressures to 15000 psia, NBS Tech. Note 622, National Bureau of Standards, September 1972.

14. Goodwin, R. D.: The Thermophysical Properties of Methane, from 90 to 500 K at Pressures to 700 Bars, NBS Tech. Note 653, National Bureau of Standards, April 1974.

15. McCarty, R. D. and Weber, L. A.: Thermophysical Properties of Oxygen from Freezing Line to 600 R for Pressures to 5000 psia, NBS Tech. Note 384, National Bureau of Standards, July 1971.

16. Angus, S. and Armstrong, B.: International Thermodynamic Tables of the Fluid State, Argon, 1971. Butterworths, London, England, 1971.

17. Gosman, A. L., McCarty, R. D. and Hust, J. G.: Thermodynamic Properties of Argon from the Triple Point to 800 K at ressures to 1000 Atmospheres, NSRDS-NBS 27, National Bureau of Standards, March 1969.

18. Keller, W. E.: Helium-3 and Helium-4, Plenum Press, 1969.

19. Wilks, J.: The Properties of Liquid and Solid Helium, Clarendon Press, Oxford, 1967.

20. McCarty, R. D.: Thermophysical Properties of Helium-4 from 2 to 1500K with Pressures to 1000 Atmospheres. NBS Tech. Note 631, National Bureau of Standards, Nov. 1972, page 11.

.1. ASM Metals Handbook, Volume 3, 9th Edition.

22. Kasen, M. B.: Mechanical and Thermal Properties of Filamentary Reinforced Structural Composites at Cryogenic Temperatures, 1: Glass-Reinforced Composites, Crogenics, Vol. 15, No. 6, June 1.75.

23. Kasen, M. B. and Schramm, R. E.: Cryogenic Mechanical Properties of Boron, Graphite, and Glass-Reinforced Composites, Materials Science and Engineering, April 13, 1977.

24. Kasen, M. B.: Properties of Filamentary-Reinforced Composites at Cryogenic Temperatures, ASTM STP 580, 1975.

25. Reed, D. L.: Point Stress Laminate Analysis, SQ5 Program, General Dynamics, FZM-5494, April 1970.

26. Page, G. R.: Acquisition/Expulsion System for Earth Orbital Propulsion System, Volume II-Cryogenic Design, Volume III-Cryogenic Test. MCR-73-97, Martin Marietta Corporation, October 1973.

27. Cady, E. C.: Study of Thermodynamic Vent and Screen Baffle Integration for Orbital Storage and Transfer of Liquid Hydrogen, NASA CR-134482, McDonnall Douglas Astronautics Company, August 1973.

28. Gille, J. P.: Development of Advanced Materials for Integrated Tank Insulation System for the Long Term Storage of Cryogens in Space. MCR-69-405, Martin Marietta Corporation, September 1969.

29. Keller, C. W.: Fiberglass Supports for Cryogenic Tanks, NASA CR-12937, Lockheed Missiles and Space Company, October 1972 (Contract NAS 3-12037)

30. Mendelson, H.D.: The Prediction of Bubble Terminal Velocity from Ware Theory, AICHE Journal, Vol. 13, March 1967.

31. Sumner I. E., Thermal Performance of Gaseous-Helium-Purged Twin Mounted Multilayer Insulation System during Ground-Hold and Space-Hold Thermal Cycling and Exposure to Water Vapor, NASA Technical Paper 1114, Lewis Research Center, August 1978.

32. Keller, C. W.: Cunnington, G. R. and Glassford, A. P.: Thermal Performance of Multilayer Insulations, NASA CR 134477, Lockheed Missiles and Space Company, April 1974 (Contract NAS3-14377).

33. Keller, C. W.: Thermal Performance of Multilayer Insulations, NASA CR-72747, Lockheed Missiles and Space Company, April 1971 (Contract NAS3-12025).

34. Stochl, R. J.: Basic Performance of a Multilayer Insulation System Containing 20 to 160 Layers, NASA TN D-7659, NASA Lewis Research Center, Cleveland, Ohio, April 1974.

35. Cunnington, G.R., Keller, C. W. and Bell, G. A.: Thermal Performance of Multilayer Insulation. Interim Report, NASA CR-72605, Lockheed Missiles and Space Company, 1971.

36. Knoll, R. H. and DeWitt, R. L.: Thermal Performance of a Modularized Replaceable Multilayer Insulation System for a Cryogenic Stage. NASA TN D-8282, Lewis Research Center, January 1977.

37. DeWitt, R. L. and Boyle, R. J.: Thermal Performance of an Integrated Thermal Protection System for Long-Term Storage of Cryogenic Propellants in Space. NASA TN D-8320, Lewis Research Center, May 1977.

38. MMC Dwg. No. 82600200102, Thermal Data Book, External Tank Project, Martin Marietta Corporation, Michoud Operations, October 1979.

39. Paynter, H. L., et al: Experimental Investigation of Capillary Propellant Control Devices for Low-Gravity Environments, Volume II-Final Report, MCR-69-585 (Vol. II), Martin Marietta Corporation, June 1970.

40. Childs, G. E., Ericks, L. J. and Powell, R. L.: Thermal Conductivity of Solids at Room Temperature and Below, NBS Monography 131, September 1973.

41. Bushnell, David: Stress, Stability, and Vibration of Complex Branched Shells of Revolution: Analysis and User's Manual for BOSOR 4, AD-748 639, U.S. Department of Commerce, March 1972.

42. Astronautics Structures Manual, Volume II, NASA TMX-73306, Marshall Space Flight Center, August 1975.

43. Warren, R. P.: Low Gravity Liquid Helium Passive Storage Concepts, Report NBPA72-48297, Martin Marietta Corporation, October 1972.

44. Cryogenic Fluid Management Experiment, Eleventh Monthly Progress Report, MCR-79-501, Issue 11, Martin Marietta Corporation, November 1979.